Department of Automation and Systems Technology

Towards Energy-Efficient Limit-Cycle Walking in Biped Service Robots: Design Analysis, Modeling and Experimental Study of Biped Robot Actuated by Linear Motors

José Luis Peralta Cabezas

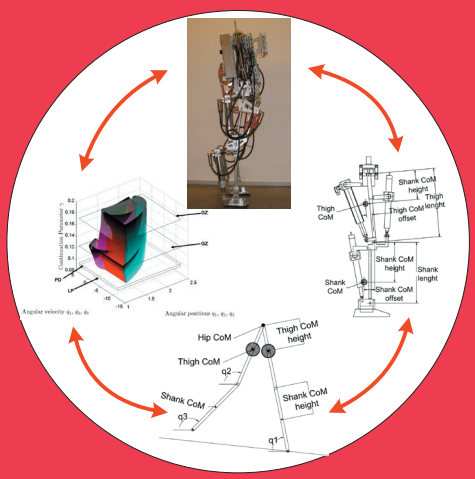

Aalto University

DOCTORAL DISSERTATIONS

Aalto University publication series
DOCTORAL DISSERTATIONS 209/2013

Towards Energy-Efficient Limit-Cycle Walking in Biped Service Robots: Design Analysis, Modeling and Experimental Study of Biped Robot Actuated by Linear Motors

José Luis Peralta Cabezas

A doctoral dissertation completed for the degree of Doctor of Science in Technology to be defended, with the permission of the Aalto University School of Electrical Engineering, at a public examination held at the lecture hall AS1, in the TUAS building (Otaniementie 17, Espoo, Finland) on the 17th of December 2013 at 12 o'clock noon.

Aalto University
School of Electrical Engineering
Department of Automation and Systems Technology

Supervising professor
Professor Aarne Halme

Preliminary examiners
Professor Manuel A. Armada, Industrial Automation Institute - Spanish Council for Scientific Research (CSIC), Madrid, Spain.

Professor Dr. ir. Bram Vanderborght, Department of Mechanical Engineering, Vrije Universiteit Brussel, Brussels, Belgium.

Opponent
Professor Andy Ruina, Sibley School of Mechanical and Aerospace Engineering, Cornell University, NY, USA.

Aalto University publication series
DOCTORAL DISSERTATIONS 209/2013

ISBN 978-952-60-5487-2
ISBN 978-952-60-5488-9 (pdf)
ISSN-L 1799-4934
ISSN 1799-4934 (printed)
ISSN 1799-4942 (pdf)
http://urn.fi/URN:ISBN:978-952-60-5488-9

Unigrafia Oy
Helsinki 2013

Finland

441 697
Printed matter

Aalto University

Abstract

Aalto University, P.O. Box 11000, FI-00076 Aalto www.aalto.fi

Author
José Luis Peralta Cabezas

Name of the doctoral dissertation
Towards Energy-Efficient Limit-Cycle Walking in Biped Service Robots: Design Analysis, Modeling and Experimental Study of Biped Robot Actuated by Linear Motors

Publisher School of Electrical Engineering

Unit Department of Automation and Systems Technology

Series Aalto University publication series DOCTORAL DISSERTATIONS 209/2013

Field of research Mobile Robotics

Manuscript submitted 5 August 2013 **Date of the defence** 17 December 2013

Permission to publish granted (date) 14 November 2013 **Language** English

☒ **Monograph** ☐ **Article dissertation (summary + original articles)**

Abstract

Researchers have been studying biped robots for many years, and, while many advances in the field have been accomplished, there still remain the challenge to transfer the existing solutions into real applications. The main issues are related to mobility and autonomy. In mobility, biped robots have evolved greatly, nevertheless they are still far from what a human can do in the work-site. Similarly, autonomy of biped platforms has been tackled on several different grounds, but its core problem still remains, and it is associated to energy issues. Because of these energy issues, lately the main attention has been redirected to the long term autonomy of the biped robotics platforms. For that, much effort has been made to develop new more energy-efficient biped robots.

The GIMBiped project in Aalto University was established to tackle the previous issues in energy efficiency and mobility, through the study and implementation of dynamic and energy-efficient bipedal robotic waking. This thesis falls into the first studies needed to achieve the previous goal using the GIMBiped testbed, starting with a detailed analysis of the nonlinear dynamics of the target system, using a modeling and simulation tools. This work also presents an assessment of different control techniques based on Limit Cycle walking, carried out on a two-dimensional kneed bipedal simulator.

Furthermore, a numerical continuation analysis of the mechanical parameters of the first GIMBiped prototype was performed, using the same approximated planar kneed biped model. This study is done to analyze the effect that such variations in the mechanical design parameters produce in the stability and energy-efficiency of the system.

Finally, experiments were performed in the GIMBiped testbed. These experiments show the results of a hybrid control technique proposed by the author, which combines traditional ZMP-based walking approach with a Limit Cycle trajectory-following control. Furthermore the results of a pure ZMP-based type of control are also presented.

Keywords Bipedal robotic walking, biped robots, nonlinear dynamics, limit cycle, limit cycle walking, ZMP-based walking, numerical continuation.

ISBN (printed) 978-952-60-5487-2 **ISBN (pdf)** 978-952-60-5488-9

ISSN-L 1799-4934 **ISSN (printed)** 1799-4934 **ISSN (pdf)** 1799-4942

Location of publisher Helsinki **Location of printing** Helsinki **Year** 2013

Pages 256 **urn** http://urn.fi/URN:ISBN:978-952-60-5488-9

Preface

This thesis is the result of the work done within the GIMBiped project in the Automation Technology Laboratory, started in the former Helsinki University of Technology and finished in the now Aalto University, during the period 2008-2013. The GIMBiped project is part of the Center of Excellence in Generic Intelligent Machines, which is partly funded by the Finnish Academy of Sciences. Also, I'm very proud of been awarded a four year scholarship (in 2009) by the prestigious Graduate School in Electronics, Telecommunications and Automation - GETA, the largest graduate school in Finland, and which the extremely successful 18 years history is coming to an end this year (2013). Within GETA I would like to thank director Prof. Ari Sihvola for providing me regular feedback and encouragement for perusing international collaboration and experience, and also Mrs Marja Lepaharju, which I personally think has been the heart and soul of GETA. I would like to thank her always friendly disposition for helping me in any matter, as well as organizing the interesting courses and networking events. Her involvement made my research and life easier, and GETA support made the overall experience as post-graduate definitely wonderful. The financial support of GETA also included a six months research visit to the Jet Propulsion Laboratory (JPL) of NASA/Caltech in USA, and for such a visit I would like to thank Richard Volpe, Adrian Stoica, Christopher Assad and Tomi Yliokorpi, for organizing the trip and supporting my work while at JPL. Furthermore, while at JPL, I wish to thank also Dr. Robert Ambrose and Dr. John Yamokoski for making my visit to Johnson Space Center possible and showing me their Robonaut project.

There are many persons that I would like to express my most deeply gratitude for their help and contribution in this process. First to Prof. Aarne Halme, who believed in me and my abilities since the beginning.

Throughout this entire journey he has provided me with all the support a student can expect from his mentor, and his lifetime dedication and contribution to research and science was an inspiration during my studies. My sincerest gratitude also goes to Tomi Yliokorpi for his support and help during this whole process. Our many fruitful discussions, his constructive feedback and his scientific contribution to the GIMBiped project definitely made a positive difference to the final outcomes of my work.

I would also like to thank and recognize the great contribution to this project made by the students whose Master's thesis I had the pleasure to supervise: Tuomas Haarnoja and Ferdi Perdana Kusumah. Their work was priceless for me, but above all I highlight their dedication and love for science, and wish them the very best in their future research career.

Furthermore, this research would have not been possible without the effort of the many researchers who worked in different aspect of the GIMBiped project, Sami Kielosto, Tapio Leppänen, Dr. Peter Jakubik, Khurram Gulzar and Asko Siitonen, their work is also highly acknowledged.

I'm grateful as well, and appreciate enormously the time and effort putted by the preliminary examiners, Prof. Manuel A. Armada and Prof. Dr. ir. Bram Vanderborght. Their remarks and suggestions helped me to improve the quality and clarity of this monograph.

Also, life in Finland wouldn't have been the same without the many good friends that I had the pleasure to meet during my time here. The sunny and beautiful summers would've been empty, and the long and cold winters unbearable without your company. Thank you all, Joan, Rosa, Helmi, Monika, Maria, Guifre, Anna, Mirva, David Lopez, David Leal, Marcela, Ana Katia, Ivan, Kaisa, Renaud, Viet-Anh, Thomas, Yesmit, Rodri, Fabricio, Julia, Jose Vallet, David Gambarte, Vilhelmina, Eric and Edinho.

I would like to specially recognize the value of Joan's friendship trough this journey. We toured side by side, since the beginning, the road towards the PhD, sharing our victories and defeats. He and his family have welcomed me and the girls, making us feel closer to home.

There are two very important sources of inspiration and role model figures that I have no longer with me and would like to acknowledge, they are my two grandfathers. They were both very different, one a man of science, and the other one a man of close contact to nature. I had the chance to experience both aspects of life living here in Finland and I know that somewhere they are watching and they are happy for me.

Above all, to my father (“o Pai”), my mother (“mamá”) and my sister (“Neni”). A boy can be as lucky to have these three supporting and loving figure in his family. All I am is thanks to you, your unconditional love and your unselfish and complete support provided during all the passages of my life. I really love you guys.

Finally, all my gratitude to my three biggest love in this life, my lovely wife Dani, (gracias por la paciencia y apoyo) and my two wonderful daughters, Sofía Isabella and María Victoria. You, Dani, have made me change all my plans by appearing in my life just a couple of months before I was leaving for a PhD. You, María Victoria, have arrived in the most stressful moments of our lives, and you, Sofía, in just 9 month have destroyed what this thesis is all about, defying with your little clumsy steps control theory and nonlinear dynamics. But for all of that I thank you, for shinning upon me humbleness, and above all, I thank you for having found and built a big space for love in the hearth in who use to be once a just work-driven-old-fool.

Espoo, December 17, 2013,

José Luis Peralta Cabezas

Contents

List of Figures

List of Tables

List of Symbols

a_1	Stance shank length below the CoM
a_2	Stance thigh length below the CoM
a_3	Swing thigh length below the CoM
a_4	Swing shank length below the CoM
b_1	Stance shank length above the CoM
b_2	Stance thigh length above the CoM
b_3	Swing thigh length above the CoM
b_4	Swing shank length above the CoM
c_{t}	Specific cost of transport
c_{mt}	Specific mechanic cost of transport
c_{et}	Total specific cost of transport
d	Traveled distance
$D_{\text{Foot Clarence}}$	Foot clearance distance
$e(t)$	Generalized coordinate position error
$\dot{e}(t)$	Generalized coordinate velocity error
$\ddot{e}(t)$	Generalized coordinate acceleration error
E	Energy
$E_{i_{Elec.}}(t)$	Electrical energy of each actuated joint
$E_{i_{Mech.}}(t)$	Mechanical energy of each actuated joint
F	Finite set
$F_d(\dot{q})$	Dynamic Friction
F_r	Froude Number
F_v	Viscous Friction
g	Gravity acceleration
g_I	State jump function
$G(q)$	Gravity vector
$G_{\text{3-link}}(q)$	Gravity vector for the 3-link dynamics
$G_{\text{2-link}}(q)$	Gravity vector for the 3-link dynamics

h_I	Event function
I	Index Vector
K_{reg}	Regeneration index
K_v	Derivative gain
K_p	Proportional gain
K_i	Integral gain
L	Lengths of the legs of the robot
m_1	Shank mass
m_2	Thigh mass
m_H	Hip mass
M	Mass of the robot
$M(q)$	Inertia matrix
$M_{\text{2-link}}(q)$	Inertia matrix for the 3-link dynamics
$M_{\text{3-link}}(q)$	Inertia matrix for the 3-link dynamics
N_q	Total number of active joints
$N(q, \dot{q})$	Combined Coriolis matrix and gravity vector
$\aleph$	Integer number space
$q = [q_1, q_2, \cdots, q_n]$	Generalized coordinates
$q(t)$	Generalized coordinate position
$\dot{q}(t)$	Generalized coordinate velocity
$\ddot{q}(t)$	Generalized coordinate acceleration
$q_d(t)$	Desired generalized coordinate position
$\dot{q}_d(t)$	Desired generalized coordinate velocity
$\ddot{q}_d(t)$	Desired generalized coordinate acceleration
$[q, \dot{q}]$	State vector
$\dot{q}^-$	Generalized coordinate velocities before the impact
$\dot{q}^+$	Generalized coordinate velocities after the impact
q_1	Stance leg angle
q_2	Thigh angle
q_3	Shank angle
$\dot{q_1}$	Stance leg angular velocity
$\dot{q_2}$	Thigh angular velocity
$\dot{q_3}$	Shank angular velocity
$\ddot{q_1}$	Stance leg angular acceleration
$\ddot{q_2}$	Thigh angular acceleration
$\ddot{q_3}$	Shank angular acceleration
Q^-	Momentum matrix before the impact
Q^+	Momentum matrix after the impact

Q_{FS}^{-}	Foot strike momentum matrix before the impact
Q_{FS}^{+}	Foot strike momentum matrix after the impact
Q_{KL}^{-}	Knee lock momentum matrix before the impact
Q_{KL}^{+}	Knee lock momentum matrix after the impact
$\Re$	Real number space
t	Time
T_I	Time interval
u	Control input
$u_i(t)$	Applied torque or force
v	Velocity of the robot
$V(q, \dot{q})$	Coriolis matrix
$V_{\text{2-link}}(q, \dot{q})$	Coriolis matrix for the 2-link dynamics
$V_{\text{3-link}}(q, \dot{q})$	Coriolis matrix for the 3-link dynamics
x	Solution vector
x_0	Equilibrium point
X	State space
w	Disturbance function

Greek

β	Duty Factor
β_{w}	Duty Factor Walking
β_{s}	Duty Factor Standing
γ	Slope Angle
κ	Gain of the velocity control
λ	Multidimensional real vector of parameters
μ	Friction coefficient
τ	Resulting generalized effort (torque) vector
τ_d	Disturbances torque
τ_{ext}	External torques
τ_{joint}	Joint actuation torques
π	Ratio of circumference of the circle to its diameter
$\Phi(x, t)$:	Vector field (flow)
ξ	Integral of generalized coordinates position error

List of Abbreviation

2D	two-dimensional
3D	three-dimensional
Aalto	Aalto University
ADAMS	MSC.Adams, engineering software commercially available from MSC Software Corporation
APS	Auxiliary Power Source
ASV	Adaptive Suspension Vehicle
ATAC	Army Tank-Automotive Center
ATL	Automation Technology Laboratory
BVP	Boundary-Value Problem
CMU	Carnegie Mellon University
CoE	Center of Excellence
CoM	Center of Mass
CoP	Center of Pressure
CoT	Cost of Transport
CTC	Computed-Torque Control
DARPA	Defense Advanced Research Project Agency
DoF	Degree of Freedom
DS	Double Support
DW	Dynamic Walking
EDB	Energy Distribution Box
EIDI	Experimental Information Distribution Infrastructure
ESS	Experimental Software Structure
FK	Forward Kinematics
FS	Foot Strike
FSR	Field and Service Robotics
GCoM	Ground Projection of Center of Mass
GE	General Electric

GIM	Generic Intelligent Machines
GUI	Graphical User Interface
GZ	Grazing bifurcation
HRP	Humanoid Robotics Project
HS	Heel Strike
HZD	Hybrid Zero Dynamic
IC	Initial Condition
IdSS	Idle State Stability
IHMC	Florida Institute for Humans and Machine Cognition
IJC	Independent Joint Control
IK	Inverse Kinematics
IMU	Inertial Measurement Unit
ISS	International Space Station
JPL	Jet Propulsion Laboratory
JSC	Johnson Space Center
KES	Kinetic Energy Shaping
KIT	Kyushu Institute of Technology
KL	Knee Lock
LC	Limit Cycle
LCW	Limit Cycle Walking
LM	Linear Motor
LP	Limit Point bifurcation
MATLAB	(MATrix LABoratory) commercially available numerical computing environment
MC	Motor Controller
MIT	Massachusetts Institute of Technology
MM	Millions
MPC	Main Processing Computer
MPS	Main Power Source
MRS	Mobility and Robotic Systems
MSB	Maximum Step Disturbance
NASA	National Aeronautics and Space Administration
ODE	Open Dynamics Engine
OS	Operating System
OSU	Ohio State University
PBC	Passivity-Based Control
PD	Proportional-Derivative
PD	Period Doubling bifurcation

PDW	Passive Dynamic Walking
PEC	Potential Energy Compensation
PID	Proportional-Integral-Derivative
PoC	Point of Clearance
R&D	Research and Development
SM	Stability Margin Criterion
SS	Single Support
StL	Stance Leg
StP	Stance Phase
SwL	Swing Leg
SwP	Swing Phase
TKK	Helsinki University of Technology
UI	User Interface
USC	University of Southern California
USD	US dollars
WU	Waseda University
WWII	Second World War
ZMP	Zero Moment Point

1. Introduction

1.1 Motivation and Background

The world has witnessed a huge increase in the robotics research during the last thirty years [1–3]. During those years, most of the main components (both hardware and software) of mobile robots have matured in such a scale that they can now be considered to be part of the off-the-shelf technology [4–8]. The applications have varied from space exploration [9–13] to entertainment robots [14, 15], and the number of non-industrial service robots has increased considerably [1, 2, 16]. As a consequence, humans are starting to accept robots as part of their everyday lives [17], and that has given the birth to a new industry and research area, the *Field and Service Robotics* (FSR) [2, 18–21].

In Aalto's *Automation Technology Laboratory* (ATL) and in the *Center of Excellence* (CoE) in *Generic Intelligent Machines* (GIM), where this study was conducted, one of the main research topics is FSR [22, 23]. *Field Robotics* study intelligent mobile machines in unstructured and dynamic environments (*e.g.* construction, forestry, agriculture, mining, underwater, military, and space applications) [2, 24], and *Service Robots* are aimed to provide services to humans instead of manufacturing [21]. These intelligent mobile machines autonomously carry out monotonous, dangerous or tedious tasks; therefore, the two crucial prerequisites for FSR are *mobility* and *autonomy*. On flat surfaces, wheels are the most efficient, however for rough terrain or in human-like environments (characterized by stairs, narrow paths and moving obstacles), leg locomotion is more advantageous [25, 26]. Within legged locomotion, humanoids-bipeds are the one of the most attractive platforms for the FSR potential applications, given that one of the goals in bipedal robotic research for FSR is to serve

as locomotion platform for a complete humanoid robot, which could replace, if desired, the human presence in the future work-site (Figure 1.1) [27].

A case could be made against the costs of *Research and Development* (R&D) for FSR and their potential to replace current human workforce. However, the goal of FSR is not to replace the current human workforce but to collaborate with humans in the future work-site, taking over heavy or hazardous tasks, generating in that way the need for a more skillful and specialized human workforce [22, 28]. Furthermore, the costs of the R&D for FSR should not be compared against simple routine industrial tasks but to potentially life-endangering jobs, where no costs are at stake. A clear example are robots for space exploration, like Robonaut [29, 30] (Figure 1.2). In space applications, the hazard to human health in outer-space is enormous (radiation, body mass loss, system failure) and the cost for training and maintaining a fleet of astronauts is huge as well [31].

Therefore, robots that walk in a human-like manner are not just a fascinating topic of research because of their connection with science fiction, but their real potential benefits indeed relate with the future objective of FSR. These applications also range from robots for entertainment [14,32], FSR [27, 33] to the restoration of damaged human leg mobility [34]. Furthermore, the research of bipedal locomotion requires the study and broad

Figure 1.1. Figure of a humanoid biped robot replacing a man in a future work-site.

Figure 1.2. Robonaut, the humanoid space platform greeting the author.

insight into the control of complex nonlinear dynamical systems, therefore being, an excellent platform for the development of new control principles [35–37].

Researchers have been studying biped robots for more than forty years [38,39,39], and, while many advances in the field have been accomplished, there still remain the challenge to transfer the existing solutions into real applications for FSR [40–42]. The foremost issue is related to what was mentioned before as one of the main requirements for FSR, *mobility* and *autonomy*. In *mobility*, biped robots have evolved greatly since their beginning, in the late 60's [25], nevertheless they are still far from what a human can do in the work-site [1]. Similarly, autonomy of biped platforms has been tackled on several different grounds (multi-sensor fusion [43–45], stability and balance [46–48], human-machine interaction [49, 50]), but its core problem still remains, and it is associated to energy issues [40, 51, 52]. Because of these energy issues, lately the main attention has been redirected to the long-time autonomy of the biped robotics platforms. For that, much effort has been made to develop new more energy-efficient biped robots, aiming to increase their productivity substantially [52–55]. In that matter, the increase of energy efficiency will also reduce ecological impact; this will help industries to fulfill new and stricter environmental regulations applied worldwide [1].

The motivation for being part of this not-yet-conquered investigation field and the need to evolve into the next generation of work-site partners autonomous machines gave birth to the GIMBiped project [41,56–60]. The GIMBiped project is part of the Motion Systems research package (RP8

[60]) in the CoE GIM, which targets research and development of non-conventional motion systems for future work-site applications. The objective of the GIMBiped project is to study and develop dynamic and energy-efficient bipedal robotic waking. This thesis falls into the first studies needed to achieve the previous goal. A detailed analysis of the nonlinear dynamics of the target system [59], the development of a simplified biped model used to analyze and compare different control approaches [41, 58, 59], the investigation of the optimal mechanical design for energy efficiency and stability [56, 59], and the study of efficient control strategies and algorithms for bipedal robotic walking [58] including practical experiments of a new proposed control approach in Aalto's biped testbed, the GIMBiped.

1.2 From Basic Locomotion Systems to Bipedal Walking in Service Robots

A locomotion system enables robots to travel along a surface (*e.g.* grass, sand, gravel) or move through a specific matter (*e.g.* water, air, vacuum). It allows the robot to avoid and overcome obstacles and reach a certain goal to perform a task. In order to fulfil FSR tasks, robots must be able to move generally just along relatively hard surfaces in indoor and/or outdoor surroundings. In indoor environments, the real challenges are mostly related to robots' capabilities to move in an infrastructure, including stairs and narrow passages, designed primarily for humans. Outdoors, the challenges are far more severe, and good locomotion capabilities are essential for field robots working on uneven outdoor terrain [19].

Some of the most important locomotion principles on ground are: wriggling, crawling, rolling, walking, running, jumping [25], and rolking [61]. The easiest and most efficient way to move on hard flat terrains is by rolling, because it preserves the momentum of the system and does not waste energy in redundant control. Rolling can be performed by any locomotion systems based on wheels (or round-shaped robots [62]). The mechanical simplicity of the wheel also allows their straightforward use, compared to the significant amount of work needed in developing the mechanical and control system for the other locomotion principles. Furthermore, through the history humans have build their entire ground transportation systems to accommodate wheel-based vehicles; nonetheless, more than half of the outdoor land areas in the world are still not

wheel-accessible [25] (and probably won't for some time to come still). In indoor working facilities, although all modern construction requires having wheel-chair access, these still are mostly built to accommodate the needs of an average-height human (*e.g.* stairs, tables, corridors, door-knobs, elevator buttons), and thus in advanced tasks and specific jobs a better locomotion system is needed. *Bipedal walking* appears therefore as the best solution, since it allows the same mobility as humans have in indoor and outdoor terrains, extending to the maximum the robots' capabilities in FSR, given that, in the future, field and service robots will work with humans.

The advantages of walking, in general, include stepping over obstacles, gaps, openings or chasm [25]. These kind of robots can also negotiate extremely broken ground and adjust the effective length of their legs to match the irregularity of the terrain, thus rendering a smooth progress useful when carrying delicate payload. Moreover, walking allows omni-directional movement on rough terrain and uses a discrete number of supporting points which can be rearranged to optimize equilibrium and grip. Consequently, there were clear reasons to impulse the study of walking systematically since the beginning of the 1960s, first with multi-legged robots for outdoor terrains [63–65] and then eventually bipedal locomotion for indoor service robots [32, 66–68].

However, besides the previously-mentioned benefits of walking, the mechanical construction as well as stability and motion control of the robotics systems that use legged locomotion are very challenging, since they are nonlinear and depend on large number of parameters. Bipeds in particular are highly unstable, because while lifting one leg the system has only one point (surface) of contact to support itself. Also the system can only apply compressive forces over the supporting point (surface), while the center of gravity of the robot is not always above it. The extensive nonlinearity of bipeds systems also prevent harsh control moves because that can drive the robot utterly out of balance. Other difficulties in biped robots have also been observed and studied in detail [69–71].

Nevertheless, researchers have actively studied many different control techniques trying to perform successful bipedal robotic walking, and, even though all these different approaches are highly computationally demanding thanks to the improvement in the computer technology for the last 20 years, several of these control techniques were effectively tested and evaluated [35, 67, 68, 72]. Other advances that allowed continued progress

in the biped robotic research were the positive results in the development of new motion drives and sensors. Many companies now offer off-the-shelf solutions for high torque and low-weight harmonic drives [73] (or servos for small robots [74, 75]), inertial measurement units (IMU) [76–78], and 6 degree of freedom (DoF) torque/force sensors (for foot or ankle torque/forces calculation) [79, 80], all essential tools for building mechanical prototypes for hardware testing which uses a traditional manipulator approach and simplified dynamic model for the control of biped robots.

So far, most of the solutions for bipedal walking that have actually been implemented in hardware use the above-mentioned, traditional manipulator approach and simplified dynamic model. These methods are known as Static-walking and Zero Moment Point (ZMP)-based walking. Static-walking is a very old technique that views walking as a rigid and defined sequence of events, meaning that it concentrates on placing the legs in the right place at the right time according to a predefined pattern to follow in position control [81]. In Static-walking, the dynamics of the robot are neglected and only static forces are considered. This brings the need for the projection of the robot's center of mass to fall into the supporting area of the feet, restricting the naturalness and velocity of the movement.

A better approach to bipedal walking came with the use of the Zero Moment Point (ZMP) concept introduced by Miomir Vukobratović [26, 38, 82, 83]. In common techniques that use the ZMP as stability indicator, some aspects of the dynamics of walking are considered but approximated. In this approach, the projection of the robot's center of mass can leave the supporting area of the feet; however, the forces and momentums acting in the robot should be controlled in such a way that at least one foot always remains flat on the ground. That is commonly referred to as the ZMP-based walking approach, and most of the modern robots [32, 67, 68, 84] use some derivation of this concept to accomplish walking.

Algorithms based on Static-walking and ZMP-based walking gave the first impulse for the bipedal robotics research, and, what is more important, they demonstrated that robotic walking was indeed possible. With increasing improvement in time, advanced controllers based on ZMP, together with new technologies in sensors and motion drives, allowed a more dynamic walking for biped and humanoid robots [32, 67, 68, 85]. The overall mobility of these robots was increased as well, transforming what were in the beginning purely interesting stiff walking machines to

Figure 1.3. Humanoid robot ASIMO performing service tasks. Courtesy of Honda Motor Co., Ltd.

the amazing humanoid robots that are seen nowadays. These state-of-the-art bipeds and humanoid robots can now climb up and down stairs [86, 87], (Figure 1.3), preform turns [86–89], walk at different speeds [86, 87, 89–94], run up to $9\ \mathrm{km/h}$ [95], fall in a controlled fashion [96–98], squat [85, 99], step over obstacles [100] and equilibrate and jump in one leg [95]. Also, apart from what the legs can do, a complete humanoid system can identify and track persons and objects [101] (thanks to cameras embedded into the robots' heads), understand speaking messages [102], manipulate and carry small objects [95, 103] and avoid moving obstacles [95].

1.3 Problem Formulation

The main problems with these previous-mentioned walking techniques for bipedal service robots, Static-walking and ZMP-based walking, are related to energy usage. The most advanced biped (humanoid) robot nowadays, based on ZMP criteria for walking, uses over 20 times more energy than a human just for walking [52], which together with their low capacity to carry their own energy source, results in very short operation times (from 20 min to 1 hour). Additionally, the long periods of time required for recharging the batteries (from 3 to 4 hours) [87, 89–95], make them unfit for use in any FSR applications. Apart from their restrictive energy consumption during walking, state-of-the-art biped and humanoid robots

still cannot be compared to humans in mobility (*e.g.* walking, jumping, climbing), in their capability to carry payloads, manipulate small objects and execute skillful tasks [1].

Therefore, an alternative to start solving the previous mobility and energy usage problems would be to build robots that walk more naturally and efficiently in terms of energy consumption. This led to a new wave of research in energy efficient bipedal walking, first impulsed by the study of unpowered walking aid by Nichols and Witt in 1971 [104], which then was made popular by McGeer, who studied cyclic stability in bipeds in his seminar paper about *Passive Dynamic Walking* (PDW) [105]. McGeer showed that a natural gait could be obtained from a simple mechanical design of a *two-dimensional* (2D) biped which takes its energy only from gravity to walk down a slight incline. If the lengths and masses of the links are correctly adjusted, a simple pendulum motion is enough to produce very fluid and human-like walking when the system reaches the *Limit Cycle* (LC). The advantage of this system is that it consumes very little energy and requires no controller. However, the plain mechanical skeleton can only walk down on a slope and cannot perform any other task, having thus poor versatility for robotic usage. The recent focus of attention has been to try to find the means of reconciling a passive and a controlled dynamic aspect in the same system for what is now known as the actuated *Limit Cycle Walking* (LCW) [106, 107].

Since hardware for driving LCW-based robots is not easily available, some researchers have chosen to develop their own tailor-made drives targeting energy efficiency [52, 72, 108–111]. However, none of the proposed solutions are as good as the human muscle in providing the compliance for passive stages of walking and, at the same time, maintaining the power to weight ratio needed for heavy duty tasks.

The problem of efficiently controlling a highly nonlinear, time-variant, under-actuated and multi-variable system, together with the current limitations in hardware for building and testing a mechanical system under innovative control approaches, generates the following broad and open-ended questions in robotics:

Is it possible to build and control a biped robot in an energy-efficient way, such that this platform could be used in FSR applications?

The broad question above covers several topics in robotics, and has been

partially addressed by some researchers who concentrate mainly in developing energy-efficient controllers for walking bipeds [52, 109, 110] and mechanical platforms which can be used to perform LCW [72, 108, 111]. However, the results are not yet ready to be ported to FSR applications, and the question remains open.

In trying to close the gap in this matter, this research then specifically addresses the following question of the above issues:

- Can this highly non-linear dynamic model be simplified for its study and analysis and, generate useful data for its design and control?

- How should the complete biped system be planned to maximize energy efficiency?

- What are the guidelines for the implementation or modification of biped robots' mechanical design to increase its energy efficiency and robustness based on Limit Cycle Walking?

- How do LCW-based control approaches compare in energy efficiency and robustness?

- How do Linear Motor (LM) actuators perform in this kind of locomotion?

All the previous questions will be addressed in this thesis, which will also present practical experiment results of a new type of control to target energy-efficient bipedal walking performed in Aalto's biped prototype, the GIMBiped.

1.4 Hypotheses and Methodology

Regardless of all technical and mathematical difficulties involved in developing biped robotic walking, humans are able to walk without any problem, and they do so unconsciously since young age. The previous-mentioned findings on PDW, and now recently in the detailed studies in LCW, point to the direction that the dynamics of the bipedal system holds a natural disposition for an energy efficiency-walking mode, referred to as the natural limit cycle (natural LC).

The hypothesis for this thesis work assumes the existence of such energy-

efficient mode, and that is governed mainly by a delicate choice in the mechanical configurations for PDW. Nonetheless, the main contribution of this thesis is the extension of the previous hypothesis to the existence of the same energy-efficient mode for actuated LCW built under a delicate equilibrium between an appropriate control scheme, suitable mechanical design and proper actuators choice.

The hypothesis above is tested first in a simulation environment, with a simplified model of the ATL's biped testbed in Aalto University. Several LCW-based controllers are compared to evaluate its performance for energy efficiency and robustness, aiming to assess the importance and influence of the control approach in the results.

Afterwards, a variational study is performed in the simplified mechanical model of the biped system to analyze the effect that changes in the mechanical parameters produce in the stability and efficiency of the natural LC.

Finally, different combinations of ZMP-based and LCW-based controllers are tested in the GIMBiped platform through the same scrutiny of efficiency and for an individual evaluation of the performance of its actuators.

1.5 Scientific and Specific Contributions

Throughout this thesis work, the author reviews the current theories and practice in bipedal legged locomotion, focusing specially on those oriented to energy-efficient bipedal walking. Based on these studies, the author further develops the scientific propositions bellow, which are the main scientific contributions of this thesis:

- The use of an approximated model of a LCW version of the actual hardware, the GIMBiped, for the variational study in parameters, to analyze the effect in the stability and efficiency (Chapter 5).

- The effective assessment between LCW-based control methods in simulation, evaluated in their energy efficiency and robustness (Chapter 4).

- The proposal of a mixed ZMP-LCW-based control for the GIMBiped robot (Chapter 6).

For the previous scientific contribution, the work developed by the author:

- All the control algorithms and simulators in MATLAB presented in this thesis were developed by the author (Chapters 3, 4 and 5).

- All codes associated to the analysis of the mechanical design using the TC-HAT software were developed by the author (Chapter 5).

- All the codes related to the control algorithms and trajectories planning for the hardware testing in the GIMBiped were developed by the author. There is a as major contribution to the GUI, communication and driver infrastructure (Chapters 3, 4 and 6).

- All the simulation and hardware experiments presented in this thesis, as well as the planning of minor mechanical changes done in the GIMBiped testbed, were planned and carried out by the author (Chapters 3, 4, 5 and 6).

- Most of the work presented in this thesis has already been partially published in the following academic papers [41, 56–60, 112],

The development of the testing platform GIMBiped was a multi-disciplinary effort which included the work of several people in different fields. A general overview of the GIMBiped platform is given in Chapter 3, the main purpose of which is to present the basic background of the testbed used to support the research. Chapter 3 however does not, in any case, represent an exhaustive study of the development of the GIMBiped prototype. The development of the GIMBiped platform does not corresponds to the author's central scientific contributions. Information related to the development of the GIMBiped testbed can be found in [41,56–60,112,113]. Furthermore, the actual mechanical design and construction of the prototype is not reviewed in detail in this thesis. The original design and initiative for adopting LMs as GIMBiped actuators shall be credited to Dr. Peter Jakubik from ATL at Aalto, and more information related to this subject can be found in [113–116].

1.6 Thesis Outline

Chapter 2 summarizes the related work and background needed to follow the work done in this thesis. It starts with a short review on legged locomotion and bipedal walking, followed by a summary of the common terminology and definitions in bipedal walking, the walking cycle and performance indices. The chapter ends with a detailed description of the concepts used for stability in bipedal walking and the common control approaches that rely on these stability concepts.

Chapter 3 shortly presents the GIMBiped testbed, the Aalto's biped prototype developed in the ATL. It first gives an overview of the mechanical layout and the main communication, sensor, actuators and processing modules. It later shows some of the first simulation experiments on the actuators oriented to support the prototype development. Finally, it presents some known concepts and new theoretical ideas towards energy-efficient walking approaches that may be applied in the future on the GIMBiped platform.

Chapter 4 starts by shortly presenting the different ways bipedal walking has been modeled for robotics research. In this chapter the approximated model used throughout this thesis is presented in detail. Next, all the simulators used in this research are presented, together with the different control techniques analyzed in the later sections and chapters. Finally, simulation results of a comparison of different LCW-based control techniques are presented, the major indicators to be noted being the robustness and energy-efficiency with such control techniques.

Chapter 5 presents a variational analysis of the mechanical parameters of the first GIMBiped prototype. The study is performed using an approximated model of the GIMBiped and applying the continuation process in the resulting nonlinear hybrid dynamic system. This study is done to analyze the effect that such variations in the mechanical design parameters produce in the stability and energy efficiency of the system.

Chapter 6 presents the experiments performed in the GIMBiped testbed. It shows the results of a hybrid control technique, as proposed by the author, which combines ZMP walking with LCW. Furthermore, the results of a pure ZMP-type of control are also presented. The results are evaluated against their energy efficiency and compared with the performance of the most relevant biped robots nowadays.

Chapter 7 presents a summary and the conclusions drawn from this

thesis work, together with some proposals for future works on both the GIMBiped project and further bipedal walking research in FSR.

2. Related Work

This chapter presents the fundamental concepts used within bipedal robotic walking research. It will be used as a support for the understanding of the work performed in this thesis. It starts, in Section 2.1, with a short history and state of the art review on legged and biped robots. Section 2.2 explains the basic terms used in biped robotic research, which includes concepts associated with bipedal walking anatomy, classification, metrics and performance indices. Finally, Section 2.3 provides theory and definitions of biped stability and their physical and mathematical representation together with the most common approaches towards biped robots controllers' implementation and their use of corresponding stability criterion.

2.1 History of Legged Robots and State of the Art in Bipedal Robotics Research

The first conjectural ideas of mechanical walking can be traced back to the work of Leonardo da Vinci, late in the XV century and at the begging of XVI century. In his sketches, he describes the designs for a humanoid automaton, referred to as Leonardo's robot. He also designed, and allegedly built, a mechanical lion which could walk, for the King Francois I, to celebrate the alliance between Florence and France. Many other authors have described theoretical designs of walking machines, including Jules Verne in his book The Steam House, where a wheeled house is pulled by a steam-powered mechanical elephant. Verne's vision of the details of its operation is quite fascinating since it anticipated hydraulic actuation, which has been one of the main drives chosen to actuate heavy walking machines. Other walking machines from the early XX century were indeed mere mechanical toys, driven by cranks and powered by a rotating

internal source based on clockwork, which could execute fixed walking cycles.

However, the real autonomous walking machines developed within the formal robotics and automation area, enfolded in universities and research institutes, did not flourish until the 1940's, with the mainstream use of the combustion engine and the interest drawn to the Defense area research at the dawn of the Second World War (WWII). The evolution in walking machines enclosed in this background has been quite similar to the evolution of walking in nature, where the first creatures were very simple animals, i.e., insects (six-legged animals), then evolving to reptiles (four-legged, but only with static motion), followed by mammals (four-legged, dynamical motion) and finally primates (two legged, dynamic motion). However, the development in walking machines did not follow the size scale seen in nature, but rather just the morphology and control complexity.

The first real attempt to build a walking machine with individually controlled legs was made by Hutchinson and Smith [64] in 1940 in the UK. The vehicle was Hutchinson's proposition to the UK War Department for a heavy-load military transport walking machine. The vehicle was ultimately built-up to scale and was remotely controlled and actuated by flexible cables. Finally it did not convince the War Department, who halted the project, but Hutchinson and Smith's proposed control mechanism was later adopted by General Electric (GE) for their *Walking Truck* built in the 1960s [117–119]. After Hutchinson and Smith's work, the mainstream in legged robotics has been divided into three major regions in the world: USA, Europe and Japan.

2.1.1 Legged Locomotion Research in the USA

In the USA, the University of Michigan led the way in legged research, thanks to its association with the USA's Army Tank-Automotive Center (ATAC), which maintained interest in the developing vehicles for rough terrain after WWII. M. G. Baker founded in 1950 the Land Locomotion Laboratory in ATAC, studied and wrote several books in legged locomotion [120–122]. His work was followed by R. A. Liston, R. K. Bernhard and J. E. Shigley, who also contributed mostly to theoretical legged locomotion research [118, 123, 124]. Shigley's work in particular laid down the first set of criteria for an ideal walking machine [124]. Successful walking machines started to emerge after ATAC joined forces with GE in

1962, ultimately resulting in the construction of the *Walking Truck*, designed by R. S. Mosher [117]. The huge 1400 kg quadruped performed relatively well; however, it proved to be awfully demanding to drive, since each of the robot's leg was coupled by hydraulic servo loops to one of the driver's legs or arms. Clearly a computer control was needed to assist the driver to command the walking machine, and that arrived shortly after, around 1965-66, with the work of R. McGhee in the University of Southern California (USC). McGhee used finite states to generate a stepping cycle on a computer, which entirely controlled their walking machine, the *Phony Pony*. Computer control was seen thereafter as the way forward and the *Phony Pony* a breakthrough in robotic legged locomotion at that time [125–127]. McGhee international and national collaboration, especially with Tomavic [128] and A. A. Frank [127, 129], boosted the legged research in other countries. McGhee later moved to Ohio State University (OSU) where he continued to work in legged locomotion in 1970s [39, 130]. He later developed, in 1984 together with K. Waldron, the Adaptive Suspension Vehicle (ASV). The ASV was the largest hexapod in the word, a quasi-industrial vehicle founded by the Defense Advanced Research Project Agency (DARPA) and able to walk on irregular terrain [131, 132].

Afterward, in the late 1970s and early 1980s, major impact research was carried out by M. Raibert, first at the Carnegie Mellon University (CMU), where he studied dynamically stable running [133, 134], and later founding the LegLab at the Massachusetts Institute of Technology (MIT). In the LegLab, Raibert developed a series of active hopping robots, including monopods, bipeds and quadrupeds, with impressive results. These robots were able to walk, run and perform flips and acrobatics [135–138]. Crucial for boosting this development was again the support of the US Army through DARPA, which in 1980 decided to fund hopping and dynamic walking machines in the LegLab. Later, in 1992, Raibert founded Boston Dynamics, a spinoff of his LegLab at MIT. The LegLab was also mostly funded by DARPA and has developed several of the most advanced quadruped and biped robots to date, the BigDog and Petman [85, 139] among others. They also recently unveiled the Cheetah, the fastest legged robot in the world, surpassing 46 km/h, a new land speed record for legged robots [140].

Parallel to the work done by Raibert, in the early 1990's several different research centers in the USA started working on legged locomotion

and continue to do so until today. C. G. Atkeson, in CMU, works in machine learning and reinforcement control on humanoid robots [141–144]. J. W. Grizzle from the University of Michigan, who introduced the Hybrid Zero Dynamic (HZD) control for biped robots, has produced several highly successful experimental results [35, 72, 145, 146]. His initial work was done with the biped RABBIT, a testbed result of a joint effort by several French research laboratories [35]. Later, together with J. Hurst, he developed Mabel [72], which is a 2D compliant under-actuated biped and, most recently MARLO/ATRIAS, the 3D version of the previous [147, 148]. Also, A. Ruina from the Cornell University, together with S. Collins (now in CMU), researched on energy efficient-biped robots in the late 1990s [52, 149, 150]. Their work was fundamentally inspired by the early work of McGeer (not to be confused with McGhee) in Passive Dynamic Walking (PDW), which will be mention in detail later because of its importance in this thesis. A. Runina together with C. Atkeson launched in 2005 the Dynamic Walking conference/meeting, a yearly summit involving the major names in the walking research [151]. Ruina's group continue to produce work on legged locomotion, and one of their recent platforms, the Cornell Ranger, managed to walk 65 km (1.5 marathons) [152].

Parallel to all the work done previously, mostly by university research centers, another important research institution working on legged locomotion in the USA was the National Aeronautics and Space Administration (NASA). NASA started to be interested in legged locomotion in the early 1960s with its potential application for mobility in space, the Moon and other planets. They opened a *Lunar Rover Competition*, and the company *Space General* proposed a walking machine named the *MoonWalker Lunar Rover* (cited in [25, 153]). After NASA canceled the earlier unmanned moon rover program, Space General re-envisioned its prototype as the *Moonwalker Disability-walker* (chair), and later as the *Iron Mule Train*, a series of walking machines intended to transport loads in the battle-field [154]. This same previous idea, of legged machines in the battle-field, was revised by D. J. Todd in 1990 and ultimately by *BostonDynamics* in the early 2000s with the BigDog [139]. NASA continued to work on the sidelines with walking machines like the LEMUR [155], ATHLETE [156] and Dante [157], but none has been on space yet. There are a couple of active projects now, involving legged locomotion, which eventually could be launched. One is the Robonaut project (initially project M), developed by a research group in the Johnson Space Center (JSC) led by R.

Ambrose (Figure 1.2) [30]. Although one of the Robonaut testbeds is currently in the International Space Station (ISS), it is just in its upper-body configuration. Robonaut is expected to initially have some type of lower body limbs, designed to attach itself to the internal supporting hooks of the ISS, and later some actual biped legs. In close relation with Robonaut and funded by NASA, a group in the Florida Institute for Humans and Machine Cognition (IHMC) developed an exoskeleton to help astronauts stay healthier in space and also a possible application for assisting paraplegics in walking. Another potential flight mission of a walking machine is the rethought of the ATHLETE project, after the canceling of the *Lunar Outpost Mission* (Figure 2.1). The new goal of this project is to land on an asteroid, explore it and gather samples.

As part of collaboration between the NASA's Jet Propulsion Laboratory (JPL) and the ATL in Aalto, T. Haarnoja (a former ATL's Master student) and the author have carried out research visits to JPL for working in a biped related project. Both T. Haarnoja and the author worked with A. Stoica and C. Assad in the Mobility and Robotic Systems group (MRS). The MRS group has now a copy of the Flame robot (Figure 2.2), developed by M. Wisse's group at Delft, and research in cerebellar models for walking pattern generation is underway in collaboration with the Northwestern University. T. Haarnoja worked on the development of an ODE simulator for biped robots, and on a model-based velocity control using

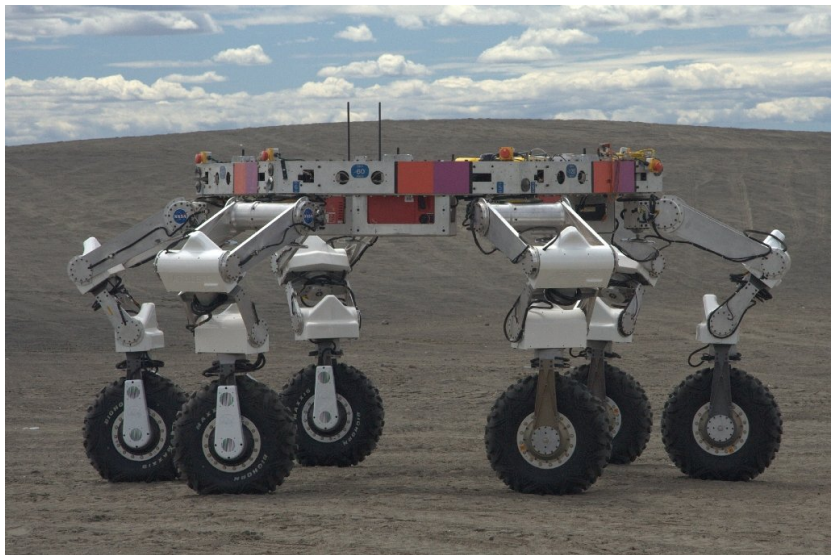

Figure 2.1. The All-Terrain Hex-Limbed Extra-Terrestrial Explorer (ATHLETE) vehicle. Courtesy NASA/JPL-Caltech

such tool [57, 158]. The author went on working in long-distance real-time control of ATL's biped system, the GIMBiped [112], and the Limit Cycle-based control of the same system [58].

Until today, a great impulse for research involving walking machines and bipeds in USA has been provided by the financial support of DARPA. Currently, DARPA is promoting the DARPA Robotic Challenge [160], a competition taking place in a rescue scenario where humanoid robots have to perform highly demanding tasks. The prize for the winner is up to $ 2 MM USD. Many of the previously mentioned research groups are taking part in the challenge, which uses, as a testebed, a robot named ATLAS, which has been developed by Boston Dynamics together with Grizzle and Hurst group, based on the Petman and Marlo platforms.

2.1.2 Legged Locomotion Research in Japan

The most prominent era in the history of legged locomotion in Japan started in the 1970s, almost at the same time at the Kyushu Institute of Technology (KIT) and at Waseda University (WU). In KIT, Taguchi

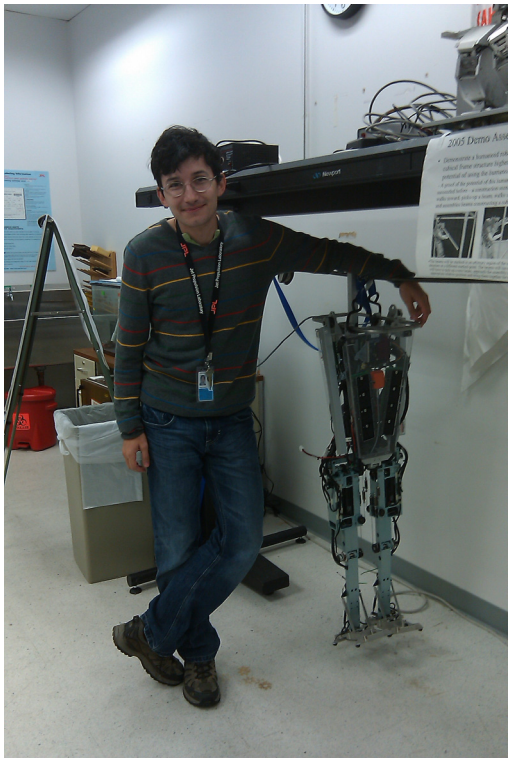

Figure 2.2. Hermes (JPL's copy of Flame [159]) and the author.

et al. built a quadruped robot which was actuated by pneumatic motors and performed a crawling gait [161]. In WU, I. Kato et al. started the WABOT Project, building a series of walking and humanoid robots, which were highly publicized. The first, WABOT-1, was built in 1973. It was a biped walker actuated by hydraulics which maintained static stability at all times. Thereafter, Kato and his group, started gradually developing robots with more dynamic capabilities and humanoid features, but the only walking one was the biped WABIAN in 1997 [162].

Noticing the attention received by robotics in their country, several private companies started to invest in R&D related to robotics, and some of them tackled walking robots. The most notable one was Honda, which in 1996 started their project to develop a humanoid robot. The first models E0 (1986), E1 (1987), E2 (1989) and E3 (1991), were mainly centered on developing walking and lower limb capabilities, and the results range from slow static walking to more dynamic walking, averaging the speed of a human (3 km/h [163]). The following series, E4 (1991), E5 (1992) and E6 (1993), focused on walking stability and stairs climbing [163, 164]. Soon after, an upper body, including torso, arms and head, was developed. These were their first humanoid series and were called P1 (1993), P2 (1996), P3 (1997) and P4 (2000). After that, in 2000 the robot was renamed ASIMO, and 3 versions (2000-02, 2004-07 and 2011) are undoubtedly the most advanced humanoid robots to date [163].

Based on the acquisition of three Honda's P3-series prototypes [165], Kawada Industries started, with the support of some Japan's state offices, the Humanoid Robotics Project (HRP). The HRP was envisioned as a domestic robotic helper and one of the few differences with ASIMO is that it can fall in a controlled fashion and stand up back again [97–99]. Thei latest version is named HRP-4C (2009-2011), and it has been built upon the database of an average young Japanese female and includes feminine face and expressions [32].

Following Honda's steps, Sony also began research on walking robots. However, their approach was towards commercial entertainment robots, and their star product was the Sony AIBO. The AIBO was a robotic pet designed to emulate a small puppy. Its first consumer version was introduced in 1999, with early updates until 2005. Although AIBO could have been considered a commercial success, selling close to 200000 units and, used in many research institutions and for education purposes, its development was canceled in 2006 due to changes in the company strat-

egy [166]. Together with the discontinuation of AIBO, Sony also canceled the development of its humanoid robot QRIO, which had started not long before, based on the knowledge acquired during AIBO's development.

Other Japanese companies which developed humanoid and biped robots include Fujitsu with the HOAP series robots (HOAP-1 (2001), HOAP-2 (2003) and HOAP-3 (2005) [167]) and Toyota with the *Toyota Partner Robots* series, from which only Version 1 (biped) and i-Foot (chair with 2 legs) are legged versions [168].

2.1.3 Legged Locomotion Research in Europe

After the work done in the UK by Hutchinson and Smith, walking research continued mainly in Eastern Europe during the cold war. R. Tomovic made one of the earliest theoretical studies on wheel-less locomotion [169] in 1961 in Belgrade. After that, Vukobratović and his colleagues, also in Belgrade at the Mihailo Puppin Institute, worked on functional rehabilitation. Their research led to the development of a biped exoskeleton for walking aid, starting with passive aid, which later evolved to the study of autonomous locomotion [170–172].

Vukobratović introduced in 1972 the concept of ***Zero Moment Point*** (ZMP) control [173], which revolutionized legged and mainly bipedal robotic locomotion, since it was the first attempt to formalize the need for dynamic stability in legged locomotion. The ZMP paradigm will be explained in detail in Section 2.3.1.

The Russians began work on walking machines in the early 1970s when Vokobratovic and Ignatiev started developing a hexapod in Saint Petersburg in 1973 [174]. By the mid-1970s, at least 3 hexapods by Vukobratović [174], Okhotsimski [175] and Platonov [176] were also developed around Moscow. Bessonov and Umnov worked in defining optimal gaits [177,178] while Kugushev and Jaroshevskii worked on free gaits [179].

The legged robotics research hype came back to Western Europe also in the early 1970s, and walking machines were built or proposed in several countries. After the work done by Hutchinson, D.C. Witt worked on leg rehabilitation systems at the University of Oxford. Witt's effort concentrated mainly on semi-passive systems although he built an autonomous testbed for proofing his walking aid system in 1971 [180]. After Hutching and Witt, computers started to play a major role in the walking systems developed in Europe. Some examples are Petternella and Salinari in Rome (1973) [181], Kessis at the University of Paris with his hexa-

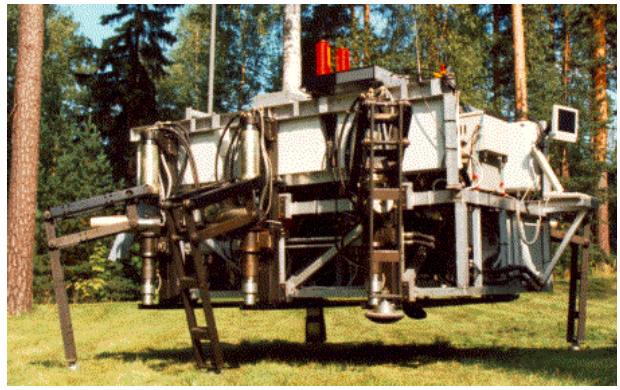

Figure 2.3. MECANT (Mechanical Ant), hydraulic six-legged fully independent walking machine.

pod [182] (1981) and D. Buckley in Britain with the *Shadow* biped walker based on pneumatic actuators [183].

More recently, walking machines research has spread all over Europe, and almost every country has a research project related to multi-legged or biped walking machines. One of the most relevant work done recently in Europe comes from the Delft University, first under M. Wisse's, who no longer is involved in the field of bipedal walking. Delft Biorobotics Lab (DBL) has developed a series of Limit Cycle Walking robots, of which the most relevant are: Denise (2004) [184], Meta (2005) [159], Flame (2007) [109], Leo (2009) [185], Tulip (2011) [109] and lately Phides (2012) [186].

Several other research institutions and commercial ventures have also developed working biped platforms in Europe: JOHNNIE from Technische Universität München (TUM) [187], DLR-Biped in DLR (Deutsches Zentrum für Luft- und Raumfahrt) [188], Lucy from Vrije Universiteit Brussel (VUB) [69, 111], NAO a commercial platform from Aldebaran Robotics [189], iCub from RobotCub Consortium [190] and COMAN from the Italian Institute of Technology (IIT) [191].

2.1.4 Legged Locomotion Research in In Finland (Aalto)

The history of walking machines in Aalto University started back in 1988 (by then the former Helsinki University of Technology-TKK; the first M.Sc. in 1988 [192] and the first PhD in 1994 [193]) with a machine called *MECANT* (MEChanical ANT), shown in Figure 2.3. It was a fully independent hydraulic six-legged walking machine. The machine weighed about 1100 kg and was driven by a 38 kW 2-cylinder ultra-light airplane engine with air cooling. The leg mechanism was a 2-dimensional pan-

Figure 2.4. Six-legged Walking Harvester of Plustech. Courtesy of Plustech Oy

tograph with vertical rotation axis and its 3 DoFs driven by a hydraulic system. The operator controlled the vehicle remotely by joysticks via a radio link. The control system consisted of a computer network connecting seven on-board computers running under a commercial real-time operating system (QNX), sensors for the vehicle body and legs and a portable operator interface with the radio control and communication facilities. For further details and complete list of publications in this project, the reader can refer to [194]. Partly based on the cooperation with the MECANT group, a Finnish company called Plustech implemented a fully operational commercially available six-legged harvester Figure 2.4. Plustech was later acquired by Timberjack, which in turn was bought by John Deere.

MECANT's successor is *Workpartner*, which is a light-weight service robot. WorkPartner is able to move in awalking, hybrid or wheel mode, depending on surface conditions (Figure 2.5). Mobility is based on a hybrid system, which combines benefits of both legs and wheels to provide a good terrain-negotiating capability and a large velocity range on variable ground [195–197]. The *rolking* of WorkPartner was a novel locomotion mode which has been introduced and studied in detail in [198, 199], proving to be one of the most widely terrain-adaptive methods of locomotion [200]. WorkPartner was developed during 1997-2006, and it is still actively used in various types of research, including locomotion, perception, and human-robot interaction studies. A full list of publications of this project and further information can be found in [201].

The next obvious step towards a more integrated service robotic platform was to embark into biped walking related research, and to tackle this

the GIMBiped project was started in 2007-08, within research package 8 (RP8) named Motion Systems, in the CoE GIM. The goal of the GIMBiped project is the research on energy-efficient bipedal robotic walking, based on its novel actuators and mechanical design, and to develop alternatives control approaches to the existing methods. Two M.Sc. theses have been written based on the GIMBiped research: F. P. Kusumah [202] (2011) and T. Haarnoja [158] (2010), and this monograph is the first PhD thesis. A further description of the GIMBiped system is given in Chapter 3.

2.2 Common Terminology, Classification and Performance Indices in Bipedal Walking Research

There are several terms and definitions commonly used within the biped research. The most important of these are related to the manner bipeds are categorized, the walking cycle and the metrics and indices used to evaluate its performance. This section will present a summary of them.

2.2.1 Classification of Biped Robots

Biped robots are classified in numerous ways, one of the most significant being related to the ***degrees of freedom*** (***DoF***) with respect to the envi-

Figure 2.5. WorkPartner, mobile centaur-like service robot

ronment. Bipeds are called ***2D-bipeds*** or ***planar-bipeds*** if their movement is restricted to the sagittal plane and ***3D-bipeds*** if they are completely free to move around all the planes in the environment. In this research, mostly the motion in the sagittal plane and planar bipeds will be discussed, since the biped model in the simulator, and the experimental hardware are restricted to 2D motion.

Bipeds can also be categorized according to their ***stability criterion*** used in their control. The common terminology is ***static-walker*** for robots using the ground projection of the CoM; ***ZMP-based walkers***, for bipeds using the ZMP as a stability measure; and ***cyclic-walkers*** for bipeds using the concept for cyclic stability. Within the cyclic-walker, the most recurrent allusions are to, ***passive-walkers***, which do not rely on actuation or active control, and the ***Limit Cycle-walker***, which tries to seize the natural ***Limit Cycle*** (LC) in its controlled gait. The previous three stability criterion will be explained in detail in the next Section 2.3.

Finally bipeds can be classified according to their ***actuation*** and ***controllable*** DoF. ***Fully-actuated*** bipeds are those which can actively control all their DoF, including the DoF related to the biped's contact with the supporting surface (typically ankle joint). ***Under-actuated*** bipeds are those which do not comply with the previous statement. Another possible denomination within the actuation category refers to ***passive-walkers***, which describes bipeds that do not have any actuators and usually rely on cyclic stability to walk, and ***active-walkers***, for bipeds which possess some kind of actuation.

2.2.2 The Walking Cycle

Another important terminology in the bipedal walking research is related to the gait description. In this thesis, only human-like bipedal walking gaits, which follow the cycle described in Figure 2.6, will be studied. In Figure 2.7, the main phases of human walking, which are shortly described below, are presented.

Step Cycle: A cycle consisting of the execution of one full phases of single and double support, either with the left leg as the supporting leg and right leg as the swing leg, or vice-versa.

Walking Cycle: Periodic progression of step cycles under the condition that the horizontal displacement of the *Center of Mass* (CoM) of the biped is strictly monotonic.

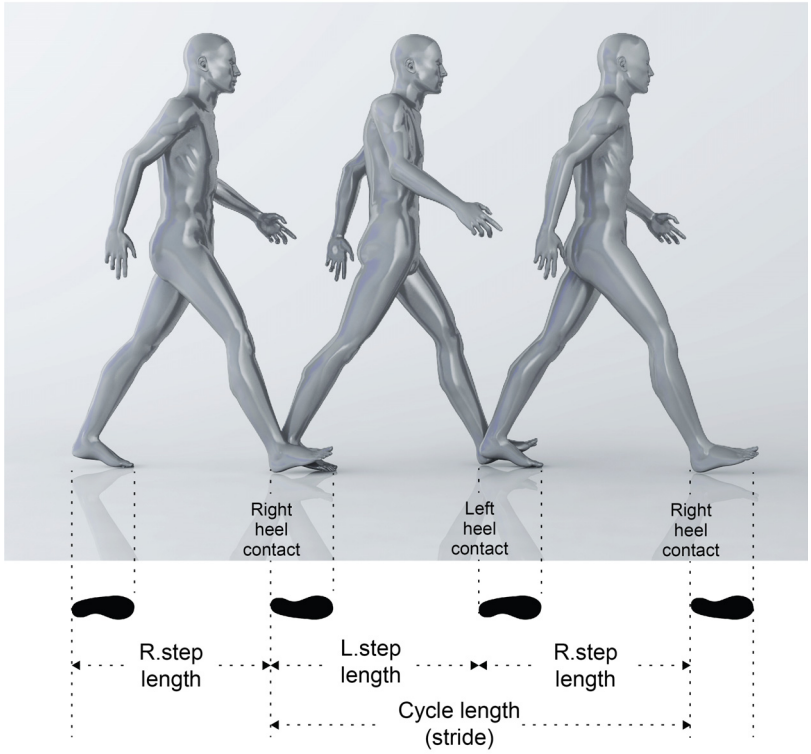

Figure 2.6. The walking cycle (reproduced from [203])

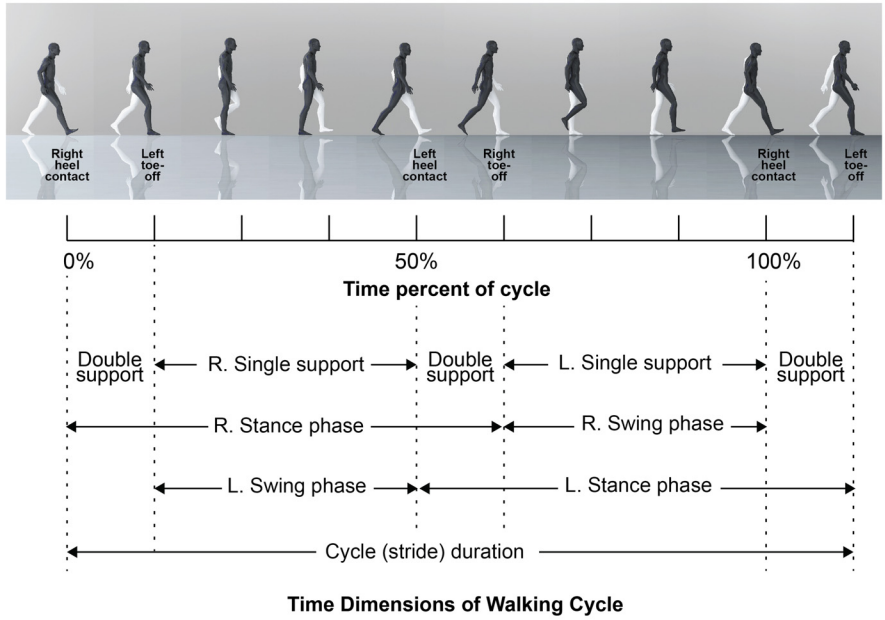

Figure 2.7. The main phases of human walking (reproduced from [203])

Stance Leg (StL): The leg that remains in contact with the ground during the period of a step cycle. In another denomination, this leg is said to be in a Stance Phase (StP).

Swing Leg (SwL): The leg that is not in contact with the ground during the step period and is performing the movement in the air. In another denomination, this leg is said to be in a Swing Phase (SwP).

Toe-off: An event in which the swing leg leaves the contact with the ground and starts the movement in the air.

Knee Lock (KL): An event in which the knee of the swing leg *locks*, maintaining thereafter the thigh and shank of this leg with the same angle and behaving as a single rigid body.

Heel Strike (HS): An event in which the swing leg's foot touches the ground (ideally with the heel) after having been in the air. This event is also generically referred to as ***Foot Strike*** (FS), and in this thesis the terms will be used indistinctively since the model uses point-feet.

Single Support (SS): The phase of the walking in which only one foot is in contact with the ground. This phase starts from the toe-off event of a given swing leg and ends in the event of the heel strike of the same swing leg.

Double Support (DS): The phase of the walking cycle where both feet are in contact with the ground. This phase starts from the heel strike event of a given swing leg and ends on the toe-off from what was before the stance leg.

Support polygon: A polygon formed by the contact between the biped's feet and the surface. In the case of DS, the support polygon is the convex hull between the two feet and, in the case of SS, the support polygon is defined by the area of the stance foot.

2.2.3 Metrics and Performance Indices in Legged Robotics

To be able to compare the performance of walking robots with different sizes, masses and number of legs, a common framework and dimensionless indices have been proposed by researches in the area [1]. Although these indices were devised to evaluate the performance of generic legged

machines, in this thesis they will be used solely in the context of bipedal walking.

Duty Factor

One of the useful indices to evaluate biped robots is the duty factor, normally symbolized by β and defined as

$$\beta = \frac{\text{support period}}{\text{cycle time}} \tag{2.1}$$

Duty factor is used to differentiate between *walking modes*, and mainly to distinguish between *walking* and *running*. Normally $\beta >= 0.5$ represents walking and $\beta <= 0.5$ running [204] in legged machines. However, the formal definition for running for bipedal robots is the existence of some instant of *fight phase*, where both legs of the biped are not in contact with the support surface. In this thesis, in addition to the normal duty factor β, the author proposes the use of the duty factor β_{w} defined as:

$$\beta_{\text{w}} = \frac{\text{time robot is walking}}{\text{total operation time}} \tag{2.2}$$

The previous index has a natural complement given by β_{s} where

$$\beta_{\text{s}} = \frac{\text{time robot is standing}}{\text{total operation time}}, \tag{2.3}$$

and normally $\beta_{\text{w}} + \beta_{\text{s}} = 1$.

The previous indices are proposed to clarify and validate the performance values presented by some sources. One example of this is the energy information on ASIMO [86, 87, 89–95], where it is not clear whether this value is taken on continuous walking or with some $\beta_{\text{w}} < 1$. The knowledge of this factor is very important to define the correct efficiency of the biped.

Froude Number

An important variable used to evaluate the biped's performance is the *velocity* of the robot. This value is normally calculated by the ratio between the horizontal displacement of the biped's CoM and the elapsed time. Nonetheless, this index is greatly dependent on the size of the robot and, more precisely, on the size of the robot's legs. Therefore, researchers in legged robotics have adopted the use of the *Froude number* (Fr). It is an index originally devised in fluid mechanics [205] and was first used in legged locomotion by Alexander, who employed it to describe animal locomotion [204, 206]. F_r is calculated here as:

$$F_r = \frac{v}{\sqrt{\text{g}L}}, \tag{2.4}$$

where v is the velocity of the robot, L is the length of the legs of the robot and g is the gravity acceleration. Fr renders a dimensionless index, which is the most commonly used index to present the speed values of legged robots.

Specific Cost of Transport

Another important variable to evaluate performance is the *energy consumption* of the robot. In this thesis in particular, *energy efficiency* is one of the main goals of the research, and therefore correct interpretation of this variable is vital. This is because to enable long-term autonomy for biped service robots, it is crucial to reduce their energy expenditure. Nonetheless, as seen before with the velocity variable, energy consumption varies significantly between robots with different masses, sizes and velocities. Consequently, another dimensionless number, *specific cost of transport* (c_{t}), has been adopted to evaluate energy efficiency of mobile robots. The specific cost of transport is defined as:

$$c_{\mathrm{t}} = \frac{E}{M \cdot g \cdot d}, \tag{2.5}$$

where E is the energy used for a traveled distance d, M is the overall mass of the robot and g is the gravity acceleration.

Specific cost of transport c_{t} was first proposed by Gabrielli and von Karman in [207] to evaluate the performance of various vehicles using the power consumption per unit of distance. They referred to this index as the specific resistance since it is analogous to the friction coefficient μ. This can be seen when evaluating the behavior of an object with mass M pushed a distance d on a floor with friction coefficient μ. During this process, the energy equivalent to $Mg\mu d$ will be consumed, and therefore $\mu = c_{\mathrm{t}}$. Consequently, this index indicates how "smooth" the motion is.

Researchers have applied this metric in several different ways to evaluate the performance of biped robots. One of the most common ways to apply it is the use of the so-called *specific mechanical cost of transport*, symbolized as c_{mt}, which just considers the mechanical energy used for the locomotion. The c_{mt} does not take into account the energy lost in the conversion from the primary energy source (*e.g.* electricity, combustion, compressed air), to mechanical energy, nor the use of energy in other activities like communication, processing or any other modules in the robotic platform. In contrast, the index c_{et} represents the overall energy consumption.

Nonetheless, there is still a need to consider how the negative work is

reflected on the calculation of c_{et} and c_{mt}, and the possibility of energy regeneration due to negative work. In this thesis, the calculation of c_{et} and c_{mt} will be extended to better evaluate the possible impact of negative work in the system. For instance, c_{mt} is is usually calculated as:

$$c_{\mathrm{mt}} = \frac{\int_0^{T_I} \sum_{i=1}^{N_q} E_{i_{Mech.}}(t)\, dt}{Mgd}, \tag{2.6}$$

where T_I is the time interval, N_q is the total number of active joints and, $E_{i_{Mech.}}(t)$ is the mechanical energy of each actuated joint. $E_{i_{Mech.}}(t)$ is calculated differently to include the effects of the actuators' efficiency towards possible regeneration of energy when negative work is performed. Some papers which include c_{mt} in their result, compute the total energy with no regeneration and assume that the negative work has been inputted by the system [208]. Some other studies [52, 209, 210] use a model where there is no regeneration but the friction (and other dynamic phenomena) is in charge of performing the negative work, and therefore no energy needs to be spent by the system to perform the negative work. The latter case is represented by:

$$E_{i_{Mech.}}(t) = \begin{cases} u_i(t)\dot{q}(t) & \text{if } u_i(t)\dot{q}(t) > 0 \\ 0 & \text{if } u_i(t)\dot{q}(t) \leq 0, \end{cases} \tag{2.7}$$

where $u_i(t)$ is the torque or force and $\dot{q}(t)$ is the angular or linear velocity. Equation 2.7 assumes that all the negative work is lost in the system, mainly dissipated by friction into heat, and therefore regeneration of negative work back into the system is not effectively possible.

However, to complement the information presented by the previous value, the author proposes the use of the following equation for a generalized case of calculating the energy in c_{mt}.

$$E_{i_{Mech.}}(t) = \begin{cases} u_i(t)\dot{q}(t) & \text{if } u_i(t)\dot{q}(t) > 0 \\ u_i(t)\dot{q}(t)K_{reg} & \text{if } u_i(t)\dot{q}(t) \leq 0, \end{cases} \tag{2.8}$$

where the value K_{reg}, named the regeneration index, can vary from -1 to 1. For the case in which $K_{reg} = -1$, total regeneration is achieved and all the negative work is restored into the system for later use. For $K_{reg} = 0$, total dissipation is assumed and none of the negative work is regenerated (the case presented by Equation 2.7). Finally, for $K_{reg} = 1$ the system needs to spend energy to break the motion and perform all the negative work.

The same principle can be applied for calculating c_{et}, which in this thesis will be computed while considering the main energy source coming from a

battery pack (electrical). The previous indices will be used to analyze the results of the simulation in Chapter 4 and experimental work in Chapter 6.

The proposition of using such methodology to calculate extreme and opposite cases of regeneration in the system does not constitute an assumption that either case would represent the real behavior of the GIMBiped testbed. These proposed indices are just a tool to evaluate the range of the possible cost of transport values (CoT) of the platform or model in the study. The real value of K_{reg} will depend on several parameters in the systems, like the efficiency of the actuators to regenerate energy back into the primary source, the capability of the system to store mechanical energy, the efficiency of the actuator and the velocity of the joints. The K_{reg} value itself will most probably not be constant in time. A further detail of its implementation will be presented in Chapter 4 and experimental work in Chapter 6.

The plot of the result values of c_{mt} vs Fr is known as the *Gabrielle-von Karman* diagram, and will be used in this thesis as a tool for comparing the performance of different control algorithms in the GIMBiped, as well as to compare the GIMBiped results with the result from other researchers. Gabrielli and von Karman first used this diagram in [207]. It was later used to compare various types of locomotion in [211], for hopping robots in [212] and for biped robots in [1, 52, 209, 210].

Stability Margin Criterion (SM)

Stability margin is defined as the boundary in which the system is known to remain stable or can be controlled to maintain its stability. The definition itself requires the existence of a *stability index*, which could be computed based on the states, variables and parameters of the system, throughout the evolution of the system in time. In the case of Static-walking, SM relies on the GCoM index, and, in the case of ZMP-based walking, the relation of SM is with the ZMP. The stability margin was first proposed by McGhee and Frank [127] for a degree of stability of the Static-walking multi-legged robots. The concept was later extended to include more dynamic types of locomotion, including cyclic bipedal walking. SM will be explained in detail for the different concepts and indices of stability in Section 2.3.1 next.

2.3 Stability and Control in Bipedal Robotic Walking

In robotics locomotion, the main concern for the control of the electro-mechanical platforms (robots) is to conserve stability. For bipedal walking robots particularly, the problem of stability is quite complex, since the platform to be controlled has a phase in which it can be represented by a close kinematic chain (double support SD) and another in which it can be represented by an open kinematic chain (single support SS). Apart from the previous issue, in the SS phase the robot is restricted to support itself in a small polygon area corresponding to the stance foot surface, in which only compressive forces can be applied (not able to apply pulling forces). Therefore, in its beginning in the late 1960's [183], stability and control of biped robot was addressed in a crude static fashion, following the principles of control for robotic manipulator, and considering the limitations in the computational power and motor drives.

Recently, great progress has been seen in the area of bipedal robotic walking, thanks to the advances in computational power, and electrical drives. However, not all the success achieved can be attributed solely to the previous advances. In fact, another very important contribution lays in the now more dynamic interpretation for the stability representation of the system. The model-based research in bipedal walking and the considerations of the dynamics of walking, both for its stability and control, have greatly pushed forward the development of agile human-like walking machines.

However, model-based investigation of the dynamics of walking in biped systems is not just constrained to robotics and has drawn interest from many other fields, such as biomechanics [213], physiology [214], biomedicine [39], orthopedics [215], neurosciences [216], sports-sciences [217], computer graphics (gaming industry) [218] and applied mathematics [219, 220]. Some of these research fields have as end-goal the construction of working mechanical prototypes. In robotics, one of the goals is the development of humanoid service robots for future work-sites, while biomedicine and orthopedics have concentrated on developing foot and leg prosthetics for human limb replacement or restoration. However, in some other fields of research, the interest may not be the development of a physical prototype. In biomechanics and sport science for instance, one goal is to study the dynamics of bipedal locomotion to generate a model for muscle behavior during different type of gaits to optimize the performance of athletes.

Nonetheless, all these research fields share the same initial core interest, the study of the dynamics of bipedal walking (human in particular) to develop mathematical models which could support their investigation. This layer of intersection between so many fields has generated much collaboration and exchange of information in what is now an active multidisciplinary research area called Dynamic Walking (DW) [151].

2.3.1 Stability in Bipeds

There are three commonly used criteria for stability during walking: the first two are ***local stability criteria*** based on the *Ground projection of the Centre of Mass* (GCoM) and the *Zero-Moment Point* (ZMP); and the last is ***cyclic stability***.

Robots that utilize the GCoM as their stability criteria are called Static-walkers, and this approach has been left aside due to its restrictions in operation velocity and poor performance in energy usage. Static-walking has been replaced with an approach in which the center of gravity can be outside of the support area, but the Zero-Momentum Point (ZMP), which is the point where the total angular momentum is zero, cannot. Today, this notion (also known as ZMP-based walking) is a well-known concept and it is used in the gait control of most of the advanced bipedal robots, like Honda ASIMO [84] and HRP [68].

Nevertheless, robots based on the ZMP principle still require plenty of energy to walk, and a better result in terms of energy efficiency can be achieved by imitating human gait as in Limit Cycle Walking (LCW) [109, 159]. Limit cycle walkers are cyclically stable, whereas both the ZMP and the GCoM criteria deal with local stability. A locally stable system will converge back to a stable state after injection of a small disturbance. Cyclic stability does not require local stability. Instead, in a cyclically stable system, the state orbits (the trajectory of the state vector in the state space) will eventually converge into a nominally stable orbit (gait). LCW is a more accurate and generic denomination, first introduced in [106], of a concept previously known as passive dynamic walking (PDW) [105], which was essentially just an un-actuated LCW where the energy was provided by gravity when the biped walked down a shallow slope.

Local Stability Criterion: Static-walking and ZMP-based walking
As stated before, locally stable systems will converge back to a stable state after injection of small disturbances. The controller using this principle

relies either on GCoM or ZMP as the stability index for defining a SM.

Once the stability index has been defined (GCoM or ZMP), there are several ways to effectively calculate the stability margin, ranging from purely geometrical limits within the support polygon to expressions dependent on the dynamics of the system [173, 221]. The most commonly used stability margin in biped control is the geometrical boundaries within the support polygon [127, 132, 222].

Stability Margin for Static-walking: GCoM stability index

Static walking assumes that the robot is statically stable: that is, during the whole walking process, if the action is stopped the robot will remain indefinitely in a stable position. For this to happen, it is necessary to restrict the GCoM within a stability margin defined inside the supporting polygon. Also, walking speed and acceleration must be kept within lower bounds so that the inertial forces are negligible. The proof of stability in this case is quite obvious, since if the GCoM falls within the support polygon and dynamic forces are neglected, there are no external torques generated, either by gravity or externally, that will cause the robot to tip over.

As the calculation of the GCoM is quite simple, the main task will be the definition of the SM. For Static-walking bipeds, the SM is defined as the minimum distance of the GCoM to the boundaries of the support polygon along the line parallel to the body motion.

The control of these types of walkers is based on precise trajectory planning and position control, requiring the detailed knowledge and calculation of ***Forward Kinematics*** (FK) and ***Inverse Kinematics*** (IK). This will be briefly addressed in Section 2.4. The problems with this type of walking are that large feet and strong ankle actuators are needed and only slow walking velocities can be attained, as quite a lot of energy is used in this process. Therefore, this method has been left aside and replaced by the dynamic walking alternative. Dynamic walking allows more realistic and agile movements and will be explained next. Some further references to static walking can be found in [127, 132, 222].

Stability Margin for Dynamic-walking: ZMP stability index

In robotic bipedal dynamic walking, the projection of GCoM can be seen outside the support polygon during the walking process but usually for brief instants. In dynamic walking, the velocities and acceleration are

not restricted and the control does not rely on neglecting the dynamics of the system. Indeed, there is no absolute criterion which would establish whether dynamic walking is stable or not, and the biped robot could be devised to recover from several types of instabilities. Nonetheless, if the robot is fully actuated and always maintains at least one foot flat on the surface, then the ZMP can be used as a stability criterion. In the previous case, an SM for dynamic walking robots can be defined within the boundaries of the support polygon, making the ZMP a natural extension of the GCoM.

ZMP Definition

The ZMP criterion was first introduced by Vukobratović and Stepanenko in 1972 [173] and defined as:

> *In Figure 2.8 an example of force distribution across the foot is given. As the load has the same sign all over the surface, it can be reduced to the resultant force R, the point of attack of which will be in the boundaries of the foot. Let the point on the surface of the foot, where the resultant R passed, be denoted as the zero-moment point, or ZMP in short.*

As seen from the previous definition, ZMP is the point where the robot's total moment at the surface of contact is zero. As long as the ZMP is inside the support polygon, the walking is considered dynamically stable, since in this state the ankle joint can effectively actuate the foot to control the robot's posture. Therefore, if the biped does not continuously maintain at least one foot flat on the ground or does not have active ankle joints, the

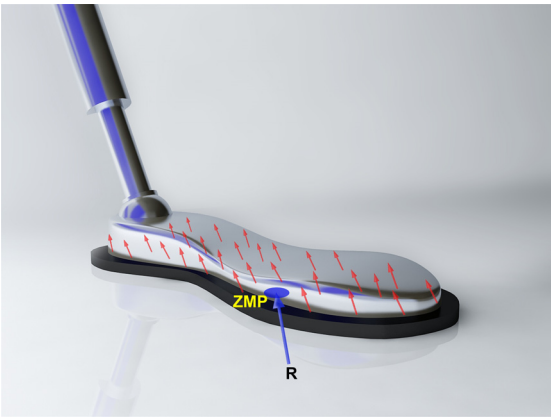

Figure 2.8. Foot reaction forces and the definition of ZMP reproduced from ([173])

ZMP criterion cannot be used to effectively control the robot's stability. As an analogy to Static-walking: if the movement is halted during the walking process, the robot will then rotate around the ZMP.

ZMP Calculation

There are different ways to calculate or identify the ZMP. The formal analytical approach was shown by Vukobratović itself in [173]. However, there are other approximations and physical interpretations of the ZMP that can lead to obtaining the location of this point by alternative approaches. The most familiar approach arises from the observation that, when at least one foot is flat on the surface of contact, the ZMP coincides with the Center of Pressure (CoP) of the surface reaction forces. Under that premise, the use of pressure sensor on the feet's sole can lead to the practical calculation of ZMP [202]. This is the approach used by many researches to calculate the ZMP in real time and to control their robots. Other comprehensive alternatives use 6 DoF force/torque sensors in the ankle joints of the biped robots to calculate more precisely the location and evolution of the ZMP.

Apart from the practical approach for obtaining the ZMP mentioned above, several analytical approximations have been proposed to the formal formula presented in [173]. These approximations simplify the dynamic model of the biped, and the most common is the use of the 2D or 3D inverted pendulum model of the biped. The use of the inverted pendulum (2D or 3D) approximates the robot dynamics to a single point mass, concentrating the total mass at the robot's CoM. This simplified model can be used to calculate the reaction force and ZMP with less effort than the formal approach in [173] requires.

Other simplified forms to compute the ZMP for 2D and 3D models can be found in [223–225].

Stability Margin in ZMP-walking

Once the ZMP is computed, the SM has to be defined to be able to effectively control the biped robot. As pointed before, since the ZMP is the natural extension of the GCoM, a similar extension can be applied to the setting of the SM, defining therefore the stability margin for dynamic walking as the minimum distance of the ZMP to the boundaries of the support polygon. This was proposed in the original work on the ZMP [173], and used implicitly by many researchers [223–225]. Other explicit

definitions of the ZMP SM can be found in [221].

Thus, ZMP walking can be attained by making sure the robot is always rotating around a point within the support polygon, or equivalently, making sure the ZMP is within the support polygon. If the biped rotates around a point outside the support polygon, the feet (or foot) will not remain flat on the surface; instead it will tip over the edges, leading to instability. In this case, the ZMP will be located on the edge of the support polygon, since by definition it cannot exist outside it [83].

The goal with the ZMP-walking technique should be total control of the robot's dynamics by planning the correct placing of the ZMP. However, most of the robots, instead, use predefined patterns for moving each joint, which results in a dynamic walk and later control the resulting ZMP to the restricted area of stability, with adjustment done basically on the hip trajectory and by actuating the ankle [48, 226–228]. Details on different ZMP control techniques will be presented in the next Section 2.4.

Cyclic Stability: Limit Cycle Walking and more

Although ZMP has been greatly helpful in the advance of bipedal robotic walking, it is still a very restrictive paradigm in terms of control and energy usage. The requirements of maintaining the ZMP inside the support polygon and ensuring that at least one foot always remain flat on the surface, result in a type of gait that is very odd-looking and unnatural for humans. Noticing such tight restriction in the definition of stability and the performance of walking, several researchers studied alternatives on how to model and define stability for controlling biped robots. In the early 1970's, Nichols and Witt were the first to identify the existence of natural stable cycles in walking, when devising their un-powered walking aid mechanism [104]. This observation was later formalized by Hurmuzlu and Moskowitz in 1986 [229]. They developed the first mathematical model based on a simple inverted double-pendulum locomotion system, and analyzed the stability of the resulting nonlinear model. The previous model was then put into practice by McGeer [230], with his celebrated compass gait [105] and kneed biped passive walkers [231], which were un-actuated biped platforms performing natural-looking gaits on a shallow slope.

The successful experimental implementation of McGeer's passive walkers boosted the research on cyclic stable robots with emphasis on underactuation and energy efficiency, which was known as the passive dynamic

walking approach. Clearly, the practical applications of PDW were very limited. However, the consideration of the essence of the mechanism and insight of the nonlinear dynamic behavior of the systems helped researchers transfer the concept of cyclic stability and energy efficiency of these passive walkers towards powered cyclic walkers. This new successor theory, based on the knowledge acquired from PDW, is now known as Limit Cycle Walking (LCW) [106]. LCW is a better-fitting and broader term, first proposed by D. Hobbelen and M. Wisse in [106], to classify cyclic stability and cyclic walking that originates from a natural dynamic behavior of the nonlinear representation of the system. In this sense, LCW can be either passive or actuated, but the core of the theory follows the principles of nonlinear dynamics for modeling the bipedal system and identifying their natural stable orbits (LC).

Parallel to the above line of research, cyclic walkers have also been studied by Raibert and his group in the LegLab at MIT since the early 1980's. Nevertheless, Raibert's group tackled cyclic stability on a more crude fashion, without too much concern foe the detailed modeling of the dynamics of the system. Their approach was instead to simplify the system by splitting it into different separated components, each with individual controls during the cycle. The resulting control algorithms are quite simple and allow real-time execution. Many impressive cyclic locomotion systems and active balance robots were implemented based on this theory [232], and this line of research seems to have been followed in the subsequent work of Raibert in Boston Dynamics [85, 140]. However, no new publications have been produced in the subject for a long time; therefore, for further details the reader is advised to refer to [232].

The work in this thesis is closely related to LCW and the use of nonlinear dynamic theory for analyzing the stability and performance of biped walking based on an approximated non-linear dynamic model of the system. Therefore, in the following sections, the results on stability proof and stability margin will be centered in the previously-mentioned LCW and non-linear dynamic theory.

Stability in Cyclic Walking

As in Static and ZMP-walkers, Cyclic-walkers need the existence of a criterion that will identify whether the behavior of the system is ***stable*** in some sense. The use of such a criterion will then enable the formulation of a proper control to perform active walking if needed. In cyclic walkers,

the stability is not evaluated in the configuration or state space, but instead in the ***phase plane*** using the concept of ***orbital stability***. Orbital stability has been qualitatively defined in [233] as:

> *A system is orbitally stable if starting from a steady closed phase trajectory any finite disturbance leads to another nearby trajectory of similar shape.*

The above definition will be mathematically formalized in Section 5.5, where nonlinear dynamic systems will be studied in more depth.

Although the concept of orbital stability can be formally defined, as in Section 5.5, for cyclic walkers, the challenge remains to demonstrate, analytically, the existence of LC in a general non-linear system. In addition, the process to find these LCs (if they exist) and their region of local stability also remains an unsolved problem. Researchers have therefore resorted to the use of numerical computational methods to determine the stability of LC once these orbits have been located. The location of the LC itself has been obtained by several different ad-hoc iterative (and sometimes manual) methods based on Genetic Algorithms (GA), Neural Networks (NN) and non-linear optimization, to mention a few.

The most recurrent method used for stability analysis in biped robotic walking research is the numerical computation of the Poincaré return map [233]. In the Poincaré map, the LC trajectories are reduced to fixed points, and the procedure to evaluate its stability relies on the introduction of small perturbations to the system's states around the LC and calculating the eigenvalues of the so-called *Mondromy Matrix*. This procedure is based on the *Floquet Theory* of non-linear dynamics. The Floquet Theory affirms that, for an LC to be stable, the eigenvalues should lie within the unit circle, meaning that their module should be strictly less than one. This concept will be seen in more detail in Section 5.5 and a demonstration of such requirement for general non-linear systems can be found in [234].

Other methods applied to prove stability and analysis of the existence and behavior of LCs use explicit and iterative integration of the system's dynamic equations, modifying the system's initial conditions (ICs) and parameters. Such methods are computationally quite demanding and not suitable for detailed studies of biped walking models.

Another approach, as taken by McGeer in [105], is to linearize the (non-linear) dynamic equation around an equilibrium point, enabling explicit

integration of the resulting expression. Then, the impact equations are concatenated and solved to find the conditions for the existence of periodic solution of this coupled system. In order to assess the stability of this cyclic solution, a second linearization around the periodic solution is needed. Nonetheless, the obtained linear solution is valid just on a small region around the point of linearization, which is usually the upright standing position, and any realistic gait will significantly deviate from this point. Based on the previous, in [233], this method has been proven unsuitable in predicting the long-term behavior of the system.

In Chapter 5, a continuation method is proposed for the stability and performance analysis of a nonlinear dynamic model representing the biped walking system. Chapter 5 will then present further details and a discussion on the stability proof and implementation of the previous methods.

Stability Margin in Cyclic Walking

The term ***stability margin*** presented in Section 2.3.1 can also be extended to the case of Cyclic-walkers. J. E. Pratt and R. Tedrake propose in [235] the use of the so-called *basin of fall* term, built upon several internal states and variables of the system. Raibert also proposes some set of rules to define a margin for stability in cyclic walking [232]. In this thesis, however, the classical nonlinear dynamic view is presented, making use of the concept of ***basin of attraction*** to define SM in cyclic walkers.

Basin of attraction is a concept derived from the non-linear dynamics, and used in the assessment of the stability for these systems. It represents the set (or region) of ICs leading to a long-time behavior that approaches the stable LC under scrutiny (walking gait). Consequently, the robustness of the resulting gait (gait is represented by the LC found in the system) can be evaluated by measuring the size of the basin of attraction.

The process of actually calculating the basin of attraction is quite challenging. Some researchers have taken the rough approach of a simple and direct iterative integration of the equations of motion, inferring then, based on the numerical results, some global properties of the system. Others, as in the stability analysis, have used iterative numerical computation methods based on the Poincaré map and analysis of the Monodromy Matrix. In [236], A. L. Schwab and M. Wisse use a cell mapping method [237] to iteratively compute the basin of attraction. However, this method is very time consuming, especially for large-dimensional state space. An extension to it, named Poincaré-like-alter-cell-to-cell mapping method,

was proposed by L. Liu et. al. [238]. It should be mentioned that the size of the basin of attraction for the simple models of passive biped walkers has been reported to be very narrow [233, 236, 238]. This implies that the resulting gait is not very robust. Therefore, active control is needed for a better performance under natural environment conditions.

Taking into consideration the lack of robustness of the passive walking platforms, this thesis studies and proposes different types of controllers to increase the robustness in these biped systems. This research, however, does not tackle the actual computation of the basin of attraction of the proposed models and experimental platform and therefore leaves it as a future work from the GIMBiped project. On the other hand, this study proposes a framework to represent the stability margin on the simulation work presented in Section 4.4, based on the tolerance to external disturbances.

2.4 Control in Biped Robots

In robotics research, the control approaches towards bipedal locomotion are closely linked with the inherent problem of stability during walking. The criterion of stability used in the control policy is thus of central importance. Several different control approaches have been proposed these are built upon the stability criteria introduced in the previous section and make use of the classical *"building block"* in robotics control. These basic foundations for developing different control algorithms will be introduced in this section. The overview will be quite brief since these are concepts widely known in robotics. The main attention and details will focus on tools used later in this thesis in the simulation and hardware experiments.

2.4.1 Kinematic Modeling and Configuration Space

In bipedal research, the biped system is typically modeled as a 3D or 2D chain of articulated rigid links. The generalized coordinates (q) used to build the configuration space are usually the joint angle, and they can be set as controllable if they are actuated or passive otherwise.

Most of the models consider the contacts between the feet and the surfaces as slip-less, and therefore a classical manipulator approach can be used on modeling and control. Nonetheless, if the robot is fully actuated,

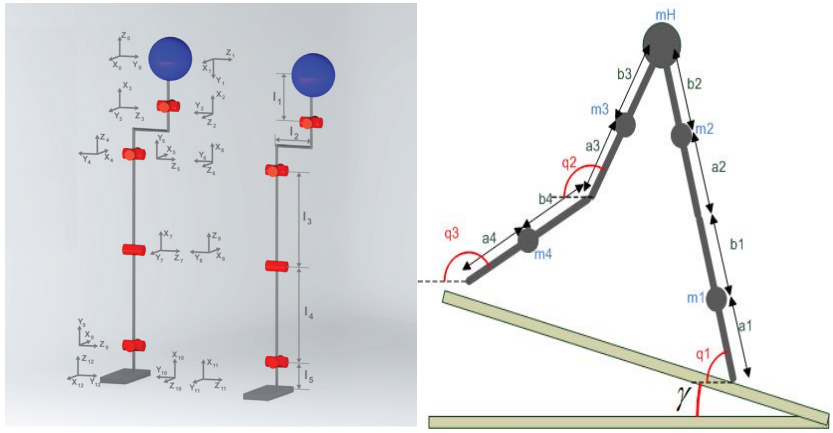

(a) Kinematic representation of the GIMBiped testbed

(b) Simplified 3-link model representation of the GIMBiped testbed

Figure 2.9. Different representations of the GIMBiped testbed

the systems will be over-actuated during the double support (DS) phase, where the robot is represented by a closed kinematic chain. Therefore, proper measures must be taken on the control approach.

On the other hand, the most generic and correct representation of the system will be to allow free motion of the robot in the space, allocating 6 DoF for the body, and assigning finite values to the contact forces and friction. However, this approach hugely increases the complexity of the control algorithm, and therefore researchers have preferred the use of simple models and have treated the effects of slippage and other non-modeled forces as disturbances, which the controller should be able to handle.

Based on the kinematic modeling and configuration space, the parameters and algorithms for the FK and the IK calculation can be obtained.

As an example, Figure 2.9-a shows the kinematic representation of the GIMBiped testbed. Figure 2.9-b shows the simplified 3-link dynamic model representation of the GIMBiped testbed and its generalized coordinates.

2.4.2 Dynamic Modeling

As in the kinematic modeling presented previously, dynamic modeling in biped research can follow several different approaches and levels of complexity. The main common points in all these approaches are the continuous dynamics of the walking motion (also called the stride function), the behavior during impacts and the contact forces.

Continuous Dynamic

Throughout this thesis, the biped will be assumed as a rigid structure, and the continuous dynamics will be expressed following the Lagrangian form as:

$$M(q)\ddot{q} + V(q,\dot{q})\dot{q} + G(q) = \tau \tag{2.9}$$

Where $q = [q_1, q_2, \cdots, q_n] \in \Re^n$ are the generalized coordinates, $M(q)$ is the inertia matrix, $V(q,\dot{q})$ is the Coriolis matrix (which includes centrifugal, gyroscopic and Coriolis effects) and $G(q)$ is the gravity vector. The resulting generalized effort (torque) vector τ includes the joint actuation torques τ_{joint} and the external torques τ_{ext}, such that $\tau = \tau_{joint} + \tau_{ext}$.

In this thesis, however, the vector of external torques τ_{ext} is considered to be zero, since τ_{ext} represent the torques generated by the ground contact forces, and in the model used in this work there is no modeling of the contact force with the surface. Instead, the stance foot of the biped is considered to be attached to the ground during SS with infinite tangential friction, and therefore only rotational movement is allowed.

Although the model used throughout this thesis does not consider the interaction of the contact forces with the surface, other advanced dynamic models of the biped system do implement it. For further details in different contact modeling approaches, the reader can refer to [239, 240].

In Chapter 4, Section 4.2.1 the equations of motion derived from this Lagrangian expression are explained in detail for the model chosen in Section 4.2.

The vector $[q, \dot{q}]$ represents the ***state*** of the robot and is used in the control algorithms.

Impacts Dynamics

The impacts in the models used in bipedal research are usually assumed to be inelastic, non-sliding and instantaneous events. The velocity of the system then jumps instantaneously from $\dot{q}^-$ to $\dot{q}^+$, following the equation:

$$Q^+\dot{q}^+ = Q^-\dot{q}^- \tag{2.10}$$

Here $\dot{q}^-$ are the generalized coordinate velocities before the impact, $\dot{q}^+$ are the same velocities after the impact and, Q^- and Q^+ are matrices obtained by using conservation of momentum before and after the impact. A detailed explanation of Eq. 2.10 and its matrices is given in Section 4.2.1 for the model chosen in Section 4.2.

Trajectory Generation

One of the most frequent approaches for the control of robotic platforms is the use of a pre-designed trajectory for each controllable joint in the machine, followed by the implementation of classical control which should allow the trajectory to be tracked. Further real-time adaptation of the trajectory can be made to overcome obstacles and external or non-modeled disturbances.

In biped research, this approach has been used since its beginnings and is still being used nowadays for the control of most of the ZMP-based bipeds. For biped robots, trajectory generation can come from the motion capture of a real human walking or be completely computer-generated. Several forms of computer generated trajectories have been proposed following coupled oscillators, parameterized splines and many others.

In this thesis, ZMP-based trajectory generation is done by separate computation of parameterized splines for each phase of walking. Therefore, there are different trajectories to follow in the swing phase, stance phase and double support, for a biped moving either in the initial step, normal step or final step. Such method is well known in the study of robotic manipulators, and further details can be found in [227, 228].

Another type of trajectory generation used in this thesis follows the states of the natural LCs of passive walkers. Further details on how the previous trajectories are generated and used in this thesis will be presented in Chapter 6.

Control

Within ***Control Theory*** there have been many different schemes proposed through the years for its use in robotic applications. Several of these different approaches can be regarded as part of same generic type of control, known as the Computed-Toque control (CTC). CTC is the main control approach used throughout this thesis. It is a particular application of the feedback linearization of nonlinear systems. CTC-like approaches can be seen in robust control, optimal control and adaptive control, to name a few.

To understand the operation of CTC, Eq. 2.9 needs to be reviewed, regrouping the terms of the dynamics of the robot as:

$$M(q)\ddot{q} + N(q,\dot{q}) + \tau_d = \tau, \tag{2.11}$$

where yet again $q(t) \in \Re^n$ represents the joint variables, τ is the input control torque, and τ_d relates to the disturbances. If a desired trajectory

$q_d(t)$ needs to be followed, a tracking error should be defined together with its derivatives as:

$$e(t) = q_d(t) - q(t) \tag{2.12}$$

$$\dot{e}(t) = \dot{q}_d(t) - \dot{q}(t) \tag{2.13}$$

$$\ddot{e}(t) = \ddot{q}_d(t) - \ddot{q}(t) \tag{2.14}$$

Solving Eq. 2.11 for $\ddot{e}(t)$ results in:

$$\ddot{e}(t) = \ddot{q}_d(t) + M(q)^{-1}(N(q,\dot{q}) + \tau_d - \tau) \tag{2.15}$$

Defining one part of the previous Eq. 2.15 as the control input function by:

$$u = \ddot{q}_d(t) + M(q)^{-1}(N(q,\dot{q}) - \tau) \tag{2.16}$$

And one part as the disturbance function by:

$$w = M(q)^{-1}\tau_d \tag{2.17}$$

Then the tracking error dynamics can be written in the canonical form as:

$$\frac{d}{dt}\begin{bmatrix} e \\ \dot{e} \end{bmatrix} = \begin{bmatrix} 0 & I \\ 0 & 0 \end{bmatrix}\begin{bmatrix} e \\ \dot{e} \end{bmatrix} + \begin{bmatrix} 0 \\ I \end{bmatrix} u + \begin{bmatrix} 0 \\ I \end{bmatrix} w \tag{2.18}$$

In this scheme, the ***computed-torque control law*** is given by the inversion of the feedback linearization presented in Eq. 2.16, which results in:

$$\tau = M(q)^{-1}(\ddot{q}_d(t) - u) + N(q,\dot{q}) \tag{2.19}$$

From which a control policy u can be defined so as to stabilize Eq. 2.18 by driving $e(t)$ to zero.

It must be noted that the CTC uses the inversion of the robots dynamics, in particular the $M(q)^{-1}$, and, therefore, due to singularities problems can arise during this process. To avoid such problems, efficient Newton-Euler inverse dynamics, instead of simple matrix multiplication, can be used to compute the torque for the cases where the system dynamics are not minimum phase.

The application of this computed-torque-type of controllers in biped walking will be addressed in Chapter 4. Further details in the implementation of certain types of control input functions are presented in Section 4.4 and summarized in Table 4.2

3. The GIMBiped

The GIMBiped is the testbed platform, developed at Aalto's ATL in the RP8 (under the CoE GIM program), for the study of bipedal waking. The development of the testing platform GIMBiped was a multi-disciplinary effort which included the work of several people in different fields.

One of the main distinctions of the GIMBiped is its novel mechanical design, focused on enabling alternative control approaches to the existing control methods. This novel design concept for bipedal walking robots is heavily based on the actuators, which are Linear Motors (LM), and on the prospect that these actuators provide to combine passive dynamic walking with active walking. The specifics of the mechanical design and its philosophy fall outside the scope of this thesis, but can be found in [114–116].

This chapter presents a general overview of the GIMBiped platform, the Aalto's biped prototype developed in the ATL. The chapter's main purpose is to present the basic background of the testbed used to support the research.

First, an overview of the mechanical layout and the main communication, sensor, actuators and processing modules are given. Further detailed descriptions can be found in [41, 56, 114–116].

Later, some of the first simulation experiments on the actuators oriented to support the prototype development are shown.

Finally, some known concepts and new theoretical ideas towards energy-efficient walking approaches that may be applied in the future on the GIMBiped platform are presented. These early results show promise on the use of LMs as actuators for more complex equilibrium control and walking algorithms.

Further analysis is desired, though, for the planning of the mechanical distribution targeting optimal performance. This is addressed by the sub-

sequent chapters. The detailed mechanical analysis and its relation with stability and energy consumption will be studied in depth in Chapter 5, and the result of an attempt to tackle energy efficient biped walking with the GIMBiped using a hybrid control will be presented in Chapter 6.

3.1 Mechanic, Sensor and Communication Systems Overview

The initial design idea of the GIMBiped envisioned a 3D biped fully actuated by LM. The platform was intended to be self-sufficient with all the controllers, computers, sensors, actuators and power source included in the robot. The first version of the GIMBiped drew near to this idea, as can be seen in Figure 3.1. However, this first prototype version did not include the power supply in the platform, and it was powered through a cable.

The biped robot was originally named The Sway. The name was changed later to GIMBiped to better relate its development with the CoE GIM. The preliminary prototype had 5 degrees of freedom per leg and an extra degree of freedom in the center of the hip, which coupled the rotational movement of both legs around the waist. The ankle's lateral DoF was not actuated.

The upper body carried the Power Distribution Box (PDB), the Walking

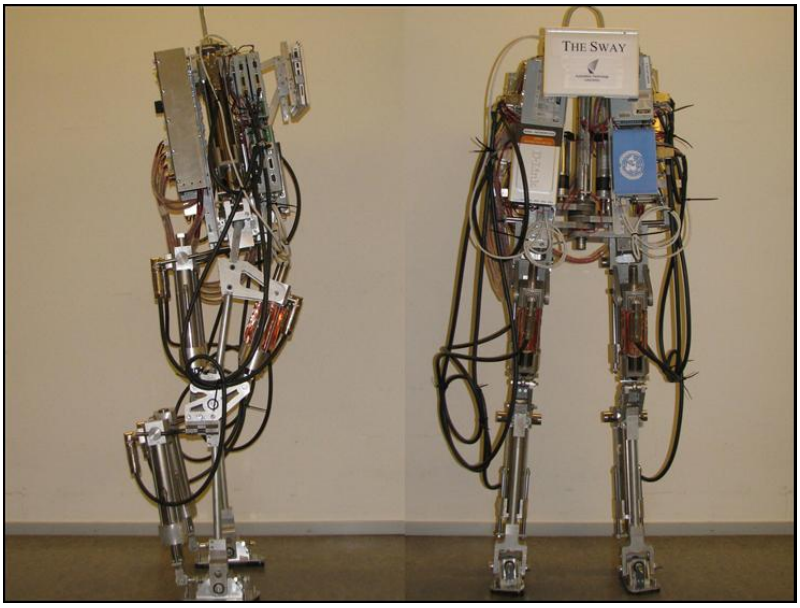

Figure 3.1. First prototype version of the GIMBiped standing by itself.

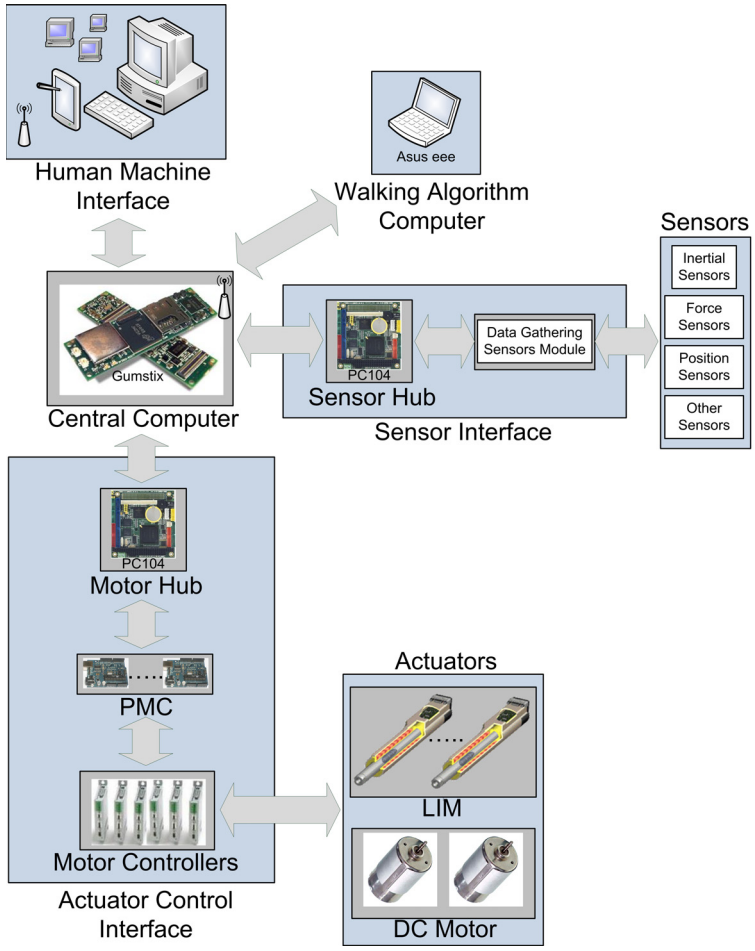

Figure 3.2. Original idea for the Information Distribution Infrastructure

Algorithm Computer (WAC) and the linear Motor Controllers (MC). The LMs in charge of moving the leg sideways in the frontal plane, were also located in the upper body, as were the motors which control the joint in the center of the hip.

As will be seen later in Chapter 6, the platform was changed to simplify the preliminary experiments and to approximate better the configuration of the model tested in the simulator. Further details on the mechanical design can be found in publications [114–116].

Regarding the sensor and communication infrastructure in Figure 3.2 illustrates the original idea. The goal was to develop a completely distributed and modular system, which could be easily upgraded or modified.

In the original infrastructure, the main processing units were two PC104 embedded computers. One, named Motor Hub (MH), was in charge of sending positioning commands to the linear motor's controller using CAN

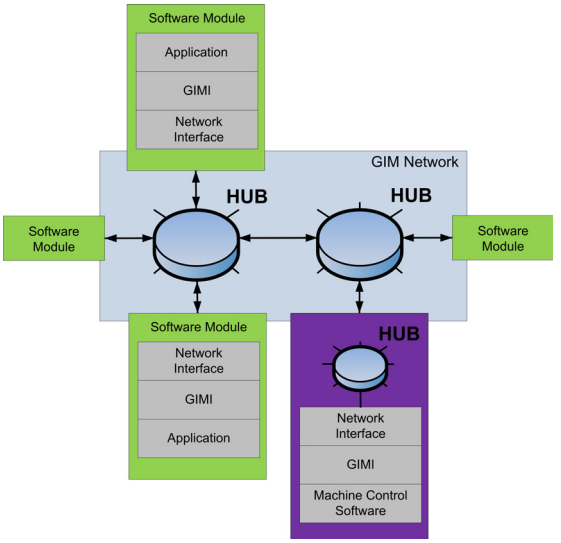

Figure 3.3. The GIMnet communication infrastructure (reproduced from [241])

protocol, and the other PC104, named Sensor Hub (SH), was responsible for collecting all the sensor's data. The CANopen interface runs at 1 $Mbit/s$ and the system uses 2 parallel CAN buses, one for the left side motors (hip, thigh, knee and ankle), and one for the right side. Sample rates are later specified in Chapter 6 according to a specific control approach.

A third computer named walking algorithm computer (WAC) was in charge of generating the walking pattern for the biped, and a fourth computer named Central Computer (CC) was in charge of managing the communication between them.

The LMs, used to drive all the biped's joints, have built-in sensors which are capable of measuring the motor's position, velocity (Hall Sensor), temperature, input voltage and current. The data can be acquired through their CAN interface. The linear motors' controllers have their own PID positioning control. These controllers receive control commands and send motors' variables data through the CAN interface that can be accessed from the Motor Hub.

Using the GIMnet communication infrastructure, all the computers, Sensor Hub, Motor Hub, WAC and CC, were connected into a network for remote access.

The GIMnet is a specially designed network architecture [241,242] (Figure 3.3), which was initially used to control the GIMBiped. GIMnet was built over TCP/IP protocol and is a combination of Client-Server and Peer-to-Peer network. GIMNet allows the robot to be controlled remotely in

"real-time", and the user can communicate through firewalls, since it has built-in VPN capability. The GIMnet is used in all the robotic platforms of the CoE GIM, and initially it was planned to be used in the GIMBiped as well. However, problems with variable and long delays over the network connections limited the "real-time" capabilities, and the communication infrastructure was modified as well, as explained later in Chapter 6.

3.2 The GIMBiped's Actuators: Novel Design Based on Linear Motors

This section presents some simulation studies and the experimental results carried on the electrical actuator of choice, the linear motors. These experiments were performed as a design support prior to the first GIMBiped prototype construction. The actual mechanical design and construction of the prototype is not reviewed in detail in this thesis. The original design and initiative for adopting LM as the GIMBiped actuators are credited to Dr. Peter Jakubik from ATL at Aalto, and more information related to this subject can be found in [113–116].

3.2.1 Actuators' Simulations and Tests

Following the premise stated in Chapter1 (Section 1.4), the hypothesis suggests that a correct choice of actuators and control technique should allow significant reduction in the energy consumption. To achieve such goal, of successfully implementing an efficient dynamic walking biped robot, one of the major tasks is to overcome the current limitations in the actuators, together with the correct application of control strategies for different walking modes during the operation.

In this thesis, Linear Motors (LMs) will be considered as the potential driver (as initial premise) for bringing together both techniques of interest, the LCW and ZMP-based type of walking, and allow them to perform at their optimum when needed.

To perform an efficient LCW, the compliance in the actuator system is essential. Until now, mainly rotational motors have been used to drive the robot's joints; however, their gearbox reduction, needed in this case to reach the desired peak torques, does not allow the natural unconstrained movement of the swinging leg. Because of that, much energy is wasted in the continuous position control of the leg.

In [56], the use of permanently actuated synchronous servo Linear Motors (LM) was proposed to efficiently address LCW. They do not have gear boxes, making them back-drivable, and for that reason nothing breaks the natural swinging movement of the leg. Also, LM can easily enable torque control because of its direct force/current relation, and thus the overuse of position control can be avoided. Furthermore, the whole actuation system can be made actively compliant with the use of a simple PD control with "soft" parameters.

If the categorization presented in paper [243] is used, this type of actuators can be classified as *variable damping actuators*, falling specifically in the category of the *eddy current dampers* (EDC), though this specific LM does not suffer from the low torque downfall mentioned in [243], since it can achieve up to 585 N.

However, LM are subjected to some mechanical friction, permanent magnetic field, back-emf and also large weight and size. This is a drawback since, in addition to the actuator dependency, the LC is highly sensitive to the design parameters of the robot (masses and lengths of the links). To avoid foot scuffing and to obtain ideal initial conditions and slope angle for the LC, the link masses and lengths of the robot have to be chosen carefully. Therefore, is important to have a thorough study on the cost versus benefit of including larger weight and size in the design of the mechanism (see Chapter 5).

Several attempts of developing more energy efficient-bipeds robots have been made [109, 111, 244]. Some of them also rely on linear actuators; however, only pneumatic and hydraulic linear actuators have been used until now. The problem with both pneumatic and hydraulic actuators is that even though the forces and torques obtained are quite large they require the use of compressors or pumps, which, with their bulky size, currently do not allow total autonomy of the biped robot for large torques/forces.

According to [69], pneumatic muscle can store energy, utilizing the compressible properties of the gas and using the actuators as an energy storage element. Also spring-based actuators can, by mechanical construction, temporarily store energy in the system. One of the future objectives of the use of LMs in the GIMBiped is to allow efficient electric regeneration to restore energy back into the system (batteries). Section 3.3.4 will present this theoretical idea, which is based on the (hypothetical) possibility to regenerate negative work.

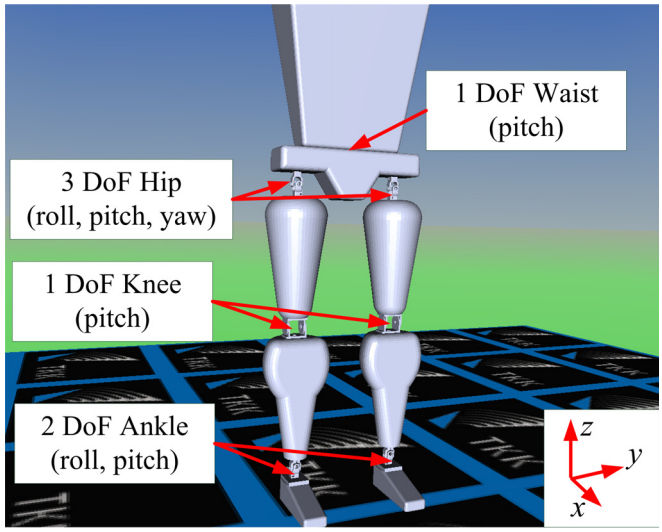

Figure 3.4. Preliminary kinematics and dynamic simulator in MATLAB.

The Linear Motors

The motors used in the GIMBiped are linear direct drives for highly dynamic motions. They are commercially available from the LinMot vendor [245], and fabricated of just two parts, the slider and the stator. These motors are in essence permanently actuated synchronous servo motors, with integrated position measurement (non-contact magnetic field sensors). Permanent magnets in the slider (like a rotor) and windings in the stator are used to generate forces, like in a brushless rotary motor. The slider and the stator are not connected by brushes or cables and, the configuration and different arrangement of the magnets generate the linear motion directly, using electromagnetic force, without the wear associated with mechanical gearboxes, belts, or levers.

The previous design characteristics allow these motors to achieve highly dynamic values, reaching acceleration of well over 200 m/s^2 and travel adjustable speed within a range of 0.001 m/s to over 4 m/s, allowing cyclical motion sequences of several Hertz [245], which are higher than human muscle bandwidth (2.2 Hz) [246]. The motors are freely positionable with no mechanical end, and they can play along the entire stroke. However such liberty in the stroke leads to a non-even force constant, given that different numbers of windings are generating the flow for different strokes (Figure 3.7).

Motor Selection

Initially an approximated dynamic and kinematics model of the biped robot was developed on MATLAB/Simulink with SimMechanics and VirtualReality ToolBoxes [247]. This simulator models the biped with 13 DoF (Figure 3.4). The main purpose of this simulation was to verify the requirements for the motors' torque in each joint. These torques were then compared with the maximum torque/force that could be obtained with the LMs available. This simulation did not include the kinematics and dynamics of the LM, instead it just calculated the torque needed, based on reaction forces in the joints. Different sizes, lengths and weights for the limbs were tested in this simulator under a ZMP-based type trajectory generated for each joint. Finally, a human-size bipedal robot was developed. Based on the previous results, a corresponding torque-force transformation was obtained and considered for the next stage.

The maximum force output allowed was set by a linear (approximated) transformation of the maximum torque obtained in the previous simulator. Two different motor sizes were selected from the LinMot vendor to be used in different parts of the robot. Their maximum force output values were 585 N for Motor 1, and 255 N for Motor 2. Complete parameter list values for Motor 1 and Motor 2 are presented in Table 3.1. LM of the type (model) Motor 1 are used on both sides of the hip, thigh and shank, and

Table 3.1. Motor's parameters

Parameters	Units	Motor 1	Motor 2
Maximum Stroke	mm	180	120
Stroke SS[a]	mm	30	40
Peak Force	N	585	255
Force Constant	N/A	39.0	17
Maximum Current [b]	A	15	15
Maximum Velocity [b]	m/s	1.7	3.9
Phase Resistance [c]	Ω	3.1/3.7	2.35/3.2
Phase Inductance	mH	3.1	1.6
Thermal Resistance	$^{\circ}K/W$	1.1	3.2
Slider Mass	g	1460	510
Thermal Time Const.	s	3000	3100

[a] Shortened Stroke. [b] At 72 V_{DC}. [c] 25/80$^{\circ}C$.

LMs of model Motor 2 are used in the knees.

Biped Motion Profile Simulation

Next, a dynamic evaluation of the biped walking motion profile was done. The motion profile was attained from the results of the previous 3D ZMP walking simulation [56]; however, in this case the computation was performed in MATLAB. This motion profile was later tested for different weights of the leg and shank. Here the vendor's sizing software tool was used (LinMot Designer 1.4.3 [245]), and, as before, a linear approximation was applied to convert the angular values to linear (stroke) movement of the LMs. This is a linear approximation of the full nonlinear Eqs.(6.3-6.5) presented later in Chapter 6.

Figure 3.5 presents the graphical result for a 4 s simulation of the thigh movement in a ZMP-based type of walking, with a velocity of 4.1 km/h (similar to the one generated in Figure 6.10 in Chapter 6). This test presents the measurements of the thigh's motor output, considering 8 kg

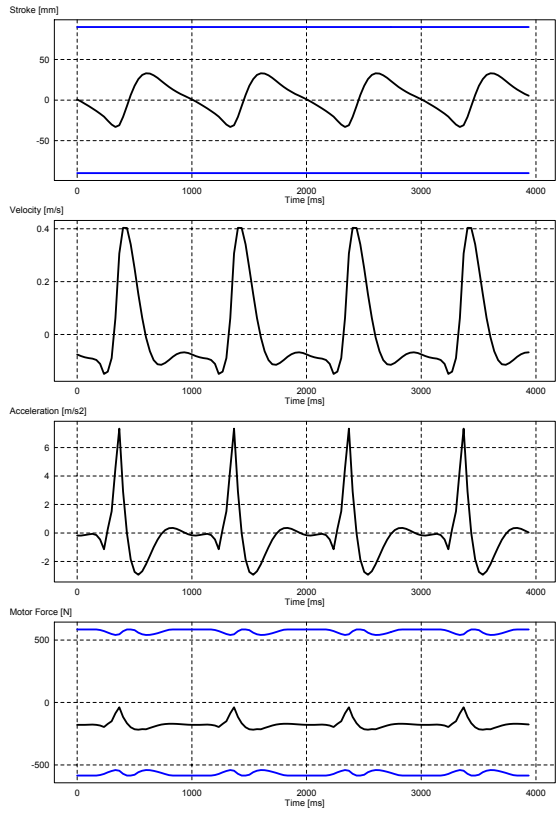

Figure 3.5. Simulation results for thigh motion profile using the simulation sizing tool LinMot Designer v1.4.3 [245]

Table 3.2. Motion profile simulation results

Parameters	Units	Motor 1	Motor 2
Zero Position	mm	65	65
Start Position	mm	0.711	41.5
Load Mass	g	8000	6000
Mounting Angle	deg	-90	-90
Dry Friction	N	5	5
Min. Strike	mm	-33.04	-41.5
Max. Stroke	mm	33.04	41.5
Total Stroke	mm	66.08	83
Peak Velocity	m/s	0.4	0.92
Peak Acceleration	m/s^2	7.33	-21.4
Peak Force	N	-217	-388
RMS Force	N	177	141
Peak Power Supply	W	130	460
Mean Power Supply	W	83	76
Mean Power Regeneration	W	0.7	2
Actual Power Dissipation	W	81	64

Numerical results for Motor 1 Hip and Knee, with supply voltage of 72 V and ambient temperature 25 $^{\circ}C$

of the thigh's own weight plus 8 kg of load weight (shank). Numerical results are presented in Table 3.2. A similar test was done for the shank's motor, assuming 5 kg load (security margin) plus 6 kg of the shank's own weight. The result can be seen in Figure 3.6 and Table 3.2.

It must be clarified that this test does not represent an actual walking simulation, instead is uses the angles trajectory (converted to strokes) of the walking motion profile, which is simulated by the motor hanging and lifting a specific weight. The angles are changed into stroke movement, and the simulation runs as if the stator were hanging from an imaginary grip, and the slider moves up and down lifting the weights according to the stroke profile. This test was performed using PID for positioning control and with no current limitation apart from the maximum allowed (no torque/current control applied). For this reason, and also because the trajectories are generated from a ZMP-based walking pattern, this result should be interpreted as the worst case scenario and not as the energy-

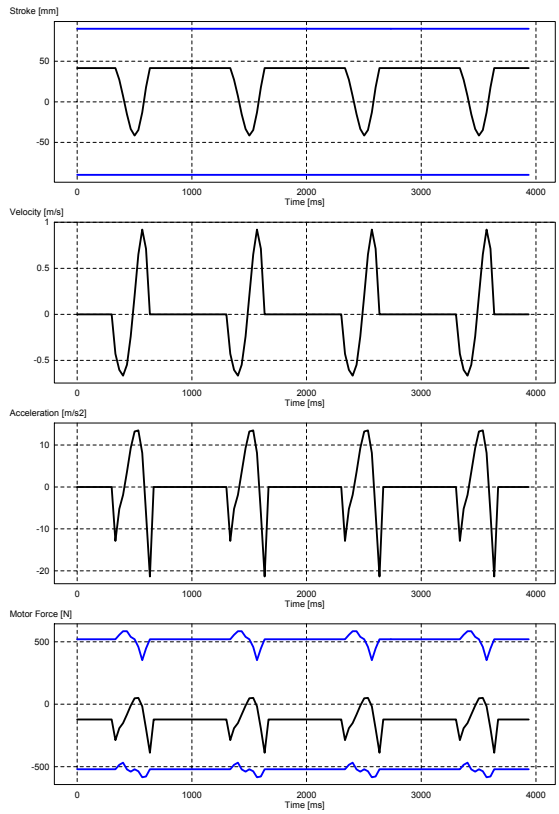

Figure 3.6. Simulation results for knee motion profile using the simulation sizing tool LinMot Designer v1.4.3 [245]

efficient case.

Later the same experiment was performed with real motors and the parameters shown in Table 3.1. The stator was fixed hanging vertically with the slider lifting a 9.5 kg weight. Fast sinusoidal motions were applied and high currents were observed; however, no overheat or failure of the system was detected.

Mechanical and Functional Considerations

After deciding to use the previous actuators, some mechanical and functional considerations needed to be taken into account to support the design concept. One of the most important issues was the non-even force constant of the LMs.

Figure 3.7 shows the actuators' force versus stroke profile and mechanical configuration of Motor 1. This figure shows a segment called the Shortened Stroke, where the force constant is invariable; however, in the remaining stroke segment, there is a linear decay of this factor. This lin-

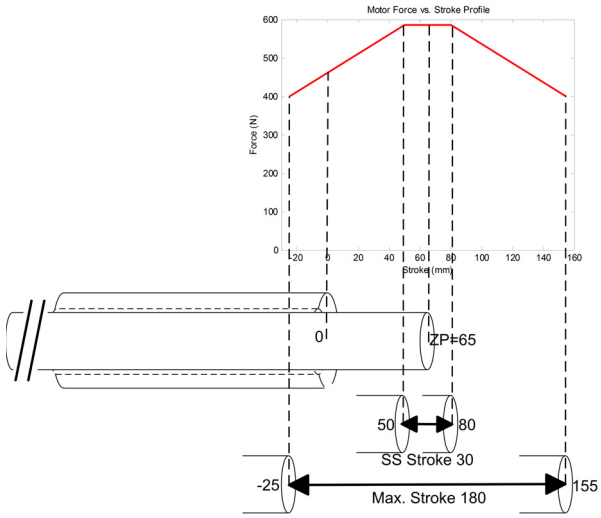

Figure 3.7. Force versus stroke profile and mechanical configuration of Motor 1

ear damping (as mentioned before), is there because different numbers of windings are generating the flow for different strokes distances. This profile then should be taken into consideration carefully when designing the mechanics, trying to match the symmetry of the human walking with the symmetry present in the torque output of these actuators. This position around which the stroke is symmetrically carried out is referred to by the vendor as the Zero Position point (ZP) [245]. In addition, because the sliders are basically permanent magnets, the ZP is also the point where the slider finds itself in steady rest when no current is applied. So this should also be thought of as the equilibrium position of the LM.

3.2.2 Kinematics and Dynamics' Simulator

A simulator was developed following the design of the first prototype [115], which was based on the previous choice of actuators and included big feet and not much detail on the upper body weight distribution (Figure 3.8 and Figure 3.9). This simulator is not a precise replica of the first prototype design but instead a simplified kinematic sketch which includes the LM kinematic and dynamic properties. The simulator was intended to analyze the mechanical constraints and physical properties of each part of the robot. The mechanical sketch was done with the IDEAS software and later exported to ADAMS, which was controlled in co-simulation by MATLAB/Simulink for the kinematic and dynamic analysis.

There are springs and dampers in each ankle sideways motion joint,

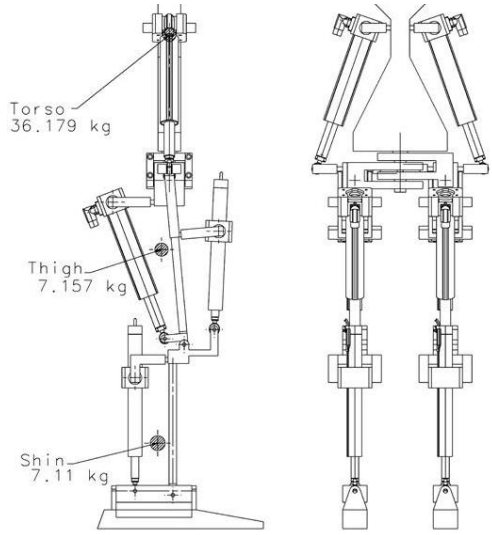

Figure 3.8. Kinematic sketch of the preliminary biped prototype done in IDEAS software

to allow foot alignment with the floor, but there is no actuator for ankle motion in this direction. Furthermore, the effect of contact parameters between the feet and floor had a strong effect on the model behavior.

Figure 3.8 also shows the CoM of the 3-Link planar approximation of the robot, which is used to perform passive walking gait analysis in the following chapters. Several tests were done in this simulator, including some ZMP-based approaches for energy consumption comparison. Nonetheless, no satisfactory performance was attained for ZMP-based walking in the 3D configuration, mainly due to lack of actuation in the ankle sideways motion and the use of traditional ZMP-based trajectory-following control. On the double support phase, the robot is able to balance itself in the frontal plane, thanks to the antagonist LM placed in the torso to articulate the lateral motion of the legs. However, on the single support phase, the robot was unstable, given that the lateral motion of the ankle was not actuated. Therefore traditional ZMP-based type trajectory-following control was not possible since strong ankle actuation is required.

To tackle such 3D motion, for an under-actuated biped due to missing ankle lateral actuators, an advanced control approach is needed. Such problem has been solved for simpler configurations such as the Acrobot in [248] and in planar bipeds like Mable [146]. Although the 3D control of walking motion falls outside the scope of this thesis, it is currently undergoing research in the GIMBiped project [113].

The simulator was successful however in balancing the robot in the

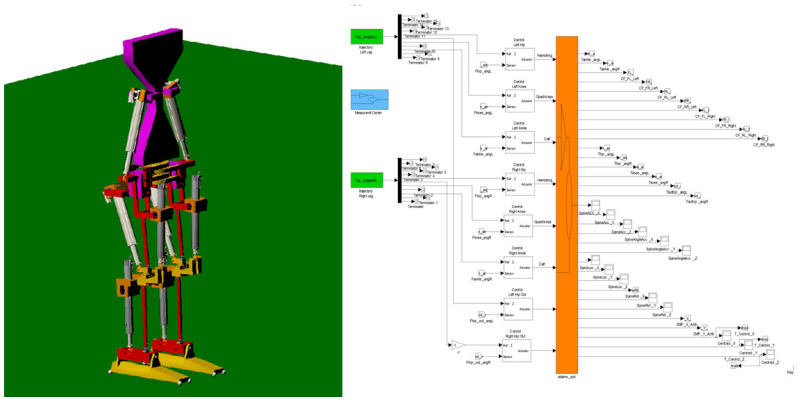

Figure 3.9. Dynamic and kinematic co-simulator with ADAMS and Simulink

standing position when facing external disturbances. Frontal and lateral balance for the biped was achieved when both feet were on the ground, and the motors could handle heavy disturbance in the frontal plane and moderate disturbance in the sagittal plane.

Such circumstances were also tested in hardware, and the outcomes inspired the idea of the *Idle State Stability* (IdSS) presented next in Section 3.3.2. The results of the simulator and its comparison with the experiments on the hardware will be presented in the following section.

3.3 Towards Long-Term Autonomy in Biped Robots

As previously mentioned in Section 2.3.1, the most advanced humanoid robots, such as Honda ASIMO [84] and HRP [68], have not taken the benefit of the fluent gait inherent for humans and animals. Instead, the traditional approach has been to control each joint angle to achieve the desired posture in terms of GCoM or ZMP. These paradigms require plenty of energy to perform and a much better result in terms of energy efficiency can be achieved by imitating human gait as in the LCW. Using the previous concepts, the new generation of energy-efficient biped robots are limit cycle walkers, which includes actuators in one or more joints enabling locomotion also on level terrain and up-hill. Nonetheless, so far the few LCW biped robots that have actually been implemented in hardware can only perform simple control maneuvers, with limitations in turning, negotiating steps or adjusting of the walking speed, being thus poor in versatility for robotic use.

Motivated by the previous challenge, the GIMBiped project also exam-

ined possible alternative sources of energy squandering in the traditional control approaches, looking to decrease energy consumption in biped service robots, and also analyzed the limitations shown by LCW bipeds, to increase mobility of these platforms.

As a result, this section proposes three separate strategies based on some known concepts and new theoretical ideas towards energy-efficient walking approaches that may be applied in the future on the GIMBiped platform.

3.3.1 Energy Issues in Biped Robots

There are three basic principles on how to save energy in a walking machine [25]:

1. By minimizing dissipative losses (*e.g.* inefficiency of power transmission).
2. By minimizing the diversion of energy into unproductive forms (such as the kinetic energy of limbs).
3. By recovering energy whenever possible.

These concepts inspired alternative theoretical approaches to tackle energy efficiency in biped service robot. To address the first two issues, the focus is centered on the correct choice of actuator and control technique for different tasks during the biped operation. Here the main operation states of bipedal robots are represented as ***Walking*** and ***Standing***. Both of these states are considered to have an energy-efficient sub-state or mode, named ***Limit Cycle Walking*** (LCW) and ***Idle State Stability*** (IdSS), respectively (Figure 3.10). LCW and IdSS are the first two proposed concepts to be followed for achieving better energy usage.The concept of ***regenerative walking*** is introduced as an addition to other existing ideas for recovering energy during walking. These three concepts will be explained in the following subsections.

From these three previous concepts, only LCW is studied in detail in the rest of this dissertation. IdSS is initially tested in hardware and confirmed in the next subsection as a valid alternative for the original design of the GIMBiped. Regenerative walking however is just offered as a theoretical proposition based on simulation results for further interesting uses of LCW approaches in biped locomotion.

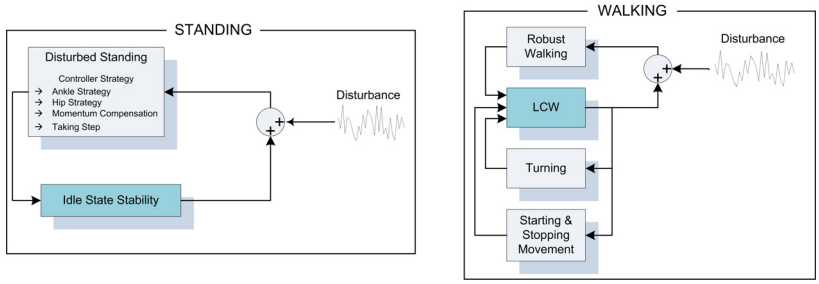

Figure 3.10. Two main states in bipedal robots operation and their respective efficient sub-states

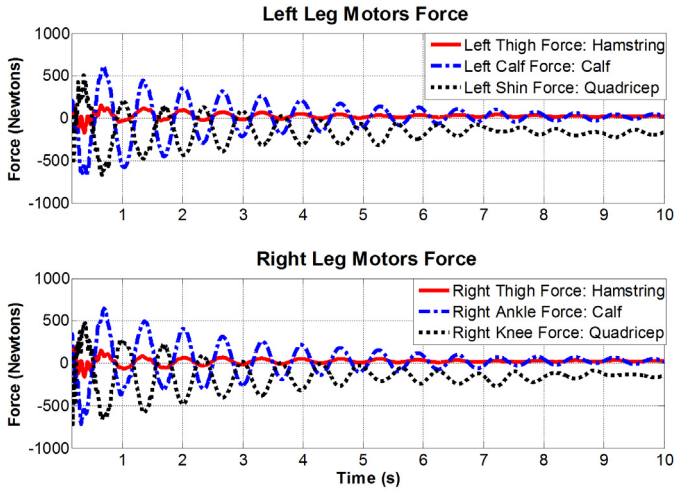

Figure 3.11. Torque outputs for position control around the equilibrium position for thigh, calf and shin motors.

3.3.2 Idle State Stability

The IdSS concept, although it may appear quite obvious, is a concept that has been missing in biped construction until now. It is essentially a rethought of the geometrical design in the mechanical structure that enables easy and efficient control of the biped in the critical equilibrium point, usually known as ***standing position***.

This is very important since the walking duty cycle β_w (presented in Section 2.2.3) in service robotic usage can be very low, making the energy saving in this stage quite significant.

In the GIMBiped, the IdSS during the experiments is maintained with zero energy expenditure from the actuators [56], and under moderate disturbance the robot will recover back to the IdSS. Figure 3.11 shows the simulated behavior for the IdSS using the simulator presented in Sec-

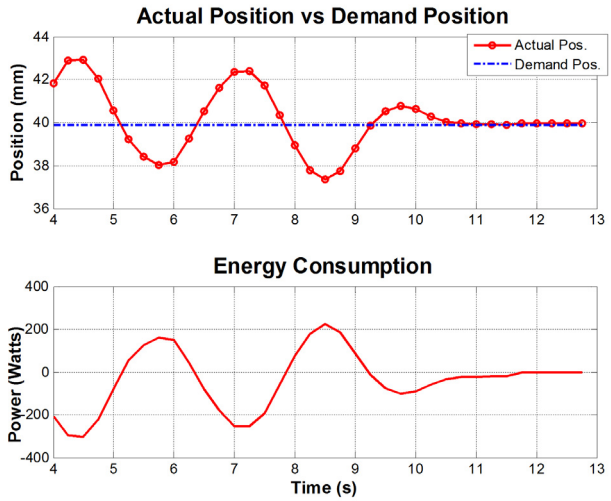

Figure 3.12. The results of the right shank's motors results for position control and energy consumption under front and back swing disturbance

tion 3.2.2. Figure 3.12 shows the experimental results in the GIMBiped testbed. The controller essentially turns off all the motor's input current once the standing equilibrium position is achieved and waits until some disturbance drives the robot away from the ideal idle position.

To this date, and to the author's knowledge, no biped robots have presented this characteristic and instead have been mostly concentrating on producing LCW. Moreover, usually performance tables do not show complete information about their consumption and duty cycles. Consequently, it is mostly mistaken to assume that the efficiency values (cost of transport) calculated for bipeds like ASIMO and HRP have been calculated under continuous walking operation.

3.3.3 Limit Cycle Walking

The LCW is a concept that has been introduced previously in Section 2.3.1, and which this thesis is focus to study and try to emulate using active control. The general idea of applying the LCW concept into an active biped platform is to try to reach the natural cyclic behavior that emanates from these systems under proper parameters settings and initial conditions and use it to avoid excessive external control.

However, the presence of a stable LC is not guaranteed in any type of system. In addition to the compliance needed in the actuators, the existence of a natural LC in biped robots is also highly sensitive to the design

parameters (link lengths and masses). To avoid foot scuffing and to obtain the ideal slope angle for the LC, the link masses and lengths of the mechanism have to be chosen carefully.

Therefore, the next chapters investigate further the possible application of LCW in active biped robots. First, as almost no robot with a realistic parameter distribution is able to perform passive LCW, Chapter 4 studies the use of a model based-control approach, with an approximated 3-link reference model that is close enough to the real hardware but still able to produce passive LCW to be used as reference trajectory for the controller.

Later, in Chapter 5, a variational analysis of the mechanical parameters of an ideal biped model is performed. This study is done with the intention to further analyze the effect of the parameters change in the evolution of LC, its stability and efficiency. The variation is done upon an ideal model derived from the GIMBiped testbed, so possible guidelines for mechanical modifications can be drawn from the study.

Finally, in Chapter 6, practical experiments using a combination of LCW- and ZMP-based control are tested in the GIMBiped platform.

3.3.4 Regenerative Walking

The study on recovering energy during walking has mainly centered in restoring the dissipated energy of the heel impact. This approach, though quite promising, still focuses on just saving energy and not harvesting it to recharge the batteries.

Here, a proposal is presented for the recovery of energy under downward walking, using Passivity Based Control (PBC) to set the biped's limit cycle reference trajectory to match a smaller slope angle than the actual walking slope used by the real hardware.

Figure 3.13 and Figure 3.14 show the results of regenerative walking for a 3-link biped walking simulator (Figure 4.3), using Passivity Based Controller (see Chapter 4 for details of the implementation of this controller), where both the controller and the dynamic simulator were developed in MATLAB (see Section 4.3 for details of the simulators).

Here the biped is simulated with the parameters presented in Table 3.3, and put it to walk on a slope $\gamma = 8^\circ$ instead of the natural LC slope ($\gamma = 6.3^\circ$). It can be observed from Figure 3.13 that negative mechanical energy is generated at some time in each joint, the ankle joint being the one that contributes the most. Figure 3.14 shows the differences of potential, kinetic and total energy between the real robot and the reference model.

Table 3.3. Parameters for a 3-link biped model approximation (Figure 4.3) used to generate plots in Figure 3.13 and Figure 3.14

Parameter	Symbol	Value
Leg Length	$L\ (m)$	0.900
Shank Length	$a_1 + b_1\ (m)$	0.450
Thigh Length	$a_2 + b_2\ (m)$	0.450
Shank CM Height	$b_1\ (m)$	0.22425
Thigh CM Height	$b_2\ (m)$	0.1849
Shank Mass	$m_1\ (kg)$	1.50
Thigh Mass	$m_2\ (kg)$	16.33
Hip Mass	$m_H\ (kg)$	10.0
Slope Angle	$\gamma\ (deg)$	6.3

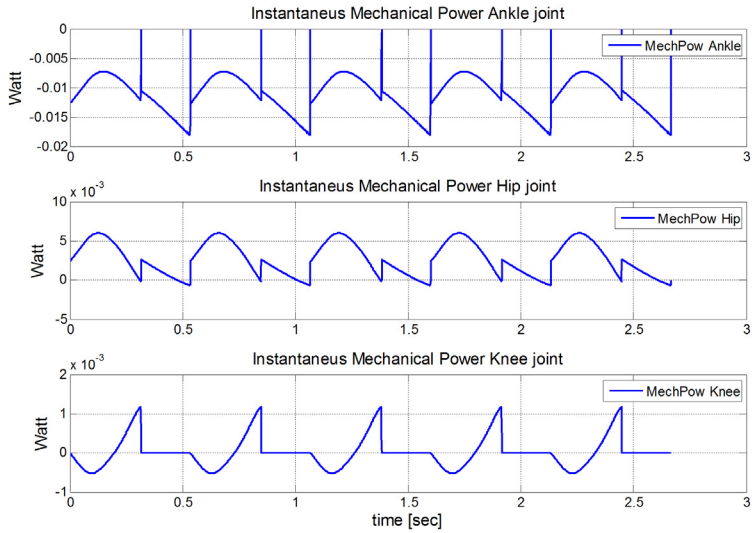

Figure 3.13. Mechanical power results under passivity-based control for a 3-link model harvesting energy walking down a 8° (deg) slope with reference LC set to 6.3° (deg)

The bottom plot shows the mechanical energy harvested. The energy is plotted as negative because that is the energy that has been "used".

For this technique to be viable, it is of central importance that the actuators used can efficiently regenerate negative mechanical work back into the form of the primary energy source. Such efficiency should be tested in the LMs, and it is part of the future work of the GIMBiped project [113].

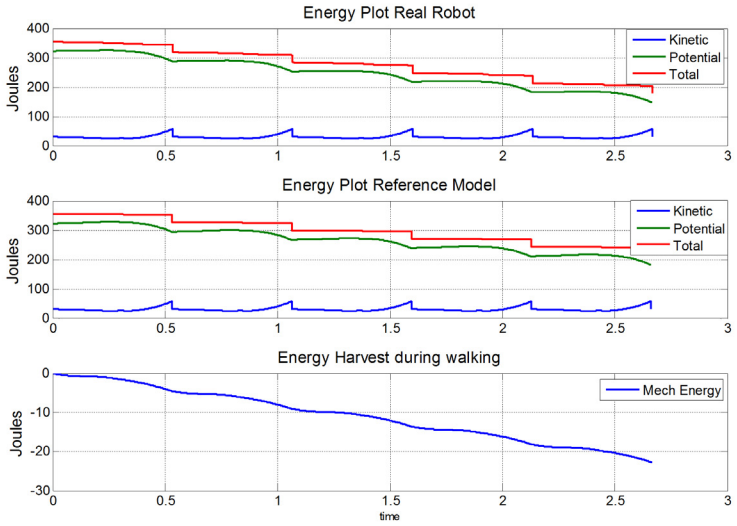

Figure 3.14. Energy results under passivity-based control for a 3-Link model harvesting energy walking down a 8° (deg) slope with reference limit cycle set to 6.3° (deg)

There are some problems related to the real implementation of this technique, since extracting energy from motors creates resistive forces, this generates some additional resistance to the motion, magnitude of which must be limited and small enough to allow the existence of LC.

In addition, the LC for a real-size robot may not be available on small slopes, as it can be observed later in the experiments in Chapter 4 and Chapter 5, and therefore high inclinations are needed to achieve a significant recharging rate. Also, it must be noticed that stability and postural control should be maintained while walking, and the compensation of those may reduce the actual amount of energy being recovered. However, also any movement in balance control that may require negative energy could be used to harvest energy under regenerative braking. Finally, the use of PBC in LCW is dependent on the prior knowledge of the slope angle and for that some prediction should be made or adequate sensors should be used.

4. Assessment of Limit-Cycle-Based Control Using Simplified Biped Model

Several walking controllers based on GCoM and ZMP stability indices have been proposed and successfully tested in simulators and hardware [68, 84]. Particularly ZMP-based controllers have been quite successful in performing advanced tasks in humanoid robots (apart from just walking), like running, jumping on one leg and navigating in unstructured environments with moving obstacles [67]. However, there is still no clear answer on which is the best control approach to target LCW, since most of the promising thoroughly proposed methods have been tested just on ideal analytical models [36] or with very favorable configuration of parameters in hardware experiments [37].

In other groups, researchers have tackled control based on practical observation, on mathematical analysis of the Limit Cycle (LC) and on applying some heuristics in controlling the actuators [249]. However, no systematical proof of stability has been carried out on the applied control. Researchers have built robots which at least in theory should be able to perform LCW. Some examples are the Delft University with Mike [108], Denise [184] (pneumatically powered) and Flame [109] (series elastic actuators), Carnegie Mellon with the Sarcos Robot (hydraulic actuators) [244] and Cornell with the Cornell Biped [249]. All previous prototypes present compliance in their system and are able to perform torque control and somehow compensate for the remaining actuators' friction. Also other control techniques have been studied for controlling bipeds and trying to achieve LCW or cyclic stability. These include Reinforcement Learning [142], Optimal Control [250], HZD [146, 209] and Neural Networks [47].

Since bipedal walking is a very complicated task, it is useful to split the task of 3D walking into smaller subtasks. This chapter will target two-dimensional gait without paying attention to the lateral balancing problem or starting and stopping the motion. Therefore, the work in this

chapter deals with a 2D model that has a similar basic structure as the existing hardware prototype GIMBiped in Chapter 3 ([41, 56]) (Figure 4.1). The goal is to define the most suitable control policy for the GIMBiped prototype based on energy efficiency and robustness, comparing (and adjusting to the needs) some of the promising control approaches for LCW found in the literature. Also, different sets of parameters (Table 4.1), which represent possible weight distribution in the hardware, are compared. Thus taking the first steps towards answering the question of which will be the best parameters for design modification in the GIMBiped, targeting energy efficiency and robustness. Further mechanical analysis of ideal weight distribution for increasing energy efficiency and stability will be performed in Chapter 5.

4.1 Methodology

As previously pointed out in Section 1.3 and Section 2.3, from the control point of view the main difficulty of bipedal walking arrives because the system is fundamentally under-actuated due to the missing actuation in the foot contact with the ground. In the foot-ground contact surface (or point), only compressive forces can be applied, preventing the direct use of classical control techniques for manipulators. The ZMP stability criterion, however, constraints the biped to maintain its foot in contact with the ground, enabling the usage of common manipulator control techniques where tight closed-loop control is used in each joint to reach the desired trajectory. The use of the ZMP concept requires detailed study of

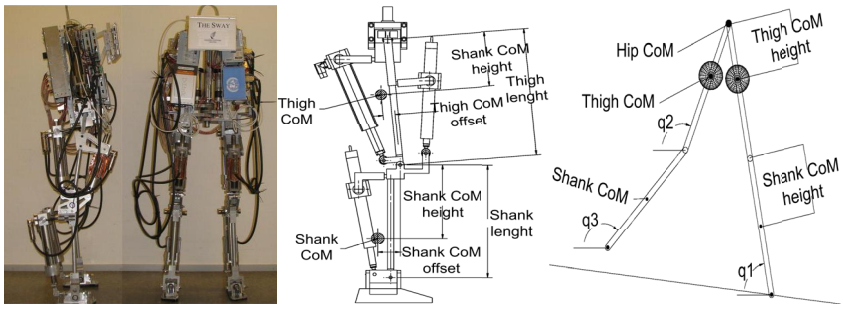

(a) GIMBiped's first prototype

(b) Kinematics sketch of preliminary design

(c) Passive LCW model based on preliminary design

Figure 4.1. Progressive approximation of the GIMBiped testbed into different simplified models

the Forward Kinematics (FK) and Inverse Kinematics (IK) of the system to generate joint trajectories that would satisfy ZMP constraints.

In LCW, the stability constraint is less restrictive and the foot does not need to be firmly (flat) on the ground during the whole step cycle [106]. Nevertheless, if normal manipulator control techniques want to be applied, there must be at least some contact with the ground, although the foot can eventually tip over the edges without that necessarily indicating that the system is becoming unstable.

This problem however, is not present in the most common analytical models of LCW, where the feet are modeled as point contacts and the ankle joint is permanently attached to the ground during the whole step cycle [36]. Some other models assume curved feet to increase the stability of the robot [231]. The previous assumptions are obviously not observed in real robots, where the contact has some sticktion and the surface has limited friction with the feet. Also the impacts are not completely inelastic and instantaneous (as assumed in most of the analytical models), therefore there is some damping and stiffness factors on the surface of the floor and in the knee joint, which leads to non-ideal dissipation of energy in the ***Knee Lock*** (KL) and to ***Foot Strike*** (FS) events.

Given that almost no robot with realistic parameters is able to perform passive LCW, the author proposes, in this chapter, the use of model-based control with a reference model that is close enough to the existing robot but still able to produce passive LCW [41,58]. In addition, in this chapter several model-based controllers are assessed on their capability to produce a stable gait based on LCW in a biped simulator that has a realistic mass distribution, link lengths and environment characteristics. The resulting gaits are evaluated for their energy efficiency and robustness. The different controllers are programmed in MATLAB and tested with a simulator built with the ***Open Dynamics Engine*** (ODE). [57,158]. Computed Torque controllers and a Passivity Based controller are compared. All of them use an ideal analytical model as a reference to compute the control input for the simulator to perform actuated LCW. The next subsections will present the analytical model, the different control policies and the ODE and other simulators.

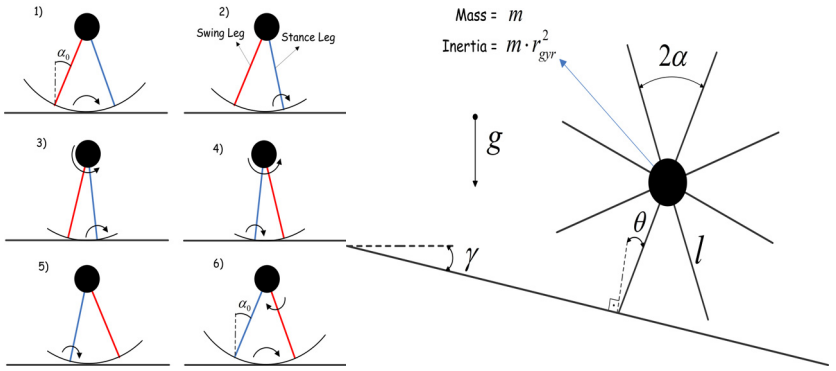

(a) Synthetic wheel **(b)** Rimless wheel

Figure 4.2. Different simplified representations of bipedal walking

4.2 Modeling of Planar Biped with Knees and Point Feet

Several two-dimensional models of LCW that differ in complexity have been proposed [149, 251–253]. Common for all the models is to assume all collisions to be inelastic and lateral friction forces on the ground large enough to prevent legs from sliding. The simplest models include the rimless wheel and the synthetic wheel [105, 254] (Figure 4.2), but since they are impractical to realize, these models are used only as a proof of the concept of passive walking [105, 231]. In the rimless wheel, the biped is represented by a point particle surrounded with mass-less bars in a planar configuration (Figure 4.2b). If the rimless wheel is located on a slope, it naturally rolls down with discrete contacts with the surface. Each bar rotates one at the time around its tip, representing in this case the legs of the biped. In this system, the FS is modeled by an instantaneous and inelastic impact, which is the only instant when two bars are in contact with the surface at the same time. McGeer used this model to explain his PDW theory which was later the foundation for the LCW research [105, 231]. The synthetic wheel is an improved version of the rimless wheel, which includes just one set of legs attached to each other and a point mass in the hip (representing the CoM), by a rotational joint (Figure 4.2a). This model was later refined by McGeer and named the compass-gait model. It was later extended again by him to include knees and curved feet. This kneed planar biped is also referred to as the three-link (3-link) biped model, due to its sequential representation of the biped as a two-link (2-link) and 3-link dynamic system.

A generalized version of this 3-link model using point feet, or alterna-

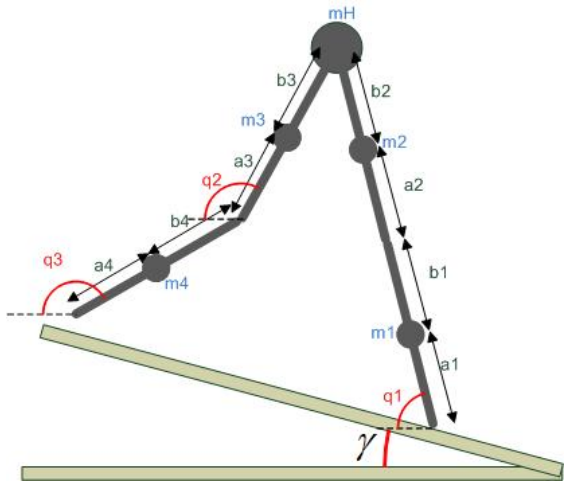

Figure 4.3. Fully parameterized planar biped model with knees and point feet.

tively named here as the planar biped with knees and point feet (Figure 4.3), was chosen as the simulator and the reference model for the controllers used in this chapter and throughout this thesis. Therefore, a detailed explanation is provided in this chapter about its functioning and the derivation of the dynamic and algebraic equations that models its behavior.

Many other models with increasing complexity and numerous DoF have been proposed for both 2D and 3D applications. However, the planar biped model with knees and point feet was chosen for its simplicity and because it has been proven to be capable of performing PDW [251], both crucial prerequisites for the control approach and analysis described in this and the following chapters.

The model is basically a kinematic chain of five rigid bodies that are connected to each other with rotational joints, or hinges, all of which allows one DoF between two links. Each leg consists of two links, shank and the thigh. Additionally, an extra dimensionless mass representing the hip is located in the joint connecting both legs. There is no upper body in this model, and therefore all the mass that may be in the upper body has to be included in the hip, which for this model will be indistinctly referred as the CoM also.

One of the legs, namely the stance leg, is always straightened, and therefore the stance leg can be regarded as a single link instead of a separate thigh and shank, leaving effectively only three free links. The links are connected to each other through frictionless hinge joints.

The presence of the knees in the model has several advantages. They ensure that the swing leg can pass the stance leg without the danger of scuffing the ground. Also, the knees will make the gait more human-like and slow down the collision speed at the FS, and slow velocities are preferable to minimize the energy dissipated in the collisions.

The surface friction is assumed to be always enough to prevent the stance foot from sliding: therefore, the foot contact with the ground can be thought of as another frictionless rotational joint (ankle joint) where torque can be applied if the biped ankle is considered to be actuated.

This model has been shown to be able to produce passive walking [36, 251], which is of great importance for the model-based control approach simulated in this chapter and tested in the hardware in Chapter 6. In addition, this model, and some derivations of it, are extensively used in LCW [41,53,57,58,251].

Therefore, the point-feet representation was chosen to keep the simulations simple and because it is one of the most commonly used configurations to study control and stability [36, 37, 55], having therefore some reference for comparison. Furthermore, the model can be gradually extended (*e.g.* adding feet, torso, 3D stability), increasing its complexity to match its real counterpart more accurately.

Figure 4.3 and Table 4.1, which present the approximated biped model and its parameters, will be referred to many times in Chapter 5 and Chapter 6. The reader should keep in mind this figure and the table for the next sections.

4.2.1 Dynamic Modeling

Since the walker consists only of rotational joints, the state of the walker is represented by joint angles and angular rates. Consequently, the state is completely defined by three angles and three angular velocities: stance leg angle q_1, thigh angle q_2, and shank angle q_3, and the three angular velocities associated to these angles $\dot{q_1}$, $\dot{q_2}$, $\dot{q_3}$. These angles are measured with respect to the world frame, as in Figure 4.3. Extensive work has been done in this model, evaluating its performance, energy efficiency and developing controllers [36,37,55,158].

This model is a hybrid dynamic system, which means that it includes continuous dynamic equations and algebraic equations. The continuous dynamic equations correspond to the 3-link phase when the knee is unlocked and to the 2-link phase when the knee is locked. The algebraic

equations represent the impact events at the KL and FS, where instantaneous changes in velocity are observed.

The continuous dynamic equations are derived in the following sections using the Lagrange method, resulting in two sets of nonlinear continuous systems, and the algebraic equations are obtained assuming conservation of momentum in the system.

The resulting concatenated sequence of the 3-link continuous dynamic equation, KL impact algebraic equation, 2-link continuous dynamic equation and FS impact algebraic equation represent a ***nonlinear hybrid dynamic system***. In particular for this model, this nonlinear hybrid dynamic system if viewed on the phase space, can present a cyclic behavior which is referred to as ***Limit Cycle*** (LC). It characterizes the performance of the biped and its walking cycle. The LC is used widely to evaluate the behavior of the walker and will be studied in detail for the 3-link model in the next section.

The Limit Cycle of the Planar Biped with Knees and Point Feet

As briefly introduced in Section 2.3.1, the LC is a particular cyclic behavior of the state variables in the phase space that may be present in a nonlinear dynamic system and can be used to evaluate the stability of the system. The LC presents itself as a ***natural*** behavior of the state variables when the system is subjected to certain ***Initial Conditions*** (ICs) and parameters values. Such LC will be referred to as the ***natural LC*** of the systems to differentiate it from a cyclic behavior or LC that may arise from the application of a control policy. Such natural LCs are present in the passive limit-cycle walkers, and in this study the ICs are found using a software developed in MATLAB. The theory and concepts behind this approach were shortly introduced in Section 2.3.1 and will be further studied in Chapter 5, where the evolution of the systems' stability, efficiency and behavior will be evaluated once the system is induced to parameters variation. Therefore, in this section, only the basic interpretation of the LC of the 3-link planar biped model with point feet will be presented.

Figure 4.4 presents the natural LC of the planar 3-link kneed biped model using the parameters in *Set 1* of Table 4.1. The LC was found using a Matlab Simulator/Program, which relies on a nonlinear optimization function to find the best ICs for the determined set of parameters' value, *Set 1* in this case (see Section 3.3.3 and Section 4.3.1 for further details in

the Simulator).

The gait starts at $t = 0$ with the 3-link phase, in which the swing leg is located behind the stance leg. In Figure 4.4, P_1 is the starting point for state variables q_1 and $\dot{q_1}$, and P_5 is the starting point for the remaining state variables q_2, $\dot{q_2}$, q_3 and $\dot{q_3}$.

With appropriate initial velocities, the walker starts to turn over the stance leg, lifting the swing leg up from the ground and letting it swing freely and pass the stance leg. The 3-link phase ends at time $t = t_1$ when the KL impact event occurs. In the KL event, the swing leg knee locks, leaving the leg in its fully extended position, preventing the shank from hyperextension. In Figure 4.4, the state jumps representing the impacts (KL and FS) are indicated by the red lines, and in particular for the KL event, $\dot{q_1}$ jumps from point P_2 to point P_3, $\dot{q_2}$ jumps from P_7 to P_8 and $\dot{q_3}$ jumps from P_6 to P_8.

The 2-link phase begins from the previous points, in which both the knees are locked. It can be noticed that the KL event occurs when both q_2 and q_3 reach the same angle, and after the event both the shank and the thigh continue with the same velocity and angle ($q_2 = q_3$ and $\dot{q_2} = \dot{q_3}$).

The overall walking cycle ends on the FS, when the swing leg foot makes contact with the ground again. Similarly, state jumps can be appreciated from Figure 4.4 in the FS event, where $\dot{q_2}$ and $\dot{q_3}$ jumps from P_9 to P_1 and $\dot{q_1}$ jumps from P_4 to P_5, therefore closing the cycle. What used to be the swing leg before, has now become the stance leg, and vice-versa.

The type of plot presented in Figure 4.4 can be used to experimentally evaluate the stability of the LC, as in the following Section 4.5, and analyze how much the state variables deviate from a constant trajectory.

Three-Link Dynamics

As described previously, during the unlocked phase of the walking, the system behaves like a three-link pendulum, as in the ballistic walker in [255, 256]. The equations of the system as anticipated can be obtained using the Lagrange formulation, calculating the kinetic and potential energy of each link, adding and deriving according to the formulation. Here however no symmetry was supposed a priory; therefore, there are more variables in the system than in the previous derivations of this model [251].

The final dynamics of the three-link phase is presented in the standard

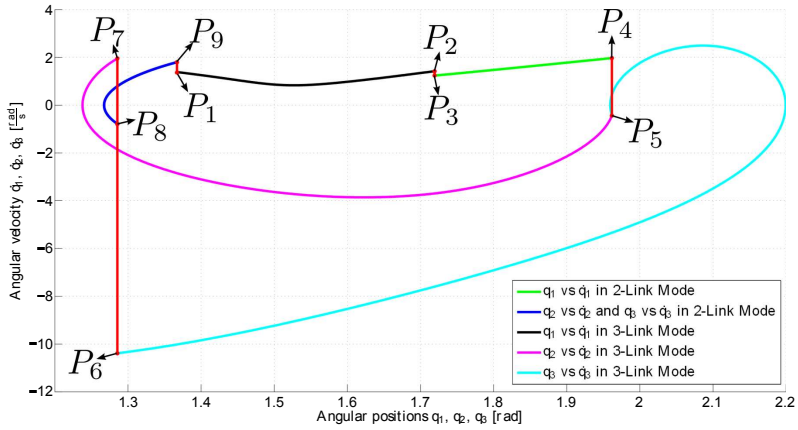

Figure 4.4. Limit Cycle for the 3-link planar biped model with knees and point feet, using parameters in *Set 1* of Table 4.1

form for manipulators' dynamics in Eq. 4.1

$$M_{\text{3-link}}(q)\ddot{q} + V_{\text{3-link}}(q,\dot{q}) + G_{\text{3-link}}(q) = \tau \tag{4.1}$$

$$V_{\text{3-link}}(q,\dot{q}) = \begin{bmatrix} V_{\text{3-link}_{(1,1)}} & V_{\text{3-link}_{(2,1)}} & V_{\text{3-link}_{(3,1)}} \end{bmatrix}^T \tag{4.2}$$

where,

$$\begin{aligned} V_{\text{3-link}_{(1,1)}} &= -L\dot{q}_2^2 \sin(q_1 - q_2)(m_3 b_3 + m_4 b_3 + m_4 a_3) \\ &\quad + L\dot{q}_3^2 m_4 b_4 \sin(q_1 - q_3) \qquad (4.2a) \\ V_{\text{3-link}_{(2,1)}} &= L\dot{q}_1^2 \sin(q_1 - q_2)(m_3 b_3 + m_4 b_3 + m_4 a_3) \\ &\quad + \dot{q}_3^2 \sin(q_3 - q_2)(m_4 b_4 b_3 + m_4 a_3 b_4) \qquad (4.2b) \\ V_{\text{3-link}_{(3,1)}} &= m_4 b_4 (L\dot{q}_1^2 \sin(q_1 - q_3) - \dot{q}_2^2 (a_3 + b_3) \sin(q_2 - q_3)), \qquad (4.2c) \end{aligned}$$

and

$$M_{\text{3-link}}(q) = \begin{bmatrix} M_{\text{3-link}_{(1,1)}} & M_{\text{3-link}_{(1,2)}} & M_{\text{3-link}_{(1,3)}} \\ M_{\text{3-link}_{(2,1)}} & M_{\text{3-link}_{(2,2)}} & M_{\text{3-link}_{(2,3)}} \\ M_{\text{3-link}_{(3,1)}} & M_{\text{3-link}_{(3,2)}} & M_{\text{3-link}_{(3,3)}} \end{bmatrix}, \tag{4.3}$$

where

$$M_{\text{3-link}_{(1,1)}} = a_1^2(m_1+m_2) + m_2(2a_1a_2 + 2a_1b_1 + a_2^2 + 2a_2b_1 + b_1^2) + L^2(m_3+m_4+m_H) \tag{4.3a}$$

$$M_{\text{3-link}_{(1,2)}} = -L\cos(q_1-q_2)(m_3b_3 + m_4b_3 + m_4a_3) \tag{4.3b}$$

$$M_{\text{3-link}_{(1,3)}} = -Lm_4b_4\cos(q_1-q_3) \tag{4.3c}$$

$$M_{\text{3-link}_{(2,1)}} = -L\cos(q_1-q_2)(m_3b_3 + m_4b_3 + m_4a_3) \tag{4.3d}$$

$$M_{\text{3-link}_{(2,2)}} = b_3^2m_3 + m_4(b_3+a_3)^2 \tag{4.3e}$$

$$M_{\text{3-link}_{(2,3)}} = m_4b_4(a_3+b_3)\cos(q_2-q_3) \tag{4.3f}$$

$$M_{\text{3-link}_{(3,1)}} = -Lm_4b_4\cos(q_1-q_3) \tag{4.3g}$$

$$M_{\text{3-link}_{(3,2)}} = m_4b_4(a_3+b_3)\sin(q_2-q_3) \tag{4.3h}$$

$$M_{\text{3-link}_{(3,3)}} = m_4b_4^2 \tag{4.3i}$$

$$G_{\text{3-link}}(q,\dot{q}) = \begin{bmatrix} G_{\text{3-link}_{(1,1)}} & G_{\text{3-link}_{(2,1)}} & G_{\text{3-link}_{(3,1)}} \end{bmatrix}^T \tag{4.4}$$

$$G_{\text{3-link}_{(1,1)}} = g\cos q_1(m_1a_1 + m_2(a_1+a_2+b_1) + L(m_3+m_4+m_H)) \tag{4.4a}$$

$$G_{\text{3-link}_{(2,1)}} = -g\cos q_2(m_3b_3 + m_4b_3 + m_4a_3) \tag{4.4b}$$

$$G_{\text{3-link}_{(3,1)}} = -m_4b_4g\cos q_3 \tag{4.4c}$$

With proper settings for the parameters a_1, a_2, b_1, b_2, a_3, a_4, b_3, b_4, m_1, m_2, m_3,m_4 and m_H and initial conditions for q, the system will enter into cyclic behavior. The necessary conditions for the existence of LC, as well as the possible range of the parameters setting will be studied in Chapter 5.

Two-Link Dynamics

After the knee lock event, the swing leg behaves as a single link, therefore switching towards two-link dynamics, which is related to the behavior of a double-link inverted pendulum. This type of system is commonly known in the biped research as the compass gait walker. However, there are still differences between the models, since this walker has a mass in the hip, which the compass gait does not.

The dynamics are derived again using the Lagrangian formulation, resulting in:

$$M_{\text{2-link}}(q)\ddot{q} + V_{\text{2-link}}(q,\dot{q}) + G_{\text{2-link}}(q) = \tau \tag{4.5}$$

$$V_{\text{2-link}}(q,\dot{q}) = \begin{bmatrix} V_{\text{2-link}_{(1,1)}} & V_{\text{2-link}_{(2,1)}} \end{bmatrix}^T \tag{4.6}$$

$$V_{\text{2-link}_{(1,1)}} = -L\dot{q}_2^2 \sin(q_1 - q_2)(m_3 b_3 + m_4 b_3 + m_4 a_3 + m_4 b_4) \tag{4.6a}$$

$$V_{\text{2-link}_{(2,1)}} = L\dot{q}_1^2 \sin(q_1 - q_2)(m_3 b_3 + m_4 b_3 + m_4 a_3 + m_4 b_4) \tag{4.6b}$$

$$M_{\text{2-link}}(q) = \begin{bmatrix} M_{\text{2-link}_{(1,1)}} & M_{\text{2-link}_{(1,2)}} \\ M_{\text{2-link}_{(2,1)}} & M_{\text{2-link}_{(2,2)}} \end{bmatrix}, \tag{4.7}$$

where

$$M_{\text{2-link}_{(1,1)}} = a_1^2(m_1 + m_2) + 2a_1 m_2(a_2 + b_1) + m_2(a_2 + b_1)^2 + L^2(m_3 + m_4 + m_H) \tag{4.7a}$$

$$M_{\text{2-link}_{(1,2)}} = -L\cos(q_1 - q_2)(m_3 b_3 + m_4 b_3 + m_4 a_3 + m_4 b_4) \tag{4.7b}$$

$$M_{\text{2-link}_{(2,1)}} = -L\cos(q_1 - q_2)(m_3 b_3 + m_4 b_3 + m_4 a_3 + m_4 b_4) \tag{4.7c}$$

$$M_{\text{2-link}_{(2,2)}} = b_3^2 m_3 + m_4(a_3 + b_3 + b_4)(a_3 + b_3 + b_4) \tag{4.7d}$$

$$G_{\text{2-link}}(q) = \begin{bmatrix} G_{\text{2-link}_{(1,1)}} & G_{\text{2-link}_{(2,1)}} \end{bmatrix}^T \tag{4.8}$$

$$G_{\text{2-link}_{(1,1)}} = g\cos q_1(m_1 a_1 + m_2(a_1 + a_2 + b_1) + L(m_3 + m_4 + m_H)) \tag{4.8a}$$

$$G_{\text{2-link}_{(2,1)}} = -g\cos q_2(m_3 b_3 + m_4 b_3 + m_4 a_3 + m_4 b_4) \tag{4.8b}$$

The previous equations complete the definition of the continuous dynamics. Now there is the need for defining the algebraic equations that model the behavior of the impact dynamics.

Knee Lock Event

The impact dynamics presented here follow the same formulation as in [251], where conservation of momentum is assumed in the discrete collision events. Since the only external force on the system is present in the stance foot, the angular momentum is conserved for the whole system around the same stance foot and the same conservation is observed for the swing leg around the hip. Using then the conservation of momentum equations, post collision states can be obtained as in the equations that follow.

$$Q_{\text{KL}}^{+} \begin{bmatrix} \dot{q}_1 \\ \dot{q}_2 \end{bmatrix}^{+} = Q_{\text{KL}}^{-} \begin{bmatrix} \dot{q}_1 \\ \dot{q}_2 \\ \dot{q}_3 \end{bmatrix}^{-}, \tag{4.9}$$

where,

$$\dot{q}_3^{+} = \dot{q}_2^{+} \tag{4.9a}$$

$$Q^{-}_{\mathrm{KL}}(q) = \begin{bmatrix} Q^{-}_{\mathrm{KL}_{(1,1)}} & Q^{-}_{\mathrm{KL}_{(1,2)}} & Q^{-}_{\mathrm{KL}_{(1,3)}} \\ Q^{-}_{\mathrm{KL}_{(2,1)}} & Q^{-}_{\mathrm{KL}_{(2,2)}} & Q^{-}_{\mathrm{KL}_{(2,3)}} \end{bmatrix}, \tag{4.10}$$

where

$$\begin{aligned} Q^{-}_{\mathrm{KL}_{(1,1)}} =& -m_2(a_1^2 + a_2^2 + b_1^2 + 2(a_1b_1 + a_2b_1 + a_1a_2)) - m_1a_1^2 \\ & - L^2(m_H + m_4 + m_3) + m_4b_4L\cos(q_1 - q_3) \\ & + (m_3b_3L + m_4L(b_3 + a_3))\cos(q_1 - q_2) && \text{(4.10a)} \\ Q^{-}_{\mathrm{KL}_{(1,2)}} =& -m_4(a_3 + b_3)^2 - m_4b_4\cos(q_2 - q_3)(a_3 + b_3) \\ & - b_3^2m_3 + L\cos(q_1 - q_2)(b_3m_4 + a_3m_4 + b_3m_3) && \text{(4.10b)} \\ Q^{-}_{\mathrm{KL}_{(1,3)}} =& -m_4b_4(b_4 + (b_3 + a_3)\cos(q_2 - q_3) - L\cos(q_1 - q_3)) && \text{(4.10c)} \\ Q^{-}_{\mathrm{KL}_{(2,1)}} =& L((m_3b_3 + m_4(b_3 + a_3))\cos(q_1 - q_2) + m_4b_4\cos(q_1 - q_3)) && \text{(4.10d)} \\ Q^{-}_{\mathrm{KL}_{(2,2)}} =& -b_3^2m_3 - m_4((a_3 + b_3)^2 + \cos(q_2 - q_3)(a_3b_4 + b_4b_3)) && \text{(4.10e)} \\ Q^{-}_{\mathrm{KL}_{(2,3)}} =& -m_4b_4(b_4 + (b_3 + a_3)\cos(q_2 - q_3)) && \text{(4.10f)} \end{aligned}$$

and

$$Q^{+}_{\mathrm{KL}}(q) = \begin{bmatrix} Q^{+}_{\mathrm{KL}_{(1,1)}} & Q^{+}_{\mathrm{KL}_{(1,2)}} \\ Q^{+}_{\mathrm{KL}_{(2,1)}} & Q^{+}_{\mathrm{KL}_{(2,2)}} \end{bmatrix} \tag{4.11}$$

where

$$\begin{aligned} Q^{+}_{\mathrm{KL}_{(1,1)}} =& -m_2(a_1^2 + a_2^2 + b_1^2 + 2(a_1b_1 + a_2b_1 + a_1a_2)) - m_1a_1^2 \\ & + (m_3b_3L + m_4L(b_3 + a_3 + b_4))\cos(q_1 - q_2) \\ & - L^2(m_H + m_4 + m_3) && \text{(4.11a)} \\ Q^{+}_{\mathrm{KL}_{(1,2)}} =& \, m_4(-2a_3b_3 - 2a_3b_4 - 2b_4b_3 - a_3^2 - b_3^2 - b_4^2) - b_3^2m_3 \\ & + \cos(q_1 - q_2)(b_3Lm_4 + b_4Lm_4 + a_3Lm_4 + b_3Lm_3) && \text{(4.11b)} \\ Q^{+}_{\mathrm{KL}_{(2,1)}} =& \, L\cos(q_1 - q_2)(m_3b_3 + m_4(a_3 + b_4 + b_3)) && \text{(4.11c)} \\ Q^{+}_{\mathrm{KL}_{(2,2)}} =& \, m_4(-2a_3b_3 - 2a_3b_4 - 2b_4b_3 - a_3^2 - b_3^2 - b_4^2) - b_3^2m_3 && \text{(4.11d)} \end{aligned}$$

Foot Strike Event

As before, now the FS is modeled as an inelastic collision, and conservation of momentum is calculated around the colliding foot for the whole system. In addition, the momentum is also conserved for the swing leg around the hip after the impact. The collision event is derived in the following equations

$$Q^{+}_{\mathrm{FS}} \begin{bmatrix} \dot{q}_1 \\ \dot{q}_2 \end{bmatrix}^{+} = Q^{-}_{\mathrm{FS}} \begin{bmatrix} \dot{q}_1 \\ \dot{q}_2 \end{bmatrix}^{-} \tag{4.12}$$

where

$$\dot{q}_3^+ = \dot{q}_2^+ \tag{4.12a}$$

$$\dot{q}_3^- = \dot{q}_2^- \tag{4.12b}$$

and

$$Q_{\mathbf{FS}}^-(q) = \begin{bmatrix} Q_{\mathbf{FS}_{(1,1)}}^- & Q_{\mathbf{FS}_{(1,2)}}^- \\ Q_{\mathbf{FS}_{(2,1)}}^- & Q_{\mathbf{FS}_{(2,2)}}^- \end{bmatrix} \tag{4.13}$$

where

$$\begin{aligned} Q_{\mathbf{FS}_{(1,1)}}^- = & -m_2(a_1^2 + a_2^2 + b_1^2 + 2(a_1b_1 + a_2b_1 + a_1a_2)) \\ & + (m_3b_3L + m_4L(b_3 + a_3 + b_4))\cos(q_1 - q_2) \\ & - L^2(m_4 + m_H + m_3) - m_1a_1^2 \end{aligned} \tag{4.13a}$$

$$\begin{aligned} Q_{\mathbf{FS}_{(1,2)}}^- = & -m_4(2a_3b_3 + 2a_3b_4 + 2b_3b_4 + a_3^2 + b_3^2 + b_4^2) - b_3^2m_3 \\ & + L\cos(q_1 - q_2)(m_4(b_3 + a_3 + b_4) + b_3m_3) \end{aligned} \tag{4.13b}$$

$$Q_{\mathbf{FS}_{(2,1)}}^- = L\cos(q_1 - q_2)(m_3b_3 + m_4(a_3 + b_4 + b_3)) \tag{4.13c}$$

$$Q_{\mathbf{FS}_{(2,2)}}^- = m_4(-2a_3b_3 - 2a_3b_4 - 2b_4b_3 - a_3^2 - b_3^2 - b_4^2) - b_3^2m_3 \tag{4.13d}$$

And

$$Q_{\mathbf{FS}}^+(q) = \begin{bmatrix} Q_{\mathbf{FS}_{(1,1)}}^+ & Q_{\mathbf{FS}_{(1,2)}}^+ \\ Q_{\mathbf{FS}_{(2,1)}}^+ & Q_{\mathbf{FS}_{(2,2)}}^+ \end{bmatrix} \tag{4.14}$$

where

$$\begin{aligned} Q_{\mathbf{FS}_{(1,1)}}^+ = & -L\cos(q_1 - q_2)(Lm_H + m_3(a_1 + a_2 + b_1) \\ & + m_2(a_3 + a_4 + b_4) + m_4a_1 + m_1a_4) \\ & + m_4(a_1a_2 + a_1b_1 + a_1b_2) + m_3(a_1b_2 + a_2b_2 + b_1b_2) \end{aligned} \tag{4.14a}$$

$$Q_{\mathbf{FS}_{(1,2)}}^+ = m_1(a_3a_4 + a_4b_3 + a_4b_4) + m_2(a_3b_3 + a_4b_3 + b_3b_4) \tag{4.14b}$$

$$Q_{\mathbf{FS}_{(2,1)}}^+ = m_3b_2(a_1 + a_2 + b_1) + m_4a_1(a_2 + b_1 + b_2) \tag{4.14c}$$

$$Q_{\mathbf{FS}_{(2,2)}}^+ = 0 \tag{4.14d}$$

4.3 Simulators

Several simulators were developed during the course of this thesis project with the intention of emulate the behavior of the real robot and test different control approaches on an approximated version of the GIMBiped testbed.

4.3.1 The MATLAB Simulator

The MATLAB simulator was developed as a tool for easy and fast verification of the previous dynamic model. The equations found in the previous Section 4.2.1 were simulated analytically in MATLAB. In the simulator, the continuous dynamic was integrated and event detection was set, which imposed a triggering condition to change from one continuous dynamic to another, following the state jump equations defined by the impact dynamics in the KL and HS.

The MATLAB simulator also served for searching for ideal parameters and ICs that could generate stable LC. For searching such parameters and ICs, nonlinear optimizations tools provided with MATLAB were used. The nonlinear optimization function searched for the best ICs, which minimized the difference between the initial states and final state values. For an ideal stable LC, the values for the states at the end of the cycle should be the same as the values in the begging of the cycle (ICs).

This simulator was of great importance since the first analysis on different parameter settings made here reveals the need for symmetry in the configuration of the parameters to be able to generate stable walking patterns. The need for symmetry in the model may appear to be an obvious matter, however here it was still tested and corroborated experimentally. Therefore, from now on the model used in the experiments will always be considered symmetric, and the necessary substitution of values is made in the previous dynamic and algebraic equations with $a_4 = a_1$ $a_3 = a_2$, $b_4 = b_1$, $b_3 = b_2$, $m_4 = m_1$ and $m_3 = m_2$.

This same simulator was used when studying the possible applications of regenerative walking presented in Section 3.3.4.

Furthermore, the model-based controller used in this chapter uses this simulator to generate the trajectory of the reference model.

4.3.2 The ODE Simulator

To simulate the dynamics of the real biped robot (Figure 4.1), a more realistic simulator than the one in previous GIMBiped project publications [41, 56] is used here. The analytical model presented in Section 4.2.1 serves then only as reference for the model-based control algorithms to control the actuated robot on level terrain. The simulator should later be replaced by the actual biped hardware, while the same analytical reference could be used for control (as it will be done later in Chapter 6).

The simulator is based on the ***Open Dynamics Engine*** (ODE), which is an open source rigid-body-physics engine library written in C. The simulator was developed to emulate any system consisting of rigidbodies and joints, but it has special features, such as a knee-locking mechanism that makes it useful for simulating LCW robots [158].

The model implemented in the simulator is the same as the reference model described in Section 4.2. However, the way the dynamics are simulated differs quite a lot from the analytical case. The analytical model is ideal, and all collisions are modeled as inelastic instantaneous collisions. In addition, the joints are assumed to be rigid and frictionless. In the ODE simulator, the collisions are not modeled as instantaneous events but as continuous counteraction defined by a spring (stiffness 5×10^5) and a damper (damping constant 5×10^5). Also the moment of inertia of each link is assumed to be similar to a thin rod with the same parameters as in Figure 4.3 and Table 4.1. The simulator has an interface to be used in co-simulations with MATLAB. This was quite advantageous because it allowed the model-based controller to run on MATLAB, which speedup the development phase of the controllers. On the other hand, the interaction between the simulator and MATLAB increased the simulation time considerably. Therefore, later in the real-time critical control on the GIMBiped platform, the control algorithm was completely rewritten in C/C++ (see Chapter 6).

The previously-mentioned ODE simulator used to evaluate the results of the controllers in this chapter was developed by T. Haarnoja in [158] and does not belong to the contributions of this thesis work. For further details on the simulators and their use, the reader should refer to [57, 58, 158]

4.3.3 The ADAMS Simulator

Another simulator developed for the GIMBiped project was the dynamic simulator in ADAMS. The simulator in ADAMS was developed to compare its results with the outcomes of the MATLAB simulator. The idea was to evaluate the influence of the simulator used on the behavior of the system. Since ADMAS is a rigid multi-body dynamics simulator, it was interesting to see the different results compared with the pure analytical method developed in MATLAB.

The major difference to appreciate was in the sensitivity of the model. Contrary to the MATLAB simulator, ADAMS models the impacts as a continuous event in time, with a spring and damping coefficients for defining

Table 4.1. Model parameters

Parameter	Symbol	Set 1	Set 2	Set 3
Leg Length[a]	$L\ (m)$	0.900	0.900	0.900
Shank Length[b]	$a_1 + b_1\ (m)$	0.450	0.450	0.450
Thigh Length[b]	$a_2 + b_2\ (m)$	0.450	0.450	0.450
Shank CM Height[b]	$b_1\ (m)$	0.22425	0.22425	0.22425
Thigh CM Height[b]	$b_2\ (m)$	0.1849	0.1849	0.1849
Shank Mass[b]	$m_1\ (kg)$	1.50	5.66	5.80
Thigh Mass[b]	$m_2\ (kg)$	16.33	11.73	11.30
Hip Mass	$m_H\ (kg)$	10.0	10.0	5.0
Slope Angle[c]	$\gamma\ (deg)$	6.3	5.5	5.8

[a] $L = a_1 + a_2 + b_1 + b_2 = a_3 + a_4 + b_3 + b_4$.

[a] In in Section 4.3.1 the model was establish to need symmetry for achieving LC, therefore $a_4 = a_1$ $a_3 = a_2$, $b_4 = b_1$, $b_3 = b_2$, $m_4 = m_1$ and $m_3 = m_2$ [c] These angles were manually and iteratively chosen as a compromise for the stability of the corresponding Limit Cycle (LC) and visual appearance of the gait.

the characteristic of the surface and contact. This simple difference made some fairly stable models in MATLAB to become unstable in ADAMS. The previous results give an idea of the great difficulty of finding and maintaining stable LC in the real word.

The ADAMS simulator was developed by T. Ylikorpi, and in [59] T. Ylikorpi and the author further analyses the difference between the passive walker simulators in MATLAB and ADAMS.

4.4 The Control Algorithms

Several techniques have been formulated to address control in LCW [106]. The basic idea is to actuate passive LCW robots, inputting just enough energy (torque) to make the system cyclically stable [249]. The major drawback with this idea is that robots that are naturally able to perform passive LCW have very favorable mass distribution and link length, and although that allows them to be actuated with small torques (light actuators) to produce actuated LCW, their application in robotic usage is limited since they are not able to withstand large disturbances, carry any

payload, start and stop the movement or perform any other task than just walking.

Therefore, [41] proposed the construction of a bipedal service robot, taking into account the requirement to produce LCW but not restricted to an ideal passive LCW mechanical design. As a result, the GIMBiped prototype has an active compliant and strong actuator system (linear motors), and different sets of weight distribution (Table 4.1) have been considered to reach the optimal performance based on an appropriate control scheme. The different values in Table 4.1 were obtained as the best approximation of weight distribution from the real hardware which can still perform LCW if represented as a point foot 3-link model as in Figure 4.3. Since the real prototype cannot produce passive LCW, the closest LCW model of the real robot is used to produce a reference trajectory. Parameter values in Table 4.1 were searched empirically based on trial and error in the MATLAB simulator. However, further mathematical proof for its stability and energy expenditure will be studied in Chapter 5.

One promising control policy to actuated LCW was presented by Spong et al [36,257,258]. They studied several methods based on energy-shaping techniques which in their most basic form correspond to ***Potential Energy Compensation*** (PEC) [259]. More sophisticated versions include ***Kinetic Energy Shaping*** (KES) [55], which allows controlling the velocity of the biped and changing it quickly in real time. PEC and KES are new denominations to an older control philosophy introduced earlier as Passivity Based Control in [260]. Potential Energy Compensation is the ***Passivity-Based Control*** (PBC) method used here. It basically provides, as input torque, the difference between the gravity vector of a reference passive LCW model (on a certain slope angle) and the robot model (on another slope angle). Its mathematical representation is shown in Table 4.2, and to perform at its optimum it assumes that the robot is very similar to the reference model, meaning that the impacts are perfectly inelastic (no bounce), the transfer between the swing and stance legs is instantaneous and there is no slipping at the foot/ground contact (assumptions that will be relaxed and studied in Section 4.5). Parallel to the previous study, Asano and Yamakita have done similar work in their Passive Velocity Fields technique. This is basically the same concept that relies on the PBC. Several stages were studied, and they also tested their results in a nearly ideal prototype [37], where their conclusion already at that point was that more robust control should be applied.

Table 4.2. Control algorithms

Robot Dynamics
$M(q)\ddot{q} + V(q,\dot{q}) + F_v\dot{q} + F_d(\dot{q}) + G(q) + \tau_d = \tau$
where,
$M(q)$ = Inertial Matrix
$V(q,\dot{q})$ = Coriolis/Centripetal Vector
F_v = Viscous Friction $= 0$
$F_d(\dot{q})$ = Dynamic Friction $= 0$
$G(q)$ = Gravity Vector
τ_d = Disturbance Torque $= 0$
τ = Torque
Computed Torque Control
PD Computed-Torque (CT-PD)
$\tau = M(q)(\ddot{q}_d + K_v\dot{e} + K_p e) + V(q,\dot{q}) + G(q)$
PID Computed-Torque (CT-PID)
$\dot{\xi} = e$
$\tau = M(q)(\ddot{q}_d + K_v\dot{e} + K_p e + K_i\xi) + V(q,\dot{q}) + G(q)$
Independent Joint Control: PD+Gravity Control
$\tau = K_v\dot{e} + K_p e + G(q)$
Independent Joint Control: Classical PD Control
$\tau = K_v\dot{e} + K_p e$
Independent Joint Control: Classical PID Control
$\dot{\xi} = e$
$\tau = K_v\dot{e} + K_p e + K_i\xi$
Passivity Based Control
Passivity Based Control (PBC) - ideal case
$\tau = G(q) - G_{Ref.}(q)$
Passivity Based Control With Soft PD (PBC+PD)
$\tau = G(q) - G_{Ref.}(q) + K_v\dot{e} + K_p e$

The other control techniques that are also evaluated here are from the ***Computed-Torque Control*** (CTC) family. CTC is a straightforward, commonly-used control scheme for robot manipulators. It was already

presented in detail in Section 2.4. These schemes generally perform well when the system's parameters are known fairly accurately. A distinction should be made in the fact that CTC targets to follow a reference trajectory (here is the trajectory of the ideal analytical LCW model) using the feedback linearization of the nonlinear model of system, while PBC indicates the exact torques that should be input into the system based on the energy difference between the model and the real system. Therefore, in principle the torques should be smoother in PBC, thus making this control more energy efficient. Table 4.2 summarizes the control algorithms compared in this study, and further details can be found in [36, 261].

To evaluate robustness, the same technique as in [262] is applied here, where different step heights are introduced in the system and robustness is related to the maximum step height that the walker can overcome without falling.

4.5 Results and Analysis

Table 4.3 shows the results of the six different control strategies (Table 4.2) used in the ODE simulator for the three different parameter sets presented in Table 4.1. These experiments report results that are different from [41], since in the previous paper the simulator consisted of only an ideal mathematical model of the robot (simulator in MATLAB) and not of a rigid body simulator as in here (ODE simulator). As the environment is not ideal here, PBC will not perform as expected. That was the first observation realized during this study, where the PBC did not manage to control the biped to walk as the reference model. This is because the simulator includes inertia for the links of the robots, and the impact events include stiffness and damping. The previous generalizations requires more energy to be inputted into the system than the one calculated by the PBC with the approximated model. To overcome this problem, a soft PD was added to the PBC, as shown in Table 4.2.

For the evaluation of the performance of the controllers, as a common practice in these types of robots, the specific mechanical cost of transport c_{mt} is also used here. The c_{mt} was already defined in Section 2.2.3, and here it is obtained by calculating E as the sum of all torque times angular velocity in each joint, using Eq.2.8. For this study, total dissipation is assumed in the system with none of the negative work being regenerated. Therefore, assuming that the systems has to input the energy needed for

Table 4.3. Result different control policies

Controller Type	Set 1				Set 2				Set 3			
	c_{mt}[a]	Fr[b]	MSD[c]	P_{time}[d]	c_{mt}	Fr	MSD	P_{time}	c_{mt}	Fr	MSD	P_{time}
Passive Walker	0.0997	0.3558	–	–	0.0871	0.2677	–	–	0.0920	0.2655	–	–
CT-PD	0.1534	0.3600	87	509e-5	0.3048	0.3618	86	514e-5	0.3285	0.3533	108	513e-5
CT-PID	0.1572	0.3619	84	511e-5	0.2956	0.3609	86	512e-5	0.2913	0.3485	90	509e-5
Ind Joint + Grav.	0.2067	0.2291	25	429e-5	0.3019	0.2386	20	407e-5	0.3135	0.2584	40	415e-5
Ind Joint PD	0.2122	0.1066	9	452e-5	0.3253	0.1622	12	433e-5	0.3520	0.1171	10	403e-5
Ind Joint PID	0.1846	0.1484	3	481e-5	0.3705	0.1673	22	458e-5	0.3660	0.1828	11	467e-5
PBC with Soft PD	0.1345	0.3398	48	476e-5	X	X	X	X	X	X	X	X

[a] Specific mechanical cost of transport, dimensionless unit. [b] Froude Number, dimensionless velocity.

[c] Maximum step disturbance, corresponding to the maximum floor height differences between two consecutive steps which the biped can overcome and stabilize within 5 steps after the disturbance its applied. Measured in $[mm]$

[d] Time needed to compute the solution in every control loop for a given controller, measured in $[s]$.

the negative work, meaning $K_{reg} = 1$ in Eq.2.8.

As reference, the result table (Table 4.3) also includes the C_{mt} of the ideal analytical Passive Walker, which is obtained by using the sole energy input into the system by the gravity when the biped is performing passive LCW. This is the minimum theoretical mechanical energy needed to perform the natural LC used as reference. Thus the C_{mt} of the Passive Walker is $C_{mt} = \frac{E_m}{mgd}$, where $E_m = E_{m_F} - E_{m_I}$, and E_{m_I}, E_{m_F} represent the total *Kinetic* plus *Potential* energy respectively in the beginning and in the end of walking down a slope. Also, the speed of traveling greatly affects the energy consumption. Therefore, the specific cost of transport has to be measured at the same normalized speeds or make that difference noticed in the evaluation. Here the speed is normalized by using the Froude number F_r introduced in Section 2.2.3.

The robustness is compared based on an index named ***Maximum Step Disturbance*** (MSB) here, measured in mm. This index corresponds to the maximum floor height differences between two consecutive steps which the biped can overcome and be stabilized within 5 steps after the disturbance its applied. Finally, the processing time P_{time}, measured in seconds (s), is the computational time of the controllers.

As previously mentioned, in CTC the controller tries to follow the trajectory of the reference model. Therefore, the reference model should be close to the set of the parameters of the real robot, but at the same time it should also have a good foot clearance to avoid falling by foot scuffing. As the LC for the parameters in *Set 2* and *Set 3* does not look natural and results in poor foot clearance, *Set 1* was always used as reference for all the CTC controllers. As a consequence, it can be observed that the F_r of the best performing controllers, like CT-PD and CT-PID, in all the cases (*Set 1*, *Set 2* and *Set 3*) resembles the F_r of the passive walker with *Set 1*.

It can be observed that the PBC with a soft PD controller has the best result in terms of cost of transport for the *Set 1* and that *Set 1* also allows to maintain a high F_r. Figure 4.5, Figure 4.7 and Figure 4.9, respectively, show the trajectory for the angles in time, LC curves and joint torques, for a 10 step simulation (5 steps in the case of Figure 4.7) of the PBC with a soft PD for *Set 1*. It can be seen from Figure 4.7 that the natural LC is not achieved constantly.

In the LC plot, the black lines correspond to the LC of the ideal reference model (natural LC), the lines in green are the trajectories of the shank of the swing leg (q_3), the lines in magenta are the trajectories of

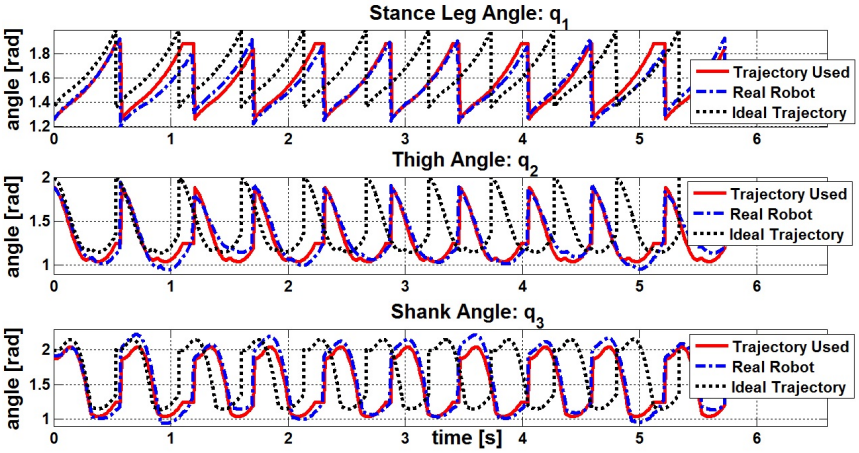

Figure 4.5. Angle vs. Time for PBC + soft PD controller with parameter *Set 1*

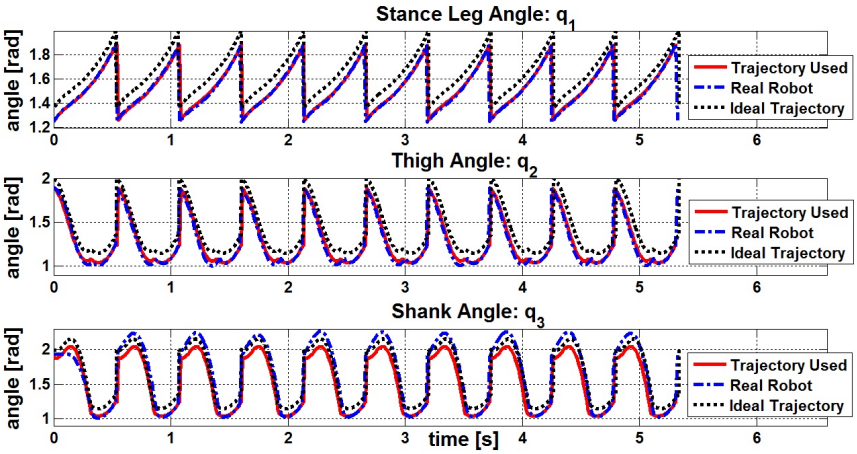

Figure 4.6. Angle vs. Time for CT-PD controller with parameter *Set 2*

the thigh (q_2) and blue lines the stance leg (q_1). Furthermore, from Figure 4.5, it can be observed that the "real" trajectory (trajectory of the model in ODE representing the real biped), lags behind the ideal trajectory, leading to a smaller value of F_r compared to the reference model. However, the torques in Figure 4.9 are kept low most of the time and without high frequency switching, thus avoiding overuse of energy in this case. Nevertheless, two high peaks are present in each step cycle, corresponding to the moments where the PD part of the controller takes over. Those two

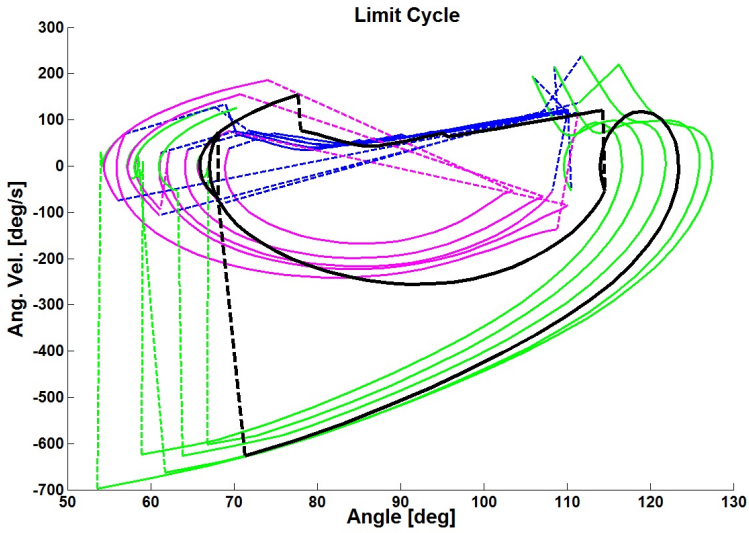

Figure 4.7. Limit Cycle plot (Angles vs. Angular Velocity) for PBC with soft PD controller with parameter *Set 1*

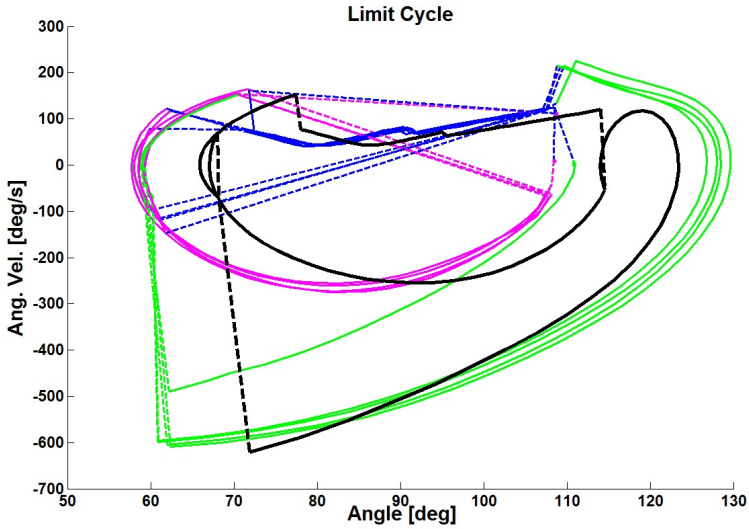

Figure 4.8. Limit Cycle plot (Angles vs. Angular Velocity) for CT-PD controller with parameter *Set 2*

moments correspond to the KL and the FS, and the difference between the reference model and the real robot is the cause of it. The processing time is also kept among the lowest.

It must be noticed, however, that PBC with a soft PD only worked with the parameter configuration from *Set 1* as the reference model, which has a natural LC with a good foot clearance. *Set 2* and *Set 3* do not present this

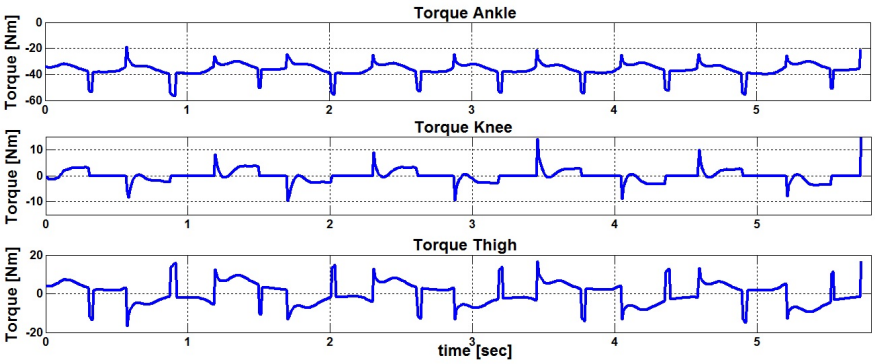

Figure 4.9. Joint Torques plot for PBC with soft PD controller with parameter *Set 1*

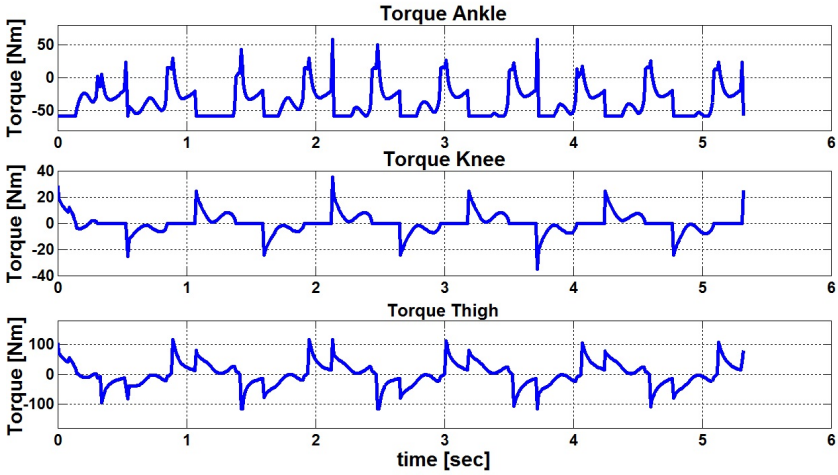

Figure 4.10. Joint Torques plot for CT-PD controller with parameter *Set 2*

feature, making it impossible for the controller to prevent foot scuffing with a soft PD. If a tighter PD were to be used, it would "take over" the controller at all times, and calling it PBC will no longer make sense. That is the reason why PBC with a soft PD is marked as unsuccessful in Table 4.3 for *Set 2* and *Set 3*.

Other satisfactory results were obtained with CT-PD and CT-PID at the cost of some processing time since the matrices $M(q)$, $V(q, \dot{q})$ and $G(q)$ must be calculated in every control loop. The results of the CT-PD controller for *Set 2* are shown in Figure 4.6, Figure 4.8 and Figure 4.10. Figure 4.6 shows that the controller manages to follow the ideal trajectory quite well, and in response the LC is kept quite stable, even when starts

far from the LC (Figure 4.8). Figure 4.10 shows however some high frequency switching in the control. That generates negative work, and as a result C_{mt} is higher.

PD+Gravity, pure PD and pure PID independent joint control do not perform as well in terms of energy efficiency as the previous controllers. They are not capable of following the desired trajectory at the natural LC speed, resulting in a slower velocity than the target model. Also their robustness values are lower than those of the previous controllers (PBC, CT-PD and CT-PID).

It should be mentioned that in the simulations, the joint input torques are limited to the values of 58.5 Nm for the ankle, 116 Nm for the hip and 35 Nm for the knee, because those are the maximum limits of the actuators that are used in the GIMBiped prototype [56] (see Chapter 3). This is accounted for in the controllers, which use an integral factor and apply an anti-windup compensation. The previous setting is reflected in the controllers' performance, as can be appreciated in the saturation for the ankle torque for the CT-PD controller in Figure 4.10.

4.6 Conclusions

The previous results could indicate promising applications in the real hardware for the PBC with a soft PD and CT-PD. However, the poor performance obtained with the PBC for parameters in *Set 2* and *Set 3* brings back to mind the trade-off between energy efficiency and versatility in robotic usage (as discussed in Section 4.4), since it proves that efficient control techniques based on energy criterion are highly dependent on mechanical parameters of the robot. This dependence is also observed (but less destructive) in CTC, which points to further research of optimal migration from passive mechanisms to robust biped robots. Such further investigation is carried out in Chapter 5that follows and, together with the result obtained in this chapter, will serve to formulate the solution applied in the GIMBiped hardware in Chapter 6.

Although PBC, CT-PD and CT-PID did perform well, PBC cannot be applied directly since it needs to know the slope value in advance. CT-PD and CT-PID use more computational resources and need precise knowledge for the matrices in the dynamic equation. Also all the gains for the CTC family were found heuristically, by searching around the natural frequency of the system and always maintaining critical damping ratio

between the gains [261]. Therefore, the gains are different for each controller, and a mathematical method to ensure optimal gain for each case should be developed.

As PD+Gravity, pure PD and pure PID independent joint controllers are not capable of following the desired trajectory, a possible solution to increase their performance could be to use slower LC as reference or scale them in time before inputting it as reference. Such solution in the case of PD and pure PID independent joint control will greatly simplify the control implementation and reduce the computation time in each control cycle, as supported by the results in Table 4.3. The use of pure PD or PID independent joint control may be encouraged as well by the impossibility to build a 3-link model close enough to the real hardware (GIMBiped), which at the same time is capable to produce PDW. In that case, or if the GIMBiped parameter values deviate considerable from the model used as reference, there won't be significant advantages of using such model and calculate the $M(q)$, $V(q, \dot{q})$ and $G(q)$ matrices used to compute the control output in each cycle.

5. Numerical Continuation of Hybrid Nonlinear Dynamic Model of the Biped System: A Design Study

This chapter presents a numerical continuation analysis of an approximated hybrid nonlinear dynamic model of the GIMBiped. This study was performed with the intention to propose proper attested guidelines for the implementation or modification of the GIMBiped mechanical design, aiming to increase its energy efficiency and robustness based on LCW. Here the biped system is simplified and modeled as a planar biped with knees and point feet, as in Section 4.2.1, where the equations of motion corresponds to the behavior of a hybrid nonlinear dynamic system. Numerical continuation analysis is performed with the software application TC-HAT, which is tailored to handle that type of problem and properly compute the continuations of dynamic systems with state jumps.

The numerical continuation analysis examines the evolution of the periodic solutions (representing walking gaits in the biped system) and its bifurcations, reaching six different boundary conditions, which characterize stable-to-unstable frontiers.

Section 5.1 presents a short motivation towards numerical continuation. Section 5.2 explains the methodology used in this chapter and Section 5.3 the potential use and problems of numerical continuation in the study of biped systems. Section 5.4 introduces the software used for the numerical continuation process and the implementation of the dynamic equations in this environment, and Section 5.5 reviews concepts of nonlinear systems. Finally, Section 5.8 and Section 5.9 present the numerical continuation experiments as well as analysis and result discussions, respectively.

5.1 Motivation and Introduction

As stated in Section 1.3, the main problem with the current biped platforms is the lack of autonomy due to their high energy consumption, which

is a consequence mainly owed to its high cost of transport. An alternative to solve the previous issue could be to build robots that walk more naturally and efficiently in terms of energy consumption. Under this scope, better results have been achieved by imitating human gait with the concept of LCW [52, 108, 208, 249, 263]. Using LCW researchers have built a new generation of biped robots which include compliant actuation systems, in one or more joints, enabling natural-looking walking cycles with better recorded performance for the cost of transport [159, 184, 208, 263].

However, the few LCW-based biped platforms built to date can only perform simple control maneuvers, lacking versatility and robustness for FSR use. The previous setbacks arise because the actuators added to power the LCW-type of biped frames are usually light and not strong enough to handle big disturbances. The use of light actuators is because of the delicate balance needed between masses' distribution and length ratio to find and conserve a suitable natural LC. Furthermore, depending of their type, there are several drawbacks in using compliant actuators [243]. Consequently, the physical characteristics of the actuators needed to better control the mechanism usually drive the robot away from a mechanical design that would allow the existence of a proper natural LC.

Therefore, it is important to have a thorough study on the cost versus benefit of including higher weight and sizes in the design of the mechanism. To accomplish the previous, and consequently to improve the performance of this new type of biped robots, a detailed study on migrating from the ideal analytical expression of passive LCW towards a more realistic modeling of actively controlled biped is required.

A numerical continuation analysis of the nonlinear hybrid dynamic model of the biped robot is proposed here as a way to find an optimal convergent point between robustness, agility and energy efficiency. This method is tested in the study of possible mechanical modifications for the GIMBiped, which could allow a better performance of the model-based controller presented in Chapter 4, looking to increase its robustness and energy efficiency.

5.2 Methodology

As introduced in Section 1.3 and Section 2.3.1, the idea of using LCW in the GIMBiped project is to follow its principles to design a well-tuned mechanical system. In the design of this type of mechanical system, much

care should be taken to choose the correct parameters, like the size and mass of the limbs, to allow the existence of a natural LC. The natural LC found will then correspond to a gait that could be used under favorable conditions (without too much external disturbances) for walking in an energy-efficient mode. For the natural LC to be used as an energy-efficient walking mode, it is primordial that the LC found exhibit a behavior that permit a viable walking cycle, with a proper step length, walking velocity, foot clearance and energy expenditure.

Given that mostly any robots with realistic parameters are not able to perform passive LCW, Chapter 4 (and [58]) propose the use of model-based control with a reference model that is close enough to the existing robot but at the same time is able to produce passive LCW. However, for this control approach to work at its best, it still needs to have a hardware that facilitates at maximum the trajectory following of the natural LC given by the reference model. There the need for further search around the possible mechanical parameters of the real biped prototype, in this case the GIMBiped testbed.

In this chapter, a numerical continuation analysis will be performed in the same approximated nonlinear hybrid dynamic model of GIMBiped presented in Section 4.2 (Figure 4.3). The analysis will be done by adjusting the masses of the above-mentioned model, starting from the parameter values in *Set 1* in Table 4.1 (see Section 4.4) and trying to steer them into the real values of the GIMBiped platform, as presented in Chapter 3. This should provide the GIMBiped project some guideline for the possible use of other type of actuators, and the expected improvement or downfalls that this could bring.

5.3 Numerical Continuation: Problems and Potential Use in Biped Studies

Numerical Continuation is the process of calculating and following approximated solutions of a system of parameterized nonlinear equations, using numerical tools (with software).

The method can be applied to ordinary differential equations of the form:

$$\dot{x} = F(x, \lambda), x \in \Re^n, \lambda \in \Re \tag{5.1}$$

where if $F(x, \lambda)$ is adequately smooth and there is an equilibrium point x_0 for a given λ_0, in which $F(x_0, \lambda_0) = 0$

Here λ can take the form of a multidimensional real vector of parameters, and F should be a sufficiently smooth function (or operator), from a suitable function-space (e.g. Banach, Euclidian) into itself.

As λ changes, usually the equilibrium solution x (also named ***steady state***, or ***fixed point***) varies too. During the process of varying this set of parameters λ (continuation), some related characteristics of the function F can be monitored and, consequently, ***bifurcations*** and ***changes of stability*** can be detected. Numerical continuation methods can also be applied to time-varying solutions, such as ***periodic***, ***homoclinic*** and ***heteroclinic orbits***, and more generally to all solutions which satisfy a ***Boundary-Value Problem*** (BVP).

Therefore, in principle it could be thought that continuation methods may be applied to identify the evolution and stability of the natural LCs (observed as a solution) in nonlinear dynamic equations that are used to model the behavior of biped systems. However, a problem may arrive due to the hybrid nature of the system, which comes from modeling the mechanical impacts as state jumps in the phase plane. The previous issue drove Goswami *et al.*, to declare, in [233], the following:

> *Although the robot has a simple kinematics, the hybrid nature of the governing equations make it impossible to utilize the traditional tools (such as the automatic detection of limit cycles [264]) developed to aid the study of non-linear systems.*

The previous statement may have been true by the time [233] was published in 1998. However, since then, researchers have advanced in the development of software for numerical continuation, which now allows its application in ***picewise-smooth autonomous systems*** [265, 266] and in more general periodic trajectories of ***hybrid dynamic systems*** [267, 268].

In [233], Goswami *et al.* finally used the full non-linear equations of the robot, relying extensively in iterative numerical simulations, and focus only on one leg (due to clear symmetries) in a compass-biped model [269], a simpler model than the one used in this study (kneed biped). [233] has been extensively referenced, and, even today, researchers in the biped area continue to use it as one of the main references in the study of the evolution of LC in biped walking under parameters variation. Other studies, as in [236, 238], have extended the previous work to analyze different types of biped models or calculating the basin of attraction. However, they

still rely on direct iterative numerical simulation of the models.

In [234], Müller first addressed the immensely important issue of correct characterization of the stability of hybrid systems. He introduced a model-based algorithm for the correct computation of the Lyapunov exponents of dynamic systems with discontinuities. In [270], Adolfsson *et al.* follow the process introduced by Müller to analyze the stability and root finding in a model of a 3D passive walking mechanism. Adolfsson *et al.* however, did not apply automatic numerical continuation but instead used direct numerical integration, as in Goswami *et al.*, implementing a semi-analytical scheme based on Müller's proposition. Adolfsson *et al.* indeed were the first to propose further automated numerical continuation in an approximated model of a biped system to study its behavior under parameter variations. They however performed the continuation with their own algorithms/program, which is not publicly available and where the parameters they variated and model used are not the ones studied in here.

Without any disregard to the great work previously done in [233, 270], the study presented in this chapter looks to update the previous works, utilizing and promoting the recent available tools in numerical continuation and showing its potential application as designing aid for the biped platforms.

5.4 The TC-HAT and AUTO Softwares

The continuation software application used in this thesis is the TC-HAT. TC-HAT itself works as a driver to a modified version of AUTO97 software, which is a fully-fledged continuation software for ordinary differential equations.

AUTO is a FORTRAN-based software widely used for the bifurcation analysis of smooth dynamical systems. Its early development stages date back to the mid-1970's and its first distributions by Doedel and Kervénez [271, 272] to the mid-1980's. AUTO later received many contributions for the update versions, which include a graphical user interface, C version of the original FORTRAN codes and programs for graphical visualization of the solutions [273–275]. The theory behind the development of AUTO and AUTO itself is highly documented, and major references can be found in [271, 276–282].

Nonetheless, AUTO cannot handle the bifurcation analysis of hybrid

dynamic systems, in which continuous (in time) dynamics are interrupted by discrete (in time) events. The previous lack of automated tools for the study of dynamic systems with discontinuities has lead researchers to rely on numerical analysis involving direct numerical integration of the related differential equations. As seen in the previous Section 5.3 and in [233], such numerical methods, based on the forward iteration of a system, apart from its computational burden can only find stable orbits. Consequently, these methods fail to give any information related to the unstable orbits or bifurcations which may derive or arrive from the stable orbits.

Inspired to cover the previous lack of automated analysis tools, P. Thota developed the TC-HAT toolbox [267, 268] to enable a thorough study of the bifurcations in (periodic) hybrid dynamic systems, in the same fashion as AUTO does it for the bifurcation analysis of smooth dynamic systems. As AUTO, TC-HAT is written in FORTRAN, and it uses AUTO 97's BVP formulation to find and continue periodic trajectories of hybrid dynamic systems. It can also perform continuation for a selected set of co-dimension-one bifurcation points under variations in the system's parameters.

Although TC-HAT was developed by P. Thota, it is inspired and closely resembles a previously developed software named ***SlideCont***, developed by F. Dercole and Y. A. Kuznetov [265, 266]. SlideCont allows bifurcation analysis of ***Filippov*** type of systems, detecting and continuing codimension-2 sliding bifurcations as well as some codimension-2 singularities. TC-HAT extended the previous capabilities, providing continuation of periodic trajectories of arbitrary sequence of events- compared to at most three segments in ***SlideCont***- including state jumps at the terminal points of solution segments, while ***SlideCont*** just handles piece-wise smooth dynamical systems without jumps. Furthermore, TC-HAT comes with a modified version of AUTO97, which contains amendments to the monodromy matrix computation, needed to correctly characterize the linearized stability properties of the trajectories in terms of the related ***Floquet multipliers*** [234]. ***SlideCont*** does not have the previous functionality. Consequently, TC-HAT can identify codimension-1 bifurcations linked with a cross through the unit circle of one or several eigenvalues, like ***saddle-node*** and ***period-doubling bifurcations***, which are of great interest in the study of the behavior of biped systems.

A short introduction of the theory and concepts of dynamic systems are

presented in Section 5.5 next, following the nomenclature in [268]. The solution for handling the numerical continuation for hybrid nonlinear dynamic systems implemented using the TC-HAT software is presented in Section 5.6 and Section 5.7. However, the complete theory, process and algorithms for the numerical continuation methods are not explained in detail in this thesis, but can be found in the related extensive literature [271–276, 278–281, 281, 282]. Furthermore, the explanation of the underlying problem of performing numerical continuation in hybrid systems, and the solution implemented in the softwares used in this thesis is detailed explained in [234, 267, 268, 270].

5.5 Theory and Concepts in Dynamical Systems

As a background source, this section presents some brief essential concepts and theory for the study and analysis of dynamical systems.

5.5.1 Smooth Dynamic Systems

In a formal generic description, a smooth dynamic system is defined over a ***state space*** (or ***phase space***) X of dimension n, with an associated vector-value function $\Phi\left(x,t\right) : X \rightarrow X$, known as the ***vector field***, where the evolution in time $t \in T$ of the states (x) of this dynamical system, map a point of the phase space X back into the phase space X.

The concept of smoothness varies depending on the type of state space X and time domain T. In the cases studied in this chapter, when T corresponds to the $\Re$ (reals), the dynamic system $\Phi(x,t)$ is named the ***flow***, and, when T corresponds to $\aleph$ (Integer) it is called a map.

Particularly for a vector field $f : R^n \rightarrow R^n$, the evolution in time of the state vector $x \in R^n$ is described by the differential equation

$$\frac{dx}{dt} = f(x) \tag{5.2}$$

A ***solution*** for the related system is a curve $x : R \rightarrow R^n$ known as a ***trajectory*** of the dynamic system, where the corresponding tangent vector at $x(t)$ is given by $f(x(t))$.

Furthermore, if $x(t_0) = x_0$ is known, x_0 is referred to as an ***initial condition*** at the ***initial time*** t_0.

5.5.2 Hybrid Dynamic Systems

A ***hybrid dynamic system***, (also named a ***picewise-smooth*** (PWS) ***hybrid system*** or the ***hybrid flow***) presents an evolution that includes both continues and discrete behavior in the dynamic system. The continuous dynamics (or ***flow*** of the system) are described by sets of differential equations, and the discrete state ***jumps*** (or ***maps***) are defined by difference or algebraic equations. Typically, hybrid systems are used for modeling mechanical impacts in dynamic systems, where they are also referred as ***impacting systems***. However, its applications have range from logic and nonlinear electrical circuit elements [283] to the modeling of the behavior of biomolecular reactions [284]. The formal definition of a hybrid system will be presented, as used by Thota in [267, 268], when implementing the changes in AUTO97 that derived in the development of TC-HAT.

As in smooth dynamics systems, a formal generic description for the hybrid dynamic systems is defined over a ***state space*** (or ***phase space***) X of dimension n, with an associated ***hybrid flow function*** $\Phi_m(x,t) : X \to X$, corresponding to the ***vector field*** f_m, parameterized by an ***index vector*** I in some ***finite set*** F.

In addition, for each value of the index vector I there exists an associate smooth ***event function*** $h_I : X \to \Re$ and a corresponding smooth ***state jump function*** $g_I : X \to X$.

Consequently, one ***solution*** to the corresponding hybrid dynamic system will correspond to a sequence $\{x_j : (t_{j-1}, t_j] \to X\}_{j=1}^{m}$ of m smooth curves and an associated sequence $\{I_j\}_{j=1}^{m}$, such that $I(t) = I_j, t \in (t_{j-1}, t_j]$.

The previous definition also implies that the resultant tangent vector at $x_j(t)$ corresponds to $f_{I_j}(x_j(t))$ and in the case in which $X = \Re^n$

$$\frac{d}{dt}x_j(t) = f_{I_j}(x_j(t)) \tag{5.3}$$

Furthermore, the j–th segment must terminate at an intersection with the ***event surface*** such that

$$\{x | h_{I_j}(x) = 0, h_{I_j,x}(x) \cdot f_{I_j}(x) \leq 0\} \tag{5.4}$$

meaning,

$$h_{I_j}(x_j(t_j)) = 0 \tag{5.5}$$

Finally, the connectivity between the j–th and $j+1$–th segments are given by the function g_{I_j}, as in

$$g_{I_j}(x_j(t_j)) = \lim_{t \to t_{j+1}} x_{j+1}(t) \tag{5.6}$$

Moreover, the sequence $\sum = \{I_j\}_{j=1}^{m}$ of values of the index vector I in some finite set F, is named ***the solution's signature***, as in [267, 268]. The previous definition and nomenclature used to express the hybrid dynamic system will be applied when implementing the biped model in the TC-HAT software in Section 5.7.

5.5.3 Stability in Dynamic Systems

Local Stability

Extending the definitions of stability given in Section 2.3.1, formally, the stability of a trajectory solution related to a known dynamic system is described by the behavior of its neighboring trajectories. Particularly, a solution $x(t)$ of a time continuous dynamic system is held to be ***stable in the sense of Lyapunov*** in the interval $[t_0, \infty)$ if $\forall\ \varepsilon > 0$, $\exists$ a $\delta(\varepsilon) > 0$ such that any other solution $\tilde{x}(t)$ for which $\|x(t_0) - \tilde{x}(t_0)\| < \delta(\varepsilon)$ assures $\|x(t) - \tilde{x}(t)\| < \varepsilon$, $\forall\ t \geq t_0$.

Likewise, a solution x_i of a discrete dynamic system is held to be ***stable in the sense of Lyapunov*** in the interval $[k, \infty)$ if $\forall \varepsilon > 0$, $\exists$ a $\delta(\varepsilon) > 0$ such that any other solution $\tilde{x}_i$ for which $\|x_k - \tilde{x}_k\| < \delta(\varepsilon)$ assures $\|x_i - \tilde{x}_i\| < \varepsilon$, $\forall\ i \geq k$.

A solution that does not comply with Lyapunov stability, is held to be ***unstable in the sense of Lyapunov***. Furthermore, if in addition of being Lyapunov stable, the solution complies with

$$\lim_{t \to \infty} \|x(t) - \tilde{x}(t)\| = 0 \tag{5.7}$$

for time continuous dynamics systems or

$$\lim_{i \to \infty} \|x_i - \tilde{x}_i\| = 0 \tag{5.8}$$

for discrete time dynamics systems, the solution is held to be ***asymptotically stable in the sense of Lyapunov***.

Cyclic Stability

Similarly, extending the definition of Section 2.3.1, a more formal presentation for cyclic stability arrives from a weaker definition of stability than the one given previously for local stability. The cyclic stability is also known as ***orbital stability***, or ***stability in the Poincaré sense***.

For that, the solution $x(t)$ of a time continuous dynamic system is held to be ***orbitally stable*** in the interval $[t_0, \infty)$ if $\forall \varepsilon > 0$, $\exists$ a $\delta(\varepsilon) > 0$ such that any other solution $\tilde{x}(t)$ for which $d(\tilde{x}(t_0), x([t_0, \infty))) < \delta(\varepsilon)$ assures $d(\tilde{x}(t), x([t_0, \infty))) < \varepsilon$, $\forall t \geq t_0$, where, $d(y, x([t_0, \infty)))$ represents the closest distance between a point y and the trajectory $x(t)$.

Likewise, a solution x_i of a discrete dynamical system is held to be ***orbitally stable*** in the interval $[k, \infty)$ if $\forall \varepsilon > 0$, $\exists$ a $\delta(\varepsilon) > 0$ such that any other solution $\tilde{x}_i$ for which $d(\tilde{x}_k, x_{[t_0,\infty)}) < \delta(\varepsilon)$ assures $d(\tilde{x}_i, x_{[t_0,\infty)}) < \varepsilon$, $\forall i \geq k$.

A solution that does not comply with orbital stability is held to be ***orbitally unstable***. Furthermore, if in addition of being orbitally stable, the solution complies with

$$\lim_{t\to\infty} d(\tilde{x}(t), x([t_0, \infty))) = 0 \tag{5.9}$$

for time continuous dynamics systems or

$$\lim_{i\to\infty} d(\tilde{x}_i, x_{[k,\infty)}) = 0 \tag{5.10}$$

for discrete time dynamics systems, the solution is held to be ***asymptotically orbitally stable***.

5.6 Modeling of 2D Biped with Knees for Continuation Analysis

Following the previous idea, of using numerical continuation to analyze the evolution of the biped system, requires the use of a simplified model of the GIMBiped system, since the continuation process of nonlinear dynamics is very demanding task for complex systems.

As reviewed in Section 4.2, many different types of simplified models of passive bipeds have been studied in detail. For a realistic application of the resulting values of the experiments, as indicators for controlling the real hardware GIMBiped, the target model should contain sufficient detail in order to predict the behavior of the real system and at the same time be simple enough to be able to run adequately the continuation process. This chapter uses the same model as the one presented in Section 4.2, where the GIMBiped is approximated by a planar biped model with knees and point feet (Figure 4.3), assuming instantaneous and inelastic collisions in the FS and KL.

As seen before, this model is a hybrid dynamic system and includes continuous dynamics equation and algebraic equations. The continuous dynamic equation corresponds to the 3-link phase when the knee is unlocked and to the 2-link phase when the knee is locked. The algebraic equations map the state jumps in the impact events at the knee lock and foot strike with the floor, where instantaneous changes in velocity are observed (Figure 4.4).

5.7 The Mathematical Model in TC-HAT

A drawback of using the TC-HAT software is that, given that it is based on AUTO97 software, it uses the same implicit form for inputting the different systems' smooth differential equation, as in:

$$\dot{x} = f(x, \lambda) \tag{5.11}$$

where x represents the states and λ the parameters. In the case of the biped model introduced in Section 4.2, there are two smooth differential equations representing the 3-link stage (Eq. 4.1) and the 2-link stage (Eq. 4.5). Both equations are in the standard form of the equation of motion with nonlinear and coupled elements present in the mass $M(q)$, Coriolis $V(q, \dot{q})$ and gravity matrix $G(q)$, and to obtain the implicit form required in Eq. 5.11 involves solving:

$$\ddot{q} = M^{-1}(q)(\tau - V(q, \dot{q}) - G(q)) \tag{5.12}$$

which is not trivial for this case, and the inversion of $M(q)$ may often lead to singular values. For solving this issue, a patch to TC-HAT was implemented in this study, which computes the result of the standard equation of motion in Eq. 5.12 for both smooth differential equations (3-link and 2-Link stage) of the biped hybrid model.

In each iteration and stages of the continuation algorithm, the patch uses FORTRAN-written LAPACK routines to solve Eq. 5.12. Specifically, the patch uses LU decomposition with partial pivoting and row interchanges to factor $M^{-1}(q)$ and then solve the resulting system of equations. The optimized functions in LAPACK allow the previous problem to be solved with relatively low extra computational cost. The solution to Eq. 5.12 is calculated using the matrices $M_{\text{3-link}}(q)$, $V_{\text{3-link}}(q, \dot{q})$, $G_{\text{3-link}}(q)$, $M_{\text{2-link}}(q)$, $V_{\text{2-link}}(q, \dot{q})$ and $G_{22\text{-link}}(q)$ for the 3-link and 2-link stage respectively, derived in the previous Section 4.2.

The author recommends this patch, or this way of approaching the solution of the equation of motion in the continuation analysis, to any research that may face interesting robotics problems that are expressed in this form with coupled state variables. The code of the patch is not annexed in this thesis, due to its length; however, it is available to download in [60].

Once the solution for the values needed in Eq. 5.12 is obtained, the dynamics of the biped may be reformulated, as a hybrid dynamical system, in the following way.

Denote the state vector x, where $x_1 = q_1$ angular displacement of the stance leg, $x_2 = q_2$ angular displacement of the upper link (thigh) of the swing leg, $x_3 = q_3$ angular displacement of the lower link (shank) of the swing leg and $x_4 = \dot{q}_1$, $x_5 = \dot{q}_5$ and $x_6 = \dot{q}_3$ their respective derivatives (Figure 4.3).

Three distinct vector fields are required to describe the rate of change of the state vector with respect to time, during 3-Link, 2-Link, and falling stages respectively, namely:

$$f_{\text{3-link}}(x) = \begin{pmatrix} f^1_{\text{3-link}}(x) = x_4 \\ f^2_{\text{3-link}}(x) = x_5 \\ f^3_{\text{3-link}}(x) = x_6 \\ f^4_{\text{3-link}}(x) = \ddot{q}_{1,\text{3-link}} \\ f^5_{\text{3-link}}(x) = \ddot{q}_{2,\text{3-link}} \\ f^6_{\text{3-link}}(x) = \ddot{q}_{3,\text{3-link}} \end{pmatrix} \tag{5.13}$$

$$f_{\text{2-link}}(x) = \begin{pmatrix} f^1_{\text{2-link}}(x) = x_4 \\ f^2_{\text{2-link}}(x) = x_5 = x_6 \\ f^3_{\text{2-link}}(x) = x_5 = x_6 \\ f^4_{\text{2-link}}(x) = \ddot{q}_{1,\text{2-link}} \\ f^5_{\text{2-link}}(x) = \ddot{q}_{2,\text{2-link}} = \ddot{q}_{3,\text{2-link}} \\ f^6_{\text{2-link}}(x) = \ddot{q}_{2,\text{2-link}} = \ddot{q}_{3,\text{2-link}} \end{pmatrix} \tag{5.14}$$

$$f_{Fall}(x) = \begin{pmatrix} NaN \\ NaN \\ NaN \\ NaN \\ NaN \\ NaN \end{pmatrix} \tag{5.15}$$

Where $\ddot{q}_{1,\text{3-link}}$, $\ddot{q}_{2,\text{3-link}}$, $\ddot{q}_{3,\text{3-link}}$, $\ddot{q}_{1,\text{2-link}}$, $\ddot{q}_{2,\text{2-link}}$ and $\ddot{q}_{3,\text{2-link}}$ are the components of the solution vector of Eq. 5.12 for the 3-Link and 2-Link stages, respectively.

NaN (***Not a Number***) indicates that the system has reached the falling state, and, once there, it cannot recover. In practice, reaching this state from direct forward simulation will halt the model; however, grazing incidents can be detected to this surface based on the continuation process.

Transitions between distinct phases of motion are governed by nine event functions. One event represents the Foot Strike (FS) and another

one the Knee Lock (KL), which, with the correct initial conditions (ICs), will lead to LC.

Other six event functions represent different ways in which the biped can become unstable, leaving one last event function corresponding to the constant state of falling. Figure 5.1 illustrates the transitions between events, and Table 5.1 summarizes all the events and their conditions.

$$\begin{aligned} h_{FS} = \tan(\gamma)(-L\cos(x_1) + (a_3 - b_3)\cos(x_2) + (a_4 - b_4)\cos(x_3)) \\ + L\sin(x_1) - (a_3 - b_3)\sin(x_2) - (a_4 - b_4)\sin(x_3) \end{aligned} \tag{5.16}$$

$$h_{KL} = x_3 - x_2 \tag{5.17}$$

$$h_{F1} = \begin{cases} x_3 - x_2 & \text{if } x_1 \leq x_2, \\ \neq 0 & \text{otherwise.} \end{cases} \tag{5.18}$$

$$h_{F2} = \begin{cases} h_{FS} & \text{if } x_1 \neq x_2, \\ \neq 0 & \text{otherwise.} \end{cases} \tag{5.19}$$

$$h_{F3} = x_1 - \gamma \tag{5.20}$$

$$h_{F4} = \begin{cases} h_{FS} & \text{if } x_1 = x_2 \text{ and } x_1 - x_2 < \varepsilon, \\ \neq 0 & \text{otherwise.} \end{cases} \tag{5.21}$$

$$h_{F5} = x_2 \tag{5.22}$$

$$h_{F6} = \pi - x_1 \tag{5.23}$$

$$h_{F7} = \begin{cases} NaN & \text{if } x_1 \text{ or } x_2 \text{ or } x_3 \text{ or } x_4 \text{ or } x_5 \text{ or } x_6 = NaN\ , \\ \neq 0 & \text{otherwise.} \end{cases} \tag{5.24}$$

Three state jump junctions finalize the connectivity graph, which is presented in Figure 5.2 and given by Eqs. 5.25-5.27.

$$g_{HS} = \begin{pmatrix} g^1_{HS}(x) = x_2 = x_3 \\ g^2_{HS}(x) = x_1 \\ g^3_{HS}(x) = x_1 \\ g^4_{HS}(x) = \dot{q}^+_{1,HS} \\ g^5_{HS}(x) = \dot{q}^+_{2,HS} \\ g^6_{HS}(x) = \dot{q}^+_{3,HS} \end{pmatrix} \tag{5.25}$$

Table 5.1. Event table for the model in TC-HAT

Events	**Abrev.**	**Description of the event**	**Flow of origin**	**Triggered event**
From 3-link stage				
Knee Lock	KL	Knee impact	$f_{\text{3-link}}(x)$	$h_{KL} \to g_{KL}$
Fall 1	F_1	KL before passing the stance foot	$f_{\text{3-link}}(x)$	$h_{F1} \to g_{Fall}$
Fall 2	F_2	FS in 3-Link stage	$f_{\text{3-link}}(x)$	$h_{F2} \to g_{Fall}$
Fall 3	F_3	Biped fall backwards	$f_{\text{3-link}}(x)$	$h_{F3} \to g_{Fall}$
From 2-link stage				
Foot Strike	FS	Foot (heel) impact	$f_{\text{2-link}}(x)$	$h_{FS} \to g_{FS}$
Fall 4	F_4	FS when $\phi < \varepsilon$[a]	$f_{\text{2-link}}(x)$	$h_{F4} \to g_{Fall}$
Fall 5	F_5	Abnormal high swing leg	$f_{\text{2-link}}(x)$	$h_{F5} \to g_{Fall}$
Fall 6	F_6	Biped fall forward	$f_{\text{2-link}}(x)$	$h_{F6} \to g_{Fall}$
From fall stage				
Fall 7	F_7	Falls continue from falling stage	$f_{Fall}(x)$	$h_{F7} \to g_{Fall}$

[a] ϕ = Angle between stance leg and swing leg (inner angle), ε = threshold for small inner leg angle so the gait is considered unstable (unrealizable).

$$g_{KL} = \begin{pmatrix} g^1_{KL}(x) = x_1 \\ g^2_{KL}(x) = x_2 = x_3 \\ g^3_{KL}(x) = x_3 = x_2 \\ g^4_{KL}(x) = \dot{q}^+_{1,KL} \\ g^5_{KL}(x) = \dot{q}^+_{2,KL} \\ g^6_{KL}(x) = \dot{q}^+_{3,KL} \end{pmatrix} \tag{5.26}$$

$$g_{Fall} = \begin{pmatrix} NaN \\ NaN \\ NaN \\ NaN \\ NaN \\ NaN \end{pmatrix} \tag{5.27}$$

where $\dot{q}^+_{1,HS}$, $\dot{q}^+_{2,HS}$, $\dot{q}^+_{3,HS}$, $\dot{q}^+_{1,KL}$, $\dot{q}^+_{2,KL}$ and $\dot{q}^+_{3,KL}$ are the components of the solution vector of Eq. 4.9 and Eq. 4.12 for the knee lock and foot strike stages, respectively. A full description of the impact dynamics and its matrices is presented in Section 4.2.1.

Now let

$$Z_f = \{\text{3-link}, \text{2-link}, Fall\} \tag{5.28}$$

$$Z_h = \{HI, KI, F1, F2, F3, F4, F5, F6, F7\} \tag{5.29}$$

$$Z_g = \{HS, KL, fall\} \tag{5.30}$$

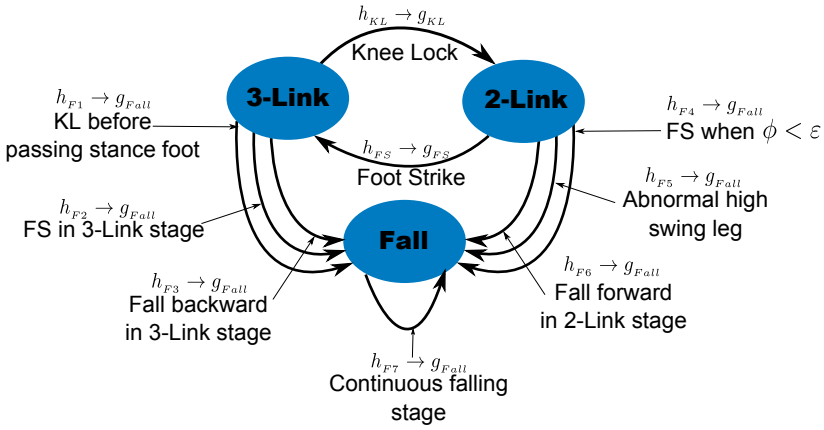

Figure 5.1. State diagram for the event transitions between continuous dynamics of the biped model in TC-HAT

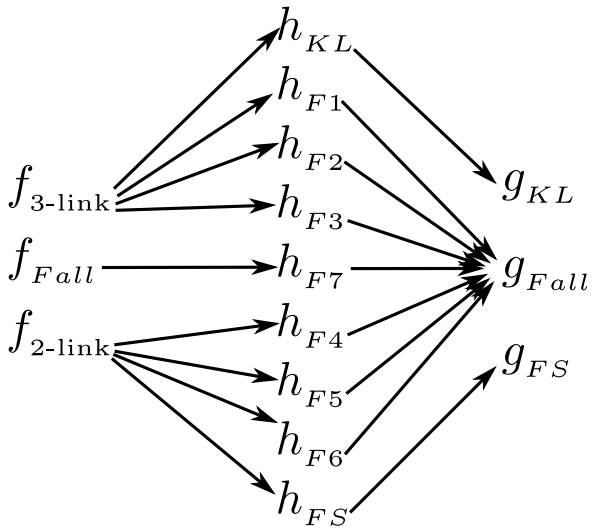

Figure 5.2. Connectivity graph between vector fields, event detection functions and jump state functions of the biped model in TC-HAT

and suppose that $\Im$ is the subset of Z_f,Z_h,Z_g corresponding to the connectivity graph in Figure 5.2 presenting the connections linking a specified vector field, the event functions that are checked during forward simulation of the corresponding vector field, and the state jump function related with the given event function. For instance, $I = (\text{3-link}, KI, KL)$ corresponds to a trajectory segment given by the vector field $f_{\text{3-link}}$ (3-link biped dynamic), terminating on the event surface h_{KL} (knee impact detection), and connected to the next trajectory segment by the state jump function g_{KL} (knee lock state jump map). For the conditions assumed in this study, every segment of a trajectory of the hybrid dynamic system describing the possible biped walking evolution matches one of the next index vectors:

$$J_1 = (\text{3-link}, KI, KL) \tag{5.31}$$

$$J_2 = (\text{3-link}, F1, fall) \tag{5.32}$$

$$J_3 = (\text{3-link}, F2, fall) \tag{5.33}$$

$$J_4 = (\text{3-link}, F1, fall) \tag{5.34}$$

$$J_5 = (\text{2-link}, HI, HS) \tag{5.35}$$

$$J_6 = (\text{2-link}, F4, fall) \tag{5.36}$$

$$J_7 = (\text{2-link}, F5, fall) \tag{5.37}$$

$$J_8 = (\text{2-link}, F6, fall) \tag{5.38}$$

$$J_9 = (Fall, F7, fall) \tag{5.39}$$

Furthermore, the cyclic signature of a periodic trajectory is specified by

the periodic repetition of some finite sequence $\left\{J_{k_j}\right\}_{j=1}^{m}$ for a finite succession $\{k_j\}_{j=1}^{m}$. For the particular case of the biped model, a periodic trajectory with signature $\{J_1, J_5\}$ corresponds to the LC of interest in bipedal walking, and it is defined by the boundary-value problem (BVP) given by:

$$\dot{x}_{J_1}(t) = f_{\text{3-link}}(x_{J_1}(t)), t \in [t_0, t_1] \tag{5.40}$$

$$\dot{x}_{J_5}(t) = f_{\text{2-link}}(x_{J_5}(t)), t \in [t_1, t_2] \tag{5.41}$$

$$h_{KI}(x_{J_1}(t_1)) = 0 \tag{5.42}$$

$$h_{HI}(x_{J_5}(t_2)) = 0 \tag{5.43}$$

$$x_{J_5}(t_1) = g_{KL}(x_{J_1}(t_1)) \tag{5.44}$$

$$x_{J_1}(t_0) = g_{HS}(x_{J_5}(t_2)) \tag{5.45}$$

The previous equations and conditions represent all the necessary information to build the numerical continuation process in TC-HAT. The source code for the implementation and simulations performed in this chapter can be found in [60].

5.8 Numerical Continuation Experiments and Analysis

The experiments performed in this section used the set of parameters indicated as Set_{Start} in Table 5.2 as the starting point of the numerical continuation. These parameters are the same as the ones in $Set1$ in Table 4.1, used for generating a *favorable* LC trajectory for the model-based controllers in Chapter 4. The reason to choose these parameters was the need for a starting trajectory originating from natural LC that would present reasonable foot clearance, speed and step length.

As previously mentioned in Section 4.2.1, the process for finding the LC itself for a particular set of parameter configuration is a very challenging task, which usually relies on manual iteration with the help of some optimization tools for finding the appropriate ICs that will lead to LC for a given set of parameters. In Chapter 4, the process used to find such set of parameters and ICs was indeed a manual iterative process. In that case, non-linear optimization tools from MATLAB were used to search for the IC when the parameter sets were fixed. The goal in that case was to search and find LCs with parameter sets close to an approximated planar 3-Link model of the GIMBiped in Figure 4.1 and Figure 4.3. Table 4.1 shows the values found and used in Chapter 4, based on the approximated planar 3-Link model of the GIMBiped.

Table 5.2. Model parameters used during continuation process

Parameters	**Symbol**	Set_{Start}	$Set_{GIMBiped}$
Leg Length	$L\ (m)$[a]	0.900	0.900
Shank lower length	$a_1\ (m)$[b]	0.22575	0.22575
Shank upper length	$b_1\ (m)$[b]	0.22425	0.22425
Thigh lower length	$a_2\ (m)$[b]	0.26510	0.26510
Thigh upper length	$b_2\ (m)$[b]	0.18490	0.18490
Shank Mass	$m_1\ (kg)$[b]	1.50	7.584
Thigh Mass	$m_2\ (kg)$[b]	16.33	9.812
Hip Mass	$m_H\ (kg)$	10.0	7.30
Slope Angle	$\gamma\ (rad)$	0.10996	–

[a] $L = a_1 + a_2 + b_1 + b_2 = a_3 + a_4 + b_3 + b_4$.

[b] The model used in this chapter assumes symmetry, therefore $a_4 = a_1$ $a_3 = a_3$, $b_4 = b_1$, $b_3 = b_2$, $m_4 = m_1$ and $m_3 = m_2$

Since the manual process performed previously for finding natural LC with similar parameters as the GIMBiped was not completely successful (given that some of the model's parameter values were still far from the real ones), in this chapter the process will be automated using the TC-HAT software tool. This study is performed to further clarify if the failure in the previous section was due to lack of proper search (algorithm), or if the system itself does not present stable or *favorable* LC with this particular configuration. Therefore, the goal is to get as close as possible to the real values of the GIMBiped and analyze the behavior of the LCs that are generated.

Furthermore, the numerical continuation process will allow for different configurations to be tested without the burden of heavy iterative computations and also to correctly characterize the stability of the cyclic trajectories, thanks to the proper computation of the Floquet Multipliers.

5.8.1 Scope of the Continuation Process

In this chapter, the study of the evolution of LCs and bifurcations started from the Set_{Start} of parameters' value presented in Table 5.2, corresponding to $Set1$ used in Chapter 4. This set was used to generate *favorable*, natural-looking walking pattern, derived from an LC that can be reached

Table 5.3. Initial conditions for the first iteration of the continuation process

State Variables	**Symbol**[a]	Set_{Start}
Stance leg angle	x_1 (rad)	1.36201
Thigh angle	x_2 (rad)	1.99949
Shank angle	x_3 (rad)	1.99949
Stance leg angular velocity	x_4 (rad/s)	1.33654
Thigh angular velocity	x_5 (rad/s)	-9.34594
Shank angular velocity	x_6 (rad/s)	-9.34594

[a] The state variables of the model used in TC-HAT relate to the model presented in Chapter 4 as: $x_1 = q_1$, $x_2 = q_2$, $x_3 = q_3$, $x_4 = \dot{q}_1$, $x_5 = \dot{q}_2$ and $x_6 = \dot{q}_3$

using the ICs presented in Table 5.3.

It must be noted that TC-HAT can perform numerical continuation of this type of hybrid dynamic system, but it cannot find steady states or stable orbits in the systems. Such trajectory solutions must be given as input to the software and, once it has this information, it can further characterize its stability (based on the principles mentioned in Section 5.5.3), and perform the continuation process. Therefore, the initial trajectory solution must be computed elsewhere, and in this case it was computed in MATLAB with the IC and parameters presented in Table 5.3 and Table 5.2, respectively. This initial solution must be inputted in a specific manner as indicated in [267], with proper sampling and segments separation.

The starting trajectory (or initial solution found with the parameters and IC in Set_{Start}), according to the analysis performed in MATLAB, was allegedly stable. The stability in the MATLAB software was evaluated using the common (not corrected) monodromy matrix (a simple Jacobian matrix of the parameters' variations), and in this case it presented all their eigenvalues within the unit circle. Additionally, an ideal biped simulator (ideal model without external disturbances) could perform more than 100 steps with these parameters and ICs without falling.

Nonetheless, as it will be shown later, this initial trajectory was actually unstable, according to the characterization of the correctly calculated Lyapunov Exponents (Floquet Multipliers). This however, does not mean

that the trajectory is not *"useful"*, since it is capable of taking several hundreds of steps before leaving the constant cyclic trajectory (under ideal conditions without external disturbances). This brings again the subject of proper classification of stability of a system, since there may be different *"levels"* or *"degrees"* of instability. Some indication of this degree of instability can be seen from the size of the Floquet Multipliers; however, due to the nonlinear nature of the system this cannot be analytically transfered to a trusted index of instability, and therefore experience and specific analysis must be used and applied for the correct interpretation of these values.

Therefore, it must be emphasized that if the system is denoted as unstable, under the previously stated criterion (see Section 5.5.3), the only assured consequence is that the solution will eventually naturally deviate from the initial cyclic trajectory. However, it is not stated how or when this will happen. Consequently, these cyclic trajectories can still be relatively easy to maintain if proper control is applied (as in Chapter 4). However, further characterizations, like controllability of the system using certain trajectories, fall outside the scope of the study performed in this chapter.

Likewise, as in *"degrees of instabilities"*, the stability itself of the trajectories can be further characterized by the strength of the attractor, in this case the LC. This can be defined by the ***basin of attraction*** (see Section 2.3.1), which is usually iteratively computed based on the forward integration of the equations of the system. As before, the stability characterization, according to the criterion in Section 5.5.3, will only indicate that under ideal conditions and without external disturbances the initial cyclic trajectory will be maintained indefinitely. That does not indicate how sensitive the system is with regard to external disturbances or how far the ICs can deviate from the ideal trajectory and still fall into the LC. Such characterization is given by the basin of attraction, and its computation and analysis also falls outside the scope of this study.

5.8.2 Characteristics of the Target LC: Overview

Now that the scope of this study has been delimited, the analysis of the results can start by observing the characteristics of the LC in the phase plane.

The basic characteristics and behavior of the LC of the 2D biped model with knees and point feet has been presented in Section 4.2.1. In Section 4.2.1 the focus was to explain the evolution of the state variables in time.

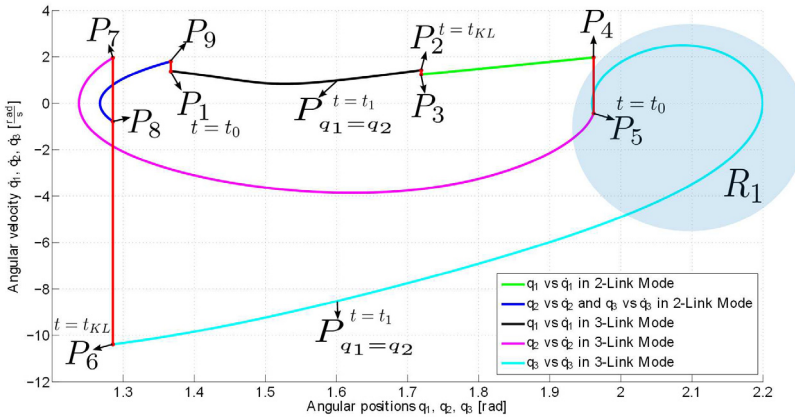

Figure 5.3. Initial Limit Cycle for the 3-link planar biped model with knees and point feet using parameters in Set_{Start} of Table 5.2 and ICs from Table 5.3

The plot in Figure 4.4, presented earlier the natural LC of the model using the parameters in *Set1* of Table 4.1. As mentioned previously, these parameters are the same as the ones in Set_{Start} in Table 5.2, and the plot was obtained using the ICs in Table 5.3. The same plot from Figure 4.4 is reproduced now in Figure 5.3, with other markers to explain further characteristics that can be observed.

As before, the state jumps representing the impacts are indicated by the red lines in Figure 5.3, and the gait starts at $t = t_0$ with the 3-link phase, in which the swing leg is located behind the stance leg. P_1 is the starting point for state variables q_1 and $\dot{q_1}$, and P_5 is the starting point for the remaining state variables q_2, $\dot{q_2}$, q_3 and $\dot{q_3}$.

With some practice and experience attained by constantly looking at these type of plots, the behavior of the system can be evaluated visually and some priori analysis can be done with this plot.

For example, the region circled with R_1 indicates how much the swing shank bends when the gait starts. Also, remembering that the state vector $x = q$, as indicated in Section 5.7, the angle difference in x_1 between point P_1 and P_5 indicates the length of the step. The actual value in m can be calculated by $2Lcos(x_1(P1) - \gamma)$ where $x_1(P1)$ is the q_1 angle at the beginning of the step in the point P_1.

Another important feature to notice is that the q_1 angle is continuously increasing during the step cycle, while both q_2 and q_3 usually change directions during the cycle, indicating some swing around different angular values.

A crucial point to observe is the instant of the knee lock event. The trajectory from point P_1 to point P_2 in q_1 corresponds to the phase previous to the knee lock. During the same phase, prior to KL, when q_2 travels from P_5 to P_6, it will eventually have the same angle as q_1. To avoid foot scuffing, at the instant in which $q_1 = q_2$, at $t = t_1 > t_0$ and marked as $P_{q_1=q_2}$, it is necessary that q_3 presents a different value from the previous angles ($q_3 \neq q_1$, $q_3 \neq q_2$), otherwise both legs will straighten with the same angle with respect to the ground and the foot will scuff. The point in which $q_2 = q_3$ is marked in Figure 5.3 as P_6, P_7 and P_8 for q_2 and q_3 corresponds to the instant of the knee impact in the KL which happens at time $t = t_{KL} > t_1 > t_0$. In the same instant t_{KL}, q_1 jumps from P_2 and P_3. Therefore, to avoid foot scuffing, the points P_8 and P_3 should not be close to each other in the horizontal axis (q_1, q_2, q_3 values), otherwise potential scuffing may occur with all the points located at the same instant in $P_{q_1=q_2}$.

The distance from the ground to the swing foot when it passes the stance foot is known as ***foot clearance***, and it has also been used somehow as a measure of robustness of the system. The actual instant or configuration for which to calculate this point is still open for interpretation. Here it is defined as the distance from the foot to the surface when the swing foot passes the line perpendicular to the surface after it has crossed the stance leg. It can be calculated as:

$$D_{\text{Foot Clarence}} = L\sin(q_1) - (a_3 + b_3)\sin(q_2) - (a_4 + b_4)\sin(q_3) \qquad (5.46)$$

when

$$-L\cos(q_1) + (a_3 + b_3)\cos(q_2) + (a_4 + b_4)\cos(q_3) = 0 \qquad (5.47)$$

Finally, the blue line corresponds to the trajectories of q_2 and q_3 after the KL event in P_6, P_7 and P_8 and, depending on how far it extends to the left, indicates how far the swing foot overshoots the landing point (angle). The point of landing in the FS is indicated in the plot by the point P_9.

5.8.3 Energy Analysis in the LC

Figure 5.4 shows the evolution of the instantaneous energy (power) in one walking cycle for the LC, with ICs and parameters given by Set_{Start} in Table 4.1 and Table 5.2 respectively.

The plot in Figure 5.4 shows that the total energy remains constant, apart for the moment in which the knee impact (KL) occurs in point P_{KL} and also at the end of the cycle in P_{FS} when the the kinetic energy

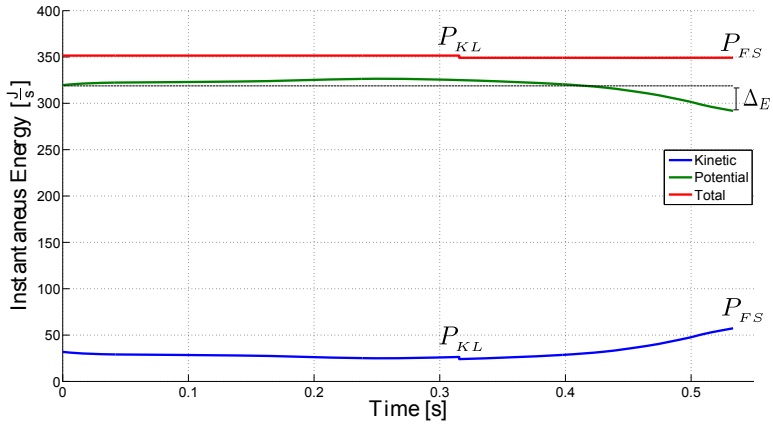

Figure 5.4. Instantaneous Energy (Power) for the Initial Limit Cycle of the 3-link planar biped model with knees and point feet using parameters in Set_{Start} of Table 5.2 and ICs from Table 5.3

presents another jump due to the impact in the FS. The energy dissipated in the impacts is compensated in the system by the potential energy gained by the biped when walking down the slope. The integration of this instantaneous energy in time (power) during a cycle corresponds to the total energy used by the system and is presented in the following continuation plots as an indicator of the efficiency of the biped.

There is a delicate balance between the kinetic energy dissipated in the impacts and the potential energy inputted in the system that drives the biped system to remain in a constant cycle (LC). Another way to interpret it is that the system must go back to its initial value, since the impact in the FS restores the original values of state variable q. So the cycle can repeat itself.

Since there should be a balance between the potential energy decrease of the system and the energy dissipated in the impact to maintain the cyclic behavior, the sum of the energy jumps at point P_{KL} (corresponding to the energy dissipated in the KL), and at point P_{FS} (corresponding to the energy dissipated in the heel strike) should add the same amount as the potential energy difference between two consecutive steps. Therefore, the total energy used in one step can also be calculated as the difference in potential energy between two consecutive steps (ΔE in Figure 5.4).

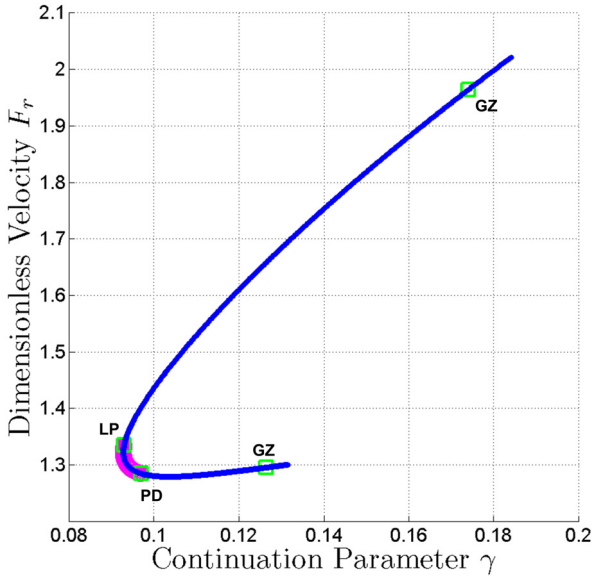

Figure 5.5. Froude Number for continuation in γ from the original parameters values in $Set_{_{Start}}$ of Table 5.2 and ICs from Table 5.3

5.8.4 Continuation in γ for $Set_{_{Start}}$

The first continuation process performed was with respect to the inclination of the surface γ. The continuation performed in this parameter will relate to the amount of energy inputted to the system. Steeper slopes will generate faster motions and higher energy dissipation in the impact, meaning that more energy is being inputted into the system.

In Figure 5.5, the dimensionless velocity F_r is plotted against the continuation parameter γ. The ***LP*** point indicates a ***saddle-node bifurcation*** (also known as ***limit-point*** or ***fold bifurcation***). The ***PD*** point indicates a ***period-doubling bifurcation***, and the point ***GZ*** indicates a ***grazing*** incident that in this case corresponds to a periodic trajectory reaching grazing contact with the event surface given by F_2.

As presented in Section 5.7, F_2 corresponds to the falling event in which the foot scuffs the floor, meaning that the FS event happened before the 2-link phase (or before locking the knee).

The continuation process showed in the plot from Figure 5.5 started at $\gamma = 0.1099557rad \approx 6.3°$ (in the point $P_{_{start}}$) with a negative value for the AUTO parameter ***DS***, which is the initial step size for the bifurcation calculation. The sign of ***DS*** indicates the direction to change the parameter. Given that the step size is adaptive, the value of ***DS*** is just an initial

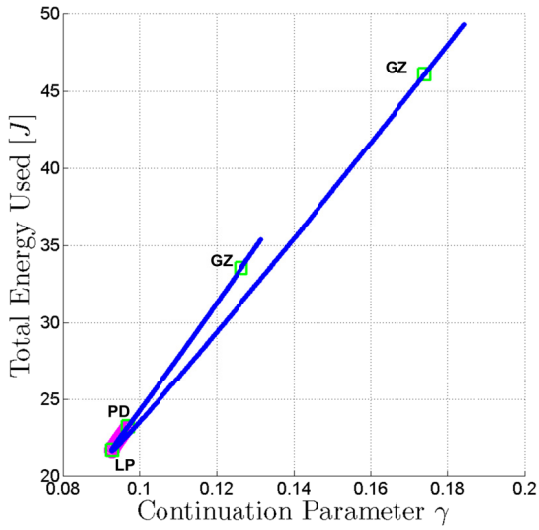

Figure 5.6. Total Energy for continuation in γ from the original parameters values in Set_{Start} of Table 5.2 and ICs from Table 5.3

suggestion.

The continuation process starts decreasing from the original value, passing through a ***PD*** bifurcation at $\gamma = 0.0969668rad \approx 5.56°$, where it enters into a region of stability indicated with the color magenta in the plot. The region evolves until a ***LP*** bifurcation at $\gamma = 0.0929538rad \approx 5.33°$, where the continuation interval ***DS*** changes sign and the trajectories become unstable and start growing on γ again. The curve finally ends in a ***grazing incident*** at $\gamma = 0.174037rad \approx 9.97°$, with the event F_2 of foot scuffing.

The continuation then is performed for the positive side of the original value of $\gamma = 0.1099557rad$, and the rest of the curve is plotted where another ***grazing incident*** is found at $\gamma = 0.126381rad \approx 7.24°$. This plot indicates that there are at least two walking patterns, with different walking velocities, for each value in $\gamma > 0.0929538rad$, and that the range from which stable cycles can be found for this set of parameters is very small $[5.33° - 5.56°]$.

The same continuation process can be seen also for a plot of the ***Energy*** vs γ in Figure 5.6. It is interesting to note that the curve branch which spends more energy is the side which presents the lower dimensionless velocity. As said before, the increase in velocity causes increase in the energy dissipated in the impacts, which is appreciated in the crescent shape of both branches. However, different characteristics of both gaits in the different branches may be the reason for the difference in energy

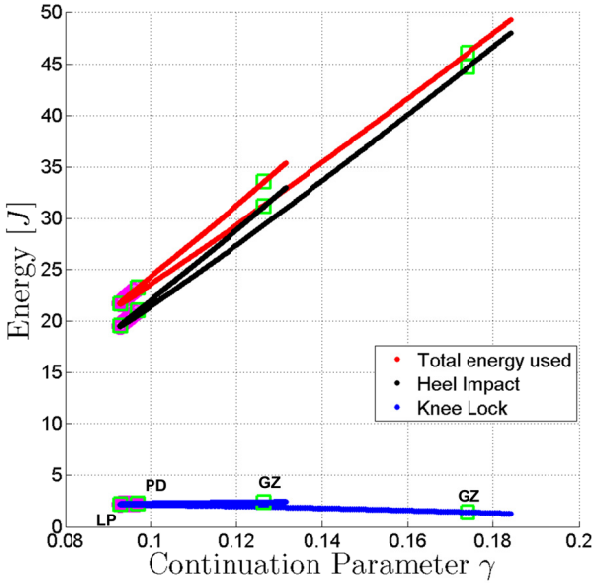

Figure 5.7. Energy consumed in the Heel Impact and in the Knee Lock for continuation in γ from the original parameters values in Set_{Start} of Table 5.2 and ICs from Table 5.3

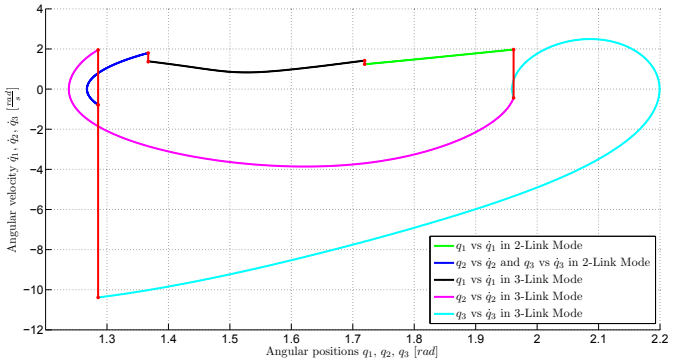

Figure 5.8. Stable LC found once continuation was performed. The LC in the figure is a stable cycle in the middle of points PD and LP, with $\gamma = 0.0935524rad \approx 5.36^{\circ}$ in the continuation curve performed for the angle γ.

expenditure between branches.

More complete information about the energy consumed by the impacts for continuation in γ can be seen in Figure 5.7, where it can be observed that most of the energy is attributed to the heel impact in the FS event. Also it can be observed that the energy in the KL in the longer branch is decreasing as γ is increasing, meaning that the KL in that branch is taking place with slower velocities compared with the other branch. For comparing stable and unstable trajectories, Figure 5.8 presents the LC of

Table 5.4. Floquet multipliers for the LCs with $\gamma = 0.109956rad$ and $\gamma = 0.0935524rad$, and with parameters values in $Set_{_{Start}}$ of Table 5.2 and IC [a] and [b]

Multiplier number	Multiplier value $\gamma = 0.109956rad$[a] Real	Im.	Multiplier value $\gamma = 0.0935524rad$[b] Real	Im.
1	1.00000	0.00000	1.00000	0.00000
2	0.167233	0.167414	0.430760	−0.324114
3	0.167233	−0.167414	0.430760	0.324114
4	-6.19474×10^{-12}	0.00000	−0.448685	0.00000
5	-8.98409×10^{-17}	0.00000	-1.75744×10^{-11}	0.00000
6	0.00000	0.00000	0.00000	0.00000
7	0.00000	0.00000	4.71550×10^{-17}	0.00000
8	0.00000	0.00000	0.00000	0.00000
9	0.00000	0.00000	0.00000	0.00000
10	0.00000	0.00000	0.00000	0.00000
11	0.00000	0.00000	0.00000	0.00000
12	−2.76294	0.00000	0.00000	0.00000

With initial conditions:

[a] $IC_{\gamma=0.109956} = \begin{bmatrix} 1.3620125248 \\ 1.9994916146 \\ 1.9994916146 \\ 1.3365397508 \\ -0.93459364080 \\ -0.93459364080 \end{bmatrix}$ [b] $IC_{\gamma=0.0935524} = \begin{bmatrix} 1.3670215509 \\ 1.9616759897 \\ 1.9616759897 \\ 1.3870815271 \\ -0.43584533360 \\ -0.43584533360 \end{bmatrix}$

a trajectory inside the stable region with $\gamma = 0.0935524rad \approx 5.36°$, located between the ***PD*** and ***LP*** points in the continuation curve performed for the angle γ. As mentioned before, the starting cyclic trajectory with $\gamma = 0.1099557rad$ was not stable according to the characterizations of the corrected Floquet multipliers in TC-HAT, and it is interesting to see the difference between the trajectories from Figure 5.8 and Figure 5.3.

The Floquet multipliers of the LC trajectories plotted in Figure 5.3 and Figure 5.8 are presented in Table 5.4. From Table 5.4 it can be seen that the unstable characterization for the LC in Figure 5.3 arrives because of the real part of multiplier number 12. Furthermore, differences in the ICs can be seen reflected in the corresponding figures, where some structural differences are observed also in the cycles, like the different swing motion of the shank and the thigh when in 3-link mode. The 2-link phase also shows different behavior in both cycles. However, the previous differ-

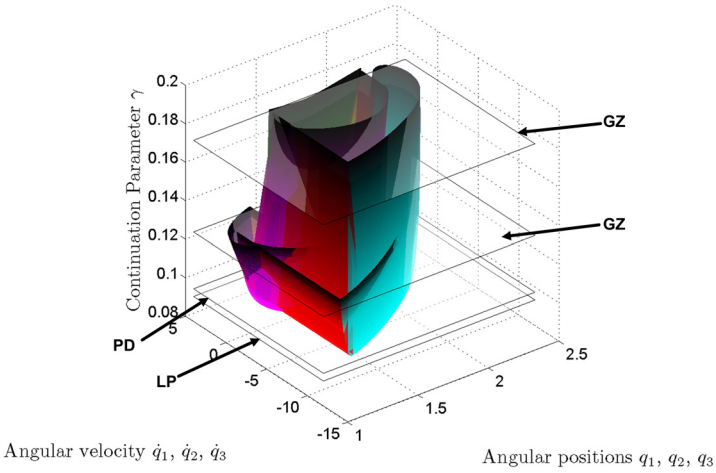

Figure 5.9. Surface plot of the evolution of the LC based on the continuation of parameter γ with parameters values in Set_{Start} of Table 5.2 and ICs from Table 5.3

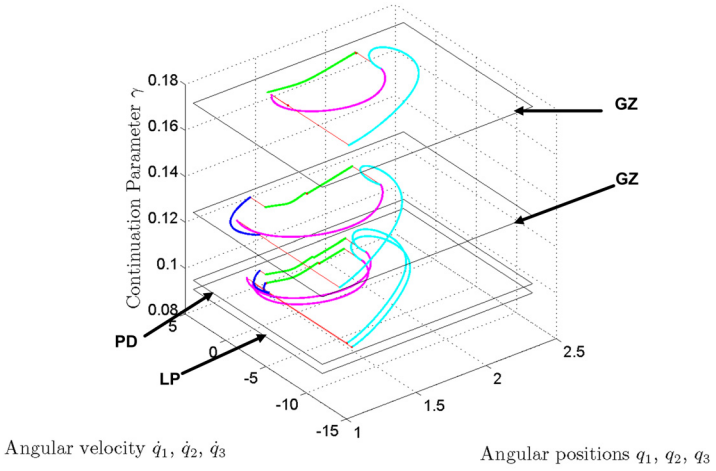

Figure 5.10. Evolution of the LC based on the continuation of parameter γ. Here only the special points in the continuation are plotted

ences do not generate dramatic changes in the gait, which could be clearly identified when running the forward (and graphical) simulator. The previous indicates already that slight unnoticed changes can greatly affect the stability of the system.

The complete information about the evolution of the LC shape in the continuation process, ran over the parameter γ, can be appreciated in Figure 5.9, where all the LCs are plotted as a surface in a 3D plot. The bifurcation points are presented as planes in the vertical axis.

Figure 5.10 shows a discrete version of Figure 5.9, where only the LC curves of the special points are presented in a slice-shaped 3D plot.

Figure 5.10 shows that the point of grazing bifurcation at $\gamma = 0.174037$ rad corresponds to the instant where the 3-link phase governs the entire gait. The KL occurs in the same instant of the FS; therefore, there is no more a 2-link mode, and foot scuffing takes place in the same instant on the FS. The feet consequently perform the FS in 3-link mode, which corresponds to event function detection number F_2.

On the other hand, for the grazing incident at $\gamma = 0.126381rad$, the LC in Figure 5.10 does not show any uncommon characteristics that may lead to the grazing incident indicated with the surface of F_2. However, running the result values in the biped simulator in MATLAB shows that the foot scuffing happens immediately after the first successful step. In other words, the biped manages to take one complete step with the given parameters and ICs. However, after the FS the velocities are not enough to carry on with the walking, and the biped scuffs the floor and collapses.

5.8.5 Two-Parameter Continuation in γ and m_1

Starting in this section, the goal of the following continuation processes was to approximate the initial parameter in $Set_{_{Start}}$ towards the "real" (approximated) parameters of the GIMBiped indicated as $Set_{_{GIMBiped}}$ in Table 5.2.

The first attempt in this task targeted the m_1 parameter, trying therefore to perform a two-parameters continuation process in m_1 and γ, where both parameters were free to change. The end purpose was to move m_1 from the value of 1.50 kg to 7.584 kg.

From the previous continuation curve of Figure 5.5, several two-parameters continuation for γ and m_1 can be performed, and Figure 5.11 shows the evolution of the Froude number in a 3D plot against γ and m_1, starting from the curve in Figure 5.5.

From the point ***GZ*** with $\gamma = 0.174037rad$ in Figure 5.5, a grazing curve was computed. The curve represents all points where the model achieves grazing contact with the event surface F_2, when variation in $m1$ and γ are allowed. In this grazing curve, every point corresponds to a grazing periodic trajectory with the same signature as the one obtained in Figure 5.5 with $\gamma = 0.174037rad$. This curve ends in several ***co-dimension-two bifurcation points*** indicated by circles in magenta. These co-dimension-two bifurcation points indicate that two parameters must be varied for the bifurcation to occur and may form centers for a variety of co-dimension-one bifurcation curves. However, in this study these points are not inves-

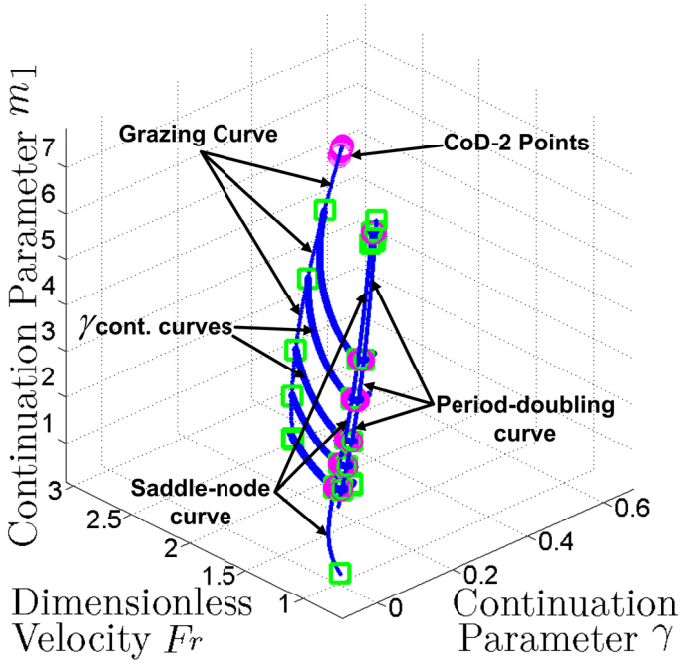

Figure 5.11. Froude number for the two-parameters continuation in m_1 and γ for several trajectories

tigated further since in practice these LCs are not realizable as walking patterns.

Also in Figure 5.11, two-parameters continuation in γ and $m1$ were computed from the points ***PD*** and ***LP*** in Figure 5.5, generating the curves indicated as the ***saddle-node curve*** and ***period-doubling curve***.

It is interesting to see that if a single parameter continuation in γ is performed on a point in any of the three previous curves (***saddle-node***, ***period-doubling*** or ***grazing curves***) a curve with similar characteristics to the one in Figure 5.5 will emanates, presenting usually two grazing points, one ***PD*** point and one ***LP*** point, with a stable region between the ***PD*** and ***LP*** points.

As m_1 increases, the region in which the curves are stable seems to remain about the same size in γ. This is illustrated in Figure 5.12.

As in Figure 5.5, in Figure 5.12 the dimensionless velocity is plotted against the continuation parameter γ. However, now the parameter $m_1 = 7.584\ kg$, which is the value that more closely reflects the weight of the shank in the GIMBiped testbed. From Figure 5.12, it can be appreciated that the range in which the curve is stable has changed to $\gamma = [0.0747533rad - 0.0838193rad]$ ($\approx [4.28° - 4.80°]$) values that indicate shal-

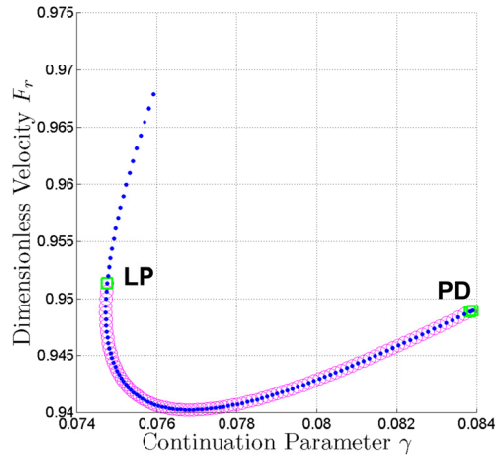

Figure 5.12. Froude number for the continuation of parameter γ with $m_1 = 7.584kg$

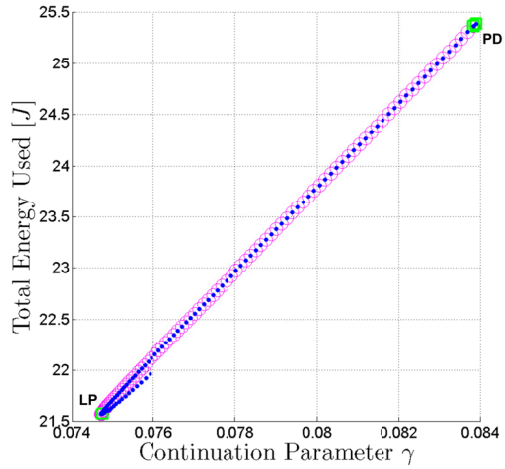

Figure 5.13. Total Energy for the continuation of parameter γ with $m_1 = 7.584kg$

lower slopes than the previous $\gamma = [0.0929538rad - 0.0969668rad]$ ($\approx [5.33° - 5.56°]$) from Figure 5.5. The size of the new stability region is twice as large for the shank with the higher weight ($m1 = 7.584\ kg$); however, this is not a clear indication yet if the resulting LCs are suitable for walking pattern generation.

Analyzing the energy plot in Figure 5.13 and comparing it with Figure 5.6, the same linear increase in energy consumption is observed as the slope increases for the stable region of the curve. However, in Figure 5.13 the energy consumption is expectedly higher due to the increase of weight in the system.

Finally, a crucial analysis to perform is that of the resulting stable LCs

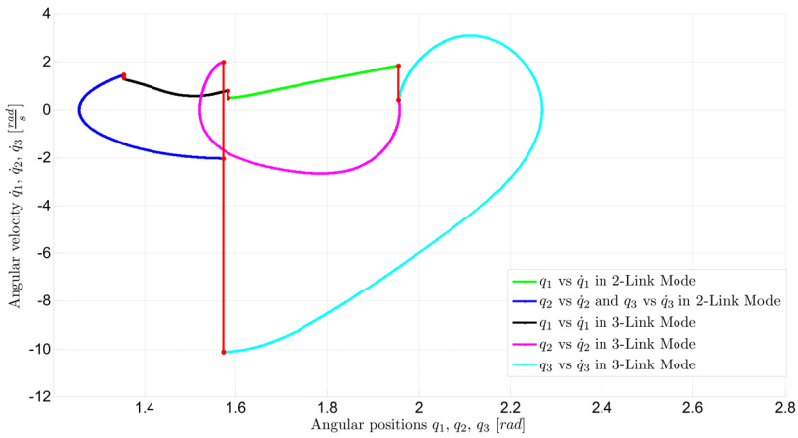

Figure 5.14. Limit Cycle for a specific trajectory from the previous continuation in Figure 5.12 and Figure 5.13 with $\gamma = 0.0773355rad$ and $m_1 = 7.584kg$

that emanate from the continuation in γ for $m1 = 7.584\ kg$ (Figure 5.12 and Figure 5.13). In Figure 5.14, an example of one of these stable LCs is plotted for $\gamma = 0.0773355rad\ (\approx 4.431°)$. From Figure 5.14, a very important observation can be made on the characteristics of the walking pattern: it reveals that the KL takes place when the swing leg angles (q_2 and q_3) have almost the same values as the angle of the stance leg (q_1).

The previous behavior indicates that foot scuffing is quite probable if this type of walking pattern is used in non-ideal model simulators or if it is used in the control of real biped platforms. Nonetheless, this is the behavior that naturally arrives from a system with the mentioned mechanical parameters. In the next sections, a further analysis and continuation will be performed to further evolve the systems towards the original design parameters.

5.8.6 Two-Parameter Continuation in γ and m_H

Figure 5.15 shows the results of a two-parameter continuation process for γ and m_H, in which the later parameter represents the weight of the hip in the model shown in Figure 4.3. The original design of the GIMbiped includes an upper body (or torso), as introduced in Chapter 3. However, in Section 4.2 the GIMbiped was modeled as a point mass system, where the hip includes the weight of the upper body. In Section 4.2, m_H took the values 10 kg, 10 kg and 5 kg for $Set1$, $Set2$ and $Set3$, respectively.

Nonetheless, in Chapter 6 the GIMbiped platform was modified and the upper-body was removed, making the GIMBiped testbed more similar to

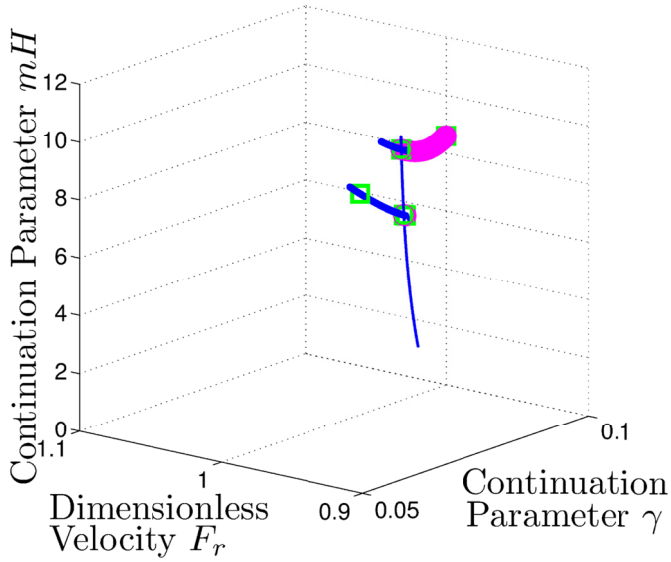

Figure 5.15. Froude number for two-parameter continuation in γ and m_H

the 3-link model of Chapter 4. The real weight of the hip in the experimental setup of Chapter 4 was $m_H = 7.30\ kg$; therefore, a two-parameters continuation was performed for γ and m_H, searching in the negative direction of m_H, starting from the original value of $m_H = 10\ kg$ in Set_{Start}, towards the value $m_H = 7.30\ kg$.

The ***LP*** point in the curve of Figure 5.12 was used as a starting solution

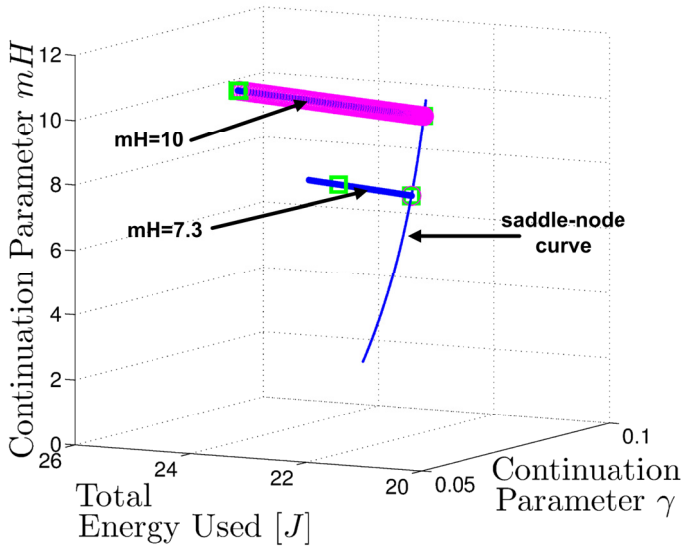

Figure 5.16. Total Energy consumed for two-parameter continuation in γ and m_H

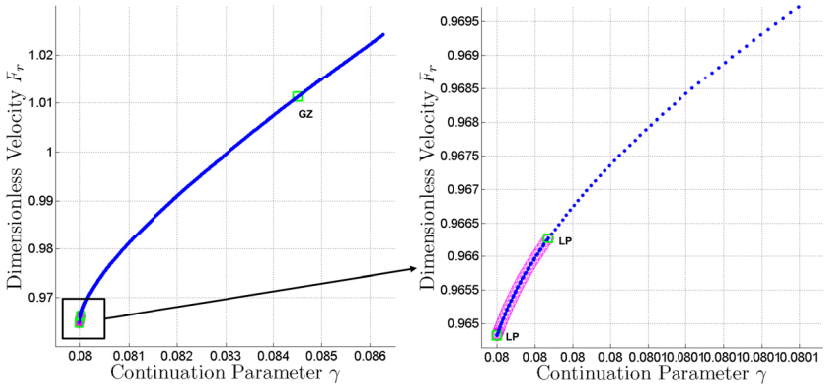

Figure 5.17. Large-scale and zoomed plot of F_r versus continuation parameter γ. A 2D view (slice) of Figure 5.15 on $m_H = 7.3\ kg$.

for the two-parameter continuation process performed in this section, and the resulting saddle-node curve can be appreciated in Figure 5.15 for a 3D plot of F_r against the continuation parameters. Figure 5.15 also shows the 1-parameter continuation in γ for $mH = 7.30kg$.

A general observation to be made from Figure 5.15 is that, as the value m_H decreases, the value of the F_r decreases as well.

Figure 5.16 presents the results of the same previous two-parameter continuation process but for the total energy used in one step cycle. As before, the result is presented in a 3D plot, now with the total energy used in one step cycle versus the continuation parameters.

It is interesting to observe that the energy consumption decreases as the m_H mass increases. The previous observation, together with the growing trend observed in the F_r values as m_H mass increases (Figure 5.15), leads to the conclusion that it is more energy-efficient to have a heavier hip for this type of modeling configuration.

Nonetheless, as always in nonlinear dynamics, this behavior and conclusion cannot be generalized for all configurations, neither can it be claimed that always the increase of the mass in the hip will lead to more energy-efficient gaits. This is a particular conclusion drawn from the study of variations around a particular set of parameters, and therefore should be interpreted in the same context. This however shows the importance of this type of studies in the development of a prototype, since small and feasible variations around the original values may lead to better overall performance.

Figure 5.17 shows the same 1-parameter continuation curve in γ with $m_H = 7.3\ kg$ presented in Figure 5.15, but in a 2D view. The region where

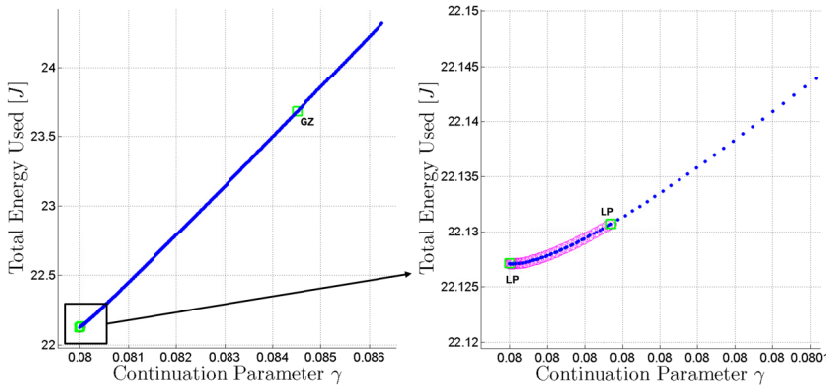

Figure 5.18. Large-scale and zoomed plot of Total Energy used versus continuation parameter γ. A 2D view (slice) of Figure 5.16 on $m_H = 7.3\ kg$.

the periodic cycles are stable has been zoomed, and it can be seen that, as m_H decreases, the range in γ, for which the cycles are stables, decreases quite noticeably.

In the curve presented in the plot from Figure 5.17, stable periodic cycles are found in the region $\gamma = [0.0799799rad - 0.0800070rad]$ ($\approx [4.5825° - 4.5841°]$) and a grazing incident happens at $\gamma = 0.0845035rad$ ($\approx 4.8417°$). With this set of parameters and ICs, also the behavior of the systems has changed: now two ***LP*** bifurcation points limit the region of stable cycles, and a ***PD*** bifurcation was not detected.

Figure 5.18 shows the same solution as in Figure 5.17 but with information regarding the total energy used in one step cycle. The same small-size stable region is obviously seen in Figure 5.18 as well.

The dramatical decrease in the size of the stable region in γ also illustrates the importance of the continuation study for the development of a prototype, given that now a tread-off between stability and energy-efficiency has to be addressed prior to evaluating any parameter changes.

Nonetheless, still the major indicator of the "usefulness" of the natural LC generated from a set of parameters and ICs is the characteristics of the walking pattern that it renders. Figure 5.19 presents one stable LC from the previous continuation curves in Figure 5.18 and Figure 5.17, corresponding to the trajectory solution with $\gamma = 0.0799824rad$ ($\approx 4.5827°$). As for the LC in Figure 5.14, this solution renders a walking pattern that is not natural-looking, and the KL event happens very close to the same angle of the stance leg q_2. Therefore, this LC, as the one in Figure 5.14, will not be an ideal solution to use as reference trajectory for walking patterns.

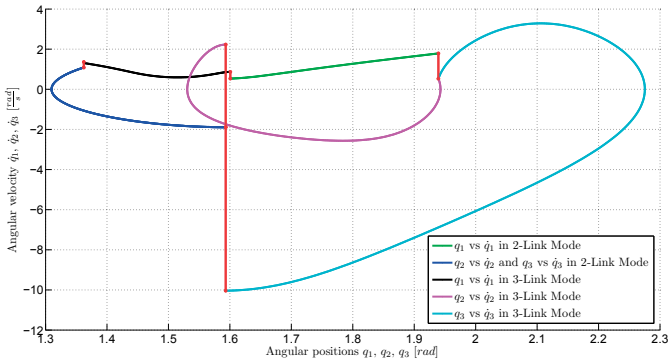

Figure 5.19. Single LC for a stable cycle in the continuation curve from Figure 5.18 and Figure 5.17 with $\gamma = 0.0799824rad$ ($\approx 4.5827^{\circ}$)

5.8.7 Two-Parameter Continuation in γ and m_2

Although the current observed LCs, for the configuration of parameters (in m_1 and m_H) reached, are not practical for its use as reference trajectories in the control algorithms proposed in Chapter 4 and Chapter 6, it is still important to try to reach the real parameter configuration of $Set_{GIMBiped}$ in Table 5.2, so as to analyze the possible changes needed to improve the system.

Therefore, the next continuation process performed was with respect to the parameter m_2, which corresponds to the thigh masses. In Table 5.2 and in [115], the total thigh mass of the GIMBiped is reported to be 9.812 kg. Consequently, a two-parameter continuation was done in γ and m_2, with a negative ***DS*** for the principal continuation parameter m_2 starting from its current value of $m_2 = 16.33$ kg.

Figure 5.20 shows the attempt of performing the previously explained

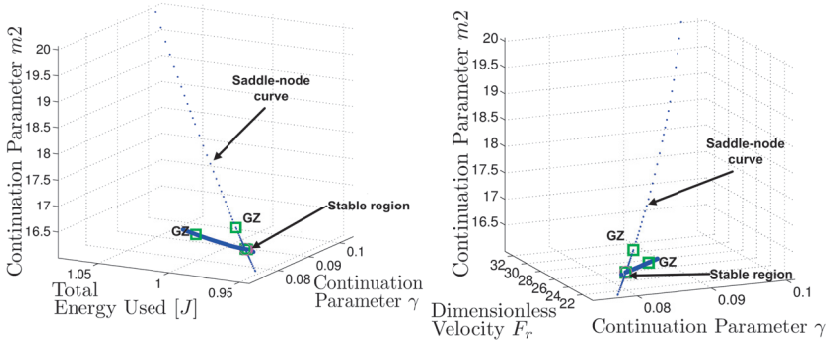

Figure 5.20. Total Energy consumed and F_r for two-parameter continuation attempt in m_2 and γ

continuation process. However, the continuation failed to converge for values of $m_2 < 16.0039$, reaching a boundary point where the ***DS*** direction needed to be changed. Continuation for higher values of the thigh weight did not present this problem; however, those values were not of interest in this study.

As a result, using the real parameter values of the GIMBiped testbed, it was not possible to reach cyclic trajectory solutions (under continuation methods) for the 3-link biped model with knees and point feet.

Given the previous problem at this stage, a decision was taken regarding possible modifications of the original parameters.

5.8.8 Seccond Trial for Two-Parameter Continuation in γ and m_1

One of the main changes observed in the characteristics of the LCs during the already performed continuation processes was the close distance between the angle values of the stance leg and the swing leg in the KL event. As mentioned before, this proximity generates an odd-looking walking pattern and decreases the foot clearance, both outcomes that are not desired for the natural LC of the system.

Since this "degradation" of the behavior of the LC was mainly due to the increase of the shank mass m_1, and given that this parameter can be easily modified in the real platform (GIMBiped) using other type of actuators, continuation was performed again in this parameter to decrease it to a reasonable value.

The target value chosen for the shank mass was $2.5\ kg$, a value that is higher than the model's original mass in Set_{Start} of Table 5.2 ($m_1 = 1.50$) but quite a lot smaller than the actual value of the prototype, presented in $Set_{GIMBiped}$ ($m_1 = 7.584\ kg$). The target value of $m_1 = 2.5\ kg$ does not relate

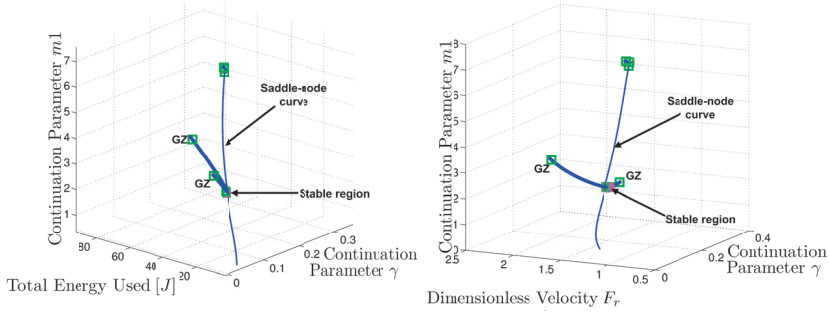

Figure 5.21. Total Energy consumed and F_r for two-parameter continuation in m_1 and γ

to any possible weight of an alternative actuator, since such changes have not been considered yet in practice, but instead it is just an arbitrary value that is used to demonstrate the procedure that can be applied for the design and performance analysis.

The continuation curve shown in Figure 5.21 looks therefore to reach $m_1 = 2.5$ from $m_1 = 7.584$. Figure 5.21 shows a 3D plot of the continuation curve for F_r and the total energy in one step versus the continuation parameters.

Such continuation was performed starting from the ***LP*** point in the curve of Figure 5.17 and Figure 5.18, where the initial inclination parameter $\gamma = 0.0800070rad$ ($\approx 4.5841°$). As seen from Figure 5.21, the two-parameter continuation was successful in reaching $m_1 = 2.5$, and also further one-parameter continuation in γ was performed, starting from the saddle-node curve for $m_1 = 2.5$.

5.8.9 Second Trial for Two-Parameter Continuation in γ and m_2

From the continuation curve in γ shown in Figure 5.21, a two-parameter continuation in γ and m_2 was attempted again to search for all the possible values that could be reached for the thigh mass, using $m_1 = 2.50\ kg$ and $m_H = 7.30\ kg$. The result is shown in Figure 5.22, where it can be seen that for this case the saddle-node curve extends over a large range in m_2.

To further study the consequences of possible variations around the original GIMBiped thigh weight and also to search for the best-suited ration between the shank and thigh, in Figure 5.23 four different LCs located in the saddle node curve from Figure 5.22 are presented.

The different LCs in Figure 5.23 correspond to the value of the thigh

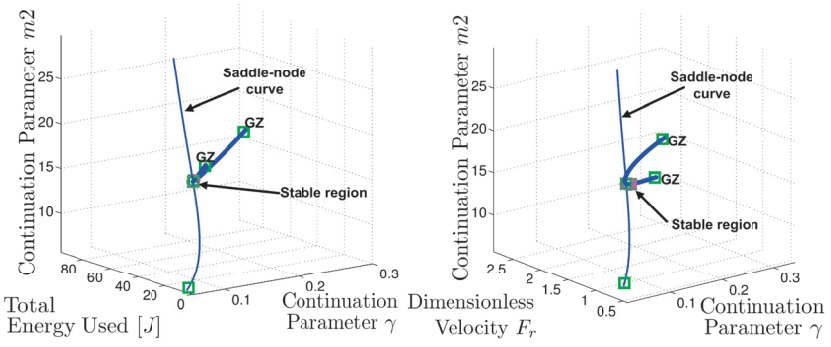

Figure 5.22. Total Energy consumed and F_r in the second attempt of two-parameter continuation in m_2 and γ

mass m_2 equaling to $10.0155\ kg$, $5.66369\ kg$, $2.00354\ kg$ and $0.100155\ kg$ as indicated in the captions of Figure 5.23.

Using the same MATLAB simulator presented in Section 4.3.1, a better and more complete analysis of these walking gaits can be performed. The analysis includes the visual appreciation of the actual walking performed by the biped.

The LC with $m_2 = 10.0155\ kg$ shows walking that looks natural, with satisfactory foot clearance, walking speed of $3.512\ km/h$ ($0.9756\ m/s$) and the step length of $0.5722\ m$.

An average human walking speed is about $1.4\ m/s$ ($5\ km/h$) [285], but the step length is highly variable depending on the human anatomy and walking speed. The acceptable average value for males is $0.75\ m$ [286]. The previously presented values for the LC in Figure 5.23.a fall below

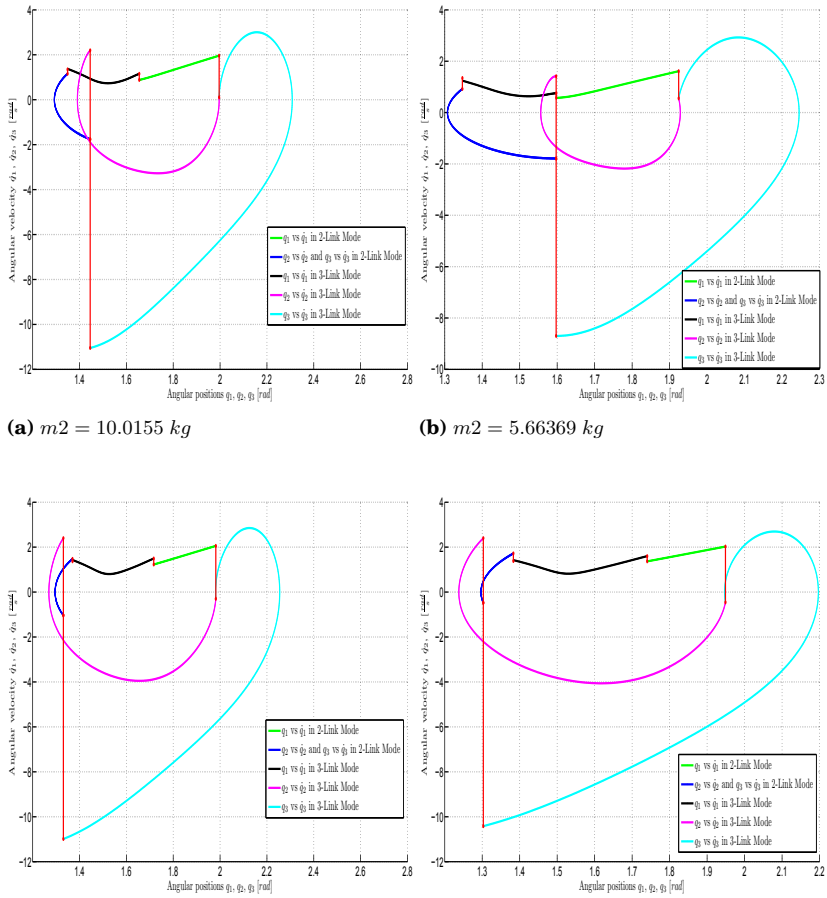

(a) $m2 = 10.0155\ kg$ **(b)** $m2 = 5.66369\ kg$

(c) $m2 = 20.0354\ kg$ **(d)** $m2 = 30.0038\ kg$

Figure 5.23. Four different LCs from the Saddle Node curve in Figure 5.22.

this average accepted value for human walking, therefore seeming fit as a reference walking pattern to use in the GIMBiped testbed.

Nonetheless, as will be discussed in Section 6.3.4 in the next chapter, experiments in the GIMBiped for walking with step length longer than $0.25\ m$ were not successful, mainly due to the restriction on the joints angle range. The maximum velocity achieved in the GIMBiped testbed was also very much below the average human walking speed, reaching only $0.1\ m/s$ ($0.36\ km/h$). Therefore, although the values attained previously may seem adequate and even slower than the normal, its application in the GIMBiped testbed may bring problem.

The LC with $m_2 = 5.66369\ kg$ presents the same problem of small foot clearance as the LCs in Figure 5.14 and Figure 5.19. The walking speed and step length are slightly smaller, $2.7792\ km/h$ and $0.5121\ m$; however, possible foot scuffing still restricts the use of this gait.

The LC with the large mass of $m_2 = 20.0354\ kg$ presents a very natural-looking LC; however, the walking speed is restrictive for its application in the GIMbiped, reaching $3.9297\ km/h$ with a step length of $0.5420\ m$.

Finally the LC with an even larger mass of $m_2 = 30.0038\ kg$, which in practice may not be possible, also presents a natural-looking gait with a faster speed of $3.9924\ km/h$ and slightly shorter step length than before, namely $0.5025\ m$.

The findings in this particular experiment are quite revealing, since until now there was a common assumption that the shank mass needed to be at least 10 to 100 times lighter than the thigh mass to be able to easily produce stable walking cycles [251]. In this experiment, some cycles were found for ratio of almost 1:2, although with very small foot clearance and stable region in γ.

Nonetheless, good cycles were found for ratio of over 1:4, with good foot clearance and stable regions in γ. Also, the curves in Figure 5.22 give a notion of the trade-off between energy efficiency and walking speed. From Figure 5.22, thigh values over $10\ kg$ show a steeper increase in energy compared to the increase in velocity, indicating a preferable region for the optimum thigh weight given the set parameters.

5.8.10 Two-Parameter Continuation in γ and Link Lengths a_1, a_2, b_1 and b_2

Following with the continuation study, the same solution curve used in Figure 5.22, with the values of the shank mass m_1 = $2.5\ kg$, the thigh

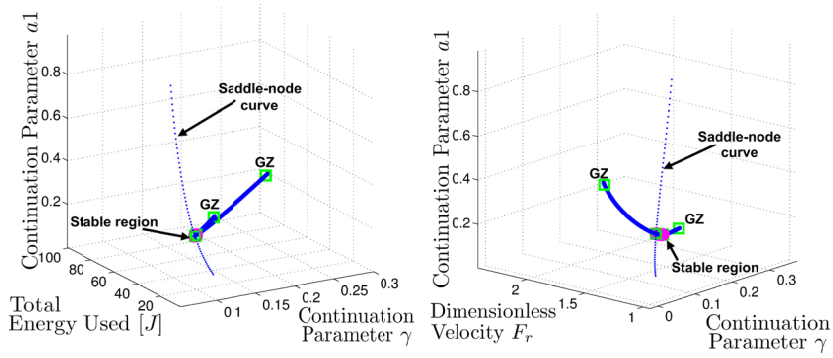

Figure 5.24. Total Energy consumed and F_r for two-parameter continuation in a_1 and γ

mass m_2 = 16.330 kg and hip mass mH = 7.30 kg, was evaluated under changes in the link length parameters a_1, a_2, b_1 and b_2.

Continuation in γ and a_1

The first continuation was performed for γ and a_1, and the solution can be seen in Figure 5.24.

As before, four different LCs are plotted in Figure 5.25 for different values of a_1 along the saddle-node curve. The values for a_1 are 0.101883, 0.000413243, 0.513839 and 1.00078 m, according to the figure's caption.

Again the MATLAB software was used to analyze the walking cycle visually and numerically, and the LC with $a_1 = 0.101883$ m showed a very natural-looking walking cycle with reasonable foot clearance. However, its walking speed was quite high, reaching 4.0410 km/h, and with a step length of 0.5915 m.

The LC with $a_1 = 0.000413243$ m visually did not look abnormal, apart from having almost a half-size shank. The clearance was good, but yet again the speed and the step length increased reaching 4.2010 km/h and 0.6224 m, respectively.

The LC with $a_1 = 0.513839$ m looked quite odd because it is no longer anatomically related to a human. However, the foot clearance was still good and the walking velocity and step length decreased in value with 3.4628 km/h and 0.4942 m.

Finally, the hypothetical LC with $a_1 = 1.00078$ m is completely out of proportion with a human walking gait. Is it interesting to see that in Figure 5.25.d the cycle looks very normal. Therefore it is important to have a simulator where the distances and shape of the model can be evaluated too. Based on pure experience, the plot in Figure 5.25.d may look like a reasonable walking pattern, however dimensions of the links convert it

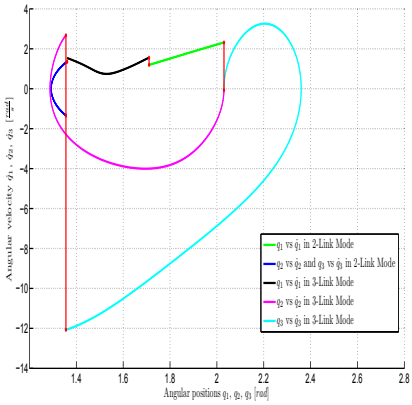

(a) $a1 = 0.101883\ m$

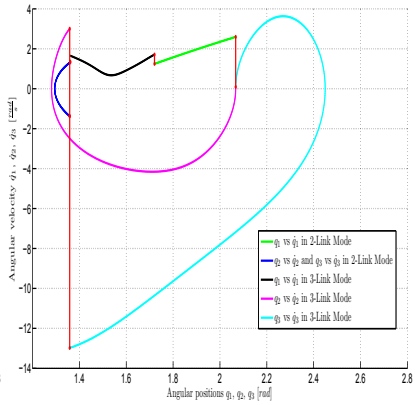

(b) $a1 = 0.000413243\ m$

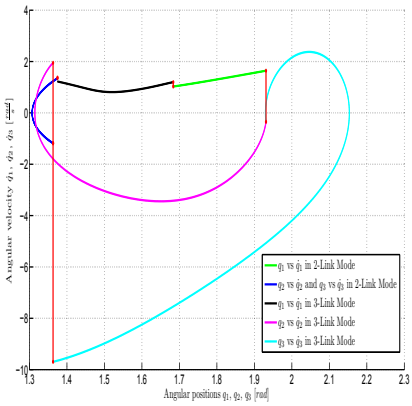

(c) $a1 = 0.513839\ m$

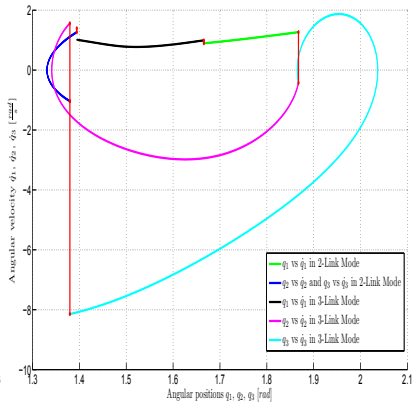

(d) $a1 = 1.00078\ m$

Figure 5.25. Four different LCs from the Saddle Node curve in Figure 5.24.

in an unpractical design. Velocity in this cycle was 3.0048 km/h and step length 0.4237 m.

Continuation in γ ***and*** b_1

The same study as before was done for b_1. Figure 5.26 shows the F_r and total energy in one step versus the continuation parameters γ and b_1. Likewise, four different LCs are plotted in Figure 5.27, where similar conclusions were drawn.

For the LC in Figure 5.27.a ($b_1 = 0.100873\ m$), the velocity is 3.6028 km/h and the step length 0.4695 m. In Figure 5.27.b ($b_1 = 0.0350671\ m$) the values are 2.8653 km/h and 0.3493 m, Figure 5.27.c ($b_1 = 0.350083\ m$) has the values of 3.8353 km/h and 0.6140 m and, finally, Figure 5.27.d ($b_1 = 0.611109\ m$) shows 3.6621 km/h and 0.6768 m.

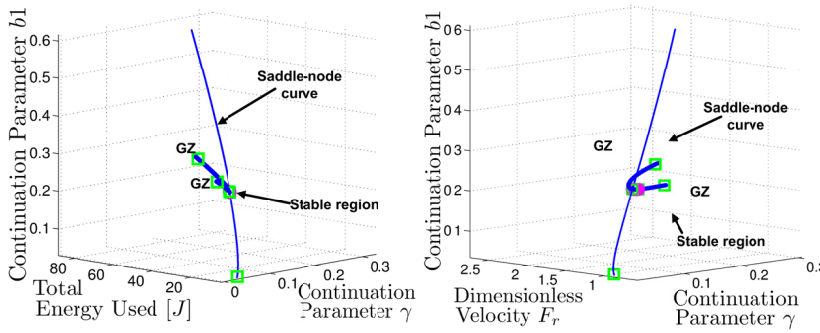

Figure 5.26. Total Energy consumed and F_r for two-parameter continuation in b_1 and γ

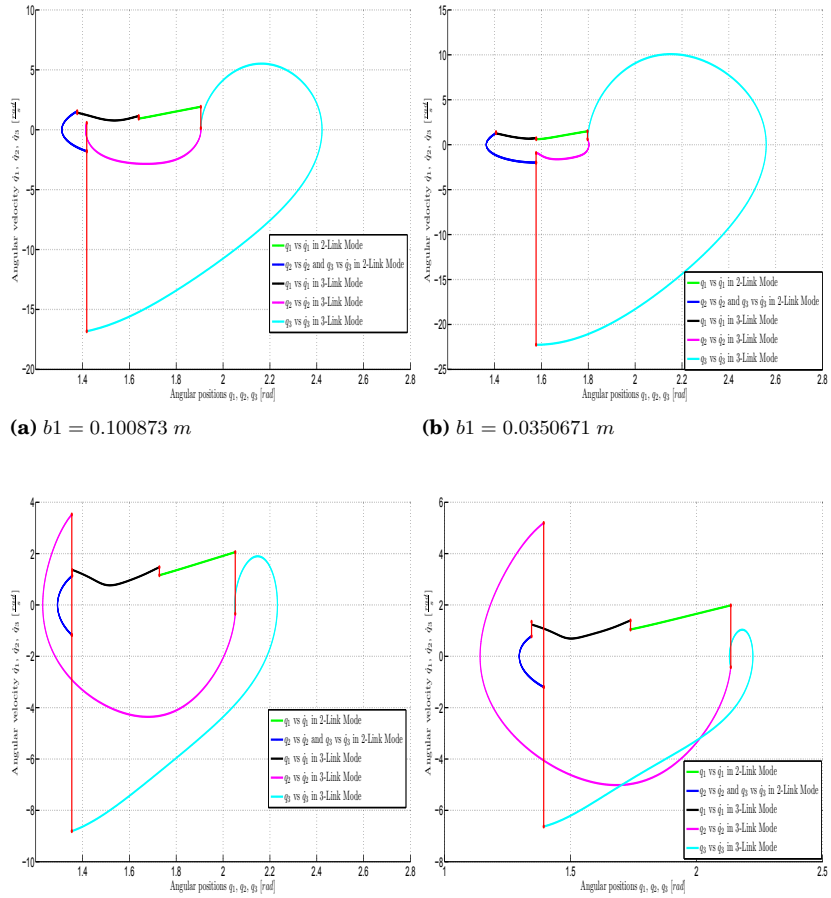

(a) $b1 = 0.100873\ m$ **(b)** $b1 = 0.0350671\ m$

(c) $b1 = 0.350083\ m$ **(d)** $b1 = 0.611109\ m$

Figure 5.27. Four different LCs from the Saddle Node curve in Figure 5.26.

None of the above results are feasible walking patterns, but it serves to demonstrate that continuation can also be performed in the other parameters in the system. All the experiments that modify the links' length

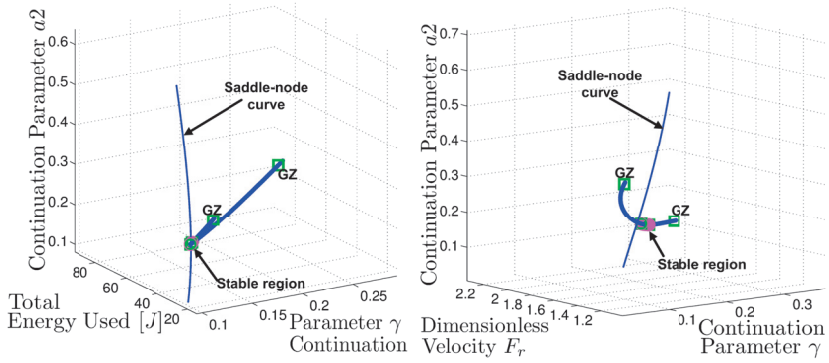

Figure 5.28. Total Energy consumed and F_r for two-parameter continuation in a_2 and γ

had a very wide range, which may not be necessary in reality but again, serves to exhibit the capabilities of the system.

Continuation in γ ***and*** a_2 ***and*** b_2

The rest of the analysis for the continuations of a_2 and b_2 is very similar to the former two procedures. Figure 5.28 and Figure 5.29 present the results for a_2, and Figure 5.30 and Figure 5.31 do the same for b_2. The information related to the walking speed and step length is summarized in Table 5.5.

5.9 Conclusions

In this chapter, the use of numerical continuation, based on a simplified model of the biped structure, has been shown to be a potentially powerful tool for the design aid and performance analysis in biped systems. The current approximated model used in this chapter does not relate exactly to the real platform configuration as it is built now. However, more ad-

Table 5.5. Results of continuation in γ and link lengths a_2 and b_2

continuation in γ and a_2			continuation in γ and b_2		
a_2 $[m]$	velocity $[m/s]$	step size $[m]$	b_2 $[m]$	velocity $[m/s]$	step size $[m]$
0.0999118	1.1425	0.5075	0.0675893	1.1771	0.6425
0.170098	1.1193	0.5330	0.112104	1.1776	0.6099
0.411527	0.9753	0.5795	0.497254	0.6529	0.4207
0.618909	0.8381	0.5871	0.998798	0.2286	0.1879

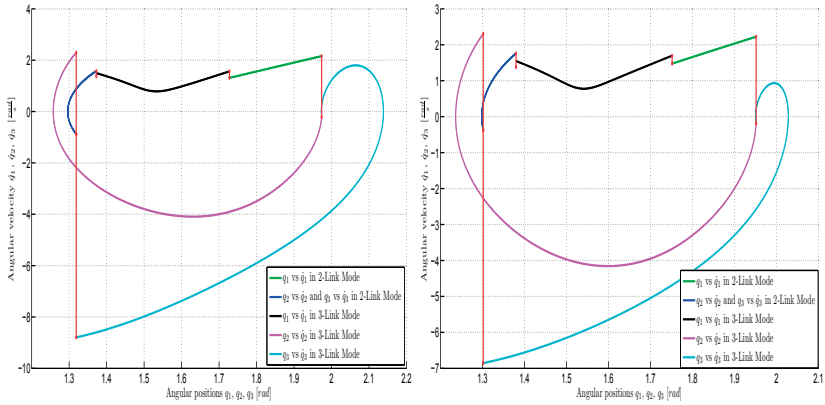

(a) $a2 = 0.170098\ m$ **(b)** $a2 = 0.0999118\ m$

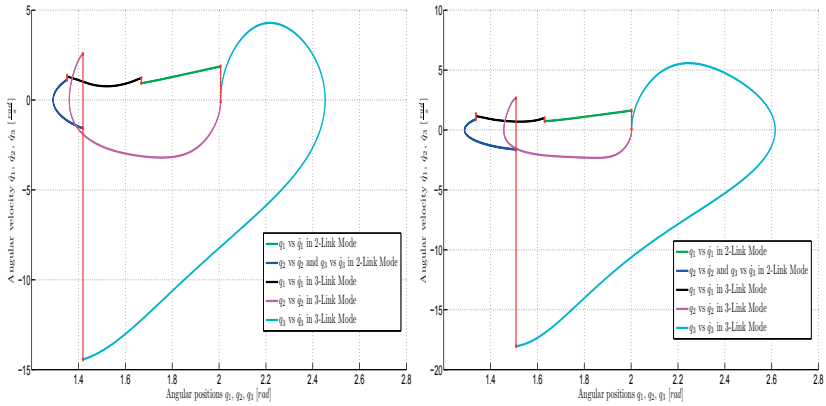

(c) $a2 = 0.411527\ m$ **(d)** $a2 = 0.618909\ m$

Figure 5.29. Four different LCs from the Saddle Node curve in Figure 5.28.

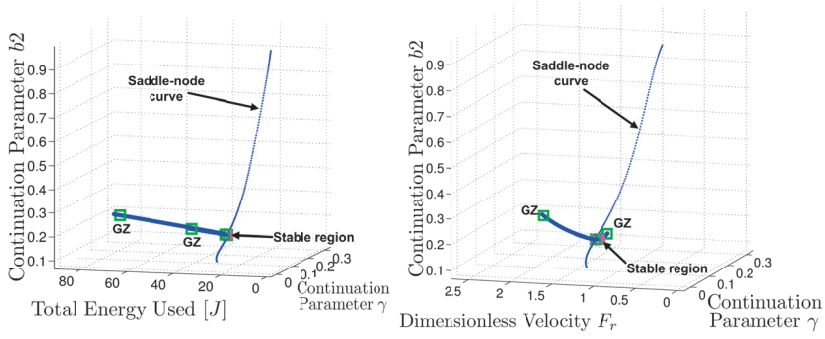

Figure 5.30. Total Energy consumed and F_r for two-parameter continuation in b_2 and γ

vanced models, which may include torso and 3D degrees of freedom, can be developed.

The use of numerical continuation has been proposed previously for the

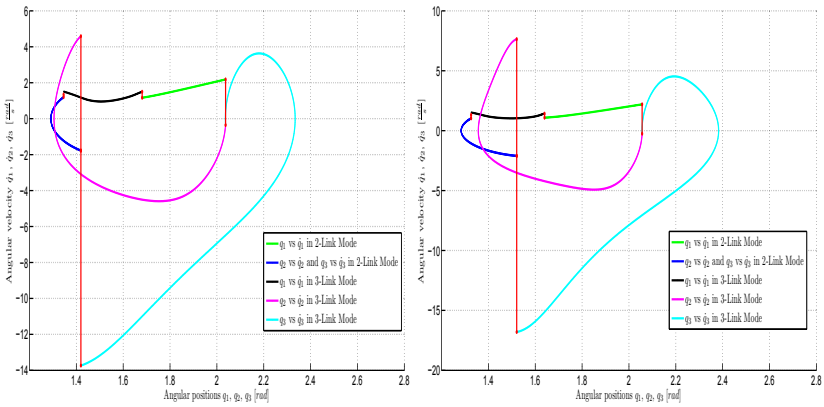

(a) $b2 = 0.112104\ m$ **(b)** $b2 = 0.0675893\ m$

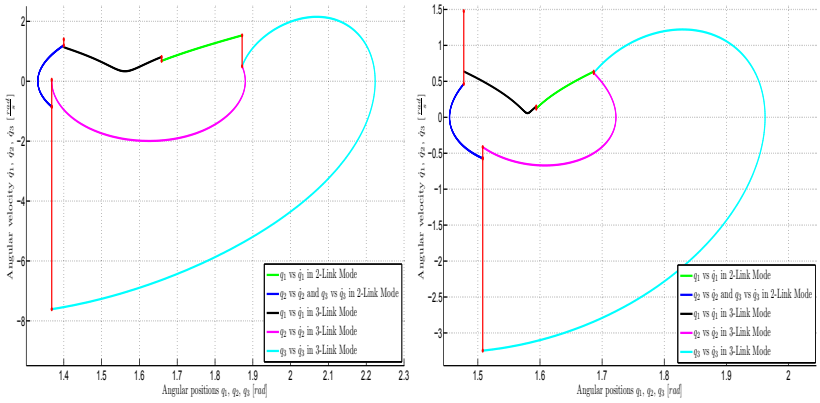

(c) $b2 = 0.497254\ m$ **(d)** $b2 = 0.998798E - 01\ m$

Figure 5.31. Four different LCs from the Saddle Node curve in Figure 5.30.

study of biped systems. Nonetheless, previous works did not target the aid in the design stage, the variation was performed just over one parameter at time, and some of the studies had incurred in errors when characterizing the stability of the system or simply ignored the stability characterization. Also an experimental analysis has been performed using a simple hardware [287] while varying some of the mechanical parameters. However, such study is not very exhaustive and reliable, due to the limited variation in the parameters, unrealistic weight distribution and high dependence on external factors during the experimental setup.

In the studies performed in this chapter, thanks to the use of the TC-HAT software, a correct characterization of the stability of the system is done and a systematic process for searching new design parameters has been presented.

Regarding the presented modeling of the system, it has to be noted that not all the possible events of falling, or potential problematic behavior of the biped system, were presented. There are some scenarios missing: *e. g.* where the knee would be bent more than 180 degrees; when the biped falls forward with the knee unlocked; or when the biped falls backwards with the knee locked. However, none of the previous fall (or fail) states were observed during the evolution of the system in the presented experiments. Furthermore, the only significant fall event detected when performing the continuation process was the foot scuffing the ground.

A better alternative for keeping the model simpler with faster simulation runs may be just to add the F_2 event and, in the case of detecting the presence of any other undesired behavior, start adding the appropriate event detection functions in the TC-HAT's biped model.

From the experiments performed in this chapter, some conclusions can be drawn for the possible changes in the mechanics of the GIMBiped testbed. The experiments revealed that, with the original design parameters of the GIMBiped, it was not possible to achieve stable cyclic trajectories nor any type of cyclic trajectory. It was necessary to change the shank to thigh ratio (that was originally $\approx$ 1:1.3) to at least 1:2 to have some sort of cyclic behavior. However, favorable LCs with adequate foot clearance, step length and walking velocity were found starting from ratio $\approx$ 1:4.

Further analysis indicates that humans do closely follow the previous mentioned ratios, with 9.7 kg shank mass and 3.2 kg thigh mass for an average weight human male, and 13.7 kg thigh mass and 4.1 kg shank mass for an obese human male [285]. The previous values result in a ratio of 1:3.03 and 1:3.34, for normal and obese human male respectively, with similar values presented also for women [285].

Furthermore, the average speeds found in these cycles are slower but quite close to the average walking velocity of humans [285, 288, 289]. Step length follows the same behavior, being slightly shorter than the human average step length [285, 288, 289].

Additional information found in the experiments was that the ratio between the step length and walking speed in the model studied varies greatly depending on the parameters, following sometimes proportional and other times inversely proportional ratio between them both.

The previous comparison between the results of the numerical continuation in the approximated biped model and the reported values of human performance lead to two possible conclusions.

One is that, if the behavior reported by the approximated model does relate closely with the real human counterpart, the slight deviation in the parameters presented in human's physiology, compared with the "optimal" distribution proposed by the model, may be compensated by the high-level control intrinsic to human walking. Such intrinsic applied control may accommodate or further optimize the CoT of a composition that is not optimally designed for passive limit cycle walking but instead evolved by nature to handle a higher versatile type of biped locomotion.

On the other hand, if the complex biped locomotion systems of the human do not directly relate to the simplified model presented here, it will mean that the approximations performed during the modeling stage obscure crucial variables of the system behavior.

In both previous cases, further study is necessary to either perform a study with active control on the current dynamic model to evaluate if the system can be driven to an efficient walking pattern or to develop a mechanical and dynamic model more closely related to human.

Some work was done already on the first hypothesis in Chapter 4 when control was applied to a model with non-ideal mechanical distribution using ideal trajectories. Further practical experiments on this will be presented in Chapter 6.

Furthermore, in this chapter the robustness evaluation was not approached, and it has been limited to the observation of the foot clearance. However, computation of the basin of attraction can give further information about robustness. Also control should be applied to increase the overall robustness of the system, and a method to calculate such robustness increment has to be devised. Nonetheless the previous study spawns through a wide field of potential solutions and therefore is left as future work for the GIMBiped project.

6. Experimental Results in Energy Consumption for a Compliant 2D-Biped Platform

The GIMBiped was originally designed to perform alternative control approaches to ZMP-based walking. In Chapter 4 (and [41, 57, 58]), the possible use of controlled Limit Cycle Walking (LCW) was studied in a simulator. Additionally, in Chapter 3 (and in [41]), a combination of ZMP and LCW to address efficiency and stability issues was proposed. This chapter presents the experimental results performed in a 2D setup of the compliant bipedal walking platform GIMBiped. Two types of controllers, based on ZMP and Limit Cycle trajectories, are evaluated to compare their performance in terms of energy consumption. The results are presented as accustomed in the literature, using the mechanical ***Cost of Transport*** (CoT) and ***dimensionless velocity*** (F_r), but also complete information of the whole system performance, including the actuators' efficiency, is provided. The disturbance and energy deviation caused by the supporting frame for 2D movement is also presented as an estimation of the frame's weight, acceleration and coefficient of friction. In contrast with Chapter 4, robustness of the system under external disturbances is not evaluated in this study. Here all the trajectories are assumed (and designed) to be sufficiently stable and capable of handling small natural disturbances to perform successful walking gaits for all the runs in the experiments.

6.1 Introduction and Motivation

Several research centers and industry-related R&D groups have successfully achieved biped walking on their experimental (and some commercial) platforms. However, precise and complete energy consumption figures have yet to be undisclosed for most of them. Some research facilities, due to the nature of their funding, understandably avoid publishing their results [66, 85]. However, a single rude approximation to ob-

tain their hypothetical energy consumption can mislead the comparison with the intended platform. That is the case of the two most advanced biped (humanoid) platforms to date, ASIMO [66, 67, 84, 164] and Petman [85]. Their energy consumption has not yet been fully revealed, and several approximations have been published using their hypothetical values [40, 52, 106, 152, 209]. In [52], Collins *et al.* approximated ASIMO's total cost of transport, considering its early performance data in [86, 90, 91], where the available data was: 510 N of weight, 1.6 $km/hour$ walking speed and draining a 38.4 V and 10 $A*hour$ battery in 30 minutes. Collins *et al.* assumed 50% drive train efficiency for the harmonic drives (HD), which, using the Equations (2.5) and (2.6) from Section 2.2.3, for ASIMO's CoT results in $C_{et(ASIMO)} = 3.2$ and $C_{mt(ASIMO)} = 1.6$.

Although ASIMO's performance data has been updated several times [88, 89, 91–95], the data in above CoT (first presented in [52]), still continue to be used [40, 106, 152, 209]. Nonetheless, even if an update in the performance data were done, the CoT calculations would still lack rigorousness, due to the assumption on the drive train efficiency and the walking duty cycle in which the data was taken. In [290], harmonic drives' efficiency has been reported to vary with applied torque, speed and lubricant viscosity. Furthermore, also in [290] the highest efficiency observed was close to 50% therefore, the $C_{mt(ASIMO)}$ may be considered quite optimistic, thus for accurate representation, the same study should be done for ASIMO's harmonic drives. In addition, the performance data presented in [86, 88–95] lacks the information about the walking duty factor (β_{w}), also presented in Section 2.2.3, leading to an assumption in the calculation of $C_{mt(ASIMO)}$ that all the energy is expended in the locomotion of the robot (none in processing, communication, etc) and that the robot is constantly walking at the same speed (for 30 minutes), meaning $\beta_{\mathrm{w}} = 1$.

Likewise, Petman's CoT has been roughly approximated using the reported performance data of its *"cousin"*, the BigDog [291]. In some conference presentations [292], Petaman was assumed to use the same type of hydraulic actuator as in [291], with a 15 hp (11190 J/s) engine powering it. Estimating its weight around 100 kg (981 N) and waking at the same speed as humans (1 m/s) results in a mere estimate of $C_{mt(Petman)} = 11$. Apart from the obvious lack of rigorousness in the correct data referencing, this calculation also overestimates the efficiency of the hydraulic actuators and the whole hydraulic system.

Therefore, this chapter, in addition to the primer objective of reporting

the results of different control approaches in the GIMBiped testbed, it also presents a full description on the performance data from such experiments. The previous data will be useful for correctly reference and interpret the performance of a biped robot (GIMBiped), and the efficiency and possible advantages or downfalls of using certain type of actuator, the ***Linear Motor*** (LM).

Another motivation for presenting the results in this chapter is that most of the information about energy consumption and energy efficiency in Biped robots are presented in small and light robots [249] that, although quite helpful for control studies and other energy efficiency analysis, have yet to be proven useful in more heavy-duty applications. In other words, there is a lack of information from the machines that could perform the same task as a human. One potential exception is MABLE [72] (and its derivation ATRIAS and MARLO [147]), which does handle high torques and potentially heavy duty task. However their results show only the CoT using Eq. 2.7 for its computation [209], missing the occasion to inform about its potential regenerative applications, efficiency of the drive train and overall consumption of the robot.

Considering these previous issues, the experimental results obtained here in the GIMBiped testbed can therefore bring some light over these hypothetical (or missing) values since, although the GIMBiped is powered by a different kind of actuator, it was built with a goal in mind that is similar to that of the previous mentioned robots: to be a robust biped robotic platform to carry out tasks comparable to those realized by humans. In this case, the GIMBiped is intended to be used in service applications.

Also, to the best of the writer's knowledge, there are no biped robots nowadays that have performed and recorded data of both the LCW and ZMP-based type of walking indistinctly and therefore are able to compare their results under the same system.

Additionally, the way that energy results are presented varies greatly between research institutions, and, consequently, a standardized and commonly accepted metrics should be proposed for this matter. In this chapter, the results are presented under the full range of possibilities for the complete system and, in Chapter 7, their value for providing helpful information will be assessed.

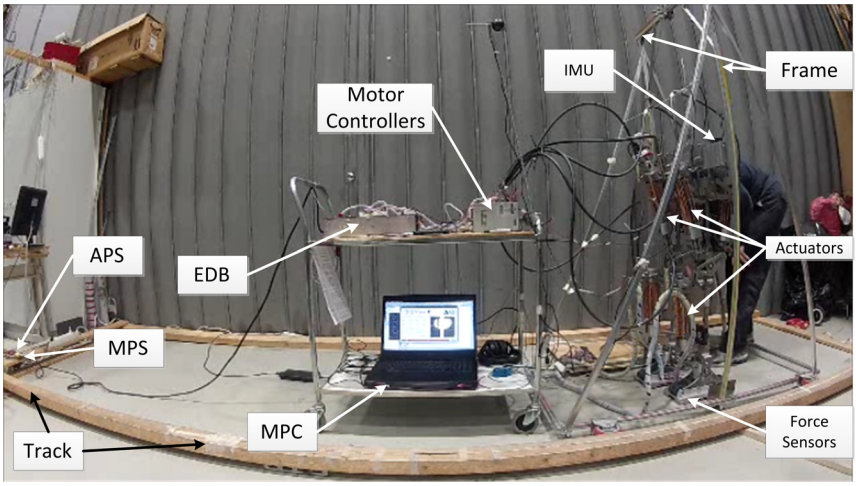

Figure 6.1. Experimental setup of the GIMBiped testbed.

6.2 Experimental Settings

This section presents the layout of the GIMBiped testbed for performing the experiments introduced in this chapter. This section also shows details on the mechanical settings and the communication and sensor infrastructure used. The final setup is a derivation of the original design view, specifically implemented to comply with the needs of the experiments planned. Details about the original design views can be found in [114–116] and in some extent in Chapter 3.

6.2.1 Hardware Setting

The experimental setup presented here uses the GIMBiped in a 2D configuration, as shown in Figure 6.1. As seen in Figure 6.1, the GIMBiped is in its ***lower body*** or ***hip-down*** configuration, one of the alternative arrangements of the original design presented in Chapter 3, which does not include the upper body [114, 116]. In this configuration, the GIMBiped is supported by a frame over a track that restricts the biped motion in 2D to the ***sagittal plane***. The frame is connected to the robot by a rotating and sliding double joint attached to both sides of the GIMBiped's hip. The joint allows the GIMBiped's hip to rotate with respect to the frame and also to slide up and down over rods placed on each side of the frame. The frame is mounted on wheels and is restricted to move over a track, rolling against the floor and the track's sideways walls.

This 2D and lower body configuration was chosen to resemble the model

used throughout this thesis. As previously said, the planar model of the biped with knees, point feet and without torso is one of the simplest models that can present LCW (Chapter 4), resulting in a natural-looking (human-like) walking gait. Since the goal of the GIMbipes project in its first stages was to examine the capabilities of the GIMbiped testbed to accomplish walking using different control approaches, and as this thesis falls within the initial attempts to achieve this, the simplest model possible was the obvious choice. Future works in the GIMBiped project will target sideways balance, upper-torso models and 3D walking.

Almost all the electronics and computers are mounted in a trolley, which is pushed along once the robot starts walking. The components that are mounted in the trolley are: 6 ***Motor Controllers*** (MCs), the ***Energy Distribution Box*** (EDB), and the ***Main Processing Computer*** (MPC). The ***Main Power Source*** (MPS) is composed of a pack of batteries that supply 72 V DC and theoretically can handle over 120 A discharge; however, the maximum that may be required by the GIMBiped is 15 A per motor (90 A max.). The MPS only provides energy for the actuators. An ***Auxiliary Power Source*** (APS) of 24 V is used to power the MCs, the sensors and other small consumption electronics and logic parts (fan, relays, etc). The MPS and APS are placed in another trolley, which remains stationary since its energy is supplied to the robot by a long cable that connects to the EDB, as shown in Figure 6.1. The EDB converts and distributes the energy where it is needed. The MPC is powered by its own battery.

An ***Inertial Measurement Unit*** (IMU) sensor is mounted in the joint that connects the frame to the biped's hip. This sensor is used, for now, mainly to measure the frame's acceleration and velocity, so as to calculate the frame's kinetic energy over time and later the energy dissipated by friction.

Finally, the feet used in the robot for this experiment are equipped with 4 force sensors in each foot. These sensors are used to calculate the location of the ***Center of Pressure*** (CoP), and in this experiment they are used mainly to indicate the level of stability and state in the walking cycle (***Single Support*** (SS) or ***Double Support*** (DS)).

In these experiments however, there is no feedback that uses the force sensors or the CoP information. For the work and results related to the use of feedback control with the force sensors and CoP data, the reader can refer to [112, 202].

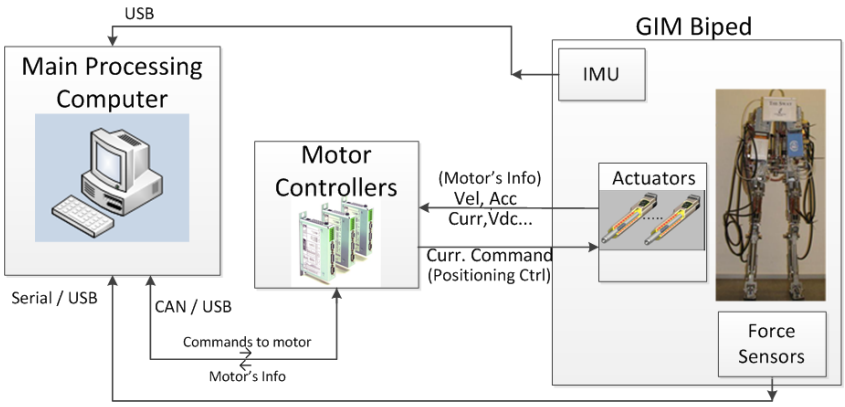

Figure 6.2. Experimental Information Distribution Infrastructure

6.2.2 Software and Information Distribution Infrastructure

For these experiments, a simplified version of the software and information distribution system is used. It is derived from the main infrastructure presented in Chapter 3.

Here, all the data collection from sensors and commands sending to actuators are executed in the same MPC. The sensor information, collected from the motors through the motor controllers, are transferred to MPC by the CAN network via a CANtoUSB converter. The data from the IMU module is inputted to the MPC directly though its USB interface. Finally, the data from the force sensor is filtered and pre-processed in its own module and sent to the MPC via USB as well [202]. The diagram in Figure 6.2 summarizes the ***Experimental Information Distribution Infrastructure*** (EIDI) described previously.

The ***Experimental Software Structure*** (ESS) used for these tests is a simplification of the one presented in Chapter 3. Here the ESS is in charge of all the processing, data collecting from sensors, and command sending to the actuators. These tasks are performed in the same MPC over 2 program. The first program, here referred to as the ***main program***, has 2 threads and is in charge of the trajectory generation, real-time command sending for the motor controllers and main data collection. The second program, here referred to as the ***auxiliary program***, is used to collect the data from the IMU module. The main thread (***Thread1***) in the ***main program*** computes first the desired trajectory off-line based on an inputted configuration file, which includes all the parameters needed by the program. Later it performs the walking control loop and data gathering, which sends trajectory commands and collects sensor data from the

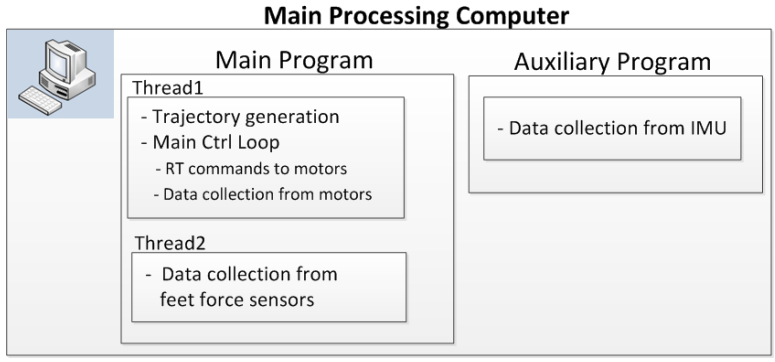

Figure 6.3. Experimental Software Structure

motors' controllers in real time through the CAN network. Figure 6.3 presents a diagram of the ESS.

The second thread (***Thread2***) in the ***main program*** collects the data from the feet's force sensors, which are not used in the walking control but are later used in the post-processing. This data is collected with time-stamp so it can be later correlated with the data gather by the motors' controller in the ***Thread1*** (which also collects and sends data with time-stamp).

Both threads work independently and run as fast as possible, performing their own tasks. Since the ***Operating System*** (OS) is not a hard-real-time OS, the time interval varies slightly for each loop. Nevertheless, the time intervals are mostly constant: the data sampling in ***Thread2*** is 2 ms, and the control loop interval in ***Thread1*** is 20 ms.

The previous control loop interval of ***Thread1*** sets the maximum sampling time for the desired trajectory planning. If the desired trajectory points are sampled faster than 20 ms, the robot won't be able to follow in time and lags behind.

The separated ***auxiliary program*** runs independently and collects data from the IMU. The ***auxiliary program*** is based on GIMnet's server and client infrastructure using the datalogger module [241, 242]. The IMU data is also time-stamped for later correlation and data post-processing.

Both simplifications, for the ESS and EIDI, are due to the problematics encountered over the real-time control needs. The GIMnet architecture presented shortly in Chapter 3 ([241, 242]), although quite flexible and suitable for remote applications, does not perform well under real-time requirement where the remote hub is the one in charge of the main control. In other words, the remote hub can be in charge of monitoring and

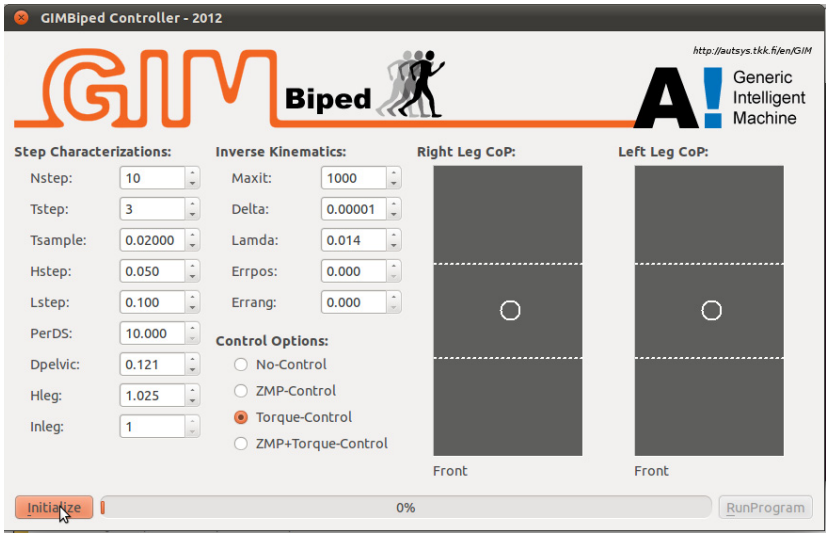

Figure 6.4. Graphical User Interface used in the hardware experiments

high level instructions like stop, walk, increase speed and turn but cannot handle the actual walking control remotely due to the potentially long and variable delays over the network. If the remote hub control were to be used, the control loop could have high variability given that the sensor information could arrive with long and variables delays, and the same problem would be seen in the resulting control commands sent to the actuators. These types of delays are restrictive for this highly critical control situation where fixed- and time-dependent interruption is needed for this time-dependent type of control.

That was the reason to include only one MPC and simplify the GIMnet structure to just one hub, which includes a simple Graphical User Interface (GUI) (Figure 6.4). The available PC104 used as local hubs in Section 3.1 were not fast enough to be used as the MPC. Therefore, the MPC used was an Alienware Notebook model M17XR3 running 64-bit Linux Ubuntu, with an Interl(R) Core(TM) i7-2820QM Processor @ 2.30 GHZ (boosted to 3.4 GHz) and 8.00 GB of RAM.

6.3 The Experiments

As mentioned previously, this chapter presents experimental results performed in the 2D configuration of the compliant biped platform GIMBiped, under ZMP- and LCW-based trajectory control. The goal was to present detailed energy consumption per step cycle in a compliant plat-

form for two different walking modes. The testing is conducted in 2 sets of experiments, here referred to as ***Experiment1*** and ***Experiment2***.

In ***Experiment1***, only a ZMP-based trajectory-following control, referred to as ***ControlType1*** here, is studied. ***Experiment1*** comprises 18 different walking trajectories (Table 6.3) obtained with variations on the parameters that describe the trajectories used in the ***ControlType1***. For each one of the 18 different trajectories, 10 sets of walking experiments were executed. ***Experiment1*** goal was to clarify the best parameters for the ZMP-based trajectory that should be used in the ***ContolType1*** (step length, step height and PD parameters for the positioning control).

Experiment2 uses both the ***ControlType1*** and an LCW-trajectory following control. Here the LCW trajectory-following control is named ***ControlType2***. In ***Experiment2***, 6 different walking speeds were tested with the ***ControlType1*** approach, using the best resulting parameters from ***Experiment1***, and 4 different walking speeds were tested using the ***ControlType2*** approach. The goal was to obtain a plot where the CoT, representing the consumption of energy, could be plotted against different sets of dimensionless velocities. For each of the 10 different walking trajectories (6 ***ControlType1s*** + 4 ***ControlType2s***), 10 runs were performed, averaging the relevant data results, as in ***Experiment1***.

Section 6.3.1 below will explain in detail the ***main controller*** overview, and the specifics for the ***ControlType1*** and ***ControlType2***. Section 6.3.3 and Section 6.3.4 present information about the parameter settings and implementation details for ***Experiment1*** and ***Experiment2***, respectively.

6.3.1 Controller Overview

Both controllers used here are different versions of the well-known PD-independent-joint trajectory-following control [261]. Therefore, the controller implementation is based on the PD version of the classical joint control, which could be represented as the case when

$$\hat{M} = I,\ \hat{N} = -\ddot{q}_d \tag{6.1}$$

From the general equation of the torque control (same as Eq. 2.16) of the ***Computed-Torque Control*** (CTC) presented in Section 2.4.2, with the approximated matrices $\hat{M}$ and $\hat{N}$ (see Table 4.2).

$$\tau_c = \hat{M}(\ddot{q}_d - u) + \hat{N} \tag{6.2}$$

This is the experimental version of the ***Independent Joint Control: Classical PD Control*** tested in the simulator in Chapter 4 and sum-

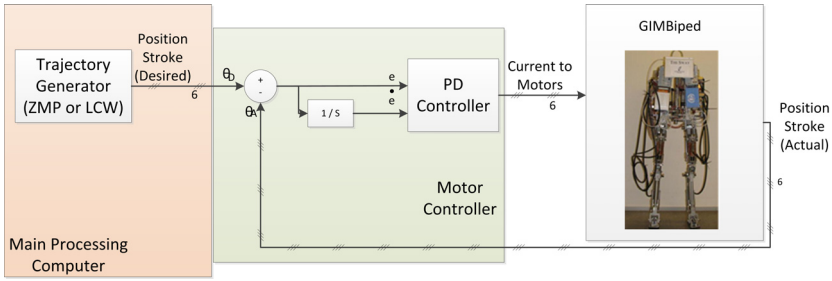

Figure 6.5. Simplified version of the control loop and block diagram for LCW and ZMP based control

marized in Table 4.2. Both control approaches, ***ControlType1*** and ***ControlType2***, are then time-dependent and therefore relying quite a lot in the real-time capability of the system and the deterministic interruption of the control loop.

The difference between the ***ControlType1*** and ***ControlType2*** is in the way the trajectories are generated. As anticipated, the ***ControlType1*** uses what is commonly known as the ZMP-based type of trajectory. This is the common terminology in the literature, however it is rather misleading and will be explained further in Section 6.3.3.

ContolType2 instead uses trajectories derived from an approximated biped model of the GIMBiped. As in Chapter 4, this model is the planar biped model with knees and point feet (Figure 4.3), which is the one that generates the trajectories finally used as references in the control. The intention was to replicate the results obtained in simulation in Chapter 4; however, the final version of the controller differs quite a lot from the one in Section 4.4 for reasons that will be explained in Section 6.3.3 more exhaustively.

The main structure of the control system of both the ***ControlType1*** and ***ControlType2*** follows the general configuration presented in the diagram of Figure 6.5. There is a module, named ***Trajectory Generator***, which is in charge of generating the trajectory for a specific type of walking (***ControlType1*** or ***ControlType2***). The commands from the trajectory generator are sent at every interval of MPC's control loop (which is approximately 20 ms, as stated in Section 6.2.2). The trajectory information is sent to the ***Position Controller***, which is programmed in the ***Motor Controllers*** and based on a PID control. Ultimately only the proportional (P) and derivative (D) gains were used (as seen in Table 6.4), since the integral (I) gain led to high currents (and therefore more energy expenditure), due to permanent errors observed in the positioning control. Such perma-

nent errors were not critical for the final trajectory following, but they did increase considerably the current because of the accumulation in time.

Finally, the ***Position Controller*** sends controlling commands to the GIMBiped actuators, which have the format of desired current for the linear motors' windings.

6.3.2 The Position Controller

As stated above, the PD positioning controller is embedded in the Motor Controllers (LinMot B1100 [245]); however, the actual value of the controller output is saturated by parameter settings used to define the motors' positioning interpolation method. This positioning interpolation is also performed by the motors' controllers. It is named maximum velocity and limited acceleration position interpolator (VA-Interpolator: VAI). The VAI follows a trapezoidal method which is limited to a maximum acceleration and deceleration, as well as a maximum velocity setting. Therefore, the VAI limits (or changes) the original output of traditional PD controllers, making it smoother. In synthesis, the VAI generates a positioning curve from the current position to the desired position, based on the parameters value of acceleration, deceleration and a maximal speed. As before, the outputs of the controllers are the current command that drives

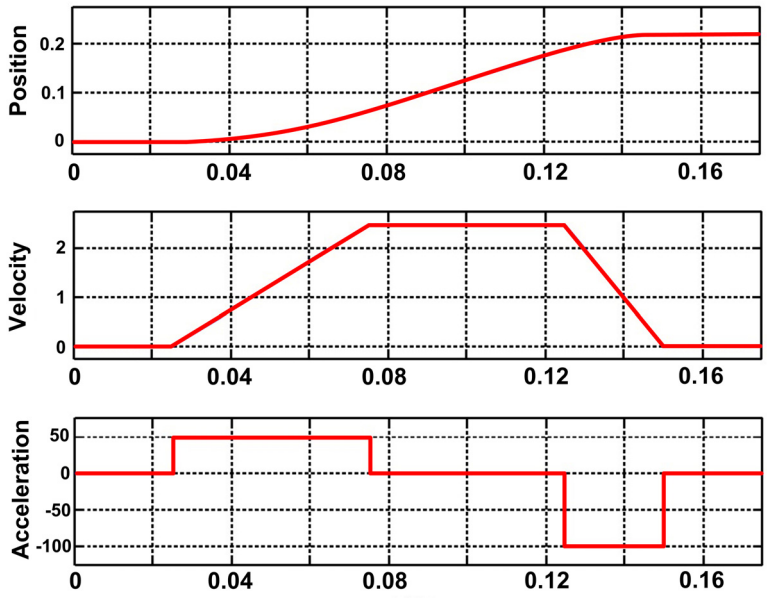

Figure 6.6. Example of Position Velocity and Acceleration profile in the VAI (reproduced from [293])

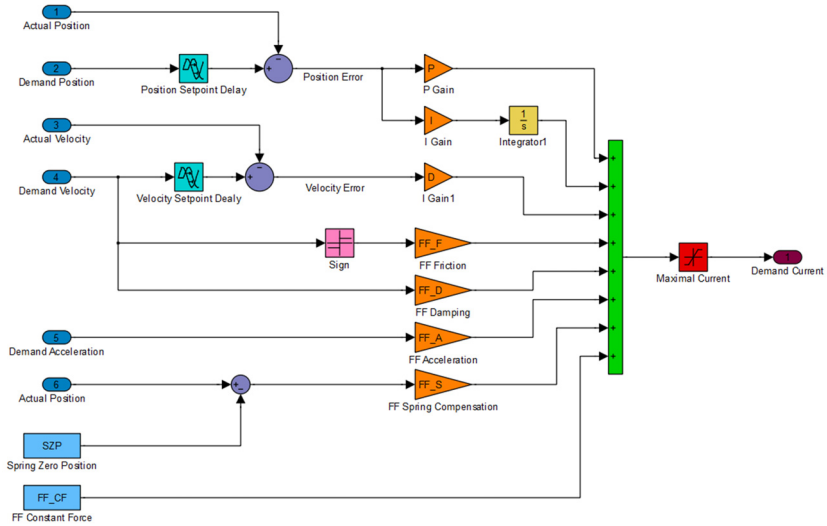

Figure 6.7. Control diagram of the positioning control in the motor's controllers (reproduced from [293])

the linear motors to the desired position but at a higher sample rate than the controlling cycle imposed by the MPC. VAI interpolation curves can be seen in Figure 6.6. The control diagram of the ***Position Controller*** is shown in Figure 6.7.

Several values for the maximum acceleration, deceleration and velocity were tested prior to the experimentation, and the best performing values were used throughout ***Experiment1*** and ***Experiment2***. The values used are presented in Table 6.1. The criterion for choosing these values was that the motors should reach their desired position within the time of every control loop (0.02 s) and the accelerations should not cause too much momentum change.

It can be noticed from Table 6.1, that the positioning parameters change depending on phase of the walking cycle of the robot. In the swing phase, the acceleration and deceleration were set higher, given that the positions

Table 6.1. Parameters for the motor positioning control

Parameters	**Units**	**Stance Phase**	**Swing Phase**
Max. velocity	$[\frac{m}{s}]$	0.16	0.16
Max. acceleration	$[\frac{m}{s^2}]$	0.3	0.5
Max. deceleration	$[\frac{m}{s^2}]$	0.3	0.5
Max. current	$[A]$	15	15

sent as set points were further apart from each-other, and therefore the robot had to react faster to reach its goal position.

Figure 6.8 and Figure 6.9 illustrate the results of the positioning control, showing the demand acceleration and actual velocity, respectively, of run #6 of trajectory #12 in Experiment1 (see Table 6.3). In the previous figures, the saturation for the acceleration and velocity can be appreciated in the different phases of the walking cycle. It should be noticed that the position controllers are of the PD-type, and, with the proper gains it would make the robot more or less compliant. It is also important to notice that a very stiff position control is not desired because in many cases it may

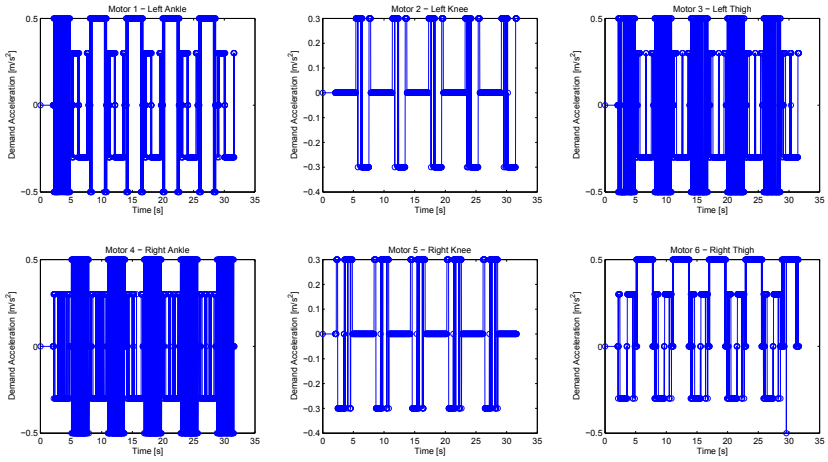

Figure 6.8. Demand acceleration plot for run #6 of trajectory #12 in Experiment1

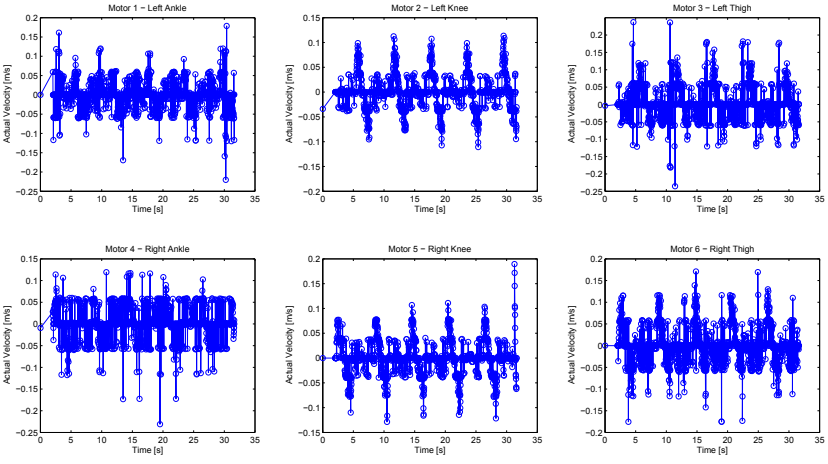

Figure 6.9. Actual velocity plot for run #6 of trajectory #12 in Experiment1

cause oscillations and unnatural motion when walking.

The specifics of how the ***ControlType1*** and ***ControlType2*** generate their trajectories for the ***Trajectory Generator*** module in Figure 6.5 is explained in the two following sections.

6.3.3 ControlType1

The ***ControlType1*** is the GIMBiped's control implementation of the most common method for controlling biped robots nowadays. It uses the traditional approach applied for the control of generic robotic manipulators. The procedure to obtain the ***Trajectory Generator*** for this ***ControlType1*** is as follows:

Trajectory Generator ControlType1:

1. ***Trajectory Planning***: first, specific trajectories are designed for the ***end-effectors*** of the GIMBiped. Here the ***CoM*** (supposed to be located at the ***hip***'s center) and the ***swing foot*** are considered as the end-effectors.

2. ***Inverse Kinematics Calculation***: after 1), the end-effectors' trajectories are converted into joint trajectories using ***Inverse Kinematic*** (IK).

3. ***Angles to Stroke Conversion***: given that the GIMbiped is driven completely by linear actuators, the joint angles calculated in 2) have to be converted into stroke values that could be used by the ***Positioning Controllers***.

The process of using the above ***Trajectory Generator*** to create time-dependent (parameterized by time) control inputs to the ***Positioning Controller*** to follow (presented in Section 6.3.2), is the same lower level structure followed by most of the ZMP-based control methods. Therefore, the outputs of the ***Trajectory Generator*** presented above are commonly known as ZMP-based type of trajectory.

However, the trajectory itself is not ZMP-dependent (or parameterized by the ZMP of the robot). The only relation with the ZMP is that these trajectories can be specifically designed to enclose the ZMP under a bounding ***stability region***, or ***stability margins*** (See Section 2.3). The goal is to generate movements that are easier to control (trajectories easier to fol-

low), that have limited accelerations (slow enough) and generate limited amount of momentum on the robot. In the ZMP-based type of trajectories generated for the GIMBiped, the foot trajectory is designed with zero speed landing to reduce shock and disturbances (at the cost of some energy efficiency).

Also, a crucial requirement is to always have at least one foot flat to the surface, so that the robot can generate torque against it, counteracting any disturbances if a close loop control is applied. Furthermore, there is a need of some percentage of the double support period (when both feet are flat on the ground) during the whole walking cycle, so the ZMP could be smoothly shifted between the two supporting areas of the feet. These trajectories can even be designed so that the projection of the CoM on the surface (GCoM) will not leave the supporting area of the feet; in this case, the biped will be following a ***Static Walking*** type trajectory. Also, the trajectory can be simulated off-line to test the dynamic behavior of the biped in a simulator and study if it will generate momentums that could drive the ZMP out of the bounding ***stability margins***.

The most common *"real"* ZMP-based type of control includes a feedback part where the information about the location of the ZMP is used to alter the originally designed trajectory in real-time. Usually the changes done in real-time are to the movements of the robot ankle and hip, which can affect directly the ZMP current location, driving it back within the ***stability margins***. Once the ZMP is again within its ***stability margins***, the controller goes back to the original trajectory-following control. Detailed information about the ZMP and all its variation of control were already introduced in Chapter 2.

Of the experiments performed in the GIMBiped for this thesis, the ***upper level control*** is not implemented. Therefore, if the robot is becoming unstable due to the inability to follow the desired trajectory or external disturbances, there is no way to bring it back to its stable state. Therefore, these experiments just consider trajectories that are inherently stable, and under no excessive external disturbances.

The GIMBiped has been experimentally tested with a control implementation which includes a ZMP feedback, and the results were reported in [112]. In [112], a fuzzy method was used to re-sample the trajectory and slow down the robot once the ZMP indicator drifted away from the stable region. However, the results and implementation of those experiments are not included within the contributions of this thesis.

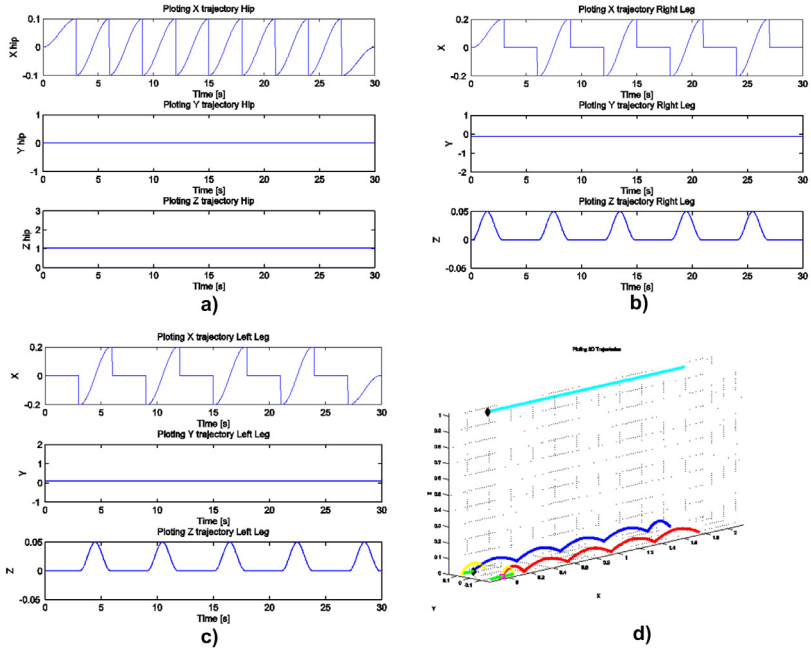

Figure 6.10. Trajectory planning for ZMP-based type of trajectory of the biped robot in 2D a) Trajectory for the CoM b) Trajectory for the Right Leg c)Trajectory for the Left Leg d) Overall planar trajectory in 3D

ControlType1: Trajectory Planning

As mentioned before, the trajectory planner for the ***ControlType1*** tackles the walking, using the common manipulator approach to solve the control problem. For that end, here, the GIMBiped is considered as a coupling of two end-effectors, the ***Swing Foot*** and the ***Hip***. In this context (and because it is a common practice in this process), the ***CoM*** will be supposed be located at the ***Hip***, and, therefore, hereafter this end-effector will be indistinctly called the ***CoM***. Independent trajectories are generated for each end-effector, with the common goal of driving the robot on a smooth walking pattern.

This whole process is well known in robotics, and therefore it will not be detailed here.

The result of one-trajectory planning is shown in Figure 6.10, where the X, Y, Z component of the left leg foot, right leg foot and CoM are indicated. It should be noticed that the Y-axis position remains constant since the robot is restricted to walk in 2D. The whole trajectory planning of the walking for a 3D biped is completed by deriving the trajectory to follow in the frontal plane. However, since the GIMBiped in these experiments will only follow 2D trajectories, the parameters for the frontal plane are

always fixed to the same value (in the Y plane). The trajectory planning of the frontal plane is very important in 3D walking since it allows to shift the ZMP or GCoM from one supporting foot to the other by moving the hip sideways.

For all the trajectories generated in these experiments, the desired height of the CoM's (hip) position is set to remain constant with the maximum allowed value L_{leg} (total length of the Leg). This was done with the intention of always keeping the stance leg straightened to save energy, since one of the major problems in the GIMBiped was the overload of the knee motors. Keeping the Z-axis reference position constant will generate an error between the reference position and the actual position, since the robot cannot reach that same height always, given that even with the straightened leg, it can only follow the trajectory corresponding to an inverted pendulum. However the ***inverse kinematics*** (IK) deals with this issue in an optimal manner and reaches the closest position to the CoM's Z-axis reference point, therefore maintaining the stance leg straight.

Once the trajectories of the end effectors are done, the calculation of the IK is needed to obtain the angular trajectories for each joint in the robot. The inverse Kinematic is an old problem in robotics. Here it is computed using the Levenberg-Marquardt algorithm, also known as the Damped Least Square (DLS), to solve the nonlinear optimization function that iteratively approximates the resulting joint angle to achieve the desired end effector position. This process in the trajectory planning is widely known in robotics, and it will not be treated in depth here either.

Angles to stroke conversion

Given that the GIMBiped is completely actuated by linear motors, once the trajectory for each joint is calculated using the previous process, the resulting angular values have to be converted into linear values to input them as a reference for the LM. Detailed descriptions of the mechanical and electrical characteristics of the motors can be found in [56,245]. Each powered joint in the robot has the same basic construction. The model and its descriptions can be seen in Figure 6.11.

It can be observed in Figure 6.11 that, if the LM's slider extends or contracts, changing the stroke x will induce a change in the angle α, which

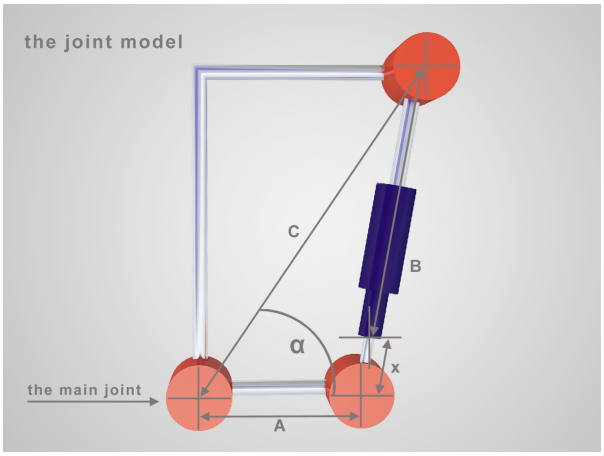

Figure 6.11. Diagram of a generic joint in the GIMBiped testbed

will follow the nonlinear function given by the equations to follow.

$$(B+x)^2 = A^2 + C - 2AC\cos\alpha \tag{6.3}$$

$$B + x = \sqrt{A^2 + C^2 - 2AC\cos\alpha} \tag{6.4}$$

$$x = \sqrt{A^2 + C^2 - 2AC\cos\alpha} - B \tag{6.5}$$

The result of applying ***ControlType1*** can be appreciated in Figure 6.12 and Figure 6.13. These figures shows the reference trajectory (the trajectory inputted to the Positioning Controller by the Trajectory Generator) and the actual position of each motor of the biped. Figure 6.12 shows these position values in angle deg units, and Figure 6.13 shows the values in stroke mm units.

6.3.4 ControlType2

The design of the Controller in this section is inspired by the same hypothesis as in Chapter 4, where allegedly using some form of walking based on the natural limit cycle of the dynamic system will reduce the energy usage. Therefore, the control implementation in this section relies, as in Chapter 4, in the use of a 3-link biped model approximation of the GIMBiped's hardware (Figure 4.1). The model is used to generate the joints' trajectories, which are then inputted as reference to the controller. This is based on the idea that using a trajectories that are natural for a simplified version of the robot should use less energy than a trajectory that forces the joints to follow a given path that are far from the natural movement of the system (far from the LC).

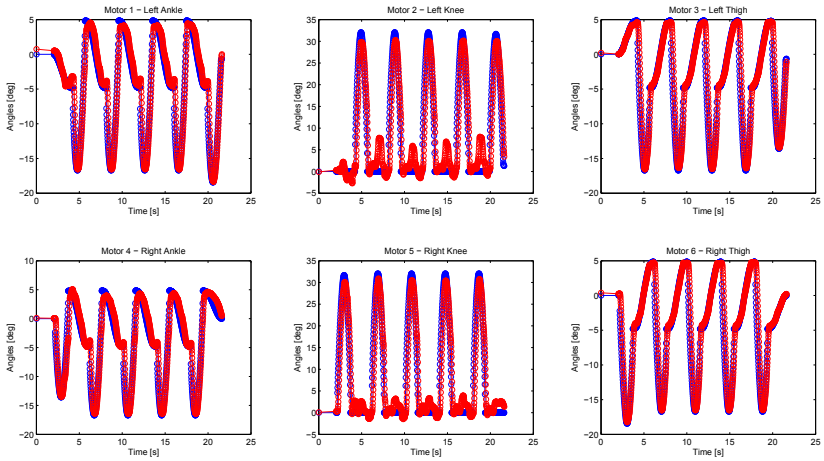

Figure 6.12. Resulting joint angles in deg for all the motors in Experiment2 with trajectory #6 in run #1. Reference trajectory in blue and actual trajectory in red

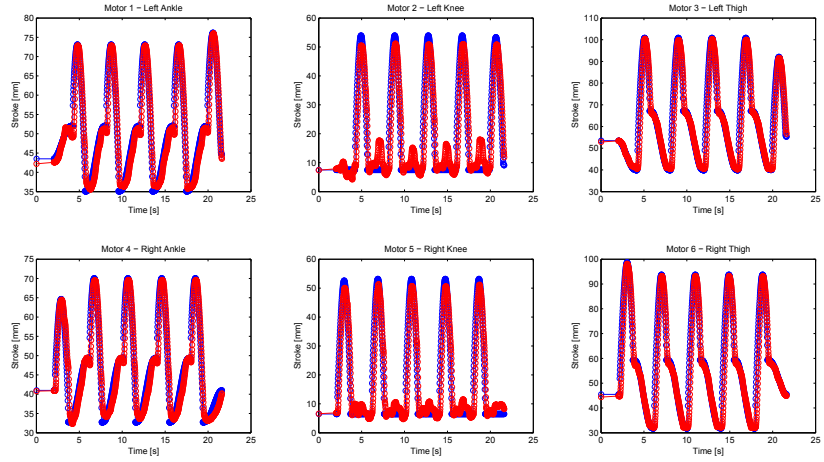

Figure 6.13. Resulting motor stroke in mm for all the motors in Experiment2 with trajectory #6 in run #1. Reference trajectory in blue and actual trajectory in red

The initial idea was to replicate the exact same controls presented in Chapter 4 (see Table 4.2). That meant implementing first the simulations' best resulting algorithm, which was the Passivity Based Control with an additional Proportional and Derivative control (PBC+PD). However, impending limitations were noticed right away in the hardware, which restricted the possibility to experimentally perform this type of control. The first indication was, that experience shows, based on [37, 53], that the

PBC-type of control does not perform well in experiments, even when the hardware is very similar to the model, which is not the case of the GIMBiped and its approximated model, since they are quite different. Further concerns arrived when evaluating the control commands resulting from the simulator and the requirements that these results would impose to the hardware. The need for a fast walking speed to match the natural limit cycle and a wider range for the joints angular positions were important drawbacks.

Additionally, after performing ***Experiment1***, the results showed that under plain position control the GIMBiped was not able to perform long strides and fast walking because of the mechanical restrictions on the joints' limited range and actuators' constraint in speed, force and temperature problems (motors overheat and shut down).

The following possibility for control, from the second best resulting control algorithms in the simulation, was to make the controller a Computed Torque Control (CTC)-type, similar to the ones in Chapter 2 (Section 2.4.2 and Table 4.2). In CTC-type for the previous biped model, a multi-variable control output for a given joint is dependent of several state variables in the model. However, this CTC-type of control suffers from the same problematic as the previous PBC and was also a source of concern when trying to implement it in the hardware.

The CTC and PBC are model-based controllers, which generally perform well when the system's parameters are known fairly accurately and the model is close to the hardware. However, with all the changes needed to be done to the reference model to generate suitable trajectories, these controllers based on the approximated model did not generate a suitable output control torque (function of current for the GIMBiped). Therefore, addition of some external PD control to compensate for the inaccuracies in the model is needed (as seen already in the case of PBC in Chapter 4). For that reason, it was decided to first evaluate the performance of a simpler Proportional and Derivative Independent Joint Control (PD-IJC) and later assess the need and potential benefits of using the information of the approximated model in the feedback loop.

ControlType2: Trajectory Planning

The use of a LCW-based trajectory, generated from a 3-link approximation of the GIMBiped (Figure 4.1 and Figure 4.3) and later controlled with a PD-IJC still included some difficulties in its implementation. An

important issue was that the 3-link approximated model assumes instantaneous and inelastic collision with the ground (also in the impact for the knee lock), which is not true in the GIMBiped testbed. Furthermore, the 3-link model approximation uses point feet and therefore is underactuated (no ankle joint and actuation). The GIMBiped instead has flat feet, and actuation is available in the ankle joint.

The previous observations mean that the whole foot strike phase in the LCW model is not repeatable with the GIMBiped, which also included a double support phase (it is not an instantaneous impact). Consequently, some different reference had to be used in foot strike and double support phase.

Given that the ZMP-based trajectory worked fine in ***Experiment1***, it was also used here as the reference trajectory for the foot strike (or heel strike HS) and double support (DS) period.

The use of the ZMP-based trajectory for the FS and DS period and a LCW for the swing phase of the walking brings the need to connect both types of trajectories, since the ZMP and LCW-based trajectories rarely end or start at the same point. To solve the connection issue, as in the previous section, third order polynomial splines were used to generate smooth trajectories between the ending points of the ZMP-based trajectories and the starting points of the LCW-based trajectories. Also the splines functions were used to connect the points from the ending of the LCW-based trajectories to the starting point of the ZMP-based trajectories.

The ZMP-based trajectory also helps to overcome the problem of ***gait initiation*** that is always present in LCW-based type of robots. Usually, to start walking, the state variables of LCW robots have to be already on the periodic orbit (LC) or be close to the basin of attraction of the LC. Therefore, ideally, the ZMP and the Connecting Trajectory should continually drive the states of the system in and out of the natural LC.

A schematic explanation of the procedure, showing both the original control idea and the final implementation of the ***ControlType2*** is presented in Figure 6.14 and Figure 6.15.

Consequently the implementation to obtain the Trajectory Generator for this ***ControlType2*** is as follows:

Trajectory Generator ControlType2:

1. ***Trajectory Planning-LCW:*** first, an LCW-based trajectory is gener-

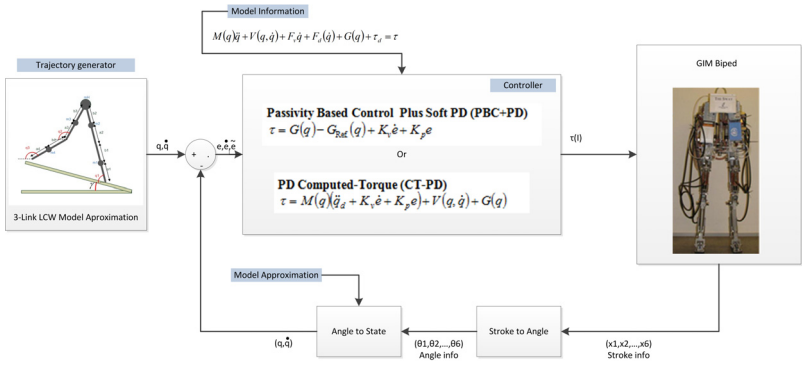

Figure 6.14. Original idea for the control algorithms based on LCW to be implemented in ***ControlType2***

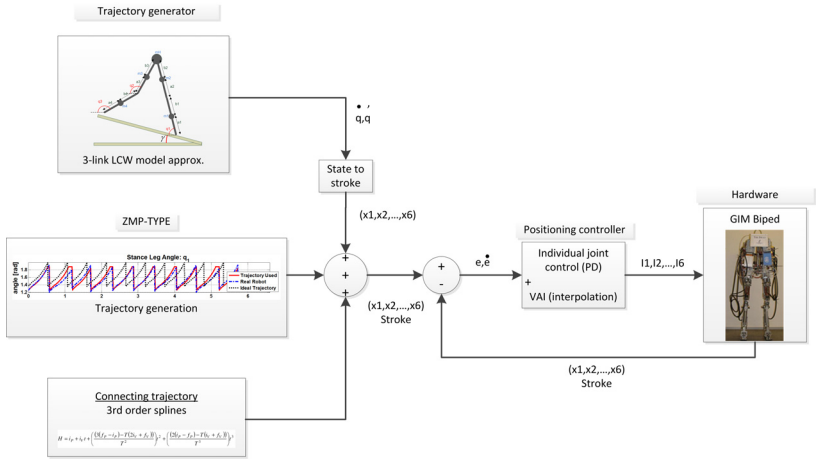

Figure 6.15. Final control algorithm implemented in ***ControlType2***. A combined strategy of ZMP-based type of trajectories and LCW-type of trajectory derived from an approximated 3-link planar biped model

ated for the GIMBiped based on a model approximation. The trajectory is scaled in velocity and step length, so the GIMBiped can perform it. Then the generated trajectory is converted from the state variable angles into stroke values.

2. ***Trajectory Planning-ZMP, IK and angles to stroke conversion:*** after 1), a ZMP-based trajectory is generated with the same approximate velocity as the LCW above and will be used for the initial and final step, as well as for the double support and foot strike phases. As in the ***ControlType1***, IK is performed and later the conversion from angles to strokes.

3. ***Trajectory Planning-Connection and Merge:*** Once the previous

trajectories are calculated, a percentage of each one is chosen and they are merged together using a third order polynomial interpolation. The final trajectory generated is inputted to the ***Positioning Controllers***.

ControlType2: Trajectory Planning-LCW planning

To plan an LCW-based trajectory the controller relies on a 3-link 2D model approximation of the GIMBiped (Figure 4.3). Using this model, the same as in Chapter 4 (Section 4.2), the natural LC for the dynamic system is calculated in the state space (Figure 4.3), and then converted into the desired robots' motor stroke and stroke velocity (Figure 6.15).

However, as already seen in Chapter 5, the real values of the mechanical design of the GIMBiped do not generate a favorable natural LC. Therefore, some changes were introduced in the model and the final trajectory in order to produce a "natural-looking" walking pattern to follow.

The main problem with the original (real) values of the GIMbiped is that it does not provide any LC without scuffing the floor with the swing leg. Therefore, these values are not useful for walking patterns. For that reason, modifications on the mechanical parameters of the model were made, as in Chapter 4, arriving to walking patterns that are more realizable but still with some important issues. The parameters used in the approximated model are shown in Table 6.2, and are the same as the ones in model $Set1$ used in the MATLAB-ODE simulation in Chapter 4, and $Set_{_{Start}}$ used in Chapter 5.

The difficulty with these new values is that they render walking patterns with long step size, high walking speed and small foot clearance, which makes this natural LC, originating from the approximated model, not very robust (due to the non-ideal mass distribution of the real hardware). This brings the need to change the resulting LC and make it slower, with shorter step length than the original LC, and also increase the foot clearance. Thus, tuning was allowed to improve its performance.

Given that the natural LC is too fast and the step length is too long for the possible range of the robot's angle joint, adjustment in the walking speed and step length was needed. The adjustment in step velocity and length follow the amplitude control proposed in [57], where the length stride and velocity are decreased in a relation formula, under the parameter κ. Therefore, the new reference trajectory can be simply achieved by

Table 6.2. Paramters for a 3-link biped model approximation (Figure 4.3) used to generate the biped's trajectory based on the rsulting LC

Parameter	Symbol	Value
Leg Length	L $[m]$	0.900
Shank Length	$a_1 + b_1$ $[m]$	0.450
Thigh Length	$a_2 + b_2$ $[m]$	0.450
Shank CM Height	b_1 $[m]$	0.22425
Thigh CM Height	b_2 $[m]$	0.1849
Shank Mass	m_1 $[kg]$	1.50
Thigh Mass	m_2 $[kg]$	16.33
Hip Mass	m_H $[kg]$	10.0
Slope Angle	γ $[deg]$	6.3

scaling both q and $\dot{q}$ by the same factor as in the equations to follow.

$$q' = \kappa q \tag{6.6}$$

$$\dot{q}' = \kappa \dot{q} \tag{6.7}$$

$$t' = t \tag{6.8}$$

Also, since no feedback control was applied in these experiments, the "robustness of the trajectory" needed to be evaluated and increased if possible. Here, as in Chapter 5, robustness is related with foot clearance. Foot clearance is the distance from the swing leg to the ground when it passes the stance foot. Here this point is named Point of Clearance (PoC), and the clearance distance is symbolized by $D_{\text{Foot Clarence}}$. These are obtained with the same Eq.5.46 and Eq.5.47 as in Chapter 5. The aim in increasing robustness is to increase this distance $D_{\text{Foot Clarence}}$ in the PoC. The desired foot clearance is achieved by linearly increasing q_2 and q_3 from heel-off to PoC and linearly decreasing it from PoC to knee-lock. It must be noticed that by doing these modifications the natural LC is broken (Figure 6.16), and positive work can be appreciated in both phases. Other alternatives should be evaluated later to better maintain the shape of the LC. These alternatives include nonlinear increment of q_2 and q_3 angles or a energy-based increase of the entire systems, as in energy-shaping control [55].

The resulting modified trajectory initially based on LCW can be seen in Figure 6.16. Points in blue, red and gray represent the original LC for the

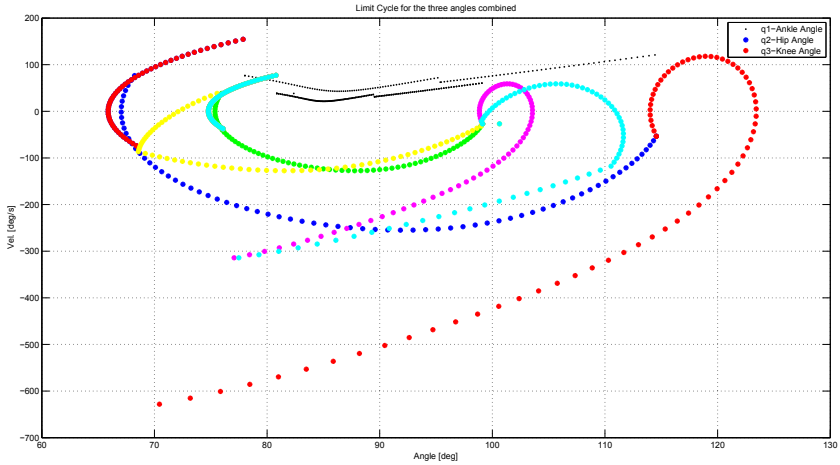

Figure 6.16. Different LC stages towards final trajectory generation. The original LC are points in blue, red and gray. LC with amplitude modification are points in magenta, green and black. The final LC with increased foot clearance are points in cyan, yellow and black

parameters of Table 6.2. Points in magenta, green and black represent the modified LC with the amplitude method after applying Eqs.5.46-5.47. Finally, the points in cyan, yellow and black show the resulting trajectory after applying the linear interpolation to increase the foot clearance.

The mathematical model used here to generate the trajectories for the LCW is the same as in Chapter 4; the only difference is in the programming platform. The simulator in Chapter 4 was developed in MATLAB, and the one used in this experiment was developed in C++, using the GSL, BLAS and LAPACK libraries for integration and matrices calculation. All the source code can be found in GIM's web page [60]. There is the implementation of the integration for the dynamics of the 3-link and 2-link model as well as the equations for the impacts in the knee and with the floor.

ControlType2: Trajectory planning and generation of ZMP phase, Connection and Merge

Given that the ideal model in Figure 4.3 supposes instantaneous and inelastic collisions, which does not correspond to reality, a mixed trajectory approached was implemented. The mixed trajectory is composed of trajectories of the ZMP-based type, which is used during the foot strike and double support phases, and, the ones generated from the 3-link model, used during the swing phase. Since the points in the robot space for both

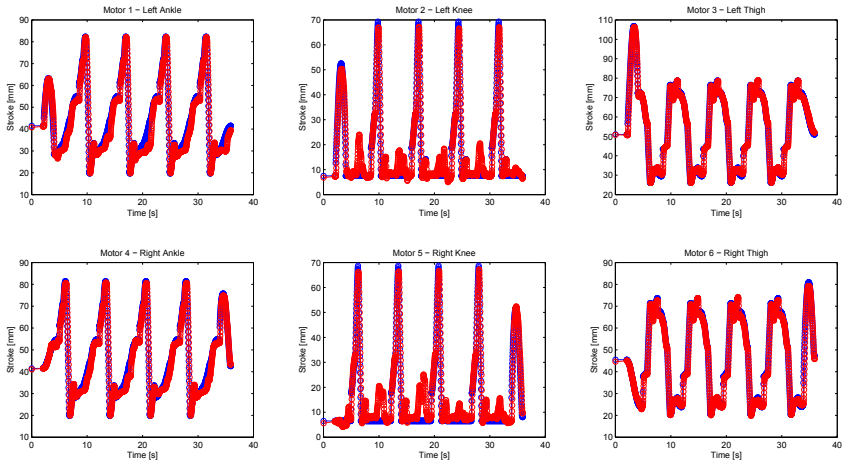

Figure 6.17. Demand position and actual position for all the motors in the GIMbiped during run # 5 in trajectory # 2 for Experiment2

trajectories usually do not match, cubic splines are used to unite the both trajectories, here named the ***connection trajectory***. Therefore, there is the possibility to choose the percentage of the ZMP and LCW trajectories, as well as the length of the connection trajectory used.

The ZMP-based trajectories are generated in the same way as in the previous ***ControlType1***, the only difference being that in here the trajectory is not used integrally and therefore should be sliced according to the percentage selected. The first and the final step are entirely used, and in the ***normal steps*** a percentage on ZMP amount of trajectory inputted defines how much of the original ***normal step*** is used for walking in the ***ControlType2***.

The resulting cut of the trajectory chosen is centered in the moment of the foot strike. Half of it is used in the beginning of the step and half at the end of the step, so it is centered where needed in the foot-strike and double support between consecutive steps.

After the previous ZMP- and LCW-based trajectories are generated and converted to stroke commands, the percentages for each of them are assigned and third order splines are generated to connect the different phases (Figure 6.15).

Figure 6.17 shows the resulting reference trajectory and the actual position tracking for each motor of the GIMBiped. Figure 6.17 shows the values in stroke mm units.

6.4 Experiment Setup

This section presents the experiment setups for each control and the basic information needed to evaluate the results.

6.4.1 Experiment1 Setup

Experiment1 shows the results of 18 different trajectories with 10 runs per trajectory. In every run, the robot walked 10 steps. In every run, the first step is the gait initiation, being half of the normal step size, and the last step is the gait ending, also half of the normal step size.

The 18 different trajectories arrived as a result of the successful walk-

Table 6.3. Parameters settings for the trajectories performed in ***Experiment1***[a]

Experiment number	Step height $[m]$	Step length$[m]$	PD value stance leg	PD value swing leg
1	0.020	0.15	M	M
2	0.020	0.15	M	H
3	0.020	0.15	H	S
4	0.020	0.15	H	M
5	0.020	0.15	H	H
6	0.020	0.20	H	S
7	0.020	0.20	H	M
8	0.020	0.20	H	H
9	0.020	0.25	H	H
10	0.035	0.15	H	S
11	0.035	0.15	H	M
12	0.035	0.15	H	H
13	0.035	0.20	H	H
14	0.050	0.15	M	H
15	0.050	0.15	H	S
16	0.050	0.15	H	M
17	0.050	0.15	H	H
18	0.050	0.20	H	M

[a] All the experiments performed with trajectory design with 3 s time per step.

Table 6.4. PID settings

Setting	Abrev.	Proportional (P) $[A/mm]$	Integral (I) $[A/mm/t]$	Derivative (D) $[A/mm \cdot t]$
Soft	S	1.00	0.00	2.00
Medium	M	2.00	0.00	3.00
Hard	H	4.00	0.00	5.00

ing experiments tried during ***Experiment1***. The whole trial set was composed by variations of the main parameter that define the Trajectory Generator and Positioning Control from Section 6.3.3. The whole trial set consisted of all the combinations of 3 different step length, 3 different step height and 9 different PD settings (for the swing leg and the stance leg positioning controllers).

The possible settings for the PID values are presented in Table 6.4, and the possible setting for the different step length and step height can be obtained from Table 6.3

Just 18 out of the 81 possible combinations of parameters resulted in successful walking patterns. The successful trajectories for the ***Experiment1*** are presented in Table 6.3 with their corresponding parameters.

6.4.2 Experiment2 Setup

In ***Experiment2***, 10 different trajectories were tested: 6 trajectories based on ***Controtype1*** and 4 based on ***ControlType2***. For the 6 trajectories

Table 6.5. Parameter settings for the trajectories in ***Experiment2*** with ***ControlType1***

Experiment number	Step height $[m]$	Step length$[m]$	Time per step $[s]$	PD value (swing-stance)
1	0.035	0.15	3.0	H-H
2	0.035	0.15	2.5	H-H
3	0.035	0.15	2.0	H-H
4	0.035	0.15	1.5	H-H
5	0.035	0.20	2.5	H-H
6	0.035	0.20	2.0	H-H

Table 6.6. Parameters setting for the trajectories in ***Experiment2*** with ***ControlType2***

	ZMP phase					LCW stage				Connect Traj.
Experiment number	Step height $[m]$	Step length $[m]$	Time per step $[s]$	PD value (swing-stance)	% ZMP phase	Clearence $[m]$	$\mathcal{K}$ [a]	PD value (swing-stance)	% ZMP phase	% Connecting trajectory phase
1	0.035	0.15	3.0	H-H	40	0.06	0.4	H-H	30	30
2	0.035	0.18	2.5	H-H	40	0.06	0.4	H-H	30	30
3	0.035	0.20	2.5	H-H	40	0.06	0.5	H-H	30	30
4	0.035	0.24	2.3	H-H	40	0.06	0.5	H-H	30	30

[a] κ is the scale factor.

from the ***ControlType1***, the goal was to look for the fastest possible walking and the longest step length, so as to achieve the maximum walking velocity for the robot. Out of several trials incrementing the speed of the 18 successful trajectories from the previous ***Experiment1***, only 6 were significantly and consistently performing well, and they are summarized in Table 6.5.

For the trajectories based on LCW, a high number of different parameter combinations were tested, looking to generate a set that would result in successful LCW-based trajectories. However, only four of them were consistently performing well and were chosen here to represent a possible initial try for the LCW-based trajectories (Table 6.6).

6.5 Metrics for the Experiment Analysis

Various metrics were employed to analyze the result of the experiments in the next sections. Two of the most commonly used metrics to evaluate the performance of biped robots were already presented in Chapter 2 (Section 2.2.3): the specific cost of transport (CoT) and the Froude Number (F_r). This section presents further definitions of this and other metrics employed to evaluate the performance of the GIMBiped in the experiments.

6.5.1 Cost of Transport

Here four different types of CoT will be used to evaluate the results: CoT1, CoT2, CoT3 and CoT4. These previous indices mainly differ in the way in which they calculate the energy variable in the CoT equation (Eq.2.5). Therefore, as in Eqs.(2.8-2.6), here the energy and the different CoT are calculated with:

$$E_{i_{Mech.}}(t) = \begin{cases} u_i(t)\dot{q}(t) & \text{if } u_i(t)\dot{q}(t) > 0 \\ u_i(t)\dot{q}(t)K_{reg} & \text{if } u_i(t)\dot{q}(t) \leq 0 \end{cases} \tag{6.9}$$

$$E_{i_{Elec.}}(t) = \begin{cases} V_i(t)I(t) & \text{if } u_i(t)\dot{q}(t) > 0 \\ V_i(t)I(t)K_{reg} & \text{if } u_i(t)\dot{q}(t) \leq 0 \end{cases} \tag{6.10}$$

$$\mathrm{CoT}_{1,2,3,4} = \frac{\int_0^{T_I} \sum_{i=1}^{N_q} E_i(t)\, dt}{Mgd} \tag{6.11}$$

CoT1 uses the electrical energy input without regeneration in the above Eqs.(6.10-6.11). Therefore in Eq. 6.10 $K_{reg} = 1$, and, as an example, CoT1

is always:

$$\mathrm{CoT}_1 = \frac{\int_0^{T_I} \sum_{i=1}^{N_q} V_i(t) I(t)\, dt}{Mgd} \tag{6.12}$$

CoT2 uses the electrical energy input with total regeneration. Therefore in Eq. 6.10 $K_{reg} = -1$.

CoT3 and CoT4 instead use mechanical energy without regeneration and with total regeneration respectively. Therefore, in Eq. 6.9 $K_{reg} = 1$ and $K_{reg} = -1$ for CoT3 and CoT4 respectively.

CoTs are also analyzed through the percentage value between them. The percentage:

$$\%_{\frac{\mathrm{CoT3}}{\mathrm{CoT1}}} = \frac{CoT3}{CoT1} \cdot 100 \tag{6.13}$$

indicates the efficiency of the conversion from electrical energy to mechanical energy, and the percentage

$$\%_{\frac{\mathrm{CoT4}}{\mathrm{CoT3}}} = \frac{CoT4}{CoT3} \cdot 100 \tag{6.14}$$

relates to the efficiency of the controller, since if too much energy can be regenerated that means that the controllers are wasting energy in a tight control.

6.5.2 Froude Number

The Froude number is used exactly as defined previously in Chapter 2 (Section 2.2.3). The velocity was calculated measuring the displacement of the hip's position during the walking period.

6.5.3 Percentage of Foot Scuffing

In the experiments, during the swing phase of the walking process, the foot of the swing leg occasionally had mild contact with the ground during moments in which, according to the reference trajectory, such contact should not exist. This mild foot scuffing indicates how tightly the reference trajectory was tracked by the controller, and eventually it has the effect of reducing the achieved step length.

In practice, the foot scuff is detected by the force sensors present in the GIMbiped's foot, and the percentage is calculated during the swing phase period of the reference trajectory.

6.5.4 External Disturbances in the System

Several external disturbances can be considered and analyzed for an experiment like the one performed in the GIMBiped. Here, however, only

external disturbances related to the frame interaction with the robot are considered and computed for its evaluation. The frame is the supporting structure that restricts the GIMBiped to move in 2D.

The disturbances of the frame were calculated as the energy "wasted" by the robot to counteract the momentum of the frame and the energy used to overcome the friction of the frame rolling against the ground and track. Since the friction coefficient cannot be calculated instantaneously, an upper and lower bounds were calculated based on the experimental measure of the highest and lowest dynamic coefficient of friction. Static friction was neglected.

The energy used to overcome the momentum of the frame is calculated by integrating the mass of the frame times the acceleration, times the velocity, where the velocity is given by a filtered measure of the acceleration provided by the IMU placed in the frame. The final values are presented in the result tables as a percentage of the total mechanical energy consumption without regeneration (the same used to calculate CoT1).

6.6 Result of Experiments in the GIMBiped

To analyze the results of the experiments with the metrics presented previously, different conditions were considered. First, out of the ***ten*** total steps performed in each run, ***one*** corresponds to the initial step, and ***one*** to the final step. These two steps are different from the rest since they are half of the size and take the same time as the normal steps to be completed. Therefore, two scenarios were considered.

Experiment Scenarios :

1. ***10-step simulation:*** All the 10 steps of each run are included in the calculation of CoT, F_r and all the rest of the coefficients. This computation includes the first and the last step of each run which are half of the length of the normal steps.

2. ***8-step simulation:*** Only the 8 middle steps are considered in the result computations, excluding the first and the last steps.

Scenario 2 should give a result pointing to the steady walking state of the GIMbiped. Most of the values from the literature use the same type of scenario to present their results and do not consider the effort for starting and finishing the walking process. Scenario 1 should give some idea of

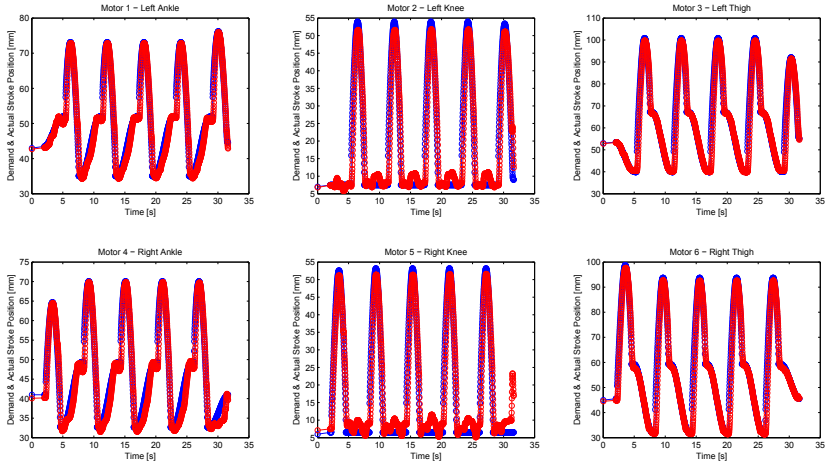

Figure 6.18. Demand position and actual position for all the motors in the GIMbiped during run # 6 in trajectory # 12 for Experiment1

the cost of starting and finishing the walking process, which is usually not presented in the studies. The results of these scenarios are presented in various result tables with the proper indication in the captions.

Another alternative way to explore the results in energy consumption is to consider or exclude the energy used during the time of double support. These values are indicated also in all the result tables as a help to explore how much energy could be save in the Double Support (DS) transition between steps, if such time is reduced or suppressed. The values are referred to in the result tables as ***With double support*** and ***Without double support***.

6.6.1 Results Experiment1

All the necessary information for data analysis and post processing from all the runs was gathered and stored. Figure 6.18 shows the result of the position tracking for all the actuators in the GIMbiped during the walking experiment of run # 6 in trajectory # 12 from Experiment1.

From the plot in Figure 6.18, it can be appreciated that the reference trajectory is followed quite well, and the main disturbance occurs in the knee's motors during the stance phase. It can be induced from the previous figure that during the stance phase these motors are working very hard to maintain the desired position.

Figure 6.19 shows however that the motor currents in the knees are not much higher than the ones in the ankle and that the knee's motors are

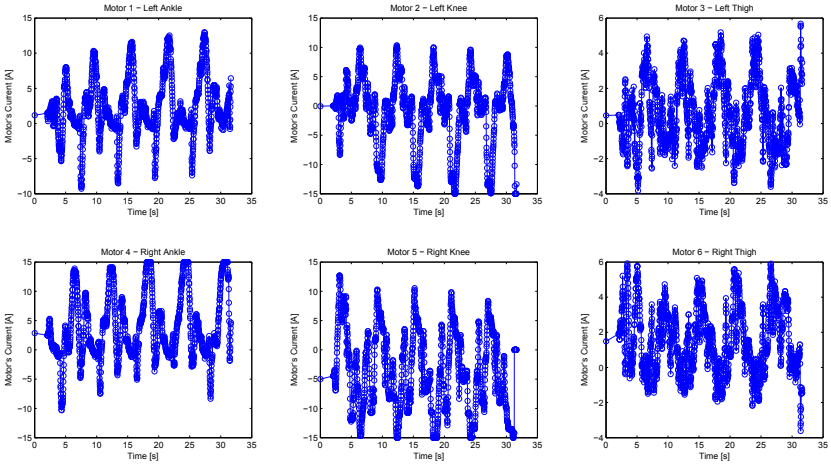

Figure 6.19. Demand current from all the motors in the GIMbiped during run # 6 in trajectory # 12 for Experiment1

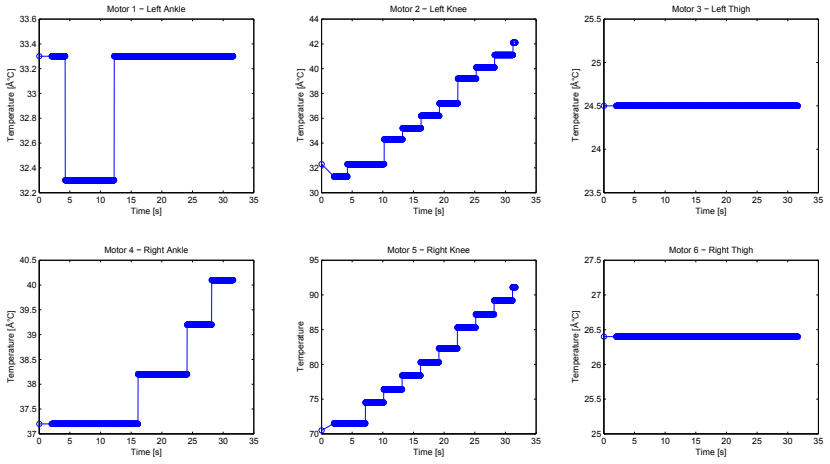

Figure 6.20. Temperature profile for all the motors in the GIMbiped during run # 6 in trajectory # 12 for Experiment1

working hard but not always in a saturated mode. This results, together with the temperature plots presented in Figure 6.20 indicates that the knee motors are working above their capabilities.

The thighs' motors are the only ones performing in a comfort zone, not surpassing often and by much, half of the allowed maximal current (15 A) and maintaining temperature constant during the whole walk.

It is concluded then that the knee motors were not built to perform with such demanding cycles; although they do not saturate at the maximum

current allowed (15 A), they still overheated and shunted down in some experiments.

The shank worked as intensively as the knee; however, it did not overheat and fail like the knee's motors. The knee motors used the stator model PS01-37x120F-HP-C, with slider model PL01-20x300/240-HP, and the other motors in the biped used sliders model PS01-48x240-C, with slider model PL01-28x350/270, all from LinMot vendor [245].

It must be mentioned that fans were installed on top of the knee motors to allow them to perform the whole experiments and speed up the cooling down process between each run. Also, special copper dissipative covers were built for all the motors.

From Figure 6.20, it can be noticed that the right-knee motor is at higher temperature than all the others. This is due to the accumulated heat during the previous runs (5 runs were performed before the one shown in Figure 6.20).

Right ankle in particular is working quite intensely, reaching saturation mode cyclically when in stance phase. The right ankle motor is actually working harder than the left ankle motor, and since the trajectories generated are symmetric, the most probable explanation for the results is that there is some slight difference between the mechanical parameters of the left and right leg, which is not balanced due to the lateral restrictions imposed by the frame. The right knee and thigh motors are also doing slightly more work than their left counterpart. That also confirms the theory of difference in mechanical layout. The difference is observed again in the higher accumulated temperature of the motors on right side.

The voltage plot in Figure 6.21 shows how much the motor's power supply is affected by the required combined currents. As detailed in Section 6.5, the current and voltage values are used to calculate ***CoT1*** and ***CoT2***, which are presented in the result tables, Table 6.7 and Table 6.8 for Experiment1.

From the result tables, several observations can be made. The first and most obvious, and maybe even the most important one, is the huge difference between CoT1 and CoT2 compared with CoT3 and CoT4. This difference is also evident in the percentage factor $\%_{\frac{\mathrm{CoT3}}{\mathrm{CoT1}}}$, which in both tables are symbolized by $\%^a$ and $\%^e$ for the calculations with DS and without DS, respectively. The previous factor indicates that the efficiency of the conversion from electrical energy to mechanical energy in the system is

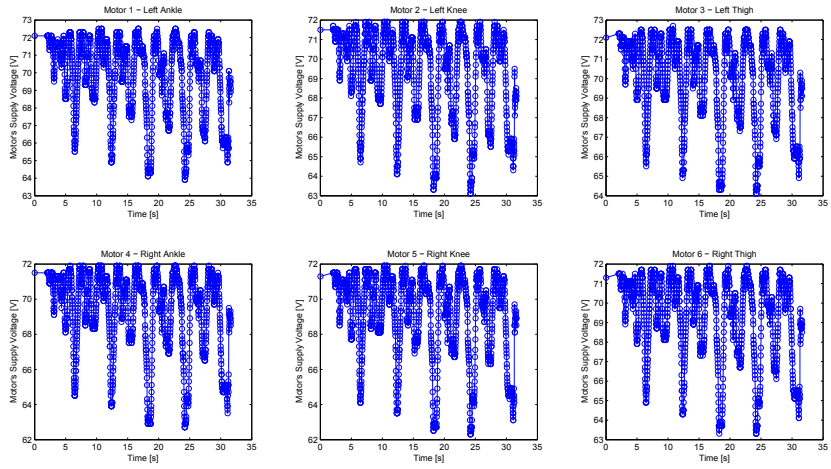

Figure 6.21. Voltage input for all the motors in the GIMbiped during run # 6 in trajectory # 12 for Experiment1

between 0.7 to 1.1%, which means that in the best cases the mechanical energy available to move the robot is 100 times less than the electrical energy inputted by the batteries. The previous values show a huge "waste" of energy already in the transmission stage.

Apart from the dreadful values, the efficiency itself is quite variable depending on the type of trajectory. Table 6.7 and Table 6.8 show more than 34% variation in the efficiency depending on the trajectory. However, Table 6.7 and Table 6.8 also show only up to 5% increase in the efficiency when DS is suppressed from the calculations. The efficiency also usually increases when only the middle 8 steps are considered; however, the variation is small and in average less than 5%.

The previous numbers indicate that the efficiency of the energy transmission, although depending heavily on the trajectory for this type of control (and also slightly on the period of DS and steady state of the biped gait), is still mainly a mechanical and driver's efficiency problem.

That said, the specific mechanical costs of transport, indicated by CoT3 and CoT4, do not present entirely bad values. Although they are higher than what was achieved by other dynamic walking bipeds, expending about twice more energy in the best cases, the best-performing values are 10 times better compared with the "reported" values of other ZMP walking bipeds like ASIMO.

The values of CoT4 and CoT3 also varies greatly, depending on the trajectory reaching 30% difference between different trajectories. Following

the same trend as before, better performance values are apparent when DS is not considered and also when only the 8 middle steps are used for the CoTs computation.

The $\%_{\frac{\text{CoT4}}{\text{CoT3}}}$ factors, which in both tables are symbolized by $\%^b$ and $\%^f$, for the calculations with DS and without DS, respectively, reveal important information about the efficiency of the controller. $\%_{\frac{\text{CoT4}}{\text{CoT3}}}$ shows that on average 30% of the energy used by the controller is negative energy, which indicates that almost $\frac{1}{3}$ of the total energy used has been "wasted" through "unnecessarily" tight control. This value indicates that a better control which does not overshoot constantly the set-point could be devised, and therefore not so much negative energy would need to be generated. The values also indicate that if this type of control is used it is important to devise a method for energy regeneration.

Focusing the attention now to velocity and displacement of the robot, another major fact is revealed from these experiments. An average human walking speed is about $1.4\ m/s$ ($5\ km/h$) [285] and the step length is highly variable depending on the human anatomy and walking speed but with an acceptable average value for males of $0.75\ m$ [286]. Table 6.3 shows that the trajectories in Experiment1 for walking patterns with step length longer than $0.25\ m$ were not successful. This is mainly due to the restriction on the joints' angle range and lack of feedback control. That means that only $\frac{1}{3}$ of a normal human step was achieved with the GIMBiped hardware, which clearly impacts on the values of CoT.

In Experiment1, only trajectories with 3 s per step were tested to make comparable all the trajectories with different step lengths and steps heights. However, the maximum velocity achieved in the GIMBiped testbed later in one of the trajectories of Experiment2 was also very much below the average human walking speed, reaching only $0.1\ m/s$ ($0.36\ km/h$).

The previous result translated in a very low dimensionless velocity for all the trajectories in Experiment1, ranging from 0.010 to 0.025 m/s. The previous values are 10 to 20 times slower than the values achieved by other dynamic walking robots (see Figure 6.35).

Relating the F_r with the CoT4, it can be seen that faster walking patterns generate better performance in CoT. This should be one of the main points to consider in the further development of the GIMBiped to allow higher range in the joints for faster and longer steps.

Analyzing now the % of scuffing during the swing phase, it can be seen from Table 6.3, together with Table 6.8 and Table 6.7, that there is a

Table 6.7. Results of Experiment1 for 10 steps, including the initial and final step

	Energy with double support						Speed	Scuffing	Frame to robot energy %			Energy without double support					
Exp. #	CoT_1	CoT_2	%[a]	CoT_3	CoT_4	%[b]	F_r	%[c]	p[d]	Friction High	Friction Low	CoT_1	CoT_2	%[e]	CoT_3	CoT_4	%[f]
1	67.80	22.91	0.69	0.466	0.321	68.7	0.015	65.9	3.537	1.271	0.323	63.766	21.542	0.71	0.4536	0.3108	68.5
2	71.27	24.64	0.77	0.549	0.365	66.5	0.014	67.7	3.112	0.942	0.239	66.895	23.377	0.79	0.5309	0.3531	66.5
3	84.46	26.63	0.71	0.598	0.412	68.9	0.010	81.9	4.559	1.250	0.318	78.129	25.338	0.72	0.5620	0.3936	70.0
4	85.61	27.30	0.73	0.623	0.429	68.9	0.010	76.9	3.517	0.901	0.229	78.047	25.988	0.75	0.5891	0.4123	69.9
5	91.09	28.97	0.78	0.712	0.481	67.5	0.010	74.7	3.821	0.922	0.235	81.737	27.596	0.83	0.6791	0.4642	68.4
6	85.72	26.88	0.74	0.635	0.437	68.8	0.012	81.5	4.667	1.009	0.257	77.618	25.215	0.75	0.5789	0.4071	70.3
7	79.48	24.92	0.75	0.599	0.412	68.7	0.013	76.5	4.960	1.071	0.272	71.757	23.336	0.78	0.5576	0.3885	69.7
8	61.27	20.89	0.87	0.535	0.365	68.1	0.017	72.4	4.798	0.869	0.221	55.893	19.796	0.91	0.5083	0.3502	68.9
9	54.65	18.53	0.88	0.483	0.335	69.4	0.022	69.6	6.123	1.024	0.260	49.657	17.451	0.92	0.4563	0.3202	70.2
10	65.33	21.26	0.79	0.514	0.362	70.3	0.015	59.5	5.419	1.267	0.322	62.446	20.566	0.80	0.4976	0.3517	70.7
11	64.33	21.39	0.83	0.531	0.366	68.8	0.015	56.8	5.698	1.298	0.330	61.791	20.949	0.84	0.5205	0.3603	69.2
12	70.93	23.86	0.83	0.592	0.407	68.7	0.014	55.7	5.339	1.127	0.287	67.108	23.336	0.86	0.5745	0.3999	69.6
13	64.86	21.66	0.86	0.555	0.379	68.5	0.017	54.2	5.207	0.926	0.235	59.972	20.559	0.88	0.5271	0.3638	69.0
14	68.44	24.53	0.89	0.607	0.408	67.1	0.016	42.3	4.604	1.107	0.286	64.390	23.316	0.90	0.5813	0.3928	67.6
15	66.32	22.31	0.86	0.572	0.390	68.2	0.016	50.2	5.943	1.326	0.337	62.411	21.112	0.86	0.5394	0.3714	68.8
16	65.84	22.89	0.90	0.591	0.404	68.3	0.016	47.8	5.946	1.204	0.306	61.883	21.727	0.91	0.5645	0.3892	68.9
17	68.31	26.61	1.01	0.691	0.471	68.2	0.015	47.1	6.918	1.217	0.309	61.694	24.942	1.04	0.6392	0.4429	69.3
18	52.38	20.43	0.99	0.516	0.359	69.5	0.022	51.3	7.453	1.158	0.295	47.318	19.074	1.02	0.4834	0.3415	70.6

Table 6.8. Results of Experiment1 for 8 steps, without including the initial and final step

	Energy with double support						Speed	Scuffing	Frame to robot energy %			Energy without double support					
Exp. #	CoT_1	CoT_2	%[a]	CoT_3	CoT_4	%[b]	F_r	%[c]	p[d]	Friction High	Friction Low	CoT_1	CoT_2	%[e]	CoT_3	CoT_4	%[f]
1	64.39	22.08	0.70	0.449	0.312	69.5	0.016	65.8	3.918	1.425	0.363	60.156	20.562	0.72	0.4349	0.3011	69.2
2	67.55	23.62	0.78	0.530	0.356	67.1	0.016	67.7	3.422	1.045	0.266	62.969	22.229	0.81	0.5105	0.3426	67.1
3	77.94	25.27	0.72	0.561	0.390	69.6	0.011	81.9	5.183	1.413	0.359	71.361	24.024	0.74	0.5252	0.3724	70.9
4	78.72	25.73	0.75	0.591	0.412	69.6	0.012	76.9	3.898	0.992	0.252	70.714	24.412	0.78	0.5546	0.3939	71.0
5	83.51	26.96	0.81	0.678	0.461	67.9	0.011	74.7	4.281	1.025	0.261	73.422	25.522	0.87	0.6423	0.4434	69.0
6	78.13	25.18	0.77	0.601	0.418	69.6	0.013	81.5	5.208	1.108	0.282	69.484	23.485	0.78	0.5435	0.3879	71.4
7	72.50	23.15	0.79	0.569	0.397	69.6	0.015	76.5	5.555	1.186	0.302	64.297	21.497	0.82	0.5267	0.3725	70.7
8	56.24	19.31	0.91	0.511	0.351	68.8	0.019	72.3	5.349	0.965	0.245	50.525	18.156	0.95	0.4814	0.3358	69.7
9	50.09	16.79	0.90	0.452	0.317	70.2	0.024	69.6	7.032	1.168	0.297	44.725	15.619	0.95	0.4229	0.3007	71.1
10	60.79	20.33	0.81	0.489	0.348	70.9	0.016	59.5	6.418	1.490	0.379	57.899	19.648	0.82	0.4729	0.3375	71.4
11	59.66	20.25	0.85	0.509	0.352	69.2	0.017	56.8	6.380	1.453	0.369	57.154	19.845	0.87	0.4979	0.3469	69.7
12	64.11	22.09	0.86	0.552	0.382	69.1	0.016	55.7	5.962	1.276	0.325	60.301	21.570	0.89	0.5339	0.3748	70.2
13	59.39	19.91	0.88	0.521	0.359	68.9	0.019	54.2	5.724	1.026	0.261	54.215	18.746	0.91	0.4917	0.3420	69.6
14	61.93	22.51	0.88	0.544	0.367	67.5	0.018	42.3	5.180	1.293	0.329	57.865	21.218	0.89	0.5175	0.3511	67.9
15	61.37	20.82	0.88	0.540	0.368	68.2	0.018	50.1	6.649	1.490	0.379	57.276	19.549	0.88	0.5062	0.3483	68.8
16	60.13	21.48	0.92	0.555	0.380	68.6	0.018	47.8	6.695	1.363	0.347	56.029	20.234	0.94	0.5260	0.3639	69.2
17	62.96	25.26	1.05	0.662	0.453	68.4	0.017	47.1	7.599	1.346	0.342	56.023	23.406	1.08	0.6060	0.4214	69.5
18	48.22	19.22	1.02	0.492	0.343	69.6	0.025	51.3	8.129	1.279	0.325	42.883	17.811	1.07	0.4576	0.3245	70.9

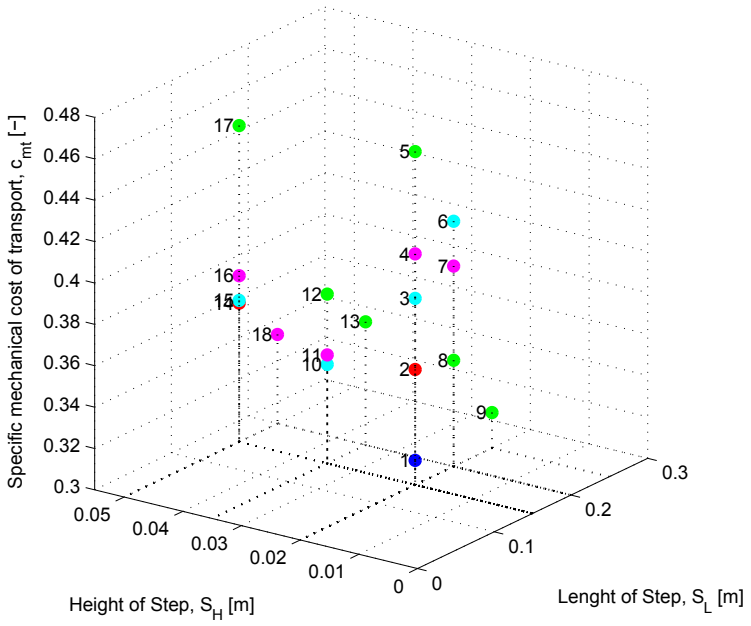

Figure 6.22. CoT4 values for Experiment1 results on a 3D-plot versus step length and step height

direct relation between the amount of foot scuffing and the stiffness of the controllers. The trajectories that present a higher percentage of foot scuffing during the swing phase have softer PID settings.

Finally, evaluating the results from the disturbance of the frame, the values indicate some active disturbance in the system due to the frame. However such disturbances are not large enough to dominate the behavior of the system. The value indicated as p^d in Table 6.8 and Table 6.7 indicates the percentage of the total energy of the system which is used to counteract the momentum of the frame. A maximum of 8% of the whole energy used by the biped is employed to counteract the frame's momentum. The highest values are presented in trajectories with longer and faster step lengths, indicating that most of the disturbance of the frame is introduced during the HS. The values for the friction bounds bare relatively small, ranging from 0.2% to 1.5% of the total energy used by the system.

Figure 6.22 shows all the experiment results for values of CoT4 on a 3D-plot versus step length and step height. The corresponding experiment number, presented in Table 6.3, is indicated besides the experiment value, and the color of the result indicates the PID settings (green=H-H; cyan=H-

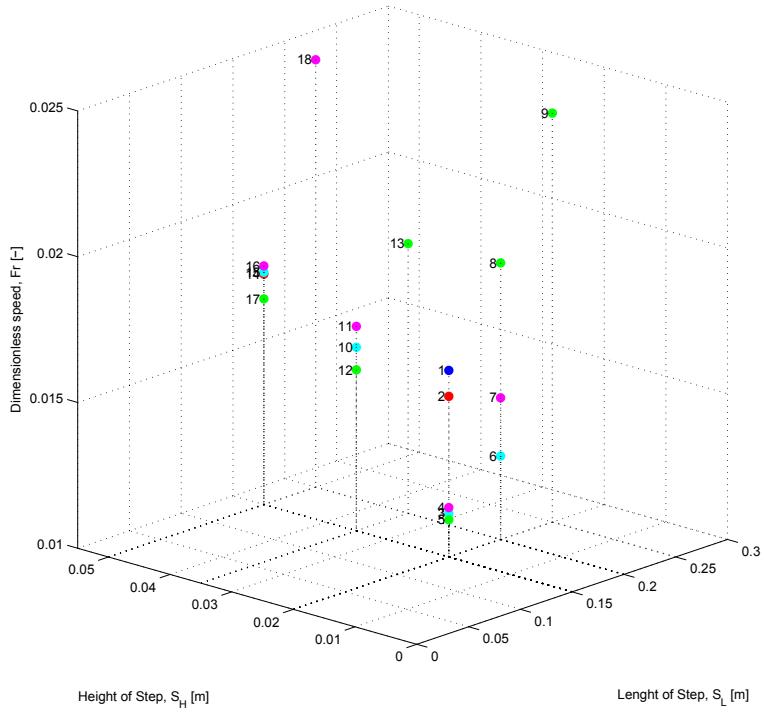

Figure 6.23. F_r values for Experiment1 results on a 3D-plot versus step length and step height

S; magenta=H-M; red=M-H; blue=M-M from Table 6.4)

Similarly, Figure 6.23 shows all the experiment results for values of the F_r on a 3D-plot versus step length and step height.

6.6.2 Results Experiment2

Considering the analysis done previously on the results of Experiment1, the best performing trajectories were chosen to continue the study now under variations of the walking speed.

Most of the trajectories with long steps were tested under different values for time per step, trying to reduce the original 3 s per step towards something closer to the human frequency $\approx$1 s per step. Most trajectories failed once the time per step was reduced (again mostly due to the lack of feedback and restriction in the angle joint range), and only trajectory #12 and trajectory #13 were successfully altered.

Trajectory #12 was gradually speed-up as shown in Table 6.5, where the time per step took the values of 3 s (original value), 2.5 s, 2.0 s and 1.5

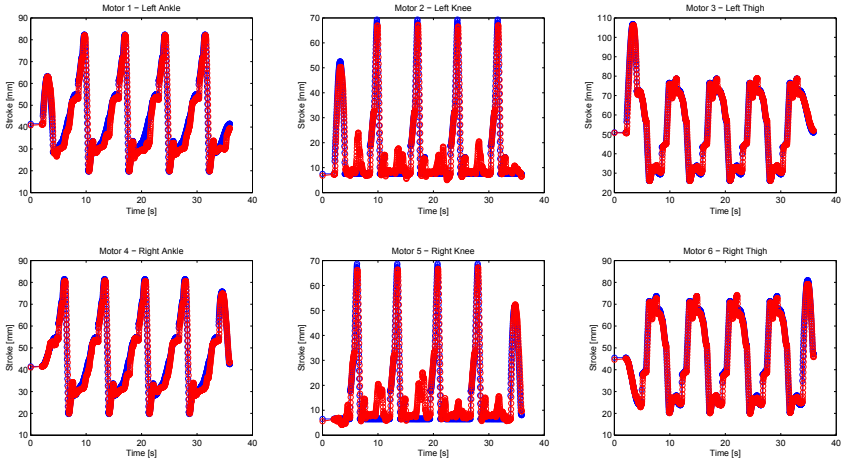

Figure 6.24. Position tracking for all the actuators in the GIMbiped during the walking experiment of run # 5 in trajectory # 9 from Experiment2

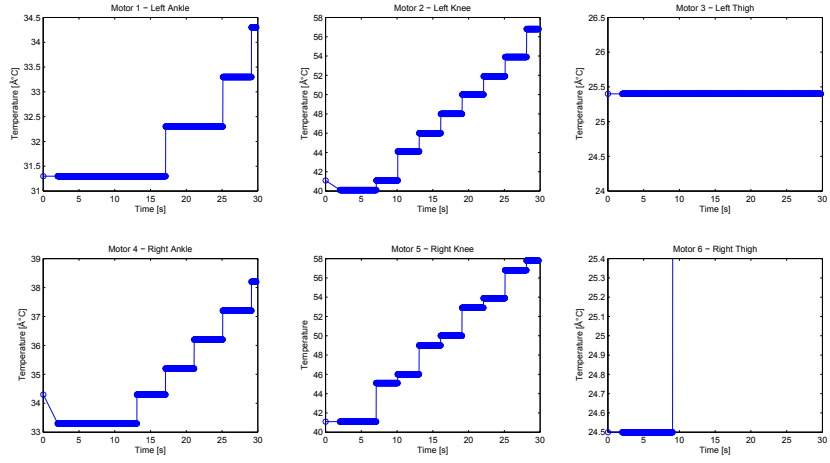

Figure 6.25. Temperature for all the actuators in the GIMbiped during the walking experiment of run # 5 in trajectory # 9 from Experiment2

s. Similarly, trajectory #13 managed to successfully perform walking with time per step values of 3 s (original value), 2.5 s and 2 s.

Alternatively, new trajectories based on the ControlType2 were implemented, as explained in Section 6.4.2, with the parameters of Table 6.6. Such trajectories also present different walking velocities, and since the variables of the trajectories generated with the ControlType1 were already analyzed graphically in Section 6.6.1, here the figures will illustrate only the behavior of the trajectories generated by the ControlType2.

Figure 6.24 shows the result of the position tracking for all the actuators

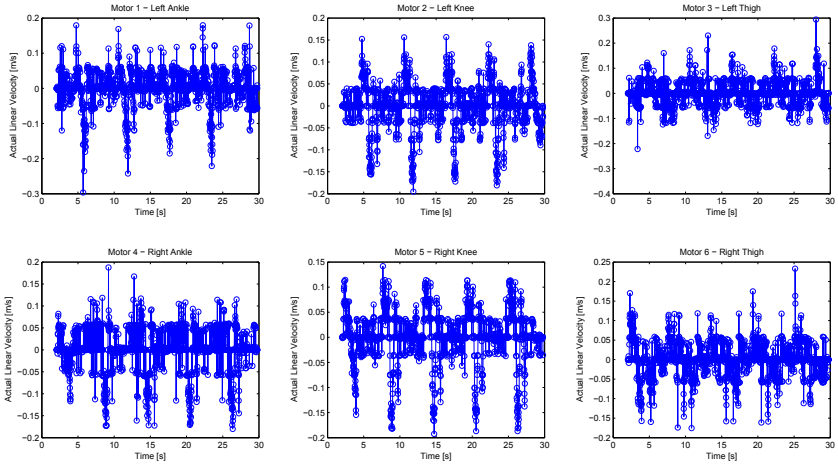

Figure 6.26. Actual linear velocity for all the actuators in the GIMbiped during the walking experiment of run # 5 in trajectory # 9 from Experiment2

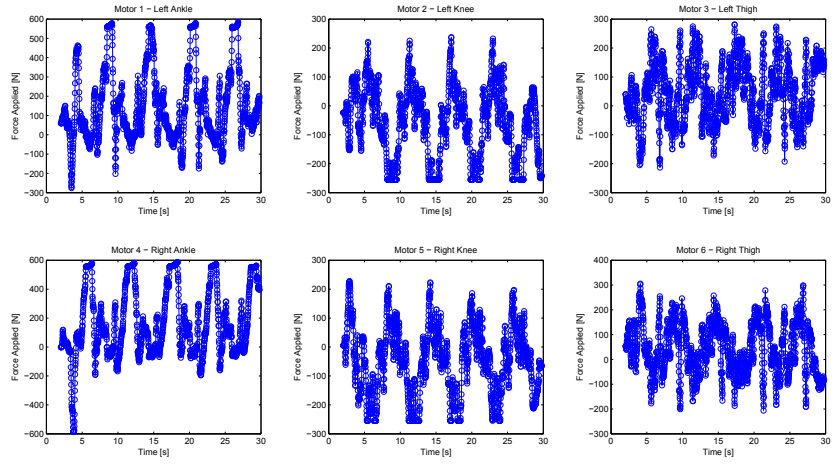

Figure 6.27. Force applied in all the actuators in the GIMbiped during the walking experiment of run # 5 in trajectory # 9 from Experiment2

in the GIMbiped during the walking experiment of run # 5 in trajectory # 9 from Experiment2.

Form the plot in Figure 6.24, it can be seen that the reference trajectory is followed fairly well and that again the main disturbance occurs in the knee's motors during the stance phase. If compared with the trajectories in Figure 6.18, the trajectory coming from the ControlType2 presents more abrupt changes. The controller seems to have some difficulty following the trajectory of the ankles during the stance phase but without any

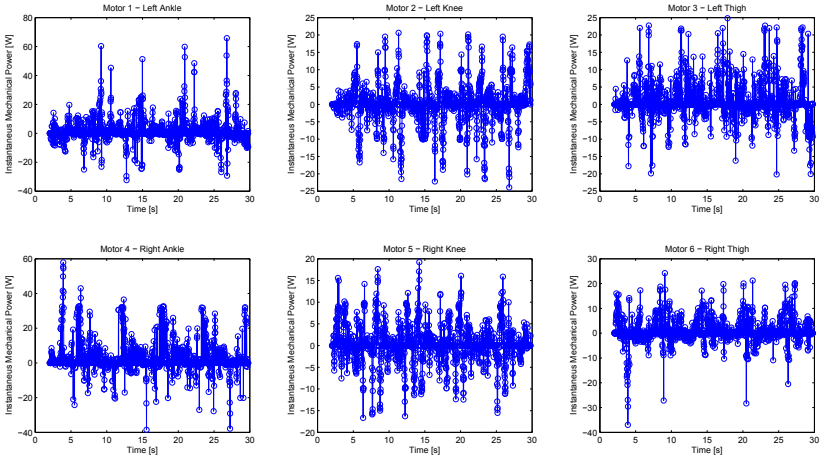

Figure 6.28. Mechanical power without regeneration for all the actuators in the GIMbiped during the walking experiment of run # 5 in trajectory # 9 from Experiment2

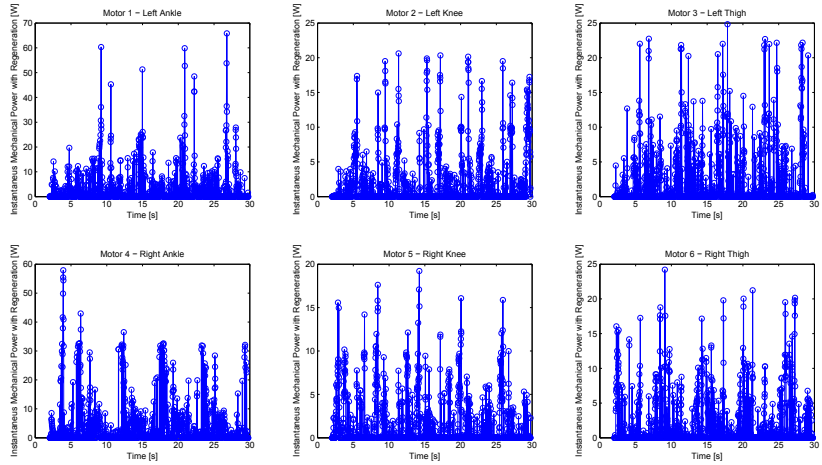

Figure 6.29. Mechanical power with regeneration for all the actuators in the GIMbiped during the walking experiment of run # 5 in trajectory # 9 from Experiment2

hard consequences in the outcome of the walking.

Looking at Figure 6.25, the same behavior as in Experiment1 is observed: the knee motors present a fast increase in temperature, the shank shows some changes in temperature and the thigh remains mostly constant.

The plots in Figure 6.26 and Figure 6.27 present the results of the actual linear velocity and force applied for every motor respectively. These are the variables used to calculate CoT3 and CoT4, which are the mechan-

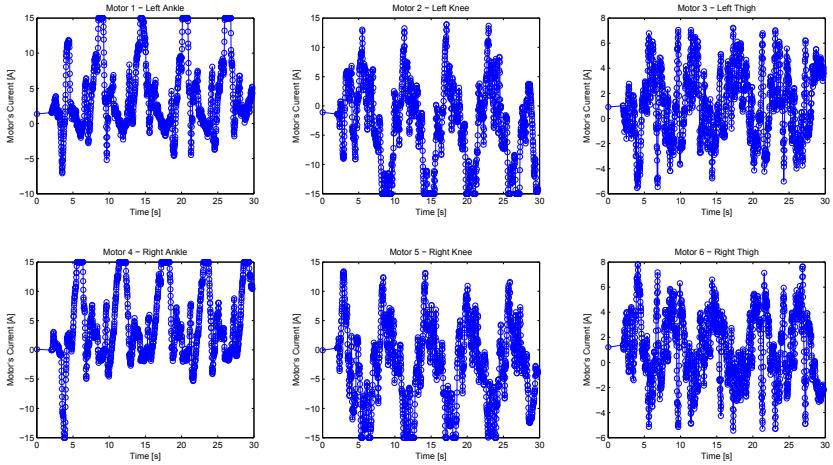

Figure 6.30. Current for all the actuators in the GIMbiped during the walking experiment of run # 5 in trajectory # 9 from Experiment2

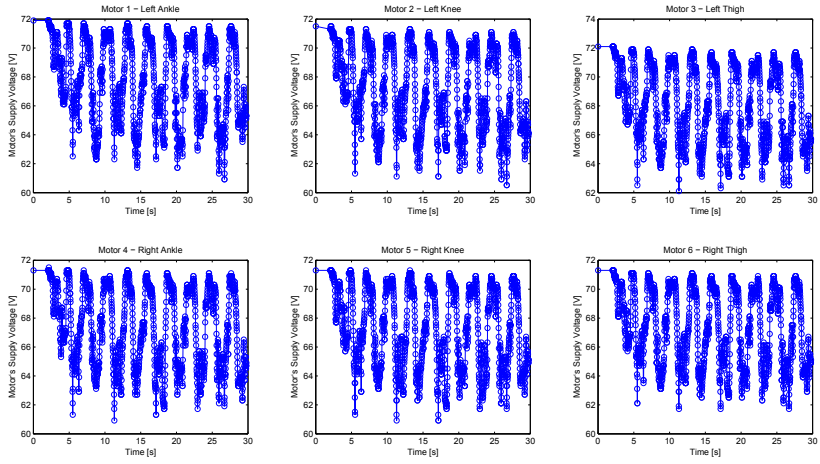

Figure 6.31. Voltage for all the actuators in the GIMbiped during the walking experiment of run # 5 in trajectory # 9 from Experiment2

ical cost of transport with and without regeneration. Figure 6.26 shows a very oscillatory behavior of the actual linear velocity, which helps to understand why so much of the total energy is used in negative work. The force presented in Figure 6.27 shows some high frequency oscillation mainly in the thighs' motors but with the force values between the boundaries (-585 N to 585 N). The knee motor plot from Figure 6.27 does reveal saturation when the knee is in the stance phase, reminding again about the importance of using active knee lock latches to avoid waisting energy.

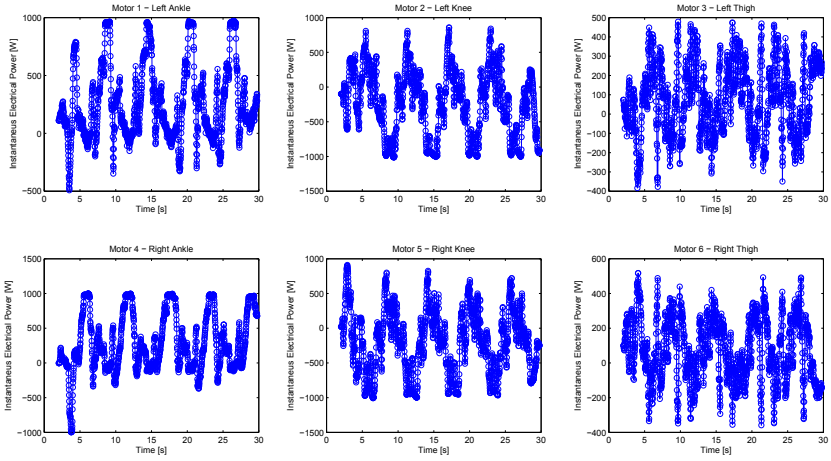

Figure 6.32. Electrical power without regeneration for all the actuators in the GIMbiped during the walking experiment of run # 5 in trajectory # 9 from Experiment2

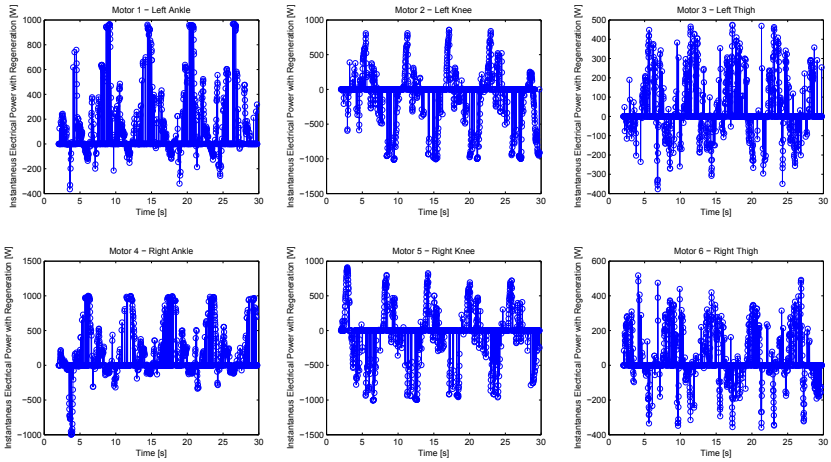

Figure 6.33. Electrical power with regeneration for all the actuators in the GIMbiped during the walking experiment of run # 5 in trajectory # 9 from Experiment2

Using the values in Figure 6.26 and Figure 6.27 mechanical power without regeneration and mechanical power with regeneration can be computed. The mechanical power with regeneration is presented in Figure 6.29, and the same without regeneration is shown in Figure 6.28. Both plots present a high-frequency component in their results, and the only visual difference is that the plots in Figure 6.29 present only positive values, as expected.

Figure 6.30 shows saturation again in both shanks and knees. The saturation in the shanks helps to explain why the trajectory during the stance

phase was not followed thoroughly. The saturation in the knee current repeats what was previously observed about the lack of force to maintain the leg straight in the stance phase.

Figure 6.31 shows that the voltage input from the power source is affected greatly by the amount current requested by all the motors. The voltage value oscillates and drops from its nominal value of 72 V_{DC} decreasing down to 61 V_{DC}.

The result of the previous variation in current and voltage can be seen reflected in the calculation of the electrical power with regeneration and without regeneration in Figure 6.33 and Figure 6.32. respectively.

Analyzing now the result tables, Tables 6.9 and 6.10 present the same information as the previous tables in Experiment1. The value Tables 6.9 and 6.10 show similar performance in efficiency of transmission, scuffing and percentage of energy used to overcome the disturbance of the frame. However, when analyzing CoT and F_r, a significant improvement in performance can be observed. CoT4 shows an improvement of almost 20% from trajectory #1, and F_r indicates that trajectory #4 is twice as fast as trajectory #1.

Unfortunately the trajectories generated with the ControlType2 do not show an improvement as strong as the one seen in the previous ControlType1. As before, Table6.11 and Table6.12 show similar values for the performance in efficiency of transmission, scuffing and percentage of energy used to overcome the disturbance of the frame. However, the values of the 4 trajectories generated with the CotrolType2 fall behind almost all the values from the ControlType1. The best performing trajectory from the ControlType2 group is trajectory #9, the same presented in all the previous figure of Experiment2. Trajectory #9 manages to outperform 3 of the 6 trajectories from the ControlType1; however, it is still 15% less efficient and almost 30% slower than the best performing trajectory from the ControlType1.

Finally to compare graphically the results from Experiment2, Figure 6.34 shows the results of CoT4 of all the trajectories plotted against the F_r. The red crosses indicate the trajectories generated with the ControlType2 and the blue crosses indicate the trajectories generated with th ControlType1.

Similarly, Figure 6.35, presents the same result but includes the values reported by other dynamic walker bipeds: the circles in magenta represent the values reported by Mable, the circles in blue are the values from

Table 6.9. Results of Experiment2 ZMP for 10 steps, including the initial and final step

	Energy with double support						Speed	Scuffing	Frame to robot energy %			Energy without double support					
Exp. #	CoT_1	CoT_2	%[a]	CoT_3	CoT_4	%[b]	F_r	%[c]	p[d]	Friction High	Friction Low	CoT_1	CoT_2	%[e]	CoT_3	CoT_4	%[f]
1	70.94	23.86	0.83	0.592	0.407	68.7	0.014	55.7	5.339	1.127	0.287	67.108	23.336	0.86	0.5745	0.3999	69.6
2	60.43	23.50	1.00	0.604	0.411	68.1	0.017	54.9	6.102	1.088	0.277	55.934	22.619	1.03	0.5762	0.3974	68.9
3	55.34	22.61	1.14	0.633	0.432	68.4	0.019	52.8	5.305	0.889	0.226	51.622	21.794	1.18	0.6074	0.4196	69.1
4	36.51	16.07	1.33	0.485	0.329	67.9	0.030	44.9	4.288	0.809	0.206	33.967	14.977	1.37	0.4653	0.3162	67.9
5	48.53	19.05	1.03	0.500	0.344	68.8	0.024	55.0	6.189	0.929	0.236	44.913	18.287	1.07	0.4794	0.3337	69.6
6	42.25	17.34	1.24	0.523	0.362	69.1	0.029	47.5	5.415	0.862	0.219	39.107	16.509	1.29	0.5031	0.3499	69.6

[a] $\%_{\frac{CoT3}{CoT1}}$ for energy calculated with double support and 10 steps. [b] $\%_{\frac{CoT4}{CoT3}}$ for energy calculated with double support and 10 steps. [c] Scuffing percentage. [d] Percentage of energy used to counteract frame's momentum. [e] $\%_{\frac{CoT3}{CoT1}}$ for energy calculated without double support and 10 steps. [f] $\%_{\frac{CoT4}{CoT3}}$ for energy calculated without double support and 10 steps.

Table 6.10. Results of Experiment2 ZMP for 8 steps, without including the initial and final step

	Energy with double support						Speed	Scuffing	Frame to robot energy %			Energy without double support					
Exp. #	CoT_1	CoT_2	%[a]	CoT_3	CoT_4	%[b]	F_r	%[c]	p[d]	Friction High	Friction Low	CoT_1	CoT_2	%[e]	CoT_3	CoT_4	%[f]
1	64.11	22.09	0.86	0.552	0.382	69.1	0.016	55.7	5.962	1.276	0.325	60.301	21.570	0.89	0.5339	0.3748	70.2
2	54.48	21.48	1.01	0.550	0.376	68.4	0.019	54.9	6.839	1.240	0.315	49.936	20.579	1.04	0.5204	0.3617	69.5
3	49.87	20.52	1.15	0.571	0.391	68.5	0.022	52.8	6.092	1.022	0.260	46.127	19.685	1.18	0.5457	0.3780	69.3
4	33.28	14.84	1.31	0.437	0.296	67.9	0.034	44.9	4.933	0.951	0.242	30.639	13.654	1.36	0.4157	0.2821	67.9
5	44.39	17.36	1.04	0.460	0.319	69.2	0.026	55.0	7.023	1.049	0.267	40.666	16.564	1.08	0.4387	0.3075	70.1
6	38.98	16.06	1.25	0.488	0.339	69.6	0.032	47.5	6.061	0.976	0.248	35.744	15.175	1.31	0.4674	0.3276	70.1

[a] $\%_{\frac{CoT3}{CoT1}}$ for energy calculated with double support and 8 steps. [b] $\%_{\frac{CoT4}{CoT3}}$ for energy calculated with double support and 8 steps.
[c] Scuffing percentage. [d] Percentage of energy used to counteract frame's momentum. [e] $\%_{\frac{CoT3}{CoT1}}$ for energy calculated without double support and 8 steps. [f] $\%_{\frac{CoT4}{CoT3}}$ for energy calculated without double support and 8 steps.

Table 6.11. Results of Experiment2 LCW for 10 steps, including the initial and final step

	Energy with double support												Speed	Scuffing	Frame to robot energy %			Energy without double support					
Exp.	CoT_1	CoT_2	%[a]	CoT_3				CoT_4				%[b]	F_r	%[c]	p[d]	Friction	Friction	CoT_1	CoT_2	%[e]	CoT_3	CoT_4	%[f]
#				Tot	LCW	Conn	ZMP	Tot	LCW	Conn	ZMP					High	Low						
7	84.71	30.86	0.90	0.760	0.249	0.244	0.266	0.497	0.177	0.145	0.175	65.46	0.0125	54.22	2.95	0.786	0.200	79.74	30.17	0.93	0.744	0.489	65.8
8	57.47	22.65	1.02	0.584	0.225	0.166	0.193	0.388	0.162	0.101	0.125	66.40	0.0203	54.48	4.47	0.892	0.227	54.44	22.03	1.05	0.572	0.381	66.7
9	51.99	20.55	1.03	0.538	0.225	0.135	0.178	0.366	0.168	0.086	0.111	68.02	0.0229	51.13	5.07	0.904	0.230	49.68	19.95	1.05	0.523	0.357	68.4
10	56.20	20.71	0.98	0.552	0.167	0.220	0.165	0.373	0.119	0.153	0.101	67.55	0.0208	51.15	4.69	0.849	0.216	53.33	20.18	1.01	0.537	0.365	67.9

[a] $\%_{\frac{CoT3}{CoT1}}$ for energy calculated with double support and 10 steps. [b] $\%_{\frac{CoT4}{CoT3}}$ for energy calculated with double support and 10 steps. [c] Scuffing percentage. [d] Percentage of energy used to counteract frame's momentum. [e] $\%_{\frac{CoT3}{CoT1}}$ for energy calculated without double support and 10 steps. [f] $\%_{\frac{CoT4}{CoT3}}$ for energy calculated without double support and 10 steps.

Table 6.12. Results of Experiment2 LCW for 8 steps, without including the initial and final step

	Energy with double support												Speed	Scuffing	Frame to robot energy %			Energy without double support					
Exp.	CoT_1	CoT_2	%[a]	CoT_3				CoT_4				%[b]	F_r	%[c]	p[d]	Friction	Friction	CoT_1	CoT_2	%[e]	CoT_3	CoT_4	%[f]
#				Tot	LCW	Conn	ZMP	Tot	LCW	Conn	ZMP					High	Low						
7	79.92	29.51	0.92	0.731	0.280	0.275	0.176	0.475	0.199	0.163	0.113	64.98	0.0133	54.22	2.87	0.832	0.212	74.85	28.81	0.95	0.714	0.467	65.3
8	54.41	21.56	1.01	0.552	0.253	0.187	0.112	0.364	0.183	0.114	0.068	65.94	0.0217	54.48	4.63	0.969	0.246	51.35	20.92	1.05	0.539	0.357	66.2
9	49.66	19.65	1.03	0.511	0.253	0.151	0.106	0.348	0.189	0.097	0.062	68.23	0.0244	51.13	5.42	0.998	0.254	47.37	19.05	1.04	0.495	0.339	68.6
10	54.15	19.55	0.96	0.519	0.188	0.247	0.083	0.352	0.134	0.172	0.046	67.86	0.0218	51.15	5.06	0.941	0.240	51.17	19.03	0.99	0.505	0.345	68.3

[a] $\%_{\frac{CoT3}{CoT1}}$ for energy calculated with double support and 8 steps. [b] $\%_{\frac{CoT4}{CoT3}}$ for energy calculated with double support and 8 steps. [c] Scuffing percentage. [d] Percentage of energy used to counteract frame's momentum. [e] $\%_{\frac{CoT3}{CoT1}}$ for energy calculated without double support and 8 steps. [f] $\%_{\frac{CoT4}{CoT3}}$ for energy calculated without double support and 8 steps.

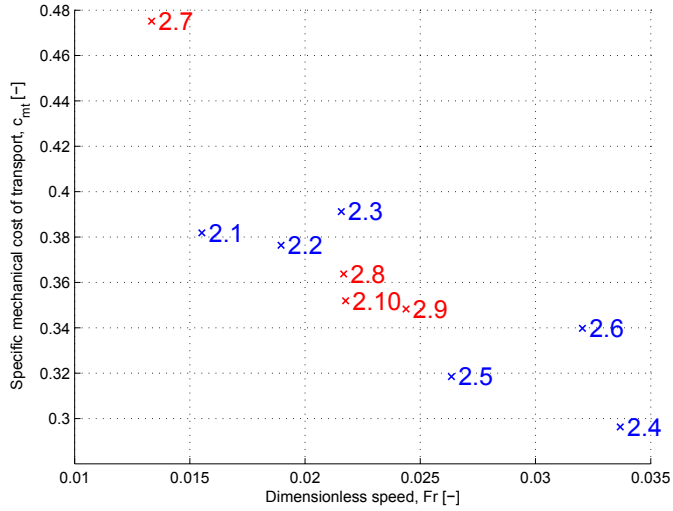

Figure 6.34. CoT4 vs F_r results plot from Experiment2 (numbers in the plot indicate respective runs in Experiment2)

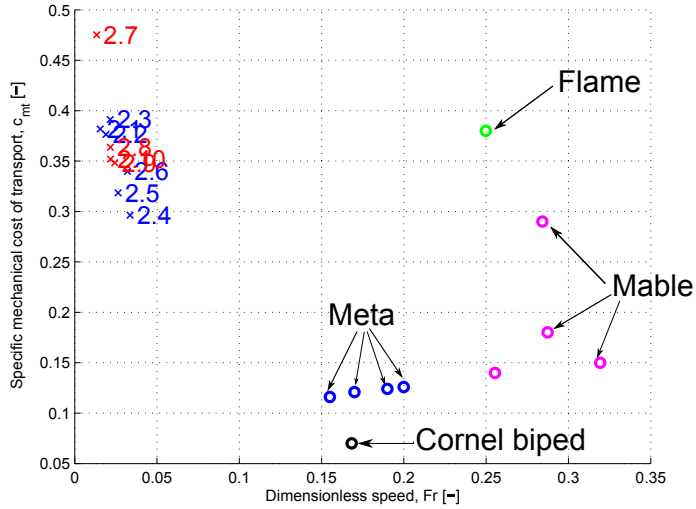

Figure 6.35. CoT4 vs F_r results plot from Experiment2 and similar biped robots

Meta, the green circle is the value of Flame and the black circle is the value of the biped built by Ruina's group.

7. Summary, Conclusions and Future Works

This thesis has presented part of the first theoretical studies and practical efforts done in Aalto University towards developing an energy-efficient biped service robot. The goal was to address the basic concepts behind energy efficiency in biped robots to help the GIMBiped project by indicating the best direction to proceed for a better performance in energy efficiency and mobility. The thesis work focused on the simplification of the biped structure into a 2D parameterized model from which different control techniques could be analyzed and compared; the design analysis of the mechanical structure parameters, which could favor energy efficiency, using the previous simplified model; and the experimental evaluation of a hybrid (ZMP-LCW) controller in Aalto's first biped prototype, the GIMBiped.

In the biped robotic walking research there is still no consensus over the best way to address energy issues in the system. One side has chosen mostly to ignore the high energy consumption and centered their efforts in developing further mobility and application of the biped robots, confident that a solution for the energy problem will eventually arrive from better efficient actuators and more compact and powerful energy sources. Meanwhile, researchers working on PDW and LCW have championed the idea to gradually actuate passive walkers up to the point in which they could perform useful tasks, drawing a simile to the evolution in aviation from gliders to airplanes.

Nonetheless, both previous points of view clash with problems: either the lack of energy efficiency, leading to short autonomy, or plenty of energy efficiency but lack of versatility and capability for heavy duty applications render both types of machines unpractical for any real use. In either case, it has to be acknowledged that the energy expenditure will constantly be a concern. Even if very small-size and unlimited energy source would be

invented, there would still be the need to eliminate the heat energy, since all the power that is not used for mechanical acceleration is converted into the heat. Therefore, reasonable power consumption should always be the goal, and energy recovery and storage should be investigated.

In this thesis, the hypothesis presented in Section 1.4 pointed to a middle ground between these two opposed ideas above. Instead of concentrating just on performing bipedal locomotion without caring about energy, the work on this thesis centered on the analysis of the natural and energy-efficient behavior of an approximated dynamic model of the hardware that leads to biped gaits. Also, instead of building up from simpler to complex systems, like from gliders to airplanes, this thesis evaluates the possible advantages of modifying the structure of previously well-performing walking machines to make them more energy efficient, resembling the process of development from regular cars to hybrid cars.

The previous concepts were investigated in Chapters 4, 5 and 6. The target was to develop a systematic method for achieving a semi-passive system that would be able to carry out efficient walking mode (that could benefit from the passive walking properties in the LCW approach under favorable conditions without external disturbances) and also be able to perform strong controlled maneuvers that will increase its possible applications in FSR.

One part of the issue is undoubtedly purely mechanical and concerned about the power conversion into mechanical energy. Large amount of power will need big actuators, or very high velocities. Big actuators will mean high volume and high weight, and high velocities would need high transmission. Actuators with high volume and weight make the design of the biped more difficult. They require more energy to move, and high velocity will imply high losses and lots of heat and wear. On the other hand, low velocity direct drives need a lot of force. Hydraulics are good in generating high forces, but creating hydraulic power from known portable power sources is difficult. Furthermore, hydraulics also generates heat, and their efficiency is currently much worse compared with electrical drives (if properly used).

However, there are numerous ways to implement mechanical solutions. The ATL, where this work was performed, is not in the best position to perform an exhaustive research on the possible alternative mechanical solutions. Therefore, the early stages of the GIMBiped project concentrated in developing the methodology and the basic science research.

The first stage was the simplification of the biped system into a 2D model with knees and point feet. This model has been used before in bipedal robotic studies; however, here the model was completely parameterized and no symmetry was supposed a priory. The model was tested in a simulator, symmetry was detected to be necessary to achieve limit cycle and the first indications of a highly sensible dynamics (to ICs and parameters) were observed.

The work followed with an assessment of different control techniques based on LCW, carried out in the same 2D biped simulator/model. The controllers were model-based driven from an analytic 2D kneed biped model. Several controllers from the CTC family together with a PBC were compared based on their energy efficiency and robustness.

The results presented in Chapter 4 at first indicate promising applications in the real hardware for the PBC with a soft PD and CT-PD. However, the poor performance obtained with the PBC for parameters in *Set 2* and *Set 3* brought back to mind the trade-off between energy efficiency and versatility in robotic usage, since it proves that efficient control techniques based on energy criterion are highly dependent on mechanical parameters of the robot. This dependence was also observed (but less disruptive) in CTC, which pointed to further research of optimal migration from passive mechanisms to robust biped robots. Such further investigation was performed later in Chapter 5, and together with the results obtained in Chapter 4, served to formulate the solution applied in the GIMBiped hardware in Chapter 6.

Although PBC, CT-PD and CT-PID did perform well, PBC as a solution cannot be applied directly since it needs to know the slope value in advance. CT-PD and CT-PID used more computational resources and needed precise knowledge for the matrices in the dynamic equation. Also, all the gains for the CTC family were found heuristically, by searching around the natural frequency of the system and always maintaining critical damping ratio between the gains. Therefore, the gains are different for each controller, and a mathematical method to ensure optimal gain for each case should be developed.

PD+Gravity, pure PD and pure PID independent joint controllers were not capable of following the desired trajectory as it is. However a solution to increase their performance, applied later in Chapter 6, was to use slower LC as reference and scale the solution in time before inputting it as reference to the controllers. Using the PD independent joint control

greatly simplified the control implementation and reduced the computation time in each control cycle. The use of pure PD independent joint control was encouraged as well by the impossibility to build a 3-link model close enough to the real hardware (GIMBiped) which at the same time would be capable of producing a favorable PDW. The previous difficulty meant that there were no significant advantages for using such model and calculate the $M(q)$, $V(q, \dot{q})$ and $G(q)$ matrices used to compute the control output in each cycle.

After evaluating some of the possible control approaches, the work focused in using the same approximated 3-link model version of the actual hardware (the GIMBiped), for the variation study in parameters, to analyze the effect in the stability and efficiency. The goal was to generate guidelines for the implementation or modification of biped robots' mechanical design, aiming to increase its energy efficiency and robustness based on LCW. Chapter 5 used then the numerical continuation method to perform a variation study in the parameters. The method demonstrated to be a potentially powerful tool for the design aid and performance analysis in biped systems.

From the experiments performed in Chapter 5, some conclusions can be drawn for the possible changes in the mechanics of GIMBiped testbed. The experiments revealed that, with the original design parameters of the GIMBiped, it was not possible to achieve stable cyclic trajectories, nor any type of cyclic trajectory. It was necessary to change the shank to thigh ratio (that was originally $\approx$ 1:1.3) to at least 1:2 to have some sort of cyclic behavior. However, favorable LCs, with adequate foot clearance, step length and walking velocity, were found starting from ratio $\approx$ 1:4.

Further analysis indicates that humans do closely follow the previous mentioned ratios, with 9.7 $[kg]$ shank mass and 3.2 $[kg]$ thigh mass for an average weight human male and 13.7[kg] thigh mass and 4.1 $[kg]$ shank mass for an obese human male [285]. The previous values result in a ratio of 1:3.03 and 1:3.34 for normal and obese human male, respectively, with similar values presented also for women [285]. Furthermore, the average speeds found in these cycles are slower but quite close to the average walking velocity of humans [285, 288, 289]. Step length being slightly shorter than the human average step length, follows the same behavior [285, 288, 289]. Additional information found in the experiments in Chapter 5 is that the ratio between step length and walking speed in the model studied varies greatly depending of the parameters, following sometimes

proportional and other times inversely proportional ratio between both.

The previous comparison between the results of the numerical continuation in the approximated biped model and the reported values of human performance, leads to two possible conclusions.

One is that, if the behavior reported by the approximated model does relate closely with the real human counterpart, the slight deviation in the parameters presented in human's physiology, compared with the "optimal" distribution proposed by the model, may be compensated by the high level control intrinsic to human walking. Such intrinsic applied control may accommodate or further optimize the CoT of a composition that is not optimally designed for passive limit cycle walking but instead evolved by nature to handle a higher versatile type of biped locomotion.

On the other hand, if the complex biped locomotion systems of the human does not directly relate to the simplified model presented throughout this thesis, it will mean that the approximations performed during the modeling stage obscure crucial variables of the system behavior.

In both previous cases, further research is necessary to either perform a study with active control on the current dynamic (non-ideal) model to evaluate if the system can be driven to an efficient walking pattern or to develop a more human-closely-related mechanical and dynamic model. Some work has been done already on the first hypothesis in Chapter 4 where control is applied to a model with non-ideal mechanical distribution using ideal trajectories and the conclusions presented previously. Further practical experiments were presented in Chapter 6.

Chapter 6 presented the experiments performed in the GIMBiped testbed. It showed the results of a hybrid control technique, proposed by the author, which combines ZMP walking with LCW. The ZMP part of the trajectory was used during the transitions between steps around the HS event, since in that instant the behavior of the hardware differs quite a lot from the trajectory imposed by the model based on LCW. Furthermore the results of a pure ZMP-based trajectory-following control were also presented.

Considering that an average human walking speed is about $1.4\ [m/s]$ ($5\ [km/h]$) [285] and that the step length is highly variable depending on the human anatomy and walking speed, but with an acceptable average value for males being 0.75 [m] [286]. Experiments in the GIMBiped for walking with step length longer than $0.25\ [m]$ were not successful, mainly due to the restriction on the joints angle range and lack of feedback control. The

maximum velocity achieved in the GIMBiped testbed was also very much below the average human walking speed, reaching only 0.1 $[m/s]$ (0.36 km/h). Therefore, the reference trajectories inputted in the control system and derived from natural LC of approximated biped models needed to be scaled down in velocity and step length.

The outcome of the hardware experiments also provided important guidelines for future improvement in the GIMBiped design and control techniques. It indicated that slower walking speeds help maintain stability without using feedback control. However, slow speed makes the robot spend more time and energy to reach its destination. Unfortunately, the current robot mechanical design does not allow the knee motor to work at its best, and consequently the temperature evolution on both knees was higher than in the hip or ankle motors. This indicated that they were working outside the area of their nominal operation.

Since one of the main problems in the GIMBiped is the knee motor overload, changes in the prototype could include lighter motors in the shank to ease the load of the knee or a relocation of the center of mass of the shank (moving it forward) to ease the bending motion of the knee. Another brute force solution to overcome the problem would be to use more powerful knee actuators and better cooling mechanism. However, this would not provide an energy-efficient solution. A better solution for the knee problem may be a complete redesign of the actuation system, considering the outcomes of other biped researches based on human physiology. The already built-in locking mechanism should also be used to further decrease the burden in the knee motor in the stance phase.

Many other derivations of ZMP-based walking and LCW-based controls can be tested in the robot, but the basic assumptions can be attained from the performance of these two methods in this particular biped platform. The previous suggestions, combined with the indication from Chapter 5, lead to the conclusion that to avoid foot scuffing and overuse of the knee motors, the best solution is to consider a design with higher weight in the thighs, maintaining a thigh to shank ration of at least 1:4, and for that reason the ankle should be as light as possible.

Also, since compliance is not strictly required in the ankle joint and the knee should not need large amount of power in normal operation, the current linear motors used in the GIMBiped testbed in those joints could be replaced. Ankle joints in humans are driven by muscle connected to tendons, and the tendons play a crucial role in storing energy. Such design

should be considered in the future works as other studies have proposed and encouraged.

Linear motors have some advantages and some disadvantages. Since mechanical design is primordial for the dynamic behavior of the robot, the main drawback is the large size and weight of these drives. Although they are backdriveable, and the actuation system can easily be made compliant by variating the controller stiffness adjusting the PID parameters, compliance is necessary only in some stages but not during the whole cycle and not in all the joints. That can be seen in the response of the knee and ankle during the stance and swing phases; therefore, an evaluation of what is the best cost-efficient solution should continue with experiments with other type of drives, since using a very stiff PID setting for the LMs consumes much energy. Weight, size, energy recovery, maximum torque and force are still issues for all biped platforms that have been built, and since many novel actuators are still being developed, the answer to which is the best solution remains open. However, the methodology presented in Chapter 5 could be used to ease and accelerate the design process and assessment of different drive applications.

In the particular case of the GIMBiped testbed, the LM seems to perform well when large torques are required for short durations of time (impulsive responses). Although such control policy could be developed, designing a robot to perform under impulsive forces is not ideal and could be a potentially danger for the surroundings. For building a versatile platform, the ideal would be a relatively good performance in both types of walking: a precision mode with slow accurate movements and an impulsive mode with fast responses to overcome sudden disturbances. The GIMBiped platform shows better behavior in the later type of walking. In the case of the GIMBiped testbed, using the linear motors under static (constant) load is not the proper application for the drives. The large power consumption in the knee and ankle motors (especially the knee), during the ZMP trajectory indicates that they are working overloaded during these stages, and a better alternative could be found.

One option for the ankle joint drive could be a combination between passive springs and small and lightweight high-geared rotational motors. The knee joint could be actuated by lighter compliant actuators, like serial elastic actuators. A proper method to lock the knee is also essential for energy efficiency, since brakes or latches are good to save energy when the joint needs to carry load without moving

To further save energy, Chap 6 showed that the correct use of an control policy is primordial. The ratio between negative work and the total energy indicates how efficient the controller is. It is also shown in the results from Chapter 6 that independent joint control is clearly not an efficient control method. However, if a more efficient control is applied, regenerative process can be devised to recover any energy wasted in negative work. The regenerative process should be relatively simple with the linear motors used in the GIMBiped, given the available connections to attach a load when negative current is induced in the system. The goal will be to use the LMs as generators when negative work is produced and perform regenerative braking when needed. Nonetheless, experimental demonstrations are still needed for regenerative walking and also other energy restoring ideas may be incorporated in this set, for example heel impact energy recovering.

Further results from Chapter 6 showed that linear motors are not very efficient, and the whole process of producing mechanical power from electric sources showed an efficiency which ranged from 0.7 to 1.1%. The previous poor values may be improved by a thorough mechanical optimization analysis, devised to solve the problem of power transmission, so that the force and stroke length are optimal and the actuators could be placed where the mass distribution is the best. Furthermore, future applications of this type of drives still depend on the further advances of the R&D of the manufacturers. Since the beginning of the GIMBiped project, better performance drives have been made available, with the same maximum toque as the one use in the construction of the GIMBiped testebed but with less weight and higher efficiency, making this still an interesting tool in bipedal robotics.

It is important to note the order in which the CoT values change, ranging between 100 and 200 times, depending on how they are computed. The CoT reduces drastically when certain conditions are not reported, including the negative work, efficiency of the transmission, inclusion of initial and final step, and double support period. Therefore, it is important to report the efficiency of the whole system, since such values help to identify where else further research is needed. In the case of the GIMBiped is the mechanics and actuators for a better power transmission.

Given the previous statement, some things that are not to be generalized are the experiment results performed under LCW- and ZMP-base type of control. The LCW-based control in particular (executed in practice

in Chapter 6), did not perform as expected, lagging some way behind in performance compared to ZMP. However, the demise of the experiments in general has to do more with the control type and the mechanical downfalls mentioned previously than the idea of LCW itself.

The mechanical shortfalls have already been addressed. On the other hand, the control policy applied in the experiments was not the best for this type of actuators and mechanical design. The final control applied in the GIMbiped was an independent joint control of a trajectory following in position; such control is parameterized by time. Control policies which are parameterized by time are not energy efficient and tend to overdrive motors to conform with the trajectory to follow. Researchers keeping track of energy-efficient methods in biped robotics have previously advised against controllers that use trajectories parameterized by time. However, since the GIMBiped was a new platform and this controller type is one of the easiest control to implement, it served to point out all the possible downfalls of the platform.

For the future, a better alternative of control drawing much attention during the development of this project, is Hybrid-Zero-Dynamics (HZD). HZD does not parameterize the trajectory in time, but instead it does it with respect to the stance leg (always a crescent angle). Such method could be the next step to go in the GIMBiped project and comparison with the current result could be made.

Bibliography

[1] B. Siciliano and O. Khatib, *Springer handbook of robotics*. Springer, 2008.

[2] A. Kelly, K. Iagnemma, and A. Howard, *Field and service robotics: Results of the 7th international conference*. Springer, 2010, vol. 62.

[3] M. Ferre, M. Buss, and R. Aracil, *Advances in telerobotics*. Springer Verlag, 2007, vol. 31.

[4] A. Brooks, T. Kaupp, A. Makarenko, S. Williams, and A. Oreback, "Towards component-based robotics," in *Proceedings of the IEEE/RSJ International Conference on Intelligent Robots and Systems*, 2005, pp. 163–168.

[5] S. Bergbreiter and K. Pister, "Cotsbots: An off-the-shelf platform for distributed robotics," in *Proceedings of the IEEE/RSJ International Conference on Intelligent Robots and Systems*, vol. 2, 2003, pp. 1632–1637.

[6] RobotShop Distribution, Inc., "Robot store for personal and professional robot technology," http://www.robotshop.com/, Retrieve January 2012.

[7] Trossen Robotics, Inc., "Robot shop for hobby, educational robot kits and robot parts," http://www.trossenrobotics.com/, Retrieve January 2012.

[8] Acroname, Inc., "Provide expertise, applications and high quality products in robotics," http://www.acroname.com/, Retrieve January 2012.

[9] A. Desrochers, *Intelligent robotic systems for space exploration*. Kluwer Academic Publishers, 1992.

[10] P. Ulivi and D. Harland, *Robotic exploration of the solar system. Part 3: The modern era, 1997-2009*. Springer, 2012.

[11] A. Ellery, *An introduction to space robotics*. Springer Verlag, 2000.

[12] Y. Xu, *Space robotics: dynamics and control*. Springer, 1993.

[13] R. Launius and H. McCurdy, *Robots in space: technology, evolution, and interplanetary travel*. Johns Hopkins Univ Pr, 2008.

[14] T. Ishida, "Development of a small biped entertainment robot QRIO," in *Proceedings of the IEEE International Symposium on Micro-Nanomechatronics and Human Science*, 2004, pp. 23–28.

[15] J. Decuir, T. Kozuki, V. Matsuda, and J. Piazza, "A friendly face in robotics: Sony's AIBO entertainment robot as an educational tool," *Computers in Entertainment*, vol. 2, no. 2, pp. 14–14, 2004.

[16] J. Jones, "Robots at the tipping point: the road to iRobot Roomba," *IEEE Robotics & Automation Magazine*, vol. 13, no. 1, pp. 76–78, 2006.

[17] A. Halme, "Intelligent machines and robots are changing our society," *Public Service Review*, vol. 19, pp. 398–399, 2010.

[18] S. Sukkarieh, *Field and service robotics: Results of the 5th international conference*. Springer, 2006, vol. 25.

[19] A. Zelinsky, *Field and service robotics*. Springer, 1998.

[20] C. Laugier, *Field and service robotics: Results of the 6th international conference*. Springer, 2008.

[21] S. Lee, I. Hong, and M. Sang, *Recent progress in robotics: Viable robotic service to human*. Springer, 2009.

[22] J. Saarinen, J. Suomela, and A. Halme, "The concept of future worksite-towards teamwork-centered field robotic systems," in *Proceedings of the 18th IFAC World Congress*, vol. 18, no. 1, 2011, pp. 14 952–14 957.

[23] ——, "Teamwork-centered field robotic systems," in *Proceedings of the 18th IFAC World Congress*, 2011.

[24] T. Oksanen and A. Visala, "Coverage path planning algorithms for agricultural field machines," *Journal of Field Robotics*, vol. 26, no. 8, pp. 651–668, 2009.

[25] D. Todd, *Walking machines: An introduction to legged robots*. Chapman & Hall, 1985.

[26] M. Vukobratović, *Biped Locomotion*. Springer, 1990.

[27] K. Yokoi, K. Nakashima, M. Kobayashi, H. Mihune, H. Hasunuma, Y. Yanagihara, T. Ueno, T. Gokyuu, and K. Endou, "A tele-operated humanoid operator," *The International Journal of Robotics Research*, vol. 25, no. 5-6, pp. 593–602, 2006.

[28] J. Suomela, J. Saarinen, A. Halme, M. Vilenius, and K. Huhtala, "GIM - towards the future worksite," in *Proceedings of the 6th IFAC Symposium on Intelligent Autonomous Vehicles*, 2007.

[29] M. Diftler, J. Mehling, M. Abdallah, N. Radford, L. Bridgwater, A. Sanders, R. Askew, D. Linn, J. Yamokoski, F. Permenter *et al.*, "Robonaut 2 - The first humanoid robot in space," in *Proceedings of the IEEE International Conference on Robotics and Automation*, 2011, pp. 2178–2183.

[30] R. Ambrose, H. Aldridge, R. Askew, R. Burridge, W. Bluethmann, M. Diftler, C. Lovchik, D. Magruder, and F. Rehnmark, "Robonaut: NASA's space humanoid," *Intelligent Systems and their Applications*, vol. 15, no. 4, pp. 57–63, 2000.

[31] NASA Research Announcement, "Research and technology development to support crew health and performance in space exploration missions," National Aeronautics and Space Administration and The National Space Biomedical Research Institute, Tech. Rep., July 2009.

[32] K. Kaneko, F. Kanehiro, M. Morisawa, K. Miura, S. Nakaoka, and S. Kajita, "Cybernetic human HRP-4C," in *Proceedings of the 9th IEEE-RAS International Conference on Humanoid Robots*, 2009, pp. 7–14.

[33] W. Bluethmann, R. Ambrose, M. Diftler, S. Askew, E. Huber, M. Goza, F. Rehnmark, C. Lovchik, and D. Magruder, "Robonaut: A robot designed to work with humans in space," *Autonomous Robots*, vol. 14, no. 2, pp. 179–197, 2003.

[34] NASA, "NASA-IHMC X1 Mina Exoskeleton," http://www.nasa.gov/offices/oct/home/feature_exoskeleton.html, Retrieve Dec 2012.

[35] C. Chevallereau, G. Abba, Y. Aoustin, F. Plestan, E. Westervelt, C. Canudas-de Wit, and J. Grizzle, "Rabbit: A testbed for advanced control theory," *IEEE Control Systems Magazine*, vol. 23, no. 5, pp. 57–79, 2003.

[36] M. Spong, J. Holm, and D. Lee, "Passivity-based control of bipedal locomotion," *IEEE Robotics & Automation Magazine*, vol. 14, no. 2, pp. 30–40, 2007.

[37] F. Asano, M. Hashimoto, N. Kamamichi, and M. Yamakita, "Extended virtual passive dynamic walking and virtual passive-mimicking control laws," in *Proceedings of the IEEE/RSJ International Conference on Intelligent Robots and Systems*, 2001.

[38] M. Vukobratović, A. Frank, and D. Juricic, "On the stability of biped locomotion," *IEEE Transactions on Biomedical Engineering*, no. 1, pp. 25–36, 1970.

[39] F. Gubina, H. Hemami, and R. B. McGhee, "On the dynamic stability of biped locomotion," *IEEE Transactions on Biomedical Engineering*, no. 2, pp. 102–108, 1974.

[40] A. Kuo, "Choosing your steps carefully: Trade-offs between economy and versatility in dynamic walking bipedal robots," *IEEE Robotics & Automation Magazine*, vol. 14, no. 2, pp. 18–29, 2007.

[41] J. L. Peralta, T. Haarnoja, T. Ylikorpi, and A. Halme, "Idle state stability, limit cycle walking & regenerative walking: Towards long time auonomy in bipeds," in *Proceedings of the International Conference on Climbing and Walking Robots*, 2010.

[42] C. Duncheon, "Robots will be of service with muscles, not motors," *Industrial Robot: An International Journal*, vol. 32, no. 6, pp. 452–455, 2005.

[43] K. Loffler, M. Gienger, F. Pfeiffer, and H. Ulbrich, "Sensors and control concept of a biped robot," *IEEE Transactions on Industrial Electronics*, vol. 51, no. 5, pp. 972–980, 2004.

[44] K. Erbatur, A. Okazaki, K. Obiya, T. Takahashi, and A. Kawamura, "A study on the zero moment point measurement for biped walking robots," in *Proceedings of the 7th IEEE International Workshop on Advanced Motion Control*, 2002, pp. 431–436.

[45] K. Loffler, M. Gienger, and F. Pfeiffer, "Sensor and control design of a dynamically stable biped robot," in *Proceedings of the IEEE International Conference on Robotics and Automation*, vol. 1, 2003, pp. 484–490.

[46] A. Goswami, "Postural stability of biped robots and the foot-rotation indicator (FRI) point," *The International Journal of Robotics Research*, vol. 18, no. 6, pp. 523–533, 1999.

[47] A. Kun and W. Miller III, "Adaptive dynamic balance of a biped robot using neural networks," in *Proceedings of the IEEE International Conference on Robotics and Automation*, vol. 1, 1996, pp. 240–245.

[48] C. Zhou and Q. Meng, "Dynamic balance of a biped robot using fuzzy reinforcement learning agents," *Fuzzy Sets and Systems*, vol. 134, no. 1, pp. 169–187, 2003.

[49] Y. Kuroki, M. Fujita, T. Ishida, K. Nagasaka, and J. Yamaguchi, "A small biped entertainment robot exploring attractive applications," in *Proceedings of the IEEE International Conference on Robotics and Automation*, vol. 1, 2003, pp. 471–476.

[50] T. Kanda, T. Miyashita, T. Osada, Y. Haikawa, and H. Ishiguro, "Analysis of humanoid appearances in human–robot interaction," *IEEE Transactions on Robotics*, vol. 24, no. 3, pp. 725–735, 2008.

[51] A. Kuo, J. Donelan, and A. Ruina, "Energetic consequences of walking like an inverted pendulum: step-to-step transitions," *Exercise and sport sciences reviews*, vol. 33, no. 2, p. 88, 2005.

[52] S. Collins, A. Ruina, R. Tedrake, and M. Wisse, "Efficient bipedal robots based on passive-dynamic walkers," *Science*, vol. 307, no. 5712, p. 1082, 2005.

[53] F. Asano, M. Yamakita, and K. Furuta, "Virtual passive dynamic walking and energy-based control laws," in *Proceedings of the IEEE/RSJ International Conference on Intelligent Robots and Systems*, vol. 2, 2000, pp. 1149–1154.

[54] S. Kajita, T. Yamaura, and A. Kobayashi, "Dynamic walking control of a biped robot along a potential energy conserving orbit," *IEEE Transactions on Robotics and Automation*, vol. 8, no. 4, pp. 431–438, 1992.

[55] J. Holm and M. Spong, "Kinetic energy shaping for gait regulation of underactuated bipeds," in *Proceedings of the IEEE International Conference on Control Applications*, 2008, pp. 1232–1238.

[56] J. L. Peralta, T. Ylikorpi, K. Gulzar, P. Jakubik, and A. Halme, "Novel design of biped robot based on linear induction motors," in *Proceedings of the 9th IEEE-RAS International Conference on Humanoid Robots*, 2009, pp. 34–39.

[57] T. Haarnoja, J. L. Peralta, and A. Halme, "Model-based velocity control for limit cycle walking," in *Proceedings of the IEEE/RSJ International Conference on Intelligent Robots and Systems*, 2011, pp. 2255–2260.

[58] J. L. Peralta, T. Haarnoja, T. Ylikorpi, and A. Halme, "Assessment of limit-cycle-based control on 2D kneed biped," in *Proceedings of the IEEE International Conference on Robotics and Automation*, 2011, pp. 3988–3993.

[59] T. Ylikorpi, J. L. Peralta, and A. Halme, "Comparing passive walker simulators in MATLAB and ADAMS," *Journal of Structural Mechanics*, vol. 44, no. 1, pp. 65–92, 2011.

[60] Center of Excellence in Generic Intelligent Machines Research, "GIM Website," http://gim.tkk.fi/, Retrieve February 2012.

[61] A. Halme, I. Leppänen, S. Salmi, and S. Ylönen, "Hybrid locomotion of a wheel-legged machine," in *Proceedings of the 3rd International Conference on Climbing and Walking Robots*, 2000, pp. 167–173.

[62] T. Ylikorpi and J. Suomela, *Climbing & Walking Robots; Towards new applications: Ball-shaped robots*, 2007, pp. 235–256.

[63] D. Higdon and R. Cannon Jr, "On the control of unstable multiple-output mechanical systems," in *Proceedings of the ASME Winter Annual Meeting*, 1963.

[64] A. Hutchinson, "Machines can walk," *The Chartered Mechanical Engineer*, vol. 11, pp. 480–484, 1967.

[65] R. A. Liston, "Walking machines," *Journal of Terramechanics*, vol. 1, no. 3, pp. 18–31, 1964.

[66] R. Hirose and T. Takenaka, "Development of the humanoid robot asimo," *Honda R&D Technical Review*, vol. 13, no. 1, pp. 1–6, 2001.

[67] M. Hirose and K. Ogawa, "Honda humanoid robots development," *Philosophical Transactions of the Royal Society A: Mathematical, Physical and Engineering Sciences*, vol. 365, no. 1850, pp. 11–19, 2007.

[68] K. Kaneko, K. Harada, F. Kanehiro, G. Miyamori, and K. Akachi, "Humanoid robot HRP-3," in *In Proceedings of IROS 2008. IEEE/RSJ International Conference on Intelligent Robots and Systems, 2008.*, 2008, pp. 2471–2478.

[69] B. Vanderborght, *Dynamic stabilisation of the biped Lucy powered by actuators with controllable stiffness*. Springer, 2010, vol. 63.

[70] J. E. Pratt, "Exploiting inherent robustness and natural dynamics in the control of bipedal walking robots," Ph.D. dissertation, 2000.

[71] C. Ridderstrom, "Legged locomotion control—a literature survey," Royal Instit. Technol., Stockholm, Sweden, Tech. Rep., 1999.

[72] J. Grizzle, J. Hurst, B. Morris, H. Park, and K. Sreenath, "Mabel, a new robotic bipedal walker and runner," in *Proceedings of the American Control Conference*, 2009, pp. 2030–2036.

[73] Harmonic Drive, LLC., "Harmonic drives specifications," http://www.harmonicdrive.ca/, Retrieve February 2012.

[74] Futaba, Inc., "Digital servos specifications," http://www.futaba-rc.com/servos/digital.html, Retrieve February 2012.

[75] ——, “Brushless servos specifications,” http://www.futaba-rc.com/servos/brushless.html, Retrieve February 2012.

[76] Xsens North America, Inc., “All products overview,” http://www.xsens.com/en/general/products-all?gclid=COiD2cXQta4CFdCb7QodJ0fjnA, Retrieve February 2012.

[77] MicroStrain, Inc., “Inertial sensors overview,” http://microstrain.com/inertial?gclid=CKCR48bQta4CFYuc7QodQ1amqQ, Retrieve February 2012.

[78] VectorNav Technologies, LLC., “Products overview,” http://www.vectornav.com/index.php?option=com_content&view=article&id=1&Itemid=2, Retrieve February 2012.

[79] ATI Industrial Automation, Inc., “Products overview - force/torque sensors,” http://www.ati-ia.com/products/ft/ft_ModelListing.aspx, Retrieve February 2012.

[80] JR3, Inc., “Products overview,” http://www.jr3.com/Products.html, Retrieve February 2012.

[81] A. Frank, “An approach to the dynamic analysis and synthesis of biped locomotion machines,” *Medical and Biological Engineering and Computing*, vol. 8, no. 5, pp. 465–476, 1970.

[82] M. Vukobratović and D. Juricic, “Contribution to the synthesis of biped gait,” *IEEE Transactions on Biomedical Engineering*, no. 1, pp. 1–6, 1969.

[83] M. Vukobratović and B. Borovac, “Zero-moment point-thirty five years of its life,” *International Journal of Humanoid Robotics*, vol. 1, no. 1, pp. 157–173, 2004.

[84] K. Hirai, M. Hirose, Y. Haikawa, and T. Takenaka, “The development of Honda humanoid robot,” in *In Proceedings of IEEE International Conference on Robotics and Automation, 1998*, vol. 2, 1998, pp. 1321–1326.

[85] Boston Dynamics, “PETMAN - BigDog gets a Big Brother,” http://www.bostondynamics.com/robot_petman.html, Retrieve March 2012.

[86] American Honda Motor Co. Inc., “ASIMO’s Fact Sheet,” http://asimo.honda.com/downloads/pdf/honda-asimo-robot-fact-sheet.pdf, Retrieve March 2012.

[87] ——, “ASIMO’s Frequently Asked Technical Questions,” http://asimo.honda.com/downloads/pdf/asimo-technical-faq.pdf, Retrieve February 2012.

[88] ——, “New ASIMO (Dec. 2005) - Turning on the Spot,” Retrieve March 2012. [Online]. Available: http://world.honda.com/HDTV/ASIMO/New-ASIMO-turning/

[89] ——, “ASIMO’s Specifications, 2005 version part 2,” http://world.honda.com/ASIMO/new/, Retrieve February 2012.

[90] ——, “ASIMO’s Specifications, 2000 version,” http://world.honda.com/news/2000/c001120.html, Retrieve February 2012.

[91] ——, "ASIMO's Specifications, 2004 version part 1," http://asimo.honda.com/asimo_specifications.html, Retrieve February 2012.

[92] ——, "ASIMO's Specifications 2004 version part 2," http://world.honda.com/news/2004/c041215.html, Retrieve February 2012.

[93] ——, "ASIMO's Specifications, 2004 version part 3," http://world.honda.com/ASIMO/next-generation/index.html, Retrieve February 2012.

[94] ——, "ASIMO's Specifications, 2005 version part 1," http://world.honda.com/news/2005/c051213.html, Retrieve February 2012.

[95] ——, "ASIMO's Specifications, 2011 version," http://world.honda.com/news/2011/c111108All-new-ASIMO/index.html, Retrieve February 2012.

[96] K. Ogata, K. Terada, and Y. Kuniyoshi, "Real-time selection and generation of fall damage reduction actions for humanoid robots," in *Proceedings of the 8th IEEE-RAS International Conference on Humanoid Robots*, 2008, pp. 233–238.

[97] K. Fujiwara, F. Kanehiro, S. Kajita, K. Kaneko, K. Yokoi, and H. Hirukawa, "UKEMI: Falling motion control to minimize damage to biped humanoid robot," in *Proceedings of the IEEE/RSJ International Conference on Intelligent Robots and Systems*, vol. 3, 2002, pp. 2521–2526.

[98] K. Fujiwara, F. Kanehiro, S. Kajita, K. Yokoi, H. Saito, K. Harada, K. Kaneko, and H. Hirukawa, "The first human-size humanoid that can fall over safely and stand-up again," in *Proceedings of the IEEE/RSJ International Conference on Intelligent Robots and Systems*, vol. 2, 2003, pp. 1920–1926.

[99] N. Kanehira, T. Kawasaki, S. Ohta, T. Ismumi, T. Kawada, F. Kanehiro, S. Kajita, and K. Kaneko, "Design and experiments of advanced leg module (HRP-2L) for humanoid robot (HRP-2) development," in *Proceedings of the IEEE/RSJ International Conference on Intelligent Robots and Systems*, vol. 3, 2002, pp. 2455–2460.

[100] B. Verrelst, O. Stasse, K. Yokoi, and B. Vanderborght, "Dynamically stepping over obstacles by the humanoid robot hrp-2," in *Proceedings of the IEEE-RAS International Conference on Humanoid Robots*, 2006, pp. 117–123.

[101] K. Nakadai, K. Hidai, H. Mizoguchi, H. Okuno, and H. Kitano, "Real-time auditory and visual multiple-object tracking for humanoids," in *International Joint Conference on Artificial Intelligence*, vol. 17, no. 1, 2001, pp. 1425–1436.

[102] I. Hara, F. Asano, H. Asoh, J. Ogata, N. Ichimura, Y. Kawai, F. Kanehiro, H. Hirukawa, and K. Yamamoto, "Robust speech interface based on audio and video information fusion for humanoid HRP-2," in *Proceedings of the IEEE/RSJ International Conference on Intelligent Robots and Systems*, vol. 3, 2004, pp. 2404–2410.

[103] R. Tellez, F. Ferro, S. Garcia, E. Gomez, E. Jorge, D. Mora, D. Pinyol, J. Oliver, O. Torres, J. Velazquez *et al.*, "Reem-B: an autonomous

lightweight human-size humanoid robot," in *Proceedings of the 8th IEEE-RAS International Conference on Humanoid Robots, 2008. Humanoids 2008*, 2008, pp. 462–468.

[104] G. Nichols and D. Witt, "An experimental unpowered walking aid," *Engineering in Medicine*, vol. 1, no. 1, pp. 7–11, 1971.

[105] T. McGeer, "Passive dynamic walking," *The International Journal of Robotics Research*, vol. 9, no. 2, pp. 62–82, 1990.

[106] D. Hobbelen and M. Wisse, "Limit cycle walking," *in book "Humanoid Robots; humanlike machines", edited by M. Hackel*, pp. 277–294, 2007.

[107] Y. Huang, B. Vanderborght, R. Van Ham, Q. Wang, M. Van Damme, G. Xie, and D. Lefeber, "Step length and velocity control of a dynamic bipedal walking robot with adaptable compliant joints," *IEEE/ASME Transactions on Mechatronics*, vol. 18, no. 2, pp. 598–611, 2013.

[108] M. Wisse and J. van Frankenhuyzen, "Design and construction of mike; a 2D autonomous biped based on passive dynamic walking," in *Proceedings of the Conference on Adaptive Motion of Animals and Machines*, 2003.

[109] D. Hobbelen, T. de Boer, and M. Wisse, "System overview of bipedal robots flame and tulip: Tailor-made for limit cycle walking," in *Proceedings of the IEEE/RSJ International Conference on Intelligent Robots and Systems*, 2008, pp. 2486–2491.

[110] R. Tedrake, T. Zhang, M. Fong, and H. Seung, "Actuating a simple 3D passive dynamic walker," in *Proceedings of the IEEE International Conference on Robotics and Automation*, vol. 5, 2004, pp. 4656–4661.

[111] B. Verrelst, R. Ham, B. Vanderborght, F. Daerden, D. Lefeber, and J. Vermeulen, "The pneumatic biped "Lucy" actuated with pleated pneumatic artificial muscles," *Autonomous Robots*, vol. 18, no. 2, pp. 201–213, 2005.

[112] F. P. Kusumah, J. L. Peralta, T. Ylikorpi, and A. Halme, "Implementation and analysis of Fuzzy-ZMP-walking control in the GIMBiped," in *Proceedings of the International Conference on Climbing and Walking Robots*. CLAWAR, 2012, pp. 449–458.

[113] Center of Excellence in Generic Intelligent Machines Research, "GIMBiped Website," http://gim.aalto.fi/GIMbiped, Retrieve November 2013.

[114] P. Jakubik, "A design concept for an anthropomorphic walker," Unpublished.

[115] ——, "Inertial parameters of the biped mechanism," Helsinki University of Technology, Tech. Rep., February 2009.

[116] ——, "An autonomous biped: Concept and design," in *Proceedings of the 9th International Conference on Informatics in Control, Automation and Robotics*, 2012, pp. 167–176.

[117] R. Mosher, "Test and evaluation of a versatile walking truck," in *Proceedings of Off-Road Mobility Research Symposium*, 1968, pp. 359–379.

[118] R. Liston and R. Mosher, "A versatile walking truck," in *Proceedings of the Transportation Engineering Conference*, 1968.

[119] R. S. Mosher, *Exploring the Potential of a Quadruped*. Society of Automotive Engineers, 1969.

[120] M. G. Bekker, *Introduction to terrain-vehicle systems*. University of Michigan Press, 1969.

[121] ——, *Theory of land locomotion: the mechanics of vehicle mobility*. University of Michigan Press, 1956.

[122] ——, *Off-the-road locomotion: research and development in terramechanics*. University of Michigan Press, 1960.

[123] R. Bernhard, "Preliminary study on jumping and running types of locomotion," *Land Locomotion Lab., Ordnance Tank Automotive Command, Rept*, vol. 43, 1958.

[124] J. Shigley, "The mechanics of walking vehicles," US Army Tank Automotive Command, Land Locomotion Laboratory, Tech. Rep., 1960.

[125] R. B. McGhee, "Finite state control of quadruped locomotion," *Simulation*, vol. 9, no. 3, pp. 135–140, 1967.

[126] ——, "Some finite state aspects of legged locomotion," *Mathematical Biosciences*, vol. 2, no. 1, pp. 67–84, 1968.

[127] R. B. McGhee and A. A. Frank, "On the stability properties of quadruped creeping gaits," *Mathematical Biosciences*, vol. 3, pp. 331–351, 1968.

[128] R. Tomovic and R. B. McGhee, "A finite state approach to the synthesis of bioengineering control systems," *IEEE Transactions on Human Factors in Electronics*, no. 2, pp. 65–69, 1966.

[129] A. Frank and R. B. McGhee, "Some considerations relating to the design of autopilots for legged vehicles," *Journal of Terramechanics*, vol. 6, no. 1, pp. 23–35, 1969.

[130] R. B. McGhee and G. I. Iswandhi, "Adaptive locomotion of a multilegged robot over rough terrain," *IEEE Transactions on Systems, Man and Cybernetics*, vol. 9, no. 4, pp. 176–182, 1979.

[131] K. J. Waldron, V. J. Vohnout, A. Pery, and R. B. McGhee, "Configuration design of the adaptive suspension vehicle," *The International Journal of Robotics Research*, vol. 3, no. 2, pp. 37–48, 1984.

[132] K. Waldron and R. McGhee, "The adaptive suspension vehicle," *IEEE Control Systems Magazine*, vol. 6, no. 6, pp. 7–12, 1986.

[133] B. K. Horn and M. H. Raibert, "Configuration space control," 1977.

[134] M. H. Raibert and J. E. Tanner, "Design and implementation of a VLSI tactile sensing computer," *The International Journal of Robotics Research*, vol. 1, no. 3, pp. 3–18, 1982.

[135] M. H. Raibert, "Hopping in legged systems—modeling and simulation for the two-dimensional one-legged case," *IEEE Transactions on Systems, Man and Cybernetics*, no. 3, pp. 451–463, 1984.

[136] M. H. Raibert, H. B. Brown, and M. Chepponis, "Experiments in balance with a 3D one-legged hopping machine," *The International Journal of Robotics Research*, vol. 3, no. 2, pp. 75–92, 1984.

[137] M. H. Raibert, "Running with symmetry," *The International journal of robotics research*, vol. 5, no. 4, pp. 3–19, 1986.

[138] M. Raibert, M. Chepponis, and H. Brown Jr, "Running on four legs as though they were one," *IEEE Journal of Robotics and Automation*, vol. 2, no. 2, pp. 70–82, 1986.

[139] M. Raibert, "Dynamic legged robots for rough terrain," in *Proceedings of the 10th IEEE-RAS International Conference on Humanoid Robots*, 2010, pp. 1–1.

[140] Boston Dynamics, "CHEETAH - Fastest Legged Robot," http://www.bostondynamics.com/robot_cheetah.html, Retrieve Jan 2013.

[141] C. G. Atkeson, A. W. Moore, and S. Schaal, "Locally weighted learning," *Artificial intelligence review*, vol. 11, no. 1-5, pp. 11–73, 1997.

[142] J. Morimoto, G. Cheng, C. G. Atkeson, and G. Zeglin, "A simple reinforcement learning algorithm for biped walking," in *Proceedings of the IEEE International Conference on Robotics and Automation*, vol. 3, 2004, pp. 3030–3035.

[143] J. Morimoto, J. Nakanishi, G. Endo, G. Cheng, C. G. Atkeson, and G. Zeglin, "Poincare-map-based reinforcement learning for biped walking," in *Proceedings of the IEEE International Conference on Robotics and Automation*, 2005, pp. 2381–2386.

[144] J. Morimoto and C. G. Atkeson, "Learning biped locomotion," *IEEE Robotics & Automation Magazine*, vol. 14, no. 2, pp. 41–51, 2007.

[145] J. Grizzle, G. Abba, and F. Plestan, "Asymptotically stable walking for biped robots: Analysis via systems with impulse effects," *IEEE Transactions on Automatic Control*, vol. 46, no. 1, pp. 51–64, 2001.

[146] E. Westervelt, J. Grizzle, and D. Koditschek, "Hybrid zero dynamics of planar biped walkers," *IEEE Transactions on Automatic Control*, vol. 48, no. 1, pp. 42–56, 2003.

[147] J. Grizzle, A. Ramezani, B. Buss, B. Griffin, K. A. Hamed, and K. Galloway, "Progress on controlling MARLO, an ATRIAS-series 3D underactuated bipedal robot," in *Proceedings of the Annual Dynamic Walking Meeting*, 2013.

[148] A. Ramezani and J. Grizzle, "ATRIAS 2.0, a new 3D bipedal robotic walker and runner," in *Proceedings of the 2012 International Conference on Climbing and walking Robots and the Support Technologies for Mobile Machines*, 2012, pp. 467–474.

[149] S. Collins, M. Wisse, and A. Ruina, "A three-dimensional passive-dynamic walking robot with two legs and knees," *The International Journal of Robotics Research*, vol. 20, no. 7, pp. 607–615, 2001.

[150] M. Garcia, A. Chatterjee, and A. Ruina, "Efficiency, speed, and scaling of two-dimensional passive-dynamic walking," *Dynamics and Stability of Systems*, vol. 15, no. 2, pp. 75–99, 2000.

[151] Dynamic Walking, "Dynamic Walking Annual Meeting," http://www.cmu.edu/dynamic-walking/, Retrieve Feb 2013.

[152] P. A. Bhounsule, J. Cortell, and A. Ruina, "Design and control of Ranger: an energy-efficient, dynamic walking robot," in *Proceedings of the 15th International Conference on Climbing and Walking Robots*, vol. 23, 2012, p. 26.

[153] R. F. Brodsky, *On the cutting edge: tales of a cold war engineer at the dawn of the nuclear, guided missile, computer and space ages*. Gordian Knot, 2006.

[154] R. Morrison, "Iron mule train," in *Proceedings of the Off-Road Mobility Research Symposium*, 1968, pp. 381–400.

[155] B. Kennedy, A. Okon, H. Aghazarian, M. Garrett, T. Huntsberger, L. Magnone, M. Robinson, and J. Townsend, "The Lemur II-class robots for inspection and maintenance of orbital structures: a system description," in *Proceedings of the International Conference on Climbing and Walking Robots*, 2006, pp. 1069–1076.

[156] B. H. Wilcox, "Athlete: An option for mobile lunar landers," in *Proceedings of the IEEE Aerospace Conference*, 2008, pp. 1–8.

[157] D. Wettergreen, H. Pangels, and J. Bares, "Behavior-based gait execution for the Dante II walking robot," in *Proceedings of the IEEE/RSJ International Conference on Intelligent Robots and Systems*, vol. 3, 1995, pp. 274–279.

[158] T. Haarnoja, "Dynamic modeling and velocity control for limit cycle walking," Master's thesis, Helsinki University of Technology, Espoo, Finland, 2010.

[159] D. Hobbelen and M. Wisse, "Controlling the walking speed in limit cycle walking," *The International Journal of Robotics Research*, vol. 27, no. 9, pp. 989–1005, 2008.

[160] DARPA, "DARPA Robotics Challenge," http://theroboticschallenge.org/, Retrieve Dec 2012.

[161] K. Taguchi, K. Ikeda, and S. Matsumoto, "Four-legged walking machine," in *Proceedings of the 2nd Symposium on Theory and Practice of Robots and Manipulators*, 1976.

[162] H.-O. Lim and A. Takanishi, "Biped walking robots created at Waseda University: WL and WABIAN family," *Philosophical Transactions of the Royal Society A: Mathematical, Physical and Engineering Sciences*, vol. 365, no. 1850, pp. 49–64, 2007.

[163] American Honda Motor Co. Inc., "History of ASIMO," http://asimo.honda.com/asimo-history/, Retrieve February 2012.

[164] K. Hirai, "The Honda humanoid robot: development and future perspective," *Industrial Robot: An International Journal*, vol. 26, no. 4, pp. 260–266, 1999.

[165] K. Kaneko, F. Kanehiro, S. Kajita, K. Yokoyama, K. Akachi, T. Kawasaki, S. Ota, and T. Isozumi, "Design of prototype humanoid robotics platform for HRP," in *Proceedings of the IEEE/RSJ International Conference on Intelligent Robots and Systems*, vol. 3, 2002, pp. 2431–2436.

[166] SONY Inc., "AIBO Official Site," http://www.sony.jp/products/Consumer/aibo/, Retrieve February 2012.

[167] FUJITSU Ltd., "Fujitsu Introduces Miniature Humanoid Robot, HOAP-1," http://pr.fujitsu.com/en/news/2001/09/10.html, Retrieve February 2012.

[168] Toyota Motor Co., "Toyota Partner Robot," http://www.toyota-global.com/innovation/partner_robot/, Retrieve February 2012.

[169] R. Tomovic, "A general theoretical model of creeping displacement," *Cybernetica, IV*, pp. 98–107, 1961.

[170] M. Vukobratović, D. Juričić, D. Hristić, V. Ćirić, and Z. Stojiljković, "Progress report to SRS (Social Rehabilitation Service): Restore the locomotion functions to severely disabled persons," Helsinki University of Technology, Tech. Rep., 1969.

[171] A. Frank and M. Vukobratovic, "On the gait stability of biped machines," *IEEE Transactions on Automatic Control*, vol. 15, no. 6, pp. 678–679, 1970.

[172] M. Vukobratovic, D. Hristic, and Z. Stojiljkovic, "Development of active anthropomorphic exoskeletons," *Medical and Biological Engineering*, vol. 12, no. 1, pp. 66–80, 1974.

[173] M. Vukobratović and J. Stepanenko, "On the stability of anthropomorphic systems," *Mathematical Biosciences*, vol. 15, no. 1, pp. 1–37, 1972.

[174] M. Vukobratovic, "Legged locomotion robots- mathematical models, control algorithms and realizations," in *Proceedings of the 5th IFAC, IIC, and ANIPLA, Symposium on Automatic Control in Space*, 1973, p. 1973.

[175] D. Okhotsimski, "Motion control system development for a mobile robot," *Automatic control in space*, pp. 251–256, 1980.

[176] A. Platonov, "Problems of motion control for mobile robots," *Automatic control in space*, pp. 303–310, 1980.

[177] A. Bessonov and N. Umnov, "Choice of geometric parameters of walking machines," *On Theory and Practice of Robots and Manipulators*, pp. 63–74, 1976.

[178] ——, "Features of kinematics of turn of walking vehicles," in *Proceedings of the 3rd Symposium on theory and practice of robots and manipulators*, 1978.

[179] E. Kugushev and V. Jaroshevskij, "Problems of selecting a gait for an integrated locomotion robot," in *Proceedings of the 4th international joint conference on Artificial intelligence-Volume 1*, 1975, pp. 789–793.

[180] J. Hall and D. Witt, “The development of an automatically-stabilized powered walking device,” in *Proceedings of the Conference on Human Locomotor Engineering*, 1971, pp. 7–10.

[181] M. Petternella and S. Salinari, “Simulation by digital computer of walking machine control system,” in *Proceedings of the 5th IFAC, IIC, and ANIPLA, Symposium on Automatic Control in Space*, 1973.

[182] J. Kessis, J. P. Rambaut, and J. Penne, “Walking robot multi-level architecture and implementation,” in *Proceedings of the 4th Symposium on Theory and Practice of Robots and Manipulators*, 1981.

[183] David Buckley, “Shadow Biped Walker by David Buckley,” http://davidbuckley.net/DB/ShadBiped.htm, Retrieve February 2012.

[184] M. Wisse and R. Q. Van der Linde, *Delft pneumatic bipeds*. Springer, 2007, vol. 34.

[185] E. Schuitema, M. Wisse, T. Ramakers, and P. Jonker, “The design of LEO: a 2D bipedal walking robot for online autonomous reinforcement learning,” in *Proceedings of the IEEE/RSJ International Conference on Intelligent Robots and Systems*, 2010, pp. 3238–3243.

[186] J. Karssen and M. Wisse, “Running robot phides,” *Dynamic Walking*, 2012.

[187] Technische Universität München, “Biped Robot JOHNNIE,” http://www.amm.mw.tum.de/en/research/current-projects/humanoid-robots/johnnie/, Retrieve November 2013.

[188] Deutsches Zentrum für Luft- und Raumfahrt, “DLR-Biped,” http://www.dlr.de/rm/en/desktopdefault.aspx/tabid-6838/11291_read-25964/, Retrieve November 2013.

[189] Aldebaran Robotics, “NAO Biped,” http://www.aldebaran-robotics.com/en/, Retrieve November 2013.

[190] RobotCub Consortium, “iCub,” http://www.icub.org/, Retrieve November 2013.

[191] Italian Institute of Technology, “COMAN,” http://www.iit.it/en/advr-labs/humanoids-a-human-centred-mechatronics/advr-humanoids-projects/compliant-humanoid-platform-coman.html, Retrieve November 2013.

[192] J. Järvinen, “Study of the technology of walking machines,” Master’s thesis, Helsinki University of Technology, Espoo, Finland, 1988.

[193] H. Lehtinen, “Force based motion control of a walking machine,” Ph.D. dissertation, 1994.

[194] Aalto University, “MECANT,” Retrieve February 2012, howpublished = "http://autsys.aalto.fi/en/MECANT".

[195] I. Leppänen, S. Salmi, and A. Halme, “Work partner - hut-automations new hybrid walking machine,” in *Proceedings of the 1st International Symposium on Climbing and Walking Robots*, 1998, pp. 391–394.

[196] A. Halme, I. Leppänen, and S. Salmi, "Development of workpartner-robot - design of actuating and motion control system," in *Proceedings of the 2nd International Conference on Climbing and Walking Robots*, 1999, pp. 657–665.

[197] A. Halme, I. Leppänen, J. Suomela, S. Ylönen, and I. Kettunen, "Workpartner: Interactive human-like service robot for outdoor applications," vol. 22, no. 7-8, pp. 627–640, 2003.

[198] S. Ylönen, I. Leppänen, S. Salmi, and A. Halme, "Hybrid locomotion of the WorkPartner service robot," in *Conference on Field and Service Robots*, 2001.

[199] A. Halme, I. Leppänen, S. Salmi, and S. Ylönen, "Hybrid locomotion of a wheel-legged machine," in *Proceedings of the 3rd International Conference on Climbing and Walking Robots*, 2000, pp. 167–173.

[200] A. Halme, "Advanced locomotion mechanism and their control systems of service robots - finding ideas from nature," in *Proceedings of the Intelligent Autonomous Vehicles*, 2001.

[201] Aalto University, "WorkPartner," http://autsys.aalto.fi/en/WorkPartner, Retrieve February 2012.

[202] F. P. Kusumah, "Foot force sensor implementation and analysis of ZMP walking on 2D bipedal robot with linear actuators," Master's thesis, Helsinki University of Technology, Espoo, Finland, 2011.

[203] V. T. Inman, H. J. Ralston, and F. Todd, *Human walking*. Williams & Wilkins, 1981.

[204] R. M. Alexander, "The gaits of bipedal and quadrupedal animals," *The International Journal of Robotics Research*, vol. 3, no. 2, pp. 49–59, 1984.

[205] J. B. C. J. Belanger, *Essai sur la solution numérique de quelques problèmes relatifs au mouvement permanent des eaux courantes*. Carilian-Goeury, 1828.

[206] R. M. Alexander, *Exploring biomechanics: animals in motion*. Scientific American Library, 1992.

[207] G. Gabrielli and T. Von, *What price speed?: specific power required for propulsion of vehicles*, 1950.

[208] D. Hobbelen and M. Wisse, "Ankle actuation for limit cycle walkers," *The International Journal of Robotics Research*, vol. 27, no. 6, pp. 709–735, 2008.

[209] K. Sreenath, H.-W. Park, I. Poulakakis, and J. W. Grizzle, "A compliant hybrid zero dynamics controller for stable, efficient and fast bipedal walking on mabel," *The International Journal of Robotics Research*, vol. 30, no. 9, pp. 1170–1193, 2011.

[210] S. H. Collins and A. Ruina, "A bipedal walking robot with efficient and human-like gait," in *Proceedings of the IEEE International Conference on Robotics and Automation*, 2005, pp. 1983–1988.

[211] Y. Umetani and S. Hirose, "Biomechanical study of serpentine locomotion," vol. 10, no. 4, 1974, pp. 513–518.

[212] J. G. Nichol, S. P. Singh, K. J. Waldron, L. R. Palmer, and D. E. Orin, "System design of a quadrupedal galloping machine," *The International Journal of Robotics Research*, vol. 23, no. 10-11, pp. 1013–1027, 2004.

[213] M. Popovic, A. Hofmann, and H. Herr, "Angular momentum regulation during human walking: biomechanics and control," in *Proceedings of the IEEE International Conference on Robotics and Automation*, vol. 3, 2004, pp. 2405–2411.

[214] N. A. Borghese, L. Bianchi, and F. Lacquaniti, "Kinematic determinants of human locomotion." *The Journal of Physiology*, vol. 494, no. Pt 3, pp. 863–879, 1996.

[215] A. G. Blanco, G. J. Munguia, and P. O. Moreno, "Development of a system for independent ambulation of patients with spinal cord injury using a dataglove and a biped robotic model," in *Proceedings of the Electronics, Robotics and Automotive Mechanics Conference*, 2008, pp. 461–466.

[216] G. Cheng, S.-H. Hyon, J. Morimoto, A. Ude, J. G. Hale, G. Colvin, W. Scroggin, and S. C. Jacobsen, "CB: a humanoid research platform for exploring neuroscience," *Advanced Robotics*, vol. 21, no. 10, pp. 1097–1114, 2007.

[217] M. Kwan and M. Hubbard, "Optimal foot shape for a passive dynamic biped," *Journal of theoretical biology*, vol. 248, no. 2, pp. 331–339, 2007.

[218] R. Boulic, P. Fua, L. Herda, M. Silaghi, J.-S. Monzani, L. Nedel, and D. Thalmann, "An anatomic human body for motion capture," in *Proceedings of the European Multimedia Microprocessor Systems and Electronic Commerce*, vol. 98, 1998.

[219] H. Hatze, "Neuromusculoskeletal control systems modeling–a critical survey of recent developments," *IEEE Transactions on Automatic Control*, vol. 25, no. 3, pp. 375–385, 1980.

[220] A. J. Ijspeert, "Central pattern generators for locomotion control in animals and robots," *Neural Networks*, vol. 21, no. 4, pp. 642–653, 2008.

[221] Q. Huang, K. Yokoi, S. Kajita, K. Kaneko, H. Arai, N. Koyachi, and K. Tanie, "Planning walking patterns for a biped robot," *IEEE Transactions on Robotics and Automation*, vol. 17, no. 3, pp. 280–289, 2001.

[222] S.-M. Song and K. J. Waldron, *Machines that walk: the adaptive suspension vehicle*. The MIT Press, 1989.

[223] I.-W. Park, J.-Y. Kim, J. Lee, and J.-H. Oh, "Online free walking trajectory generation for biped humanoid robot KHR-3 (HUBO)," in *Proceedings of the IEEE International Conference on Robotics and Automation*, 2006, pp. 1231–1236.

[224] S. Kajita, F. Kanehiro, K. Kaneko, K. Fujiwara, K. Harada, K. Yokoi, and H. Hirukawa, "Biped walking pattern generation by using preview control of zero-moment point," in *Proceedings of the IEEE International Conference on Robotics and Automation*, vol. 2, 2003, pp. 1620–1626.

[225] A. Takanishi, H.-o. Lim, M. Tsuda, and I. Kato, "Realization of dynamic biped walking stabilized by trunk motion on a sagittally uneven surface," in *Proceedings of the IEEE International Workshop on Intelligent Robots and Systems*, 1990, pp. 323–330.

[226] E. Cuevas, D. Zaldívar, R. Rojas *et al.*, "Incremental fuzzy control for a biped robot balance," in *Proceedings of the International Conference on Robotics and Applications*, 2005.

[227] E. Cuevas, D. Zaldívar, and R. Rojas, "Dynamic control algorithm for a biped robot," in *Proceedings of the 7th International Conference on Control and Applications*, 2005.

[228] ——, "Walking trajectory control of a biped robot," 2004.

[229] Y. Hürmüzlü and G. D. Moskowitz, "The role of impact in the stability of bipedal locomotion," *Dynamics and Stability of Systems*, vol. 1, no. 3, pp. 217–234, 1986.

[230] T. McGeer, "Powered flight, child's play, silly wheels and walking machines," in *Proceedings of the IEEE International Conference on Robotics and Automation*, 1989, pp. 1592–1597.

[231] ——, "Passive walking with knees," in *Proceedings of the IEEE International Conference on Robotics and Automation*, 1990, pp. 1640–1645.

[232] M. H. Raibert *et al.*, *Legged robots that balance*. MIT press Cambridge, MA, 1986, vol. 3.

[233] A. Goswami, B. Thuilot, and B. Espiau, "A study of the passive gait of a compass-like biped robot symmetry and chaos," *The International Journal of Robotics Research*, vol. 17, no. 12, pp. 1282–1301, 1998.

[234] P. C. Müller, "Calculation of Lyapunov exponents for dynamic systems with discontinuities," *Chaos, Solitons & Fractals*, vol. 5, no. 9, pp. 1671–1681, 1995.

[235] J. E. Pratt and R. Tedrake, "Velocity-based stability margins for fast bipedal walking," in *Fast Motions in Biomechanics and Robotics*. Springer, 2006, pp. 299–324.

[236] A. Schwab and M. Wisse, "Basin of attraction of the simplest walking model," in *Proceedings of the ASME Design Engineering Technical Conference*, vol. 6, 2001, pp. 531–539.

[237] C. S. Hsu, *Cell-to-cell mapping: a method of global analysis for nonlinear systems*. Springer-Verlag New York, 1987.

[238] L. Liu, Y. Tian, and X. Huang, "A method to estimate the basin of attraction of the system with impulse effects: application to the biped robots," in *Intelligent Robotics and Applications*. Springer, 2008, pp. 953–962.

[239] P.-B. Wieber, "Constrained dynamics and parametrized control in biped walking," in *International Symposium on Mathematical Theory of networks and systems*, 2000.

[240] F. Pfeiffer and C. Glocker, *Multibody dynamics with unilateral contacts*. Wiley-VCH, 1996, vol. 9.

[241] J. Saarinen, A. Maula, R. Nissinen, H. Kukkonen, J. Suomela, and A. Halme, "Gimnet-infrastructure for distributed control of generic intelligent machines," *provider (server)*, vol. 586, no. 029, p. 525, 2007.

[242] A. Maula, M. Myrsky, and J. Saarinen, "GIMnet 2.0-enhanced communication framework for distributed control of generic intelligent machines," in *Embedded Systems, Computational Intelligence and Telematics in Control*, no. 1, 2012, pp. 62–67.

[243] B. Vanderborght, A. Albu-Schaeffer, A. Bicchi, E. Burdet, D. Caldwell, R. Carloni, M. Catalano, O. Eiberger, W. Friedl, G. Ganesh *et al.*, "Variable impedance actuators: a review," *Robotics and Autonomous Systems*, vol. 61, no. 12, pp. 1601–1614, 2013.

[244] D. C. Bentivegna, C. G. Atkeson, and J.-Y. Kim, "Compliant control of a hydraulic humanoid joint," in *Proceedings of the 7th IEEE-RAS International Conference on Humanoid Robots*, 2007, pp. 483–489.

[245] LinMot Inc., "Manufacturer of the linmot linear motors, guided actuators, servo controllers, and magspring constant force springs." http://www.linmot.com/, Retrieve January 2012.

[246] S. Aaron and R. Stein, "Comparison of an EMG-controlled prosthesis and the normal human biceps brachii muscle," *American Journal of Physical Medicine & Rehabilitation*, vol. 55, no. 1, pp. 1–14, 1976.

[247] MATLAB, *version 7.10.0 (R2010a)*. Natick, Massachusetts: The MathWorks Inc., 2010.

[248] M. W. Spong, "The swing up control problem for the acrobot," *IEEE Control Systems*, vol. 15, no. 1, pp. 49–55, 1995.

[249] S. Anderson, M. Wisse, C. Atkeson, J. Hodgins, G. Zeglin, and B. Moyer, "Powered bipeds based on passive dynamic principles," in *Proceedings of the 5th IEEE-RAS International Conference on Humanoid Robots*, 2005, pp. 110–116.

[250] J. Denk and G. Schmidt, "Synthesis of a walking primitive database for a humanoid robot using optimal control techniques," in *Proceedings of IEEE-RAS International Conference on Humanoid Robots*, 2001, pp. 319–326.

[251] V. Chen, "Passive dynamic walking with knees: A point foot model," Master's thesis, Massachusetts Institute of Technology, 2007.

[252] M. Wisse, A. Schwab, and F. Van Der Helm, "Passive dynamic walking model with upper body," *Robotica*, vol. 22, no. 06, pp. 681–688, 2004.

[253] A. Kuo, "Energetics of actively powered locomotion using the simplest walking model," *Journal of biomechanical engineering*, vol. 124, p. 113, 2002.

[254] M. J. Coleman, A. Chatterjee, and A. Ruina, "Motions of a rimless spoked wheel: a simple three-dimensional system with impacts," *Dynamics and Stability of Systems*, vol. 12, no. 3, pp. 139–159, 1997.

[255] S. Mochon and T. A. McMahon, "Ballistic walking," *Journal of biomechanics*, vol. 13, no. 1, pp. 49–57, 1980.

[256] ——, "Ballistic walking: An improved model," *Mathematical Biosciences*, vol. 52, no. 3, pp. 241–260, 1980.

[257] M. W. Spong, "Passivity based control of the compass gait biped," in *Proceedings of the IFAC World Congress*, 1999.

[258] M. W. Spong and F. Bullo, "Controlled symmetries and passive walking," *IEEE Transactions on Automatic Control*, vol. 50, no. 7, pp. 1025–1031, 2005.

[259] M. W. Spong and G. Bhatia, "Further results on control of the compass gait biped," in *Proceedings of the IEEE/RSJ International Conference on Intelligent Robots and Systems*, vol. 2, 2003, pp. 1933–1938.

[260] R. Ortega and M. W. Spong, "Adaptive motion control of rigid robots: A tutorial," *Automatica*, vol. 25, no. 6, pp. 877–888, 1989.

[261] F. L. Lewis, D. M. Dawson, and C. T. Abdallah, *Robot manipulator control: theory and practice*. CRC Press, 2003, vol. 15.

[262] D. G. Hobbelen and M. Wisse, "Swing-leg retraction for limit cycle walkers improves disturbance rejection," *IEEE Transactions on Robotics*, vol. 24, no. 2, pp. 377–389, 2008.

[263] M. Wisse, "Three additions to passive dynamic walking; actuation, an upper body, and 3D stability," in *Proceedings of the 4th IEEE/RAS International Conference on Humanoid Robots*, vol. 1, 2004, pp. 113–132.

[264] T. S. Parker, L. O. Chua, and T. S. Parker, *Practical numerical algorithms for chaotic systems*. Springer New York, 1989.

[265] F. Dercole and Y. A. Kuznetsov, "Slidecont: An auto97 driver for bifurcation analysis of filippov systems," *ACM Transactions on Mathematical Software*, vol. 31, no. 1, pp. 95–119, 2005.

[266] ——, "User guide to slidecont 2.0," 2004.

[267] P. Thota and H. Dankowicz, "TC-HAT ($\hat{TC}$): A novel toolbox for the continuation of periodic trajectories in hybrid dynamical systems," *Journal on Applied Dynamical Systems*, vol. 7, no. 4, pp. 1283–1322, 2008.

[268] P. Thota, "Analytical and computational tools for the study of grazing bifurcations of periodic orbits and invariant tori," Ph.D. dissertation, Virginia Polytechnic Institute and State University, 2007.

[269] A. Goswami, B. Thuilot, B. Espiau *et al.*, "Compass-like biped robot part I: stability and bifurcation of passive gaits," 1996.

[270] J. Adolfsson, H. Dankowicz, and A. Nordmark, "3D passive walkers: Finding periodic gaits in the presence of discontinuities," *Nonlinear Dynamics*, vol. 24, no. 2, pp. 205–229, 2001.

[271] E. J. Doedel, "Auto: A program for the automatic bifurcation analysis of autonomous systems," *Congressus Numerantium*, vol. 30, pp. 265–284, 1981.

[272] E. Doedel and J. P. Kernevez, *AUTO, software for continuation and bifurcation problems in ordinary differential equations*. California Institute of Technology, 1986.

[273] E. Doedel, A. Champneys, T. Fairgrieve, Y. Kuznetsov, B. Sandstede, and X. Wang, "Auto 97: Continuation and bifurcation software for ordinary differential equations, user's manual," *Center for research on parallel computing, California Institute of Technology, Pasadena*, 1997.

[274] Doedel, EJ and Paffenroth, RC and Champneys, AR and Fairgrieve, TF and Kuznetsov, Yu A and Oldeman, BE and Sandstede, B and Wang, XJ, "AUTO-07P: Continuation and bifurcation software for ordinary differential equations (2007)," http://indy.cs.concordia.ca/auto, Retrieve February 2012.

[275] E. Doedel, X. Wang, and T. Fairgrieve, "Auto 94: Software for continuation and bifurcation in ordinary differential equations," *Applied Mathematics Report, California Institute of Technology*, 1994.

[276] J. J. Dongarra and C. B. Moler, "Eispack: A package for solving matrix eigenvalue problems," Argonne National Lab., IL (USA), Tech. Rep., 1983.

[277] H. Keller, "Lectures on numerical methods in bifurcation problems," *Applied Mathematics*, vol. 217, p. 50, 1987.

[278] T. F. Fairgrieve and A. D. Jepson, "OK floquet multipliers," *journal on numerical analysis*, vol. 28, no. 5, pp. 1446–1462, 1991.

[279] E. Doedel, H. B. Keller, and J. P. Kernevez, "Numerical analysis and control of bifurcation problems (I): Bifurcation in finite dimensions," *International journal of bifurcation and chaos*, vol. 1, no. 03, pp. 493–520, 1991.

[280] ——, "Numerical analysis and control of bifurcation problems (II): bifurcation in infinite dimensions," *International Journal of Bifurcation and Chaos*, vol. 1, no. 04, pp. 745–772, 1991.

[281] E. Doedel, "Numerical analysis of bifurcation problems," *Spring School on Numerical Software*, 1997.

[282] E. J. Doedel, "Nonlinear numerics," *Journal of the Franklin Institute*, vol. 334, no. 5, pp. 1049–1073, 1997.

[283] M. Goldfarb and N. Celanovic, "Modeling piezoelectric stack actuators for control of micromanipulation," *IEEE Control Systems*, vol. 17, no. 3, pp. 69–79, 1997.

[284] R. Alur, C. Belta, F. Ivančić, V. Kumar, M. Mintz, G. J. Pappas, H. Rubin, and J. Schug, "Hybrid modeling and simulation of biomolecular networks," in *Hybrid Systems: Computation and Control*. Springer, 2001, pp. 19–32.

[285] R. C. Browning, E. A. Baker, J. A. Herron, and R. Kram, "Effects of obesity and sex on the energetic cost and preferred speed of walking," *Journal of Applied Physiology*, vol. 100, no. 2, pp. 390–398, 2006.

[286] R. Tanawongsuwan and A. Bobick, "A study of human gaits across different speeds," Georgia Tech, Tech. Rep., 2003.

[287] R. Ferández, H. Montes, J. Sarriá, M. Armada, P. Solaeche, and G. Fernández, "Experimental evaluation of passive biped under structural parameters variations." CLAWAR, 2010.

[288] P. G. Weyand, B. R. Smith, M. R. Puyau, and N. F. Butte, "The mass-specific energy cost of human walking is set by stature," *The Journal of Experimental Biology*, vol. 213, no. 23, pp. 3972–3979, 2010.

[289] F. Danion, E. Varraine, M. Bonnard, and J. Pailhous, "Stride variability in human gait: the effect of stride frequency and stride length," *Gait & Posture*, vol. 18, no. 1, pp. 69–77, 2003.

[290] S. Krishnan and C. Voorhees, "The use of harmonic drives on NASA's Mars Exploration Rover," 2001.

[291] M. Raibert, K. Blankespoor, G. Nelson, R. Playter *et al.*, "Bigdog, the rough-terrain quadruped robot," in *Proceedings of the 17th World Congress*, 2008, pp. 10 823–10 825.

[292] A. K. Azad, N. Cowan, M. Tokhi, G. Virk, and R. Eastman, *Adaptive Mobile Robotics: Proceedings of the 15th International Conference on Climbing and Walking Robots and the Support Technologies for Mobile Machines*. World Scientific Publishing Company, 2012.

[293] LinMot Inc., "Motion control sw user manual, documentation of the motion control sw - e1100 / b1100 drive series," http://www.linmot.com/fileadmin/doc/Manuals/E1100/Usermanual_MotionCtrlSW_e_recent.pdf, Retrieve November 2013.

Researchers have been studying biped robots for many years, and, while many advances in the field have been accomplished, the challenge still remains in transferring the existing solutions into real applications. The main issues are related to mobility and autonomy, and, the underlying problem is associated to energy issues.

The GIMBiped project in Aalto University was established to tackle the previous issues in energy efficiency and mobility, through the study and implementation of dynamic and energy-efficient bipedal robotic waking.

This thesis focused on the development of a simplified biped model used to analyze and compare different control approaches. Later the same model is used to evaluate a redesign of the hardware, searching for better energy efficiency and stability. Furthermore, a new control approach combining ZMP-based and LCW is tested in a modified version of the original GIMBiped hardware

ISBN 978-952-60-5487-2
ISBN 978-952-60-5488-9 (pdf)
ISSN-L 1799-4934
ISSN 1799-4934
ISSN 1799-4942 (pdf)

Aalto University
School of Electrical Engineering
Department of Automation and Systems Technology
www.aalto.fi

BUSINESS + ECONOMY

ART + DESIGN + ARCHITECTURE

SCIENCE + TECHNOLOGY

CROSSOVER

DOCTORAL DISSERTATIONS

Aalto-DD 209/2013